Nonlinear Control for Linear Motion Systems
An Exploratory Study

PROEFSCHRIFT

ter verkrijging van de graad van doctor
aan de Technische Universiteit Eindhoven,
op gezag van de Rector Magnificus, prof.dr.ir. C.J. van Duijn,
voor een commissie aangewezen door het College voor Promoties
in het openbaar te verdedigen
op woensdag 24 september 2008 om 16.00 uur

door

Wilhelmus Henricus Theodorus Maria Aangenent

geboren te Gennep

Dit proefschrift is goedgekeurd door de promotor:

prof.dr.ir. M. Steinbuch

Copromotoren:
dr.ir. M.J.G. van de Molengraft
en
dr.ir. W.P.M.H. Heemels

The research reported in this thesis is part of the research program of the Dutch Institute of Systems and Control (DISC). The author has successfully completed the educational program of the Graduate School DISC.

A catalogue record is available from the Eindhoven University of Technology Library.

Nonlinear Control for Linear Motion Systems. An Exploratory Study./
by Wilhelmus H.T.M. Aangenent. – Eindhoven : Technische Universiteit Eindhoven, 2008. Proefschrift. – ISBN: 978-90-386-1378-9

This thesis was prepared with the pdfLaTeX documentation system.
Cover Design: Dovile Jurgelenaite
Reproduction: Universiteitsdrukkerij TU Eindhoven, Eindhoven, The Netherlands

Summary

Nonlinear Control for Linear Motion Systems
An Exploratory Study

Both industrial and commercial high-tech mechatronic devices, such as printers, robotic manipulators, CD/DVD players, electron microscopes and wafer scanners, constitute a major economic value. These machines have to perform their motion tasks satisfying stringent speed and accuracy requirements. Increasing performance demands motivate a re-examination of the current designs. Since most motion systems are (mechanically) designed to have approximately linear behavior, the implemented control strategies generally rely on classical linear control theory. However, these linear controllers suffer from inevitable trade-offs that restrict the achievable system performance.
The trade-offs that are encountered during the design of the control system are caused by fundamental performance limitations in feedback systems. Part of these limitations is inherently linked to the plant and thus holds irrespective of how the input is generated, be it via linear, nonlinear, hybrid or time-varying feedback. Other limitations are a consequence of the plant acting in combination with linear time-invariant (LTI) causal feedback control. This naturally raises the question whether these latter limitations can be circumvented by using time-varying or nonlinear feedback controllers.
Such a study is motivated by several examples which have been presented in literature, showing that nonlinear control can, in certain circumstances, outperform linear time-invariant feedback control for linear plants. However, knowledge about robustness, systematic controller synthesis methods, and performance limitations is still lacking for these nonlinear control schemes. Taking the above into account, the goal of this thesis is stated as follows:

Develop systematic and generic control synthesis methods for nonlinear feedback controllers for linear motion systems, overcoming the limitations imposed by linear feedback.

This thesis explores three main directions to contribute to the solution of this challenging research question.

Time-domain performance based control design: We propose a method to design a nonlinear state feedback controller that meets a set of time-domain specifications that are not attainable by linear state feedback. This is done using an existing constrained polynomial interpolation technique. Stability of the obtained nonlinear state feedback controller is analyzed using sum-of-squares techniques. Additionally, we present an extension of recent results where linear matrix inequality (LMI) techniques were used to synthesize a fixed order linear controller that satisfies certain time-domain specifications. This extension enables the assignment of complex conjugate closed-loop poles as opposed to the original method in which only real poles were allowed.

Reset control: This thesis extends the results in the field of reset control in two directions, namely in the sense of the $\mathcal{L}_2$ gain and with respect to the $\mathcal{H}_2$ norm. We generalize the $\mathcal{L}_2$ gain analysis to general reset control systems fitting in the common $\mathcal{H}_\infty$ framework, and include the possibility to analyze tracking problems. With respect to the $\mathcal{H}_2$ norm, we derive convex optimization problems based on LMIs to compute an upperbound on the $\mathcal{H}_2$ norm.

LPV control: In standard linear parameter varying (LPV) control systems, the plant that is considered depends on a real-valued parameter. In this thesis, however, the plant is considered to be linear and time-invariant, and the parameter dependence is introduced through the performance requirements. We propose a method to design a nonlinear controller for a linear motion system to improve the transient response to a step reference. Furthermore, we propose a nonlinear controller setup for the active control of a vibration isolation system. This setup consists of two parts: (i) a real-time multiresolution spectrum analyzer that is able to identify the currently dominating disturbance characteristics, and (ii) an LPV controller that adapts itself to the available disturbance information. This way, a control system is obtained that is able to adapt itself to the current operating condition, resulting in a closed-loop system with an overall increased performance when compared to the original controller.

This thesis presents initial steps towards systematic design methods for nonlinear controllers for linear systems, which obtain performance levels that are not attainable by using linear controllers. The obtained results are promising on the one hand, but, on the other hand they also show that still a lot of developments are needed before complete systematic synthesis methods are available. However, the potential benefits for the high-tech industry will drive such further developments in this appealing and challenging area, for which the results presented in this thesis can form a starting point.

Contents

Part I

Motivation

Chapter 1

Introduction

In this introductory chapter, the research of this thesis is motivated. Some of the limitations imposed on linear control systems that are caused by the use of linear feedback are discussed. The problem statement, the main contributions, and the structure of this thesis are stated.

1.1 Trade-offs in linear control design

Both industrial and commercial high-tech mechatronic devices, such as printers, robotic manipulators, CD/DVD players, electron microscopes and wafer scanners, constitute a major economic value worldwide and especially in the Netherlands. These machines have to perform their motion tasks with increasingly high performance demands, which cannot be obtained by the current designs. Examples of performance demands are high speed and high accuracy. Engineering practice tries to meet these demands by posing stringent requirements on the components and the mechanical construction. Additionally, disturbances are reduced by operating the motion system in highly optimized environments, such as clean rooms. Although these solutions are beneficial for performance, they are also very costly. A potentially less costly option is to improve the control design. Since motion systems are usually designed to have approximately linear behavior, the implemented control strategies generally rely on classical linear control theory. However, the resulting linear controllers suffer from inherent limitations and require additional, possibly mechanical, solutions to achieve system performance.
An example of this is given by the linear servo control design of optical storage drives for the automotive industry, see Figure 1.1(a). To assure sufficient suppression of low-frequency shocks and vibrations, induced for example by road or

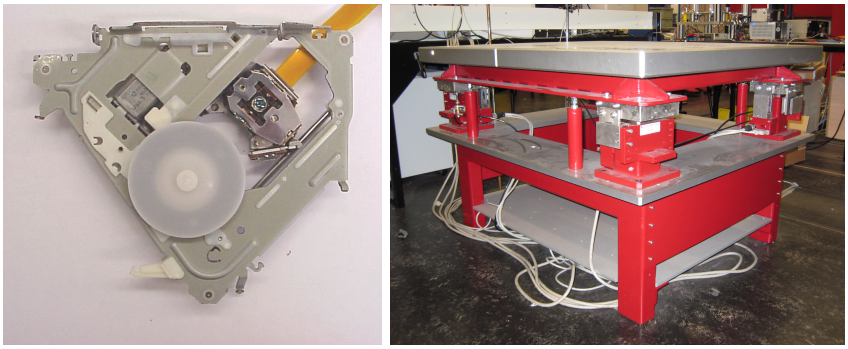

(a) (b)

Figure 1.1: Industrial applications hampered by trade-offs. (a) Optical storage drive for car applications, (b) vibration isolation table.

engine vibrations, the bandwidth of the linear control design should be chosen as high as possible. However, by choosing the bandwidth too high, the control design becomes very sensitive to high-frequency measurement noise, induced for example by disc defects, such as scratches and fingerprints. To deal with this trade-off, manufacturers integrate passive dampers in their modules to reduce the vibration level to which the drive is being exposed. Unfortunately, these dampers are undesirable because they are both expensive, and space and energy consuming.
As a second example of the trade-offs that are encountered in linear control, consider vibration isolation systems, see Figure 1.1(b). Such systems generally possess low resonance frequencies resulting from supporting large payload masses by weak undamped springs. The reason for doing so is that high-frequency disturbances from the ground are not passed to the payload mass in this manner. This effect can be represented by the so-called transmissibility function, or complementary sensitivity function in control engineering terminology. Using linear control, we are now essentially facing the trade-off formalized by the Bode sensitivity integral [12]. Namely, if low-frequency transmissibility is to be suppressed by applying active damping near the undamped resonance frequency, then this comes at the price of increased high-frequency transmissibility.

1.2 Nonlinear control of linear systems

The trade-offs that are encountered during the design of the control system are caused by fundamental performance limitations in feedback systems. Part of these limitations is inherently linked to the plant and thus holds irrespective of how the input is generated, be it via linear, nonlinear, hybrid or time-varying feedback.

Other limitations are a consequence of the structure imposed on the controller, as typically linear time-invariant (LTI) causal feedback is considered. This naturally raises the question whether these latter limitations can be circumvented by using time-varying or nonlinear feedback control.
Being aware of the difficulties and negative effects normally associated with the presence of nonlinearities, it may appear a step backwards to intentionally introduce nonlinearities into an otherwise linear system. In some cases however, there may be good reasons to do so. In literature, several examples have been presented showing that nonlinear control can, in certain circumstances, outperform linear time-invariant feedback control for linear plants. For instance, in [35, 82], it is shown that a simple PI controller, whose integrator is switched on and off depending on the size of the error, performs better than its linear time-invariant counterpart considering certain performance specifications. In the same spirit of switching between controllers, [93] discusses potential performance benefits of hybrid control for LTI systems. Optimal nonlinear feedback control derived from higher-order performance criteria is examined in [3, 118, 123], while the use of non-smooth filters like the SPAN (split-path nonlinear) filter and the driven limiter are proposed in [38] and [2], respectively. A servo mechanism with a nonlinear gain element is treated in [73], while nonlinear damping is proposed in [87]. Another strategy for nonlinear control of an LTI plant is reset control. A reset controller is an LTI system whose states, or subset of states, are reset to zero whenever its input and output satisfy certain conditions. The concept of reset control was first introduced in 1958 by means of the resetting integrator of Clegg [26]. In 1975, this concept was extended to first-order reset elements (FOREs) by Horowitz [62] and several analysis methods for reset control systems were developed later on [5, 23, 60]. However, knowledge about robustness, systematic controller synthesis and performance limitations is still lacking for this kind of nonlinear control schemes.
Most of these approaches were proposed during the sixties and seventies, and no serious recent attempts have been made to further investigate their potential. However, several nonlinear solutions are used in industry to obtain better performance of an LTI motion system, especially in (optical) data storage systems [19, 52, 142, 148] and automotive applications [36, 71, 74]. Typically, their design is based on heuristics and experience, while a systematic design method is lacking.

1.3 Problem statement and followed approach

This thesis focusses on the design of nonlinear controllers for linear motion systems as these systems are widely used in industrial applications. The main requirements for nonlinear controllers to be accepted as a viable alternative for linear controllers are:

(i) The advantages with respect to performance in comparison to well-accepted

linear control should be evident.

(ii) The control design techniques should be generic, and hence not application-specific.

(iii) A systematic design procedure.

Taking these requirements into account, the goal of this thesis can be stated as follows:

Develop systematic and generic control synthesis methods for nonlinear feedback controllers for linear motion systems, overcoming the limitations imposed by linear feedback.

Both the analysis and synthesis methods for linear controllers for linear systems are well-developed and understood. Therefore, in this thesis we will use several of these well-developed analysis and synthesis methods as a starting point, and extent or adapt these methods by introducing different nonlinear or time-varying elements. The linear methods that we will use and the corresponding nonlinear extensions that we explore are:

1) Linear state feedback controller synthesis extended to polynomial state feedback controller synthesis incorporating input and state constraints.

2) Analysis of linear $\mathcal{H}_\infty$ and $\mathcal{H}_2$ controllers extended with resets of the states.

3) Synthesis of linear controllers via the generalized plant framework extended to the synthesis of nonlinear controllers via linear parameter varying (LPV) synthesis techniques.

1.4 Contributions

In this thesis, we explore several principles to design nonlinear controllers for linear systems as just mentioned. The main contributions in these directions are stated next.

1.4.1 Time-domain performance based control design

Recently, in [56] linear matrix inequality (LMI) techniques have been used to synthesize a fixed order linear controller that satisfies certain time-domain specifications. This approach was originally limited to the assignment of distinct

strictly negative rational closed-loop poles, which is a severe restriction in the case of lightly damped systems. We propose two relaxations, which enable the assignment of complex conjugate poles, but at the expense of introducing some conservatism. The proposed method is evaluated by conducting an experiment on a fourth order motion system. Although the proposed approach is a completely linear one, it is a good example of the idea of improving time-domain performance by a two-step controller design.
Additionally, we propose a method to design a nonlinear static state feedback controller that meets a set of prescribed time-domain requirements that are not attainable by linear static state feedback. Using an existing constrained polynomial interpolation technique, an input signal is computed that satisfies the desired time-domain constraints on the input and state-trajectories. A nonlinear state feedback controller is designed and stability of the resulting closed-loop system is analyzed using sum-of-squares techniques [107]. An illustrative example is presented, showing that the proposed nonlinear controller outperforms the best linear static state feedback. To validate the proposed method, experiments on a fourth-order motion system have been carried out as well.

1.4.2 Reset control

A reset controller is a linear time-invariant system whose states, or subset of states, reset to zero whenever its input and output satisfy certain conditions. Reset controllers have been shown to be favorable over linear controllers with respect to the transient response performance [6]. This thesis extends the results in the field of reset control in two directions, namely in the sense of the $\mathcal{L}_2$ gain as introduced in [101, 151] and with respect to the analysis of the $\mathcal{H}_2$ norm. We propose an extension to [101, 151] in several ways. First, whereas [101, 151] are restricted to the Clegg integrator and FOREs, we generalize the $\mathcal{H}_\infty$ analysis to a general class of reset control systems. Second, arbitrary tracking problems are successfully included in our results, as opposed to [152], which only considers constant reference signals. We will show that this might introduce conservatism, for which a solution will be provided via input filtering.
With respect to the $\mathcal{H}_2$ norm, we derive convex optimization problems in terms of LMIs to compute an upperbound on the $\mathcal{H}_2$ norm, using dissipativity theory with piecewise quadratic Lyapunov functions [72]. The results can be used to approximate the energy content of the output resulting from specific input signals. We provide a simple though convincing example to illustrate the accuracy of our proposed $\mathcal{H}_\infty$ and $\mathcal{H}_2$ norm analysis and show that, for an input constrained $\mathcal{H}_2$ problem, reset control can indeed outperform the non-resetting linear controller designed via a commonly used optimization method.

1.4.3 LPV control

In 1953, Lewis introduced the use of nonlinear feedback to improve the rise-time and overshoot of the transient response of a servo mechanism [87]. He achieved this by introducing variable damping in a second order closed-loop system instead of using a constant damping coefficient. The idea of designing controllers that result in closed-loop systems with parameter (e.g. error) dependent performance is applicable in a broader context. A promising link with respect to the synthesis of this kind of nonlinear controllers for linear systems, is the control theory of linear parameter varying (LPV) plants. We aim to use LPV controllers for LTI systems. Such controllers are able to account for performance measures that are designed for different operating conditions of the closed-loop system including an LTI plant. When these operating conditions depend on a state variable, as is the case for the Lewis servo, the resulting LPV controller is consequently nonlinear. We propose an LPV approach to systematically design a nonlinear closed-loop servo system with the same characteristics as the Lewis servo by specifying the performance via parameter dependent weighting functions.
In the same LPV context, the closed-loop performance of motion systems that suffer from non-stationary disturbances could benefit from knowledge of these disturbances. Indeed, if the disturbance could be measured, this measurement could be used to enable an LPV controller to adapt itself to the current operating condition resulting in a closed-loop system with an overall increased performance. We use this idea to control an active vibration isolation system that is affected by non-stationary disturbances.

1.5 Outline

This thesis consists of five parts. In the remainder of Part I, Chapter 2 discusses the fundamental limitations in linear and nonlinear control systems. Opportunities and performance measures of nonlinear control systems are discussed as well. Chapter 3 discusses two examples of frequency domain based nonlinear controller design for linear systems.
Part II deals with time-domain performance based control design. It is shown in Chapter 4 that time-domain constraints on closed-loop signals of linear systems can be cast into an LMI problem, even when complex conjugate poles are assigned. Chapter 5 describes a method to design a nonlinear state feedback controller that meets a set of time-domain specifications that are not attainable by linear state feedback.
The topic of Part III is reset control. Chapter 6 introduces the reset control concept and in Chapter 7, we present a general LMI-based analysis method to determine an upperbound on the $\mathcal{L}_2$ gain performance of a reset control system. The focus in Chapter 8 is to study the performance of a reset control system in $\mathcal{H}_2$ sense. Chapter 9 concludes this part.
The fourth part is concerned with LPV control for linear systems. Chapter 10

introduces the basic concepts of LPV controller synthesis, which are used in Chapter 11 to design a closed-loop servo system that mimics a Lewis servo. In Chapter 12 we propose a nonlinear controller setup to control a vibration isolation system. This setup consists of two parts: (i) a real-time spectrum analyzer that is able to identify the currently dominating disturbance, and (ii) an LPV controller that adapts itself to the available disturbance information. This combination results in a control system that is able to adapt itself to the current operating condition resulting in a closed-loop system with an overall increased performance when compared to a non-adapting LTI controller.
Finally, in Part V, Chapter 13, we reflect on the obtained results by stating the conclusions and propose possible future research directions.

Chapter 2

Fundamental limitations in control systems

This chapter discusses the most important fundamental limitations in linear and nonlinear control systems. Furthermore, the opportunities and performance measures of nonlinear control systems are discussed.

2.1 Introduction

This thesis describes some new methods to design nonlinear controllers for linear systems, which overcome the limitations that are inherent to linear feedback controllers. Therefore, it is important to understand what these limitations are, and how they actually limit the attainable performance. Since the focus of this work is on single-input single-output (SISO) systems, this chapter reviews the most important fundamental limitations for feedback control systems such as depicted in Figure 2.1. In this figure, the plant is denoted by P, and the controller by C. The controller has to be designed such that the output y tracks the reference input r under the influence of disturbances affecting the loop, such as input and output disturbances d_{i} and d_{o}, and measurement noise n. We start this chapter by reviewing limitations in linear feedback control systems in Section 2.2. These fundamental limitations are expressed via integral relations both in the frequency domain, Section 2.2.2 and 2.2.3, as well as in the time-domain, Section 2.2.4. The limitations can also be interpreted from the analysis of limiting optimal control problems, which is discussed in Section 2.2.4.
Although there has been considerable attention in the control community for fundamental limitations in linear closed-loop systems, similar results for nonlinear

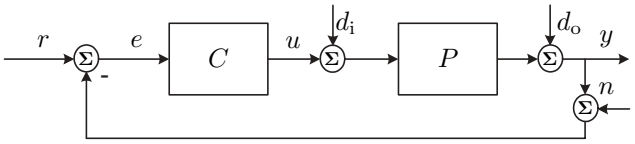

Figure 2.1: Feedback control system.

closed-loop systems are scarce and premature. Section 2.3 discusses the available results from literature. Finally, in Section 2.4 the insights from Sections 2.2 and 2.3 are used to make a statement about the possible benefits of nonlinear control for linear systems.

2.2 Limitations in linear control systems

Fundamental limitations in linear feedback loops result in unavoidable trade-offs between conflicting criteria such as stabilization, disturbance attenuation, and sensitivity reduction on the one hand, and noise amplification, poor stability margins and excessive control signals on the other hand. The study of fundamental limitations in linear feedback systems has its origin in the seminal work of Bode [12]. His work on integral relations in the frequency domain was applied to the feedback control problem by Horowitz [61], who obtained results on logarithmic integral constraints on the sensitivity function of continuous-time, stable minimum phase systems. Freudenberg and Looze [41, 42] extended the classical Bode integral relations to continuous-time systems that are non-minimum phase, open-loop unstable, or include time delays. A similar result for the complementary sensitivity function was obtained in [97]. Extensions to discrete-time systems were made in [94, 139], while integral relations for multi-input multi-output (MIMO) systems are considered in [21, 22]. The derivation of all these results mostly relies on analytic properties of the sensitivity and complementary sensitivity functions and can be traced back to specific applications of the Cauchy and Poisson integral formulas [131]. There exist alternative proofs based on e.g. elementary analysis [146], properties of the Laplace and z-transforms [20], and the extended argument principle [24, 25], which lead to new integral relations for specific cases. Similar as in the frequency domain, in the time-domain linear control systems are subject to integral relations as well [94, 98]. These limitations are best illustrated by the step response with particular reference to rise-time, settling-time, overshoot and undershoot.

In this section, it is assumed that the plant P and controller C are SISO continuous-time linear time-invariant systems, described by the transfer functions $P(s)$ and $C(s)$, respectively, where s denotes the Laplace variable. From this point onward, with some abuse of notation, we will use the same symbol to denote a system and its transfer function, and omit the dependency on the frequency variable when-

ever it is convenient and does not introduce any confusion. The response of the feedback system from Figure 2.1 is governed by four closed-loop transfer functions

$$\left[\begin{array}{c|c} S & PS \\ \hline CS & T \end{array}\right] = \left[\begin{array}{c|c} \frac{1}{1+PC} & \frac{P}{1+PC} \\ \hline \frac{C}{1+PC} & \frac{PC}{1+PC} \end{array}\right] \tag{2.1}$$

via

$$\begin{aligned} Y &= SD_{\mathrm{o}} + T(R-N) + PSD_{\mathrm{i}}, \\ E &= S(R - D_{\mathrm{o}} - N - PD_{\mathrm{i}}), \\ U &= -TD_{\mathrm{i}} + CS(R - N - D_{\mathrm{o}}), \end{aligned} \tag{2.2}$$

where the capital letters Y, R, D_{i}, D_{o}, and N are used to denote the Laplace transforms of the corresponding time-domain signals. Assume that P and C contain no unstable hidden modes. Then the closed-loop system from Figure 2.1 is internally stable if and only if the four transfer functions (2.1) are stable, i.e, have all of their roots in the open left half plane (OLHP) [134]. The open-loop transfer function is defined as $L=CP$.
Two functions are of central interest in the design of feedback systems, namely the sensitivity function S and the complementary sensitivity function T, since S maps the output disturbance to the output and reference input to the error, and T maps both the reference input and sensor noise to the output, see (2.2). Design of linear feedback controllers in the frequency domain is closely related to attaining a desired shape for the frequency response of these transfer functions (disturbance rejection, reference following, robustness, etc.). However, there are some fundamental limitations in shaping S and T, which hold for all possible linear controller designs. These are dictated by integral relations such as the Bode sensitivity theorems and Bode's gain-phase relationship, which are discussed next.

2.2.1 Bode sensitivity theorems

The sensitivity function S and the complementary sensitivity function T are complementary mappings, meaning that they satisfy the constraint

$$S + T = 1. \tag{2.3}$$

This identity represents an algebraic trade-off, merely due to the presence of a feedback loop, and states that $|S|$ and $|T|$ cannot both be small at the same frequency. Hence, desirable properties such as disturbance attenuation and noise rejection must be traded off against each other at each frequency. In practice, the algebraic relation (2.3) does not pose a severe restriction in the design of feedback systems. The reason is that although (2.3) implies that both S and T cannot be small at the same time, the frequency content of the reference signal r and the noise signal n are usually concentrated in different frequency regions. Good reference tracking is achieved if the sensitivity function S is small, while

suppression of measurement noise requires the complementary sensitivity function T to be small. Therefore, controllers with good (low-frequent) tracking properties and (high-frequent) noise suppression can be obtained by making S small at low frequencies and making T small at high frequencies. For instance, suppose that a controller needs to be designed to track reference signals with frequency content in the range $[0, \omega_c]$, and that the measurement noise has frequency content above ω_c. Then the ideal shapes of S and T that are consistent with (2.3) are given by

$$|S(i\omega)| = \begin{cases} 0 & \text{if } \omega \leq \omega_c \\ 1 & \text{if } \omega > \omega_c \end{cases}, \quad |T(i\omega)| = \begin{cases} 1 & \text{if } \omega \leq \omega_c \\ 0 & \text{if } \omega > \omega_c \end{cases}. \tag{2.4}$$

In contrast to (2.3), another class of design trade-offs is related to feedback properties in different frequency ranges. Based on Bode's attenuation theorem and corollary [12], Horowitz [61] obtained results on integrals on the sensitivity and complementary sensitivity function for stable and minimum phase open-loop systems. The extensions of these to unstable open-loop plants and plants with time delay were derived by Freudenberg and Looze [41, 42]. The complementary result for T with non-minimum phase open-loop systems was obtained by Middleton and Goodwin [97]. They are referred to as the Bode integrals for S and T.

Theorem 2.1 (Bode integral for S) *Let $S(s)$ be the sensitivity function and let $\{p_i \mid i = 1, \ldots, n_p\}$ be the set of poles in the open right half plane (ORHP) corresponding to the proper open-loop transfer function $L(s) = C(s)P(s)$. Then, assuming closed-loop stability,*

$$\int_0^\infty \log \left| \frac{S(i\omega)}{S(i\infty)} \right| d\omega = \frac{\pi}{2} \lim_{s\to\infty} \frac{s[S(s) - S(\infty)]}{S(\infty)} + \pi \sum_{i=1}^{n_p} p_i. \tag{2.5}$$

For a proof see e.g. [131]. Theorem 2.1 states that open-loop unstable poles of L worsen the integral constraint. Poles further from the $i\omega$-axis pose a greater difficulty in shaping S. If the relative degree is greater than 1 and if the plant has no poles in the ORHP, then (2.5) reduces to the well-known version of the Bode sensitivity integral

$$\int_0^\infty \log |S(i\omega)| \, d\omega = 0, \tag{2.6}$$

since $S(i\infty) = 1$ in this case.
An equivalent relation holds for the complementary sensitivity function.

Theorem 2.2 (Bode integral for T) *Let $T(s)$ be the complementary sensitivity function and let $\{q_i \mid i = 1, \ldots, n_q\}$ be the set of zeros in the ORHP corresponding to the proper open-loop transfer function $L(s) = C(s)P(s)$, and suppose that $L(0) \neq 0$. Then, assuming closed-loop stability,*

$$\int_0^\infty \log \left| \frac{T(i\omega)}{T(0)} \right| \frac{d\omega}{\omega^2} = \frac{\pi}{2} \frac{1}{T(0)} \lim_{s\to 0} \frac{dT(s)}{ds} + \pi \sum_{i=1}^{n_q} \frac{1}{q_i}. \tag{2.7}$$

For a proof see e.g. [131]. Non-minimum phase zeros of $L(s)$ worsen the integral constraint for the complementary sensitivity function. Zeros closer to the $i\omega$-axis pose a greater difficulty in shaping T. It is obvious that the ideal shape for S and T (2.4) do not satisfy (2.5) and (2.7). Indeed, Theorem 2.1 states that sensitivity reduction ($|S(i\omega)| < 1$) in a certain frequency range is always accompanied by a frequency range of increased sensitivity ($|S(i\omega)| > 1$). This property is known as the waterbed effect and, as opposed to the algebraic relation (2.3), does pose restrictions on the achievable system behavior in practice as discussed next.

2.2.2 Waterbed effect

Unstable poles and non-minimum phase zeros limit the achievable shape of the sensitivity and complementary sensitivity functions, respectively. As a consequence, most controlled motion systems are designed such that no unstable poles and/or non-minimum phase zeros are present in the open-loop system. Hence, for now we focus on the Bode sensitivity integral (2.6) that holds for open-loop stable linear systems with a relative degree of at least two. This relation does not necessarily imply that a peak ($|S(i\omega)| \gg 1$) will occur outside the frequency range over which the sensitivity function has been reduced. In principle, although the area of sensitivity reduction (region A_{SR} in Figure 2.2) is always compensated by an area of sensitivity increase (region A_{SI} in Figure 2.2) according to (2.6), the latter can be smeared out over an arbitrary large range of frequencies. Any practical

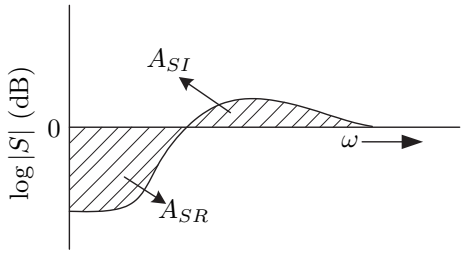

Figure 2.2: Typical shape of the sensitivity function, A_{SR} is the region of sensitivity reduction while A_{SI} is the region where the sensitivity is increased.

design however, is limited by bandwidth constraints which typically require that the open-loop transfer function $L(s)$ is small above a certain frequency. These constraints can arise due to actuator and sensor limitations but are mostly caused by uncertain and unmodeled dynamics in the plant. Indeed, since the frequency response fidelity of a physical system is limited beyond a certain bandwidth, it is required that the open-loop gain rolls off above that frequency to provide some stability robustness. Such a bandwidth constraint can be cast into an open-loop

gain specification of the type

$$|L(i\omega)| \leq \delta \left(\frac{\omega_c}{\omega}\right)^{1+k}, \quad \forall \omega \geq \omega_c, \tag{2.8}$$

with $\delta < \frac{1}{2}$ and $k > 0$. The parameters k, ω_c and δ can be used to provide upper limits to the slope of magnitude roll-off, the frequency where roll-off starts and the gain at that frequency, respectively. It follows that a bandwidth constraint such as (2.8) puts an upper limit on the part of the area of sensitivity increase A_{SI} that can be present at frequencies greater than ω_c.

Corollary 2.3 *Suppose that $L(s)$ is a transfer function with relative degree two or more and satisfies the bandwidth constraint* (2.8)*. Then*

$$\left| \int_{\omega_c}^{\infty} \log |S(i\omega)| d\omega \right| \leq \frac{3\delta\omega_c}{2k}. \tag{2.9}$$

For a proof see [131]. This result states that the part of the area A_{SI} of the tail of the Bode sensitivity integral over the infinite frequency range $[\omega_c, \infty)$ is bounded. Suppose that

$$A_{SR} = \left| \int_{0}^{\omega_d} \log |S(i\omega)| d\omega \right| = \alpha > \frac{3\delta\omega_c}{2k}, \tag{2.10}$$

then (2.9) implies that

$$\left| \int_{\omega_d}^{\omega_c} \log |S(i\omega)| d\omega \right| \geq \alpha - \frac{3\delta\omega_c}{2k}. \tag{2.11}$$

Hence, if $\omega_c - \omega_d$ is small, then necessarily $|S(i\omega)| \gg 1$ in the frequency range $[\omega_d, \omega_c]$. This phenomenon is referred to as the waterbed effect and was first observed in [39] for systems with non-minimum phase zeros. Indeed, unlike the trade-off due to the Bode sensitivity integral (2.6), there exists a guaranteed peak in $|S(i\omega)|$ (even when there are no bandwidth constraints) imposed by non-minimum phase zeros. A similar result holds for the complementary sensitivity function T [131]. The waterbed effect can be made more explicit for non-minimum phase and unstable systems with alternative expressions for the sensitivity trade-offs, the Poisson integral formulae [131]. It can be shown that a peak will occur in S (T) that is larger than 1 for non-minimum phase (unstable) systems, even if there is no bandwidth constraint. Based on these formulas, constraints on the bandwidth can be formulated for open-loop unstable non-minimum phase systems in order to have acceptable performance. It turns out that unstable poles result in a lower bound on the bandwidth while unstable zeros and/or time delays provide an upper bound [94].

The waterbed effect is inevitable in linear systems and holds irrespective of which method is used to design the linear controller, be it via classical or modern techniques, see Figure 2.3. Even if desired shapes of S and T have been designed that satisfy (2.3), (2.5), and (2.7), it still may be possible that there does not exist a stabilizing linear controller that achieves these shapes. This is due to another well-known limitation, which is formulated via Bode's gain-phase relationship.

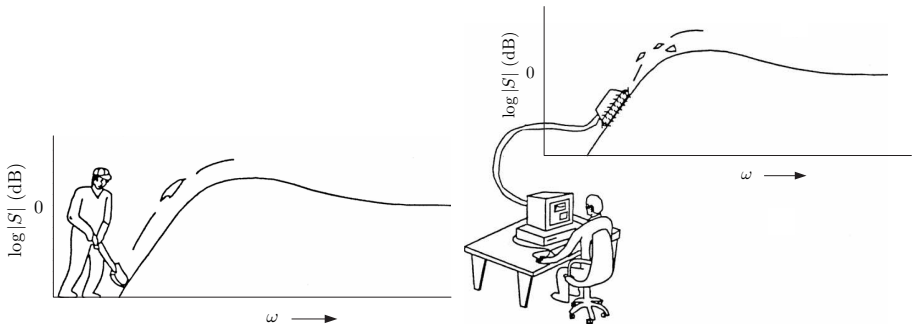

Figure 2.3: Representation of the waterbed effect. (a) Waterbed effect in classical control, (b) waterbed effect in modern control.

2.2.3 Gain-phase relationship

As discussed in Section 2.2.1, controllers with good (low-frequent) tracking properties and (high-frequent) noise suppression can be obtained by making S small at low frequencies and making T small at high frequencies, in the ideal case this is formulated by (2.4). In terms of the open-loop gain $|L(i\omega)|$ this amounts to

$$\begin{cases} |L(i\omega)| \gg 1 & \text{if } \omega \leq \omega_c \\ |L(i\omega)| \ll 1 & \text{if } \omega > \omega_c \end{cases} . \tag{2.12}$$

Furthermore, for the closed-loop system to be stable, the phase of the open-loop transfer function must satisfy

$$\arg L(i\omega_c) > -\pi. \tag{2.13}$$

Specifications (2.13) and (2.12) are known as the *Bode loop shaping specification* [44], which states that the open-loop should posses (i) high gain at low frequencies, (ii) low gain at high frequencies, and (iii) a reasonable phase-margin (phase bounded away from $-\pi$ near the crossover frequency ω_c). Ideally, the gain and phase should be designed separately such that any desired combination of the gain and phase can be obtained. Unfortunately, it is impossible to manipulate gain and phase independently. Indeed, the gain-phase relationships originally developed by Bode establish that, for a stable minimum phase transfer function, the phase of the frequency response is uniquely determined by the magnitude of the frequency response and vice versa. Hence, the gain and phase of the frequency response of a stable, minimum phase transfer function are dependent on each other, as is stated in the following theorem.

Theorem 2.4 (Bode's gain-phase relationship) *Let H be a proper, stable, and minimum phase transfer function, such that $H(0)>0$. Then, at any frequency*

ω_0, the phase $\phi(\omega_0) := \arg H(i\omega_0)$ satisfies

$$\phi(\omega_0) = \frac{1}{\pi}\int_{-\infty}^{\infty} \frac{d\log|H(i\omega_0 e^u)|}{du} \log|\frac{\omega+\omega_0}{\omega-\omega_0}|du, \tag{2.14}$$

where $u = \log(\frac{\omega}{\omega_0})$.

For a proof, see for instance [131]. Since the weighting function

$$\log|\frac{\omega+\omega_0}{\omega-\omega_0}|$$

becomes infinite at the point $\omega = \omega_0$, the slope of the magnitude curve of $H(i\omega)$ in the vicinity of ω_0, denoted by c, determines the phase $\phi(\omega_0)$

$$\phi(\omega_0) \approx \frac{c}{\pi}\int_{-\infty}^{\infty} \log|\frac{\omega+\omega_0}{\omega-\omega_0}|du = \frac{c}{\pi}\frac{\pi^2}{2} = c\frac{\pi}{2}. \tag{2.15}$$

Due to Bode's gain-phase relationship, attempts to specify certain loop shape specifications in one frequency range may compromise specifications in other ranges. For instance, because of the necessary phase-margin together with relation (2.15), the open-loop should crossover with a slope approximately equal to $c = -1$. This requirement restricts the achievable Bode loop shaping gain specification as is illustrated in Figure 2.4.

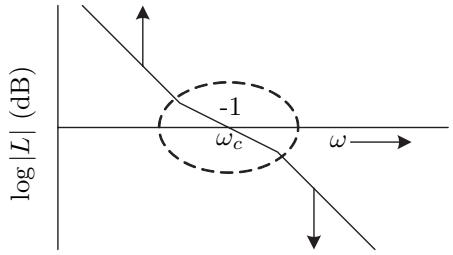

Figure 2.4: The Bode loop shaping specification.

To summarize, there are restrictions on the achievable performance of linear plants that are controlled by a linear feedback controller. For stable, minimum phase plants these limitations can be appreciated in the frequency domain by Bode's gain-phase relationship and the waterbed effect. In case the plant is unstable and/or non-minimum phase, the limitations are even more severe.

2.2.4 Time-domain integral relations

Similar to the limitations that are formulated in the frequency domain, in the time-domain there are also trade-offs and limitations that hold in linear feedback

systems. Consider for example a second order linear closed-loop system in the standard form

$$T(s) = \frac{\omega_n^2}{s^2 + 2\zeta\omega_n s + \omega_n^2}, \tag{2.16}$$

where ζ is the damping ratio and ω_n denotes the natural frequency. The nature of the response to a step function depends on the value of ζ. For large ζ there is little to no overshoot, but as ζ decreases, the response develops an overshoot. However, large values of the damping ratio also imply a sluggish response while the speed of response increases when the damping ratio decreases. This means that there will be a trade-off between the speed of the response and the amount of overshoot, see Figure 2.5.

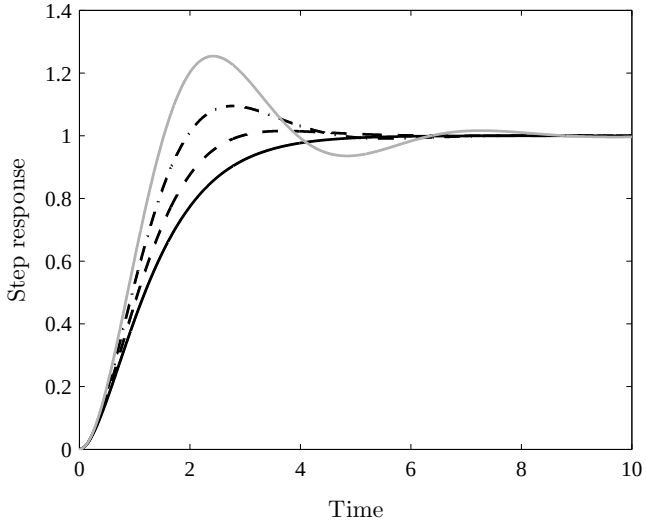

Figure 2.5: Step responses for $\omega_n = 2$: $\zeta = 1.0$ (solid black), $\zeta = 0.8$ (dashed), $\zeta = 0.6$ (dash-dotted), and $\zeta = 0.4$ (solid grey).

Relations based on interpolation constraints

Although less well-known than the integral relations in the frequency domain, integral relations in the time-domain also exist. However, these relations are only available for unstable and non-minimum phase open-loop transfer functions and can be derived from the following interpolation constraints that S and T must satisfy when the closed-loop system is stable: (i) if p is an unstable pole of $L(s)$, then $S(p) = 0$ and $T(p) = 1$, (ii) if q is a non-minimum phase zero of $L(s)$ then $S(q) = 1$ and $T(q) = 0$. The time-domain results are generally formulated with

respect to the step response. These results are weighted equal area criteria and imply amongst others that (i) the closed-loop step response of a plant with a real unstable pole and possibly time delay must overshoot, and (ii) the closed-loop step response of a plant with a real non-minimum phase zero must undershoot [94]. Similar results on bandwidth constraints as based on the Poisson integral formulae can be obtained by considering the time-domain relations in [94].

Limiting optimal control problems

The integral relations that represent the fundamental limitations and that were discussed in the preceding sections, are derived from analyticity of the various transfer functions. Another line of research with respect to performance limitations considers limiting optimal control problems formulated in the time-domain, resulting in similar results as were obtained in the frequency domain approach. The cost function in the limiting optimal control problems typically consists of quadratically weighted components in both the state and the control signal. If one of the weighings approaches zero, two limiting cases arise.
The first is the *minimum energy control* problem where the weighting of the states is allowed to approach zero. Suppose that a system with state $x(t)$ is subject to an initial condition $x(0)=x_0$. The stabilizing control u with minimum energy (in $\mathcal{L}_2$ sense) can be found by optimizing the cost functional

$$\lim_{\varepsilon\to 0} J_u(\varepsilon) := \lim_{\varepsilon\to 0} \frac{1}{2}\int_0^\infty \left(u^2(t)+\varepsilon^2 x^T(t)x(t)\right) dt. \tag{2.17}$$

In [132] it is shown that for linear systems

$$\lim_{\varepsilon\to 0} J_u(\varepsilon) = \sum_{p_i\in \mathrm{CRHP}} p_i, \tag{2.18}$$

where p_i denotes an open-loop pole and CRHP is the closed right half plane.
The second limiting optimal control problem is the so-called *cheap control* problem, where the input weighting approaches zero. In this case, the initial condition is assumed to be zero, $x(0)=0$, and the control which minimizes the $\mathcal{L}_2$ norm of the output error e to a step reference is obtained via

$$\lim_{\varepsilon\to 0} J_e(\varepsilon) := \lim_{\varepsilon\to 0} \frac{1}{2}\int_0^\infty \left(e^2(t)+\varepsilon^2 v^2(t)\right) dt, \tag{2.19}$$

where $v=u-u(\infty)$ with $u(\infty)$ the final control which gives a zero steady-state error. For the cheap control case, it can be shown [115, 132] that for linear systems

$$\lim_{\varepsilon\to 0} J_e(\varepsilon) = \sum_{q_i\in \mathrm{CRHP}} \frac{1}{q_i}, \tag{2.20}$$

where q_i denotes an open-loop zero. Explicit relations between the sensitivity integrals (2.5) and (2.7) and the optimal costs (2.18) and (2.20) are presented in [95]. The main result in [132] is that the lowest attainable $\mathcal{L}_2$ norm of the error to a step reference equals the least amount of energy that is needed to stabilize the unstable zero dynamics of the linear plant. Hence, non-minimum phase zeros pose a fundamental performance limitation in terms of a lower bound on the $\mathcal{L}_2$ norm of the tracking error.

2.3 Nonlinear fundamental limitations

In literature, several articles have appeared in which the fundamental limitations that are known for linear feedback loops have been extended to time-varying and nonlinear systems. Although these results will not be used in the sequel of the thesis, they give insight in what can be expected when nonlinear controllers are applied to linear plants. There are three research directions on this topic that are worth mentioning. First, there is a version of the waterbed effect for non-minimum phase and unstable open-loop nonlinear systems that is based on an extension of the linear waterbed effect from Section 2.2.2. This extension is discussed in Section 2.3.1. Second, in the context of the limiting optimal control problems from Section 2.2.4, an extension of the fundamental limitations has been proposed for non-minimum phase nonlinear plants, see Section 2.3.2. A third approach to quantify limitations in nonlinear control systems is shortly reviewed in Section 2.3.3, where the information theoretic concepts of entropy and finite capacity feedback are used to derive a Bode like sensitivity integral for general nonlinear feedback systems. For the interested reader, several links are provided to the corresponding literature. Unfortunately, although the fundamental limitations in linear control systems have been extended to some extent to nonlinear systems, an explicit link between the fundamental limitations and the performance of nonlinear systems is still missing.

2.3.1 Nonlinear extensions of the logarithmic integral relations

The complex analysis results such as the sensitivity and complementary sensitivity integrals (2.5) and (2.7) cannot be straightforwardly extended to the case where there is a nonlinear controller and/or plant. For instance, the concept of a frequency response function has to be generalized. An interpretation of a nonlinear non-minimum phase system is given in [133], where a nonlinear open-loop is said to be non-minimum phase if there are restrictions on the output that can be generated if the input is bounded. For such a nonlinear non-minimum phase open-loop system, it was shown in [133] that making the sensitivity (which is in this case defined to be a signal-based measure) arbitrary small over a frequency range necessarily implies a large response to some specific admissible disturbance. This is a nonlinear version of the waterbed effect. A related approach can be

found in [130], where a nonlinear open-loop is said to be unstable if there are restrictions on the input in order to have a bounded output. It is established that for any Lipschitz open-loop nonlinear system the sensitivity and complementary sensitivity (for a definition, see [130]) fulfill the complementarity mapping $S+T=I$. The open-loop L is considered to be a nonlinear operator and the main results of [130] on the sensitivity limitations are (i) if L is non-minimum phase, then $\|S\|_L \geq 1$, and (ii) if L is unstable, then $\|T\|_L \geq 1$. Here $\|X\|_L$ denotes the Lipschitz constant, or Lipschitz gain of X. These results are well-known for linear feedback systems (see Section 2.2.2) and hence, at a fundamental level, extend the fundamental limitations analysis to any Lipschitz nonlinear open-loop system. Extensions to specific nonlinear feedback systems such as sampled data control and periodic control are available in for instance [43, 82] and [102, 122], respectively.

2.3.2 Time-domain extensions

In attempting to extend the results on fundamental limitations to nonlinear systems, it is most natural to explore extensions of time-domain constraints as they are also defined for nonlinear systems. It is well-known that the step response of a stable linear plant which has a real, right half-plane open-loop zero must undershoot. It is less well-known, however, that this holds for any (nonlinear, time varying) control signal generated in open or closed-loop, provided that the input step response is bounded [94]. In [132] the results of cheap control as discussed in Section 2.2.4 have been extended using the concept of zero dynamics for the characterization of non-minimum phase nonlinear plants. In that context, a non-minimum phase plant is one with unstable zero dynamics. This is done for a class of nonlinear plants of a particular structure, i.e., plants whose zero dynamics are driven by the output of the plant (as is also the case for LTI systems). It is shown that if the nonlinear plant has unstable zero dynamics, then there is a fundamental bound on the achievable tracking performance in the same sense as for linear plants, i.e., the lowest attainable $\mathcal{L}_2$ norm of the output error to a step reference is the least amount of energy that is needed to stabilize the unstable zero dynamics of the nonlinear plant. These results have been used in [83, 96] to derive undershoot and settling-time trade-offs for nonlinear plants with unstable zero dynamics. In case of non-minimum phase linear plants, the obtained trade-offs boil down to the well-known undershoot and settling-time trade-offs from [94]. Unfortunately, no extensions of other known time-domain trade-offs in linear feedback systems seem to be available for nonlinear systems.

2.3.3 Limitations in an information theoretic perspective

More recently, extensions have been obtained by means of a connection between Bode's integral and the information theoretic concept of *entropy* [66, 68], a time-domain concept. This concept is well defined for systems that do not admit

a transfer function, and can hence be used to analyze nonlinear systems. In [66, 68] a time-domain characterization of Bode's sensitivity integral for linear time-varying systems is obtained. In [67, 153], the following characterization is derived for discrete-time linear plants,

$$\frac{1}{2\pi}\int_{-\pi}^{\pi} \ln|S(e^{i\omega})|d\omega = \mathcal{H}_c(e_k) - \mathcal{H}_c(r_k). \tag{2.21}$$

The left hand side of this equation resembles the discrete version of the Bode sensitivity integral while the right hand side denotes the difference between the *entropy rates* [67, 153] of the reference signal r and the error e from Figure 2.1. The entropy rate of a signal can be computed directly from the signals without having to resort to frequency domain methods. It is shown in [67, 153] that, provided the (possibly nonlinear) open-loop is strictly proper and stable, the right hand side of (2.21) is zero, irrespective of the choice of controller. This result is comparable to Bode's classical result for discrete-time systems and is valid in case a nonlinear controller is used to control a linear system.
A similar approach is followed in [34] where Bode's integral is derived for feedback systems in the presence of a communication channel. In this framework, the measurements of the LTI plant are transmitted over a communication channel to the controller C. In the case that this channel has a maximum rate with which information can be transmitted, also known as *finite capacity feedback*, fundamental limitations were investigated in [91]. The main conclusion is that the fundamental performance limitation similar to the waterbed effect is due to causality alone. For continuous-time LTI feedback systems, the effects of unstable poles, non-minimum phase zeros and time delay have been investigated in this context in [16, 17, 99].

2.4 Opportunities and performance measures of nonlinear control systems

Although attempts have been made to develop fundamental limitations for nonlinear systems, these cannot be straightforwardly used to draw conclusions about the performance of a nonlinear control scheme. The question that remains is whether causal nonlinear control can perform better than causal linear control for linear systems. If we assume that there are no unstable poles or non-minimum phase zeros present, the main limitation in linear systems is imposed by the waterbed effect and Bode's gain-phase relation. Taking into account the nonlinear extensions of the fundamental limitations discussed in Section 2.3 (especially (2.21)), the existence of a similar trade-off as the waterbed effect seems to be inevitable. However, there is no direct link between this nonlinear waterbed effect and the performance of the controlled system, and therefore it is not clear at this point to what extent this waterbed-like effect is limiting for the performance.

In posing the question whether we can do better with a nonlinear controller for a linear system, it is instrumental to find appropriate performance measures that can discriminate between linear and nonlinear controllers and reflect the real practical objectives of the control design problem at hand. For linear motion control systems, performance is typically evaluated using traditional Bode frequency response methods or modern $\mathcal{H}_\infty$ (or related) techniques, see for example [134] for an overview.

The first category, often referred to as loop shaping, hinges on the property that a linear stable system exhibits, for each bounded disturbance, a bounded globally asymptotically stable response and obeys the superposition property. Namely, by the grace of these facts, the performance related to these unique responses can be assessed analytically through frequency response functions, such as the sensitivity and complementary sensitivity functions. Clearly, these standard analysis techniques do not straightforwardly extend to the nonlinear domain, since they exist by the grace of linearity. Nonlinear extensions of these steady-state measures are the well-known describing function [49] and the recently developed 'nonlinear response function' [109, 110]. For linear systems these measures are a valid choice as the frequency response function contains all information about a linear system. For nonlinear systems however, using these measures one can only draw conclusions about the evaluated signals since the superposition principle does not hold.

The second category based on $\mathcal{H}_\infty$ or related methods constitutes a more systematic approach, which supports the design of linear controllers for linear systems ensuring an optimal (i.e., minimal) bound on the induced norm of the closed-loop transfer function (reflecting the optimization of a worst case frequency domain performance for a large class of disturbances). The $\mathcal{H}_\infty$ norm is the $\mathcal{L}_2$ induced norm (from inputs to outputs), which indicates that it reflects a (maximum) gain from the energy of the input to the energy of the output. An important drawback of $\mathcal{H}_\infty$ design is that it guarantees that the $\mathcal{L}_2$ gain is lower than a certain value for whole classes of disturbances or references, while in practice one is often interested in the performance related to particular disturbance and reference signals. For linear control systems one can always assess the obtained closed-loop behavior exactly by analytical means, which allows for exact performance assessment for a given class of disturbances (be it in retrospect). For nonlinear systems this is not possible due to, firstly, the lack of analytical solutions and, secondly, the fact that for arbitrary disturbances nonlinear systems generally exhibit non-unique steady-state solutions. The latter hampers an accurate and unique performance assessment and tempts to use performance measures such as the ones based on $\mathcal{L}_2$ gain relationships [45, 46]. However, performance evaluation taking into account *all* possible disturbance signals is often far too conservative for the *particular* disturbances present in the real plant.

Although the existence of a similar trade-off as the waterbed effect seems to be inevitable also when nonlinear controllers are employed, it could be that in specific cases a nonlinear controller outperforms the best linear controller. As an example, consider hybrid control of linear systems. Classical linear control seeks to achieve a trade-off between multiple performance objectives using a sin-

gle controller, while hybrid linear control seeks to achieve multiple performance objectives by switching between pre-specified linear controllers [93]. If the switching logic is appropriately defined, then the hybrid closed-loop can reflect multiple performance properties thereby enriching the spectrum of achievable trade-offs. Explicit examples of performance improvement using hybrid control can be found in [6, 35, 52, 93].

It is therefore expected that the benefits of nonlinear control of linear systems are most apparent in specific situations and that there are few to no benefits when worst case performance is considered for large classes of possible input and disturbance signals. This is also motivated by the observation that in the standard linear $\mathcal{H}_\infty$ problem for LTI plants, arbitrary nonlinear time-varying controllers offer no performance improvement over LTI controllers [76, 116]. Instead of the induced bounds that relate norms of the output of the system to norms on the input of the system, there is a need for performance measures that depend on specific input and disturbance characteristics. For instance, the 'transient measures' rise-time, settling-time, and overshoot are related to a single disturbance signal being the step function, while 'steady-state' measures such as the frequency response functions give information on harmonic disturbance signals.

To summarize, on the one hand there exist norm-based measures for nonlinear systems which guarantee performance for large classes of input and disturbance signals, but which may be fairly conservative for the practical problem at hand. On the other hand, the often less conservative transient and steady-state measures provide only information about specific signals and using these, it is generally impossible to obtain conclusions about the performance to other signals.

Unfortunately, at the current state-of-the-art, no mature performance analysis tools exist for nonlinearly controlled linear motion systems. Therefore, in this thesis we will use the various kinds of performance measures that are available. The choice between time-domain, steady-state, and norm-based measures will depend on the specific problem setting.

Chapter 3

Examples of frequency domain based nonlinear controller design

In this chapter, we review two classical and heuristic examples of nonlinear control of linear systems, i.e., the SPAN (split-path nonlinear) filter and the driven limiter. The goal of this chapter is to show that the introduction of nonlinear elements in a linear motion system can improve the step response with respect to the combination of overshoot and settling-time when compared to standard linear feedback.

3.1 Introduction

In feedback control of servo and positioning systems, the most commonly used controller is a PID (Proportional, Integral, Derivative) controller. While the proportional and the integral part are mainly used to increase the performance of the PID controller (high-gain feedback and steady-state error elimination), the derivative action is often used to stabilize the closed-loop system by providing a reasonable phase margin via the introduction of damping. The major drawback of the derivative action is that it results in open-loop magnitude amplification for higher frequencies, which is not desirable as formulated by the Bode loop shaping specification in Section 2.2.3. This can be partly overcome by replacing the pure derivative action by a phase lead compensation filter, since then the magnitude amplification can be reduced to some extent. However, it cannot be completely

removed. The major drawback of the integral action is that the desired low frequent magnitude amplification results in (destabilizing) phase lag.
These drawbacks are typical and inherent to the use of linear compensation filters. Indeed, Bode's gain-phase relationship (see Theorem 2.4) states that phase lead (derivative action) is always accompanied by an increase of the gain, while gain reduction with increasing frequency (integrating action) is always accompanied by phase lag. Therefore, in the fifties and sixties research was started to design nonlinear filters that are free of this limiting gain-phase relationship [2, 26, 38, 86]. Of course, since the superposition principle does not hold for such nonlinear filters, one cannot speak of a gain-phase relationship in the same manner as for linear filters. Therefore, the frequency domain properties (such as the gain-phase relationship) of this kind of nonlinear filters are represented in an approximate way by the describing function [49]. The describing function is a quasi-linear description of the nonlinear element that depends on the type of input signal. To characterize the input/output behavior of a nonlinear element in the frequency domain, sinusoidal input describing functions (SIDFs) are commonly used. The SIDF results in magnitude and phase information of the fundamental output frequency of the nonlinear element with respect to the frequency of the sinusoidal input, and hence, resembles the frequency response function for linear systems.
Notable examples of proposed nonlinear filters that show an improved gain-phase relation ship in the describing function sense are the Clegg integrator [26] (see Part III of this thesis), the SPAN (split-path nonlinear) filter [38], and the driven limiter [2]. In the case of the Clegg integrator, the describing function showed that such an integrator has considerably less phase lag than the corresponding linear integrator [26], and in [78] the Clegg integrator was used to control a motion system. The main idea behind the SPAN filter and driven limiter is that the gain and phase of these filters can be designed separately [2, 38]. In this chapter we will analyze the potential of the SPAN filter and driven limiter when used in a PID controlled motion system. The goal of this chapter is to investigate whether these nonlinear filters can result in an improved step response when they are applied as the derivative element in a PID controller.
In Section 3.2 we present the closed-loop control setup incorporating the SPAN filter and driven limiter. The controller synthesis procedure is discussed in Section 3.3, simulation results are presented in Section 3.4, and conclusions are given in Section 3.5.

3.2 Closed-loop control setup

As stated in Section 3.1, the most commonly used controller to control a servo system is a PID controller. The standard control setup of the corresponding closed-loop system is depicted in Figure 3.1. In this figure, G denotes the plant, P, I, and D stand for respectively the proportional, integral and derivative (in the form of a lead filter) parts of the controller, signal r denotes the reference signal, y is the plant output, and $e = r - y$ is the servo or tracking error. As

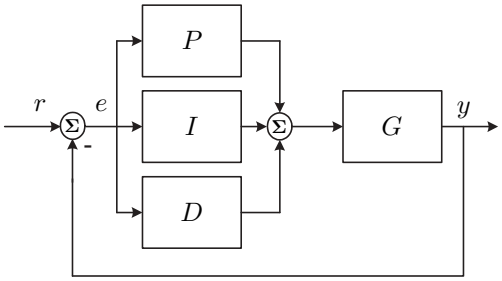

Figure 3.1: Standard PID controlled system.

already mentioned, the major drawback of the lead filter is that the desired phase lead is accompanied by an undesired magnitude amplification. To circumvent this drawback, we propose to use the SPAN filter and the driven limiter as the derivative action (i.e., they replace the block D in Figure 3.1), as they were originally intended to be able to design the gain and phase characteristics separately. The following discussion on the SPAN filter and driven limiter uses a frequency domain point of view to reason about the performance of these filters. This reasoning should be interpreted with care, since nonlinear elements are considered, and the describing function cannot be seen as an equivalent replacement of the frequency response function for linear systems. However, we reason now from a frequency point of view as historically the ideas to use the SPAN filter and driven limiter were conceived in this manner [2, 38].

3.2.1 SPAN filter

The SPAN filter is an attempt to obtain a filter that has independent gain and phase characteristics. In Figure 3.2, a block scheme of a SPAN filter is depicted. This filter processes the input in two paths and multiplies the output of the two branches. The upper path containing the *absolute value* element destroys all sign

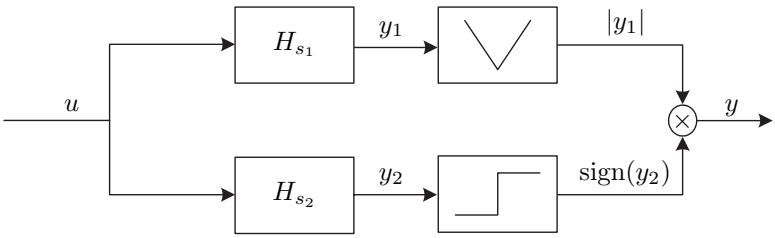

Figure 3.2: Block diagram of a SPAN filter.

information, and therefore controls the magnitude information, while the lower

path with the *sign* element destroys all magnitude information and controls the phase of the signal. The SPAN filter could be used to provide phase lead while attenuating the magnitude, by using a low-pass filter in the absolute value path, and a linear phase lead filter in the sign-path, given in the Laplace domain by

$$H_{s_1}(s) = \frac{1}{1+\tau_1 s}, \quad H_{s_2}(s) = \frac{1+\tau_2 s}{1+\tau_3 s}. \tag{3.1}$$

In this way, the SPAN filter can be used as the derivative element of the PID controller with similar phase characteristics as a linear lead filter, but without the undesired magnitude amplification.

3.2.2 Driven limiter

The driven limiter [2] is another classical and heuristic attempt to obtain independent gain and phase characteristics. In a driven limiter, the input is again split in two paths. The upper path generates the signal to be limited, while the lower path generates the limiting signal, see Figure 3.3. To achieve phase lead, a linear lead filter is placed in the upper path, i.e.,

$$H_{\mathrm{dl}_1}(s) = \frac{1+\tau_1 s}{1+\tau_2 s}, \tag{3.2}$$

while a static gain

$$H_{\mathrm{dl}_2}(s) = K, \tag{3.3}$$

is used in the lower path to limit the high frequency gain of the lead filter. The

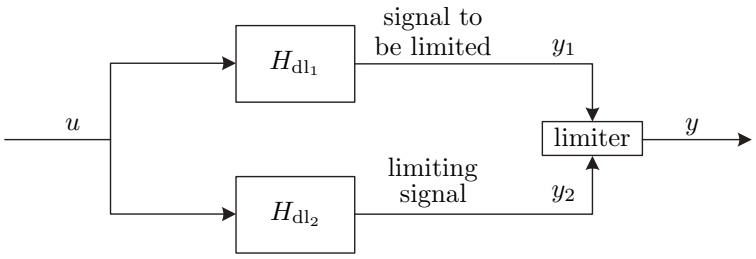

Figure 3.3: Block diagram of a driven limiter.

combined output y is limited as:

$$y = \begin{cases} |y_2|\ sign(y_1) & \text{if } |y_2| \le |y_1|, \\ y_1 & \text{if } |y_2| > |y_1|. \end{cases} \tag{3.4}$$

Figure 3.4 shows an example of how the signal is limited for the chosen linear functions in both paths. Loosely speaking, the driven limiter behaves linearly

according to the lead filter $H_{\mathrm{dl}_1}(s)$ for frequencies where $|H_{\mathrm{dl}_1}(i\omega)| < |H_{\mathrm{dl}_2}(i\omega)|$. When limiting occurs, the modulus of the driven limiter is limited to the gain K in the limiting path, while the phase is still that of the lead filter. This way, it is possible to create phase lead, without the increase in modulus for higher frequencies. Since the limiting value is not a fixed value, the limiter is called a *driven* limiter. Just as the SPAN filter, the driven limiter replaces the derivative element in Figure 3.1.

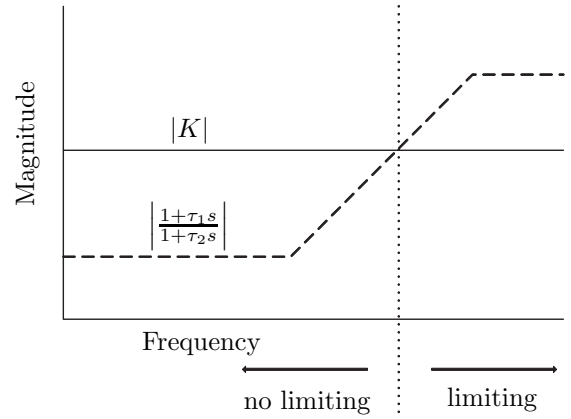

Figure 3.4: Magnitude plot of the linear filters H_{dl_1} (dashed) and H_{dl_2} (solid).

3.3 Controller synthesis

The goal of this chapter is to investigate if the nonlinear PID controllers can outperform a linear PID controller (where the derivative action is obtained via the application of a linear lead filter) with respect to the response to a unit step input. Although the loop shaping procedure is an attractive method to design a linear feedback controller, the classical rules-of-thumb used in this procedure do not apply during the design of nonlinear feedback controllers using the describing function, since, as stated before, the superposition principle is not valid anymore. As a consequence, the tuning of a nonlinear controller such as the PID controllers proposed in Sections 3.2.1 and 3.2.2 can be quite tedious. To be able to compare the three controllers, i.e., the linear PID controller, the PI controller with the SPAN filter, and the PI controller with the driven limiter, we synthesize these controllers via optimization. During the last decades, good results have been achieved in the field of controller optimization based on genetic algorithms [59]. These algorithms search for an optimal solution with respect to the requirements specified via an objective function, which is often referred to as the *fitness function*. The time-domain criteria that are used to define the performance via

the fitness function are the settling-time $t_{\rm s}$, the percentage overshoot $p_{\rm os}$, and the integral of the absolute error IAE, defined by

$$\begin{aligned} t_{\rm s} &= \min\{T \in \mathbb{R}_+ \mid |y_p(t) - 1| \leq \varepsilon, \text{ for all } t \geq T\}, \\ p_{\rm os} &= \max\{y_p(t) - 1 \mid t \geq 0\} \times 100\%, \\ IAE &= \int_0^{T_{IAE}} |e(t)| dt, \end{aligned} \tag{3.5}$$

where ε is the error band, which is in this case selected to be $\varepsilon = 0.02$, and where T_{IAE} denotes the time over which the integral of the absolute error is computed, which is in this case $T_{IAE} = 5$ seconds. This integral is used in the fitness function to obtain a fast response. The fitness value f that is assigned to each design is computed via

$$f = t_{\rm s} + \frac{p_{\rm os}}{5} + IAE + f_u, \tag{3.6}$$

where f_u is an additional penalty to enforce that the control output is limited to 2.5. The results of the genetic optimization are presented in the next section.

3.4 Simulation results

In this section we present simulation results of the optimized controllers and compare them with respect to the requirements in (3.5). The controllers are designed for a fourth-order dual rotary motion system, which consists of two masses that are connected by a flexible shaft, see Figure 3.5. One of the masses is driven by a motor while the position of the other mass is measured and used for feedback. The model of this system is represented by the state-space representation

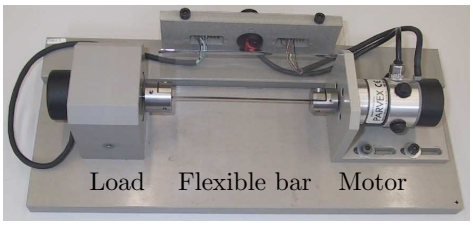

Figure 3.5: The fourth order dual rotary motion system.

$$\begin{aligned} \dot{x} &= \begin{bmatrix} 0 & 1 & 0 & 0 \\ -47829 & -0.8006 & 47829 & -0.8006 \\ 0 & 0 & 0 & 1 \\ 61131 & 1.0232 & -61131 & -1.0232 \end{bmatrix} x + \begin{bmatrix} 0 \\ 4880 \\ 0 \\ 0 \end{bmatrix} u \quad . \\ y &= \begin{bmatrix} 0 & 0 & 1 & 0 \end{bmatrix} x \end{aligned} \tag{3.7}$$

The optimized controllers have the following performance characteristics:

	fitness	**settling-time [s]**	**overshoot [%]**
PID controller	2.1004	2.5304	7.4851
Controller with a SPAN filter	0.3946	1.4557	0.0088
Controller with a driven limiter	1.0877	2.1802	2.9164

The corresponding step responses are depicted in Figure 3.6. As can be seen from

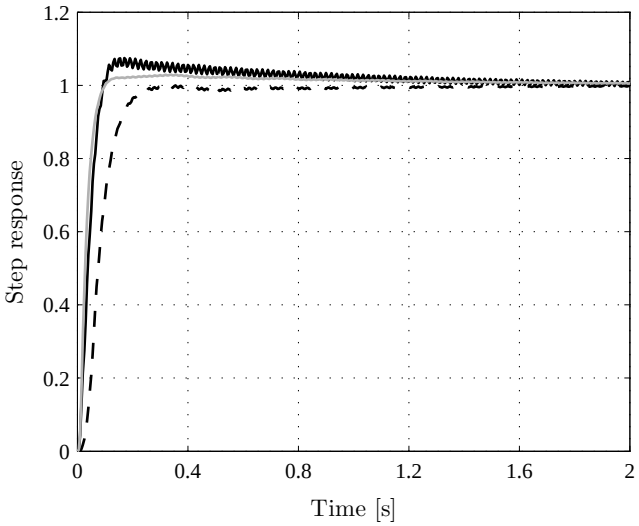

Figure 3.6: Step response of the linear PID controller (solid black), the PID with SPAN filter (dashed black), and the PID with the driven limiter (solid grey).

both the above table and Figure 3.6, the PID controllers with the nonlinear elements both perform better in terms of the optimized time-domain requirements than the linear PID controller does. As stated in Section 3.2, the initial idea behind the SPAN filter and the driven limiter was that the frequency domain description in the form of the describing function could show phase lead without the undesired side effect of increasing gain. The describing functions of the optimized SPAN filter and driven limiter are depicted in Figure 3.7. The describing function of the SPAN filter in Figure 3.7(a) shows that the filter provides phase lead with magnitude attenuation. This indeed corresponds to the initial idea behind the filter and such a characteristic is clearly not attainable by any linear controller. The describing function of the driven limiter in Figure 3.7(a) also results in the expected behavior. Although there is some magnitude amplification with increasing frequency, it is much less than that of a linear filter with a similar phase characteristic. The gain of the driven limiter in Figure 3.7(b) indeed resembles Figure 3.4.
The Bode diagrams of the open-loop with the linear filter and with the describing functions of the SPAN filter and driven limiter are depicted in Figure 3.8. From

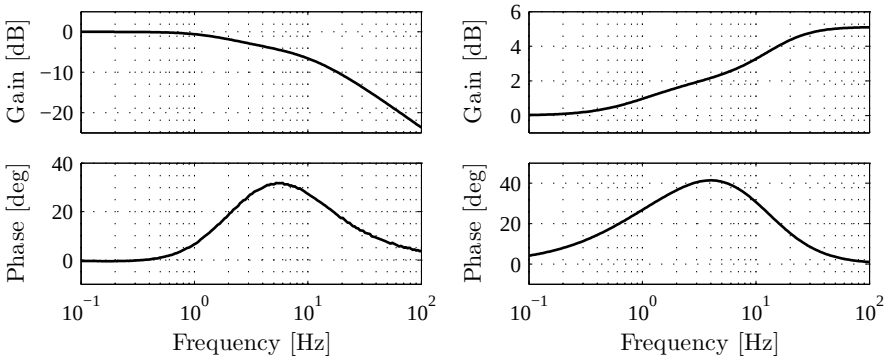

Figure 3.7: Describing functions of (a) the optimized SPAN filter and (b) the driven limiter.

these figure, it cannot directly be concluded that the SPAN filter and driven limiter should perform the way they do. The PID controller with the SPAN filter results in a higher bandwidth than the linear PID controller. This would suggest that the rise-time of the nonlinear PID controller is smaller than that of the linear one, however, the response to the unit step input is much slower as can be seen in Figure 3.6. Moreover, the linear PID controller provides more phase margin around the bandwidth than both nonlinear controllers, which normally indicates that the closed-loop system has more damping, and hence, less overshoot. Clearly, this is not the case as can be seen in Figure 3.6.

3.5 Conclusions

In this chapter, we compared a linear PID controller to a PID controller with a SPAN filter as the derivative element, and a PID controller with a driven limiter as the derivative element, all designed via optimization using a genetic algorithm. Both the PID controllers featuring the SPAN filter and the driven limiter have been shown to outperform a linear PID controller with respect to the considered performance measures for the unit step response. The initial idea behind the SPAN filter and the driven limiter was that they are able to obtain phase lead without the normally accompanying magnitude increase. Describing function analysis showed that the optimized nonlinear filters indeed have this characteristic. From a loop shaping perspective however, the obtained behavior does not correspond to the describing function of the optimized nonlinear PID controllers. Therefore, we expect that nonlinear controller design in the frequency domain based on the describing function is not a useful method. This is in agreement

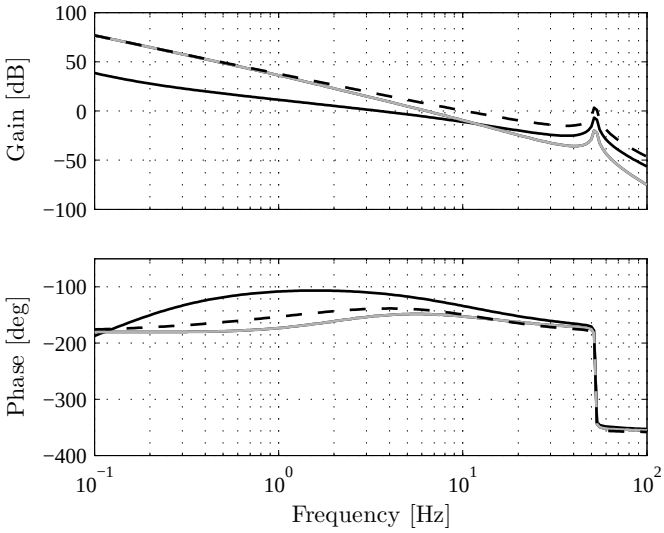

Figure 3.8: Bode diagrams of the open-loop with the linear PID (solid black), PID with SPAN filter (using the describing function, grey), and PID with driven limiter (using the describing function, dashed black).

with [145], which states that although the describing function can be useful for the analysis of, for instance, limit cycling, loop shaping based on the describing function generally does not lead to the desired results. The results in this chapter showed that there are potential benefits when using nonlinear controllers for linear motion systems. However, these results are obtained using heuristic ideas and methods, and the question arises whether such benefits can be obtained via a systematic design procedure for nonlinear controllers for linear motion systems. In the remainder of this thesis, we will try to answer this question.

Part II

Time-Domain Performance based Control Design

Chapter 4

Linear Control of Time-Domain Constrained Systems

This chapter presents an extension of recent results on the control of linear systems subject to time-domain constraints. It is shown that time-domain constraints on closed-loop signals of linear systems can be incorporated in an LMI problem, even when complex conjugate poles are assigned. The proposed method is evaluated by applying it to a fourth order motion system using both simulations and experiments.

4.1 Introduction

The transient response to commands or disturbance inputs is a performance qualifier in many control systems. However, most control design strategies cannot cope directly with requirements on time-domain signals. A commonly used method to capture the essence of time-domain specifications in the controller design is the reformulation into frequency domain requirements [33]. In general, such reformulations are either approximate, conservative or both.
Several methods have been proposed that can cope with time-domain constrained control problems directly. In predictive control theory, (non)linear controllers can be formulated that satisfy hard time-domain constraints on the closed-loop signals. Model predictive control (MPC) [92], for example, prescribes a control action that is obtained by solving an finite or infinite horizon optimization problem.

In [8], the concept of on-line reference management using a command governor is addressed. This command governor is a system that adjusts the reference signal based on predictive control theory, such that the constraints are fulfilled. A drawback of predictive control concepts and online optimization-based methods in general is that they require a high computational effort with the consequence that they cannot be implemented on fast motion systems where high sampling rates are required, typically in the order of kHz. Explicit MPC [9], where a piecewise linear state feedback for discrete-time systems can be constructed off-line might offer a solution, although the explicit control law often leads to a complex description, which cannot be evaluated at high sampling rates either. As an alternative approach, some specific types of constraints, such as saturation, can be dealt with after the control design, for instance by means of anti-windup schemes [40].

A methodology to enforce time-domain constraints on the input and output of a continuous-time linear control system is presented in [56], where linear matrix inequality (LMI) techniques are used to synthesize a fixed order controller that satisfies the constraints. This is done in a polynomial setting, i.e., a controller is designed according to the well-known pole placement method using the Diophantine equation. This method allows the design of a controller that results in a closed-loop transfer function with prescribed pole locations, either exact, or within an admissible region of the complex plane. In [56], the objective of assigning closed-loop poles is replaced by assigning a characteristic polynomial. This polynomial can be easily computed from fractional representations of the transfer functions of the controller and the plant, and allows for a parametrization of all stabilizing controllers using the Youla-Kučera parametrization [79]. After a controller has been designed that achieves the prescribed closed-loop pole locations, the degrees of freedom of the Youla-Kučera parametrization are used to enforce certain time-domain constraints, such as bounds on the input amplitude and output overshoot, exploiting results on positive polynomials [55, 100]. Unfortunately, the approach in [56] is limited to the assignment of distinct strictly negative rational (in the sense of quotients of integers) closed-loop poles, which is a severe restriction in the case of lightly damped systems.

In this chapter, we propose an extension to the method in [56] in the form of two relaxations, which enable the assignment of complex conjugate poles, but at the expense of some conservatism. The proposed methodology from [56] is briefly reviewed in Section 4.2, while the extension to complex conjugate poles is treated in Section 4.3. Section 4.4 discusses the proposed control design method, and Section 4.5 provides an illustrative example. Section 4.6 shows the effectiveness of the proposed method in an experiment and discusses numerical issues related to the involved optimization problem. Finally, the conclusions are stated in Section 4.7.

Although the proposed approach in this chapter is a completely linear one, it is a good example of the idea of improving time-domain performance by a two-step controller design as discussed in Chapter 1.

4.2 Methodology involving real poles

In [56] a method is presented to incorporate time-domain constraints on input and output signals of a linear system. It is shown that finding a controller of fixed order that satisfies these constraints boils down to solving a set of LMIs. In this section, we shortly review this procedure.

4.2.1 Youla-Kučera parametrization

Consider the control system depicted in Figure 4.1 with a linear strictly proper single-input-single-output plant P given in transfer function notation by

$$P(s) = \frac{b(s)}{a(s)}, \tag{4.1}$$

where $a(s)$ and $b(s)$ are polynomials in the the Laplace variable s. The controller

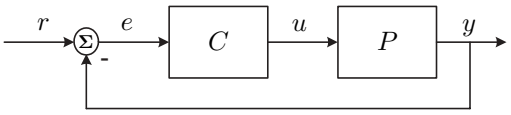

Figure 4.1: Block diagram of the closed-loop system with controller C, plant P, and reference signal r, control output signal u, and output signal y.

C which is to be designed is accordingly described by

$$C(s) = \frac{d(s)}{c(s)}, \tag{4.2}$$

and the complementary sensitivity is as a consequence given by

$$T(s) = \frac{y(s)}{r(s)} = \frac{b(s)d(s)}{a(s)c(s) + b(s)d(s)}. \tag{4.3}$$

If $a(s)$ and $b(s)$ are coprime (i.e., their greatest common divisor is 1), then arbitrary pole placement can be achieved by designing the corresponding controller polynomials. This is done by solving the polynomial Diophantine equation

$$a(s)c(s) + b(s)d(s) = z(s), \tag{4.4}$$

where $z(s) = (s + p_1)(s + p_2)\dots(s + p_n)$, is the polynomial with given roots $-p_1, \dots, -p_n$ which are the desired poles of the closed-loop system. There are infinitely many solutions to (4.4), but there is a unique solution pair $(c_0(s), d_0(s))$ such that $\deg d_0(s) < \deg a(s)$. In this case we have that $d_0(s)$ is of minimal order

(the d-minimal solution pair). All possible solutions to the Diophantine equation can be written as

$$\begin{aligned} c(s) &= c_0(s) + b(s)q(s), \\ d(s) &= d_0(s) - a(s)q(s), \end{aligned} \tag{4.5}$$

where $q(s) = \sum_{i=0}^{d_q} q_i s^i = q_0 + q_1 s + \ldots + q_{d_q} s^{d_q}$ is an arbitrary polynomial of degree d_q such that $c_0(s) + b(s)q(s)$ is non-zero. This polynomial, called the Youla-Kučera parameter, creates extra freedom in the design of the controller. While the closed-loop poles are invariant, the Youla-Kučera parameter enables placement of closed-loop zeros to alter the response. Only proper controllers are considered and therefore there is a degree constraint on $q(s)$. Since the plant was assumed to be strictly proper, and under the additional assumption that $\deg z(s) \geq 2\deg a(s) - 1$ (to enable arbitrary pole placement), this constraint is given as [80]

$$\deg q(s) \leq \deg z(s) - 2\deg a(s). \tag{4.6}$$

The extra freedom in the control design parameterized by $q(s)$ satisfying (4.6) can now be used to satisfy additional time-domain constraints as explained in the following section.

4.2.2 A positive polynomial formulation of time-domain constraints

Suppose that the response to a step input ($r(s) = \frac{1}{s}$) is considered. The Laplace transform of the closed-loop system's output is then given by

$$y(s) = \frac{1}{s}\frac{b(s)d(s)}{z(s)} = \frac{1}{s}\frac{b(s)d_0(s)}{z(s)} - \frac{1}{s}\frac{a(s)b(s)}{z(s)}q(s). \tag{4.7}$$

According to [56], in order to continue with the controller synthesis, a *restrictive assumption* has to be made,

Assumption 4.1 *All the assigned poles p_i are distinct strictly negative rational numbers.*

If this is the case then, since $z(s) = \prod_{i=1}^{n}(s+p_i)$, (4.7) can be decomposed as

$$y(s) = \sum_{i=0}^{n} \frac{y_i(q)}{s + p_i}, \tag{4.8}$$

where $p_0 = 0$ and $y_i(q)$, $i = 1, \ldots, n$ are appropriate coefficients following from the decomposition, which are influenced by the choice of the design parameter $q(s) =$

$\sum_{i=0}^{d_q} q_i s^i$. For ease of exposition, from now on we omit the explicit dependency of y_i on q. The corresponding time-domain signal is given by

$$y(t) = \sum_{i=0}^{n} y_i e^{-p_i t}. \tag{4.9}$$

Let $p_i = \frac{n_i}{d_i}$ be the ratios of the integers n_i and d_i, and let m denote the least common multiple of the denominators such that $p_i = \frac{\bar{p}_i}{m}$ for some positive integers $\bar{p}_i$. This means that the time-domain output signal at time $t \in \mathbb{R}_+$ can now be expressed as the polynomial

$$y(\lambda) = \sum_{i=0}^{n} y_i \lambda^{\bar{p}_i} \tag{4.10}$$

in the indeterminate $\lambda = e^{-t/m}$, which obviously lies in the interval $[0, 1]$. Suppose that the output $y(t)$ of the system needs to be bounded according to

$$y_{\min} \leq y(t) \leq y_{\max} \quad \forall\, t \in \mathbb{R}_+. \tag{4.11}$$

Formulation (4.11) is equivalent to enforcing the polynomial bound constraints

$$y_{\min} \leq y(\lambda) \leq y_{\max} \Leftrightarrow \left\{ \begin{array}{l} P_1(\lambda) := y(\lambda) - y_{\min} \geq 0 \\ P_2(\lambda) := y_{\max} - y(\lambda) \geq 0 \end{array} \right. \quad \forall\, \lambda \in [0, 1]. \tag{4.12}$$

This is a special case of the more general problem of minimizing a polynomial with polynomial constraints over a semialgebraic set $\mathcal{D}$:

$$\begin{array}{ll} \min\limits_{z} & p(z, x) \\ \text{s.t.} & \begin{array}{ll} g_i(z, x) \geq 0, & i = 1, \ldots, \ell \\ h_j(z, x) = 0, & j = 1, \ldots, m \end{array} \quad \forall\, x \in \mathcal{D} \end{array} \tag{4.13}$$

with in this case $z = \{y_0(q), y_1(q), \ldots, y_n(q)\}$, $x = \lambda$, $\ell = 2$, $m = 0$, $p(z, x) = 0$, $g_1(z, x) = P_1(\lambda)$, $g_2(z, x) = P_2(\lambda)$, and $\mathcal{D} = \{\lambda \in \mathbb{R} \mid 0 \leq \lambda \leq 1\}$. Although the bounds $y_{\min}$ and $y_{\max}$ in (4.12) are constants, they can be chosen polynomial in λ, i.e., in the form $y_{\min}(\lambda)$ and $y_{\max}(\lambda)$ without additional effort. In case of univariate positive polynomial constraints such as (4.12) an LMI formulation, as stated in the following lemmas, can be obtained.

Lemma 4.2 Odd degree polynomial, [56]. *A given polynomial $p(\lambda) = p_0 + p_1\lambda + p_2\lambda^2 + \ldots + p_n\lambda^n$ of odd degree $n = 2m+1$ for some $m \in \mathbb{N}$, is nonnegative along the interval $\lambda \in [\lambda_{min}, \lambda_{max}]$ if and only if there exist polynomials $g_i(\lambda)$, $j_i(\lambda)$ of degree $m = (n-1)/2$ such that*

$$p(\lambda) = (\lambda - \lambda_{min}) \sum_i g_i^2(\lambda) + (\lambda_{max} - \lambda) \sum_i j_i^2(\lambda). \tag{4.14}$$

Condition (4.14) *is fulfilled if and only if there exist symmetric matrices $G = G^T \succeq 0$, $J = J^T \succeq 0$ of dimension $m+1$ solving the constraints*

$$\begin{array}{l} p_i = \mathit{trace}\; G \left(H_{i-1}^{m+1} - \lambda_{min} H_i^{m+1} \right) \\ \qquad + \mathit{trace}\; J \left(\lambda_{max} H_i^{m+1} - H_{i-1}^{m+1} \right), \quad i = 0, 1, \ldots, n, \end{array} \tag{4.15}$$

where $H_i^r \in \mathbb{S}^r$ *is the* i^{th} *Hankel matrix,*

$$H_i^r(k,l) = \begin{cases} 1, & \text{if } k+l = i+2 \\ 0, & \text{otherwise} \end{cases} . \tag{4.16}$$

If $i<0$ *or* $i>2(r-1)$ *then* H_i *is the zero matrix of dimension* r*.*

For the proof, see [56].

Lemma 4.3 Even degree polynomial. *Consider a given polynomial* $p(\lambda) = p_0 + p_1\lambda + p_2\lambda^2 + \ldots + p_n\lambda^n$ *of even degree* $n = 2m$ *for some* $m \in \mathbb{N}$*. In accordance with Markov-Lukacs theorem,* $p(\lambda)$ *is nonnegative along the interval* $\lambda \in [\lambda_{min}, \lambda_{max}]$ *if and only if there exist polynomials* $g_i(\lambda)$*,* $j_i(\lambda)$ *of degree* $m = n/2$ *such that*

$$p(\lambda) = \sum_i g_i^2(\lambda) + (\lambda - \lambda_{min})(\lambda_{max} - \lambda) \sum_i j_i^2(\lambda). \tag{4.17}$$

Condition (4.17) *is fulfilled if and only if there exist symmetric matrices* $G = G^T \succeq 0$*,* $J = J^T \succeq 0$ *of dimensions* $m+1$ *and* m*, respectively, solving the constraints*

$$\begin{aligned} p_i = {} & \text{trace } G H_i^{m+1} \\ & + \text{trace } J \left((\lambda_{min} + \lambda_{max}) H_{i-1}^m - (\lambda_{min}\lambda_{max}) H_i^m - H_{i-2}^m \right), \\ & i = 0, 1, \ldots, n, \end{aligned} \tag{4.18}$$

where $H_i^r \in \mathbb{S}^r$ *is the* i^{th} *Hankel matrix,*

$$H_i^r(k,l) = \begin{cases} 1, & \text{if } k+l = i+2 \\ 0, & \text{otherwise} \end{cases} . \tag{4.19}$$

If $i<0$ *or* $i>2(r-1)$ *then* H_i *is the zero matrix of dimension* r*.*

Since the coefficients of the polynomial $y(\lambda)$ are affine in the unknown design parameters q_i, a controller satisfying the time-domain constraints can be designed using the following theorem.

Theorem 4.4 [56] *Under the pole placement assumption (Assumption 4.1), the closed-loop time-domain constraints* (4.11) *are satisfied by the controller polynomials* (4.5) *if and only if there exists a polynomial Youla-Kučera parameter* $q(s)$ *with degree bound* (4.6)*, whose coefficients satisfy the LMIs* (4.15) *or* (4.18)*.*

The approach discussed in this section is not restricted to bounding only the output of a system. Indeed, by using the appropriate transfer functions, any signal in the loop can be constrained. The control output u, for example, can be bounded using

$$u(s) = r(s)\frac{a(s)d_0(s)}{z(s)} - r(s)\frac{a^2(s)}{z(s)}q(s) \tag{4.20}$$

in addition to, or instead of (4.7). Also, other Laplace transformable inputs can be used as long as the poles of the Laplace transform of the input signal are distinct strictly negative rational numbers and differ from the closed-loop poles p_i. A combination of requirements on different reference signals can easily be handled at the cost of increasing the size of the set of LMIs.

4.3 Extension to complex poles

As stated in the former section, the polynomial representation (4.9) of the time response of a linear system to a Laplace transformable input is only possible when strictly negative rational closed-loop poles are assigned (see Assumption 4.1). However, the assignment of purely real poles can be undesirable, especially in lightly damped systems such as most motion systems. In the case of resonant systems for instance, this would imply that the closed-loop system should be (over)critically damped. Furthermore, many reference signals have Laplace transforms with complex poles. If, for instance, a sinusoid is used as the reference signal instead of a step, the Laplace transform is given by $r(s) = \frac{\omega}{s^2+\omega^2}$ resulting in complex poles in the system's response. Therefore, such reference signals cannot be handled by the approach from [56]. When we allow both distinct rational real and rational complex poles to be present in the closed-loop transfer function $T(s)$ and the Laplace transformed reference signal $r(s)$, the Laplace transform of the system's output can be decomposed as

$$y(s) = \sum_{i=0}^{n_r} \frac{y_i}{s+p_i} + \sum_{i=n_r+1}^{n_r+n_c/2+1} \frac{y_i}{s+\alpha_i+j\beta_i} + \frac{y_i^*}{s+\alpha_i-j\beta_i}, \tag{4.21}$$

where n_r and n_c denote the number of real and complex poles, respectively, $-p_i$ is the location of a real pole, $-\alpha_i \pm j\beta_i$ is the location of a complex pole, and y_i are the possibly complex coefficients (with complex conjugate y_i^*) that depend on the design parameter q. The corresponding time-domain signal is then described by

$$y(t) = \sum_{i=0}^{n_r} y_i e^{-p_i t} \quad + \sum_{i=n_r+1}^{n_r+n_c/2+1} (y_i e^{-j\beta_i t} + y_i^* e^{j\beta_i t}) e^{-\alpha_i t}. \tag{4.22}$$

As before, p_i, α_i, and β_i are assumed to be rationals and we denote $p_i = \frac{\bar{p}_i}{m}$, $\alpha_i = \frac{\bar{\alpha}_i}{m}$, $\beta_i = \frac{\bar{\beta}_i}{m}$, $\tau = \frac{t}{m}$ for a sufficiently large integer m such that $\bar{p}_i$, $\bar{\alpha}_i$, and $\bar{\beta}_i$ can be taken as integers. Furthermore, let

$$\lambda = e^{-\tau}. \tag{4.23}$$

Using Euler's formula and decomposing the complex coefficients as $y_i = a_i + jb_i$, $y_i^* = a_i - jb_i$, yields

$$y(t) = \sum_{i=0}^{n_r} y_i \lambda^{\bar{p}_i} + \sum_{i=n_r+1}^{n_r+n_c/2+1} \left(a_i 2\cos(\bar{\beta}_i\tau) + b_i 2\sin(\bar{\beta}_i\tau)\right) \lambda^{\bar{\alpha}_i}. \tag{4.24}$$

Obviously, the terms involving the complex poles are non-polynomial in the indeterminate λ because of the terms involving products of $\cos(\overline{\beta}_i\tau)$ and $\sin(\overline{\beta}_i\tau)$ with $\lambda^{\overline{\alpha}_i}$, which make it impossible to directly use the positive polynomial approach to bound the output as in (4.11). Although the parameters $\overline{\alpha}_i$ and $\overline{\beta}_i$ are fixed as a result of the pole placement, there still is freedom in the choice for the coefficients a_i, b_i (which depend on q_i) which makes it possible to shape the part of the response caused by the complex poles. We propose two relaxations to determine the values a_i, b_i via convex optimization to shape the time response $y(t)$.

4.3.1 Exponential bounds relaxation

To resolve the problem of the products $\cos(\overline{\beta}_i\tau)\lambda^{\overline{\alpha}_i}$ and $\sin(\overline{\beta}_i\tau)\lambda^{\overline{\alpha}_i}$ in (4.24) we relax the problem by using the fact that

$$\cos(\overline{\beta}_i\tau),\ \ \sin(\overline{\beta}_i\tau) \in [-1,1] \quad \forall\tau \in \mathbb{R}, \tag{4.25}$$

and instead of the exact time-response (4.24), we consider

$$\begin{aligned} y_{\text{upper}}(\lambda) &= \sum_{i=0}^{n_r} y_i\lambda^{\overline{p}_i} + \sum_{i=n_r+1}^{n_r+n_c/2+1} \left(2|a_i| + 2|b_i|\right)\lambda^{\overline{\alpha}_i}, \\ y_{\text{lower}}(\lambda) &= \sum_{i=0}^{n_r} y_i\lambda^{\overline{p}_i} - \sum_{i=n_r+1}^{n_r+n_c/2+1} \left(2|a_i| + 2|b_i|\right)\lambda^{\overline{\alpha}_i}. \end{aligned} \tag{4.26}$$

In contrast to (4.24), these exponential bounds on the closed-loop time response are univariate polynomials in the indeterminate $\lambda = e^{-\tau}$ and can be bounded by specified polynomials $g_u(\lambda)$ and $g_l(\lambda)$ via the polynomial non-negativity constraints

$$\begin{aligned} P_3(\lambda) &:= g_u(\lambda) - y_{\text{upper}}(\lambda) \quad \geq 0 \\ P_4(\lambda) &:= y_{\text{lower}}(\lambda) - g_l(\lambda) \quad \geq 0 \end{aligned} \qquad \forall\lambda \in [0,1]. \tag{4.27}$$

Enforcing non-negativity of (4.27) on the interval $\lambda \in [0,1]$ is again a special case of (4.13) with $z = \{y_i, a_i, b_i\},\ x = \lambda,\ \ell = 2,\ m = 0,\ p(z,x) = 0,\ g_1(z,x) = P_3(\lambda)$, $g_2(z,x) = P_4(\lambda)$, and $\mathcal{D} = \{\lambda \in \mathbb{R} \mid 0 \leq \lambda \leq 1\}$. Therefore, it is possible to determine the values y_i, a_i, b_i (and hence q_i), such that the upper and lower bounds (4.26) of the closed-loop time response are bounded by $g_u(\lambda)$ and $g_l(\lambda)$.

4.3.2 Multivariate polynomial relaxation

In this section, we propose a second relaxation. An equivalent expression for the time response (4.24) is given by

$$\begin{aligned} y(t) = &\sum_{i=0}^{n_r} y_i \lambda^{\overline{p}_i} + \\ &\sum_{i=n_r+1}^{n_r+n_c/2+1} \left(a_i 2w_i(\cos(\tau),\sin(\tau)) + b_i 2r_i(\cos(\tau),\sin(\tau))\right) \lambda^{\overline{\alpha}_i} \end{aligned} \tag{4.28}$$

with $w_i(\cdot,\cdot)$ and $r_i(\cdot,\cdot)$ appropriate polynomial functions of their argument, see Appendix A.3. Let $u = \cos(\tau)$ and $v = \sin(\tau)$ so that

$$u^2 + v^2 = 1. \tag{4.29}$$

The time response (4.28) can now be written as the multivariate polynomial

$$y(u,v,\lambda) = \sum_{i=0}^{n_r} y_i \lambda^{\bar{p}_i} + \sum_{i=n_r+1}^{n_r+n_c/2+1} \left(a_i 2w_i(u,v) + b_i 2r_i(u,v)\right) \lambda^{\bar{\alpha}_i} \tag{4.30}$$

with the constraints (4.23) and (4.29). Bounding the output as in (4.11) is therefore equivalent to enforcing the polynomial non-negativity constraints

$$\begin{aligned} P_5(u,v,\lambda) &:= y(u,v,\lambda) - y_{\min} \geq 0, \\ P_6(u,v,\lambda) &:= y_{\max} - y(u,v,\lambda) \geq 0 \end{aligned} \tag{4.31}$$

subject to (4.23) and (4.29). If constraint (4.23) is released and replaced by

$$\lambda \in [0,1], \tag{4.32}$$

then, since constraint (4.29) is already algebraic, enforcing non-negativity of (4.31) subject to (4.29) and (4.32) again is a special case of (4.13) with $z = \{y_0, a_i, b_i\}$, $x = (u,v,\lambda)$, $\ell = 2$, $m = 0$, $p(z,x) = 0$, $g_1(z,x) = P_5(u,v,\lambda)$, $g_2(z,x) = P_6(u,v,\lambda)$, and $\mathcal{D} = \{(u,v,\lambda) \in \mathbb{R}^3 \mid u^2 + v^2 = 1, \quad 0 \leq \lambda \leq 1\}$. However, since the polynomial positivity constraints (4.31) are now multivariate instead of univariate, Lemmas 4.2 and 4.3 cannot be used. In general, checking positivity of a multivariate polynomial on a semialgebraic set is a hard problem, but it can often be approximated as closely as desired by a hierarchy of convex relaxations, see Appendix A.2. To reduce the conservatism introduced through replacing (4.23) by (4.32), one can attempt to approximate the connection between constraints (4.23) and (4.29) through polynomial Fourier series expansion. In general, it is not possible to describe (4.23) by a polynomial in u and v, however, in some specific situations a polynomial approximation of this relation can result in less conservatism as is shown in the example in Section 4.5.2.

Remark 4.5 As already mentioned, both the exponential bounds relaxation as well as the multivariate polynomial relaxation are special cases of the more general

problem of minimizing a polynomial over a semialgebraic set (4.13). Therefore, it is straightforward to add an objective function $p(z, x)$ which can be used to express additional desired properties of the response (such as the contribution of certain poles and the steady-state error) in terms of the design parameters y_i, a_i, and b_i. We will discuss these additional design options in the the following section.

4.4 Control design procedure

In this section, we will discuss some issues on the control design procedure such as the choice of the objective function $p(z, x)$ and the numerical tractability of the optimization problem (4.13). Suppose that the d-minimal controller (4.2) for system (4.1) has been designed via the Diophantine equation (4.4) such that the desired closed-loop pole locations are achieved. Also suppose that more closed-loop poles are assigned than twice the number of poles of the plant. Then, according to (4.6) there is additional control design freedom in the form of the Youla-Kučera parameter, which can be used to shape the closed-loop time response via optimization problem (4.13). In case there are complex closed-loop poles assigned, either of the proposed relaxations from Section (4.3) can be used to arrive at the form (4.13).
In case the exponential bounds relaxation from Section 4.3.1 is used, we propose the following design procedure to shape the closed-loop time response. The originally designed diophantine controller (4.2) results in the upper bound $g_{u_{\text{original}}}(\lambda)$ and the lower bound $g_{l_{\text{original}}}(\lambda)$ on the closed-loop response $y(t)$. These bounds can be optimized via optimization problem (4.13). Suppose for instance that $y(t)$ is the response to a step input. Desirable properties of a step response are a zero steady-state error, a short settling-time and small overshoot. To ensure that the exponential bounds of the transient response are not deteriorated by the Youla-Kučera parameter and that a zero steady-state error is achieved, the upper and lower bound in (4.27) are specified as $g_u(\lambda) = g_{u_{\text{original}}}(\lambda) + c_u$ and $g_l(\lambda) = g_{l_{\text{original}}}(\lambda) + c_l$, where c_u and c_l are constants used to express the zero steady-state error specification. Then the transient response can be improved by specifying an objective function $p(z, x)$ that minimizes slow modes to improve the settling-time. The exponential bounds relaxation is not suited to directly minimize the overshoot. This procedure will be illustrated with an example in Section 4.5.1.
As opposed to the exponential bounds relaxation, the multivariate polynomial relaxation from Section 4.3.2 is typically suited to minimize the overshoot of a step response by constraining the response (4.30) as $y(u, v, \lambda) \leq \gamma$ and specifying an objective function that minimizes γ. This procedure will be illustrated Section 4.5.2.
Theoretically, all pole locations can be handled in the proposed framework. However, when the real parts of the poles are ratios of large integers, i.e., when the least common multiple m is large, a high degree polynomial would be required.

This will lead to a large LMI problem, which could be untractable for the current state-of-the-art solvers. Therefore, to facilitate the computations the desired closed-loop pole locations should be such that m is small.
Even when m is small, the combination of the order of the characteristic equation $z(s)$ and the choice of the closed-loop poles can result in a relatively large difference between the smallest and largest coefficient in the characteristic equation. This affects both the numerical solution of the Diophantine equation as well as the LMI solver since both (4.4) and (4.13) are then ill-conditioned. To improve the conditioning of the characteristic equation $z(s)$, time-scaling can be applied. The control design procedure as proposed in this section will be illustrated by an example in the next section.

4.5 Example

We start with a simple example to illustrate the proposed design method. Consider the simple model describing a water tank as depicted in Figure 4.2 with inflow-to-level transfer function

$$P(s) = \frac{y(s)}{u(s)} = \frac{1}{s+1}. \tag{4.33}$$

The control objective is to let the level y track a step reference from 0 to 1 as close as possible. Moreover, the controller (4.2) will be designed such that the assigned complex closed-loop poles are $p_{1,2} = -1 \pm 2j$, $p_{3,4} = -2 \pm 4j$. This is done

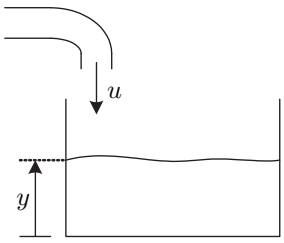

Figure 4.2: Water tank with inflow u and level y.

by solving the Diophantine equation (4.4) leading to the d-minimal controller

$$C(s) = \frac{d_0(s)}{c_0(s)} = \frac{68}{s^3 + 5s^2 + 28s + 32}, \tag{4.34}$$

resulting in the closed-loop system given by the complementary sensitivity function

$$T(s) = \frac{68}{s^4 + 6s^3 + 33s^2 + 60s + 100}. \tag{4.35}$$

By virtue of the Youla-Kučera parameter and in accordance with the constraint $\deg q(s) \leq 2$, i.e., $q(s) = q_0 + q_1 s + q_2 s^2$, the set of allowable controllers assigning the specified closed-loop polynomial is parameterized as

$$\begin{aligned} C(s) &= \frac{d(s)}{c(s)} = \frac{d_0(s) - a(s)q(s)}{c_0(s) + b(s)q(s)} \\ &= \frac{68 - (q_0 + (q_0 + q_1)s + (q_1 + q_2)s^2 + q_2 s^3)}{s^3 + 5s^2 + 28s + 32 + (q_0 + q_1 s + q_2 s^2)}, \end{aligned} \tag{4.36}$$

resulting in the set of closed-loop transfer functions

$$T(s) = \frac{68 - (q_0 + (q_0 + q_1)s + (q_1 + q_2)s^2 + q_2 s^3)}{s^4 + 6s^3 + 33s^2 + 60s + 100}. \tag{4.37}$$

The Laplace transform of the time response of (4.37) to a step input is parameterized as

$$y(s) = \frac{1}{s} T(s) = \frac{68 - (q_0 + (q_0 + q_1)s + (q_1 + q_2)s^2 + q_2 s^3)}{s(s + 1 + 2j)(s + 1 - 2j)(s + 2 + 4j)(s + 2 - 4j)}. \tag{4.38}$$

The values y_0, a_1, b_1, a_2, b_2 of the corresponding partial fractional decomposition

$$y(s) = \frac{y_0}{s} + \frac{a_1 + jb_1}{s + 1 + 2j} + \frac{a_1 - jb_1}{s + 1 - 2j} + \frac{a_2 + jb_2}{s + 2 + 4j} + \frac{a_2 - jb_2}{s + 2 - 4j} \tag{4.39}$$

can be solved from the linear system of equations

$$\begin{bmatrix} 100 & 0 & 0 & 0 & 0 \\ 60 & 40 & 80 & 20 & 40 \\ 33 & 48 & 16 & 18 & 16 \\ 6 & 10 & 4 & 8 & 8 \\ 1 & 2 & 0 & 2 & 0 \end{bmatrix} \begin{bmatrix} y_0 \\ a_1 \\ b_1 \\ a_2 \\ b_2 \end{bmatrix} = \begin{bmatrix} 68 \\ 0 \\ 0 \\ 0 \\ 0 \end{bmatrix} + \begin{bmatrix} -1 & 0 & 0 \\ -1 & -1 & 0 \\ 0 & -1 & -1 \\ 0 & 0 & -1 \\ 0 & 0 & 0 \end{bmatrix} \begin{bmatrix} q_0 \\ q_1 \\ q_2 \end{bmatrix}, \tag{4.40}$$

where q_0, q_1, q_2 are the free variables to shape the time response. The goal is to determine values of y_0, a_1, b_1, a_2, b_2 (via q_0, q_1, q_2), attainable by a proper controller, such that the closed-loop time response to the step input can be optimized. Both relaxations described in Section 4.3 are demonstrated to show their effectiveness.

4.5.1 Application of the exponential bounds relaxation

The exponential bounds on the step response of closed-loop system (4.37) are given by

$$\begin{aligned} y_{\text{upper}}(t) &= y_0 + (2|a_1| + 2|b_1|)e^{-t} + (2|a_2| + 2|b_2|)e^{-2t}, \\ y_{\text{lower}}(t) &= y_0 - (2|a_1| + 2|b_1|)e^{-t} - (2|a_2| + 2|b_2|)e^{-2t}, \end{aligned} \tag{4.41}$$

where y_0, a_1, b_1, a_2, b_2 are related to q_0, q_1, q_2 via (4.40). The goal of this relaxation is to determine values of q_0, q_1, q_2 such that

$$\begin{array}{ll} P_3(\lambda) = g_u(\lambda) - y_{\text{upper}}(\lambda) & \geq 0, \\ P_4(\lambda) = y_{\text{lower}}(\lambda) - g_l(\lambda) & \geq 0 \end{array}, \tag{4.42}$$

where

$$\begin{aligned} \lambda &= e^{-t}, \\ y_{\text{upper}}(\lambda) &= y_0 + (2|a_1| + 2|b_1|)\lambda + (2|a_2| + 2|b_2|)\lambda^2, \\ y_{\text{lower}}(\lambda) &= y_0 - (2|a_1| + 2|b_1|)\lambda - (2|a_2| + 2|b_2|)\lambda^2. \end{aligned} \tag{4.43}$$

The original upper and lower bounds on the step response, i.e., of (4.38) with $q(s) = 0$, are given by

$$\begin{aligned} g_{u_{\text{original}}}(\lambda) &= 0.68 + 1.58\lambda + 0.38\lambda^2, \\ g_{l_{\text{original}}}(\lambda) &= 0.68 - 1.58\lambda - 0.38\lambda^2, \end{aligned} \tag{4.44}$$

respectively. According to the design method from Section (4.4), $g_u(\lambda)$ and $g_l(\lambda)$ are specified to be

$$\begin{aligned} g_u(\lambda) &= g_{u_{\text{original}}}(\lambda) + c_u = 1.01 + 1.58\lambda + 0.38\lambda^2 \\ g_l(\lambda) &= g_{l_{\text{original}}}(\lambda) + c_l = 0.99 - 1.58\lambda - 0.38\lambda^2. \end{aligned} \tag{4.45}$$

where $c_u = 0.33$ and $c_l = 0.31$ are used to specify a small steady-state error (smaller than 0.01). The dominant term in the upper and lower bound corresponds to the slow mode e^{-t} with coefficient $(2|a_1| + 2|b_1|)$. To minimize the contribution of this term and to bring the steady-state error close to zero, we specify the objective function

$$p(y_0, a_1, b_1) = 10|1 - y_0| + 2|a_1| + 2|b_1|, \tag{4.46}$$

resulting in the optimization problem

$$\begin{array}{ll} \min\limits_{q_0, q_1, q_2} & p(y_0, a_1, b_1) \\ \text{s.t.} & (4.40) \\ & (4.42) \quad \forall\ \lambda \in [0, 1]. \end{array} \tag{4.47}$$

The constraints (4.42) cannot straightforwardly be implemented as an LMI since the nonlinear operator $|\cdot|$ is used in these equations. However, each of the two nonlinear inequalities can be expressed as 2^4 equivalent linear inequalities (2 inequalities for each absolute value expression). The Youla-Kučera parameter resulting from minimization problem (4.47) is

$$q(s) = -32.0 - 23.0s - 3.0s^2, \tag{4.48}$$

which yields the controller and closed-loop

$$C(s) = \frac{3s^3 + 26s^2 + 55s + 100}{s^3 + 2s^2 + 5s}, \tag{4.49}$$

$$T(s) = \frac{3s^3 + 26s^2 + 55s + 100}{s^4 + 6s^3 + 33s^2 + 60s + 100}, \tag{4.50}$$

together with the new bounds

$$\begin{aligned} g_{u_{\text{new}}}(t) &= 1.00 + 1.25e^{-2t}, \\ g_{l_{\text{new}}}(t) &= 1.00 - 1.25^{-2t}. \end{aligned} \tag{4.51}$$

This shows that the steady-state error is zero and the contribution of the slow mode has been completely eliminated. The step responses together with their bounds of the original closed-loop system (4.35) and of the new, optimized closed-loop system (4.50) are depicted in Figure 4.3(a), while the Bode diagrams of the original controller (4.34) and the new controller (4.49) are shown in Figure 4.3(b). From Figure 4.3(a) it is obvious that the step response of the designed closed-loop

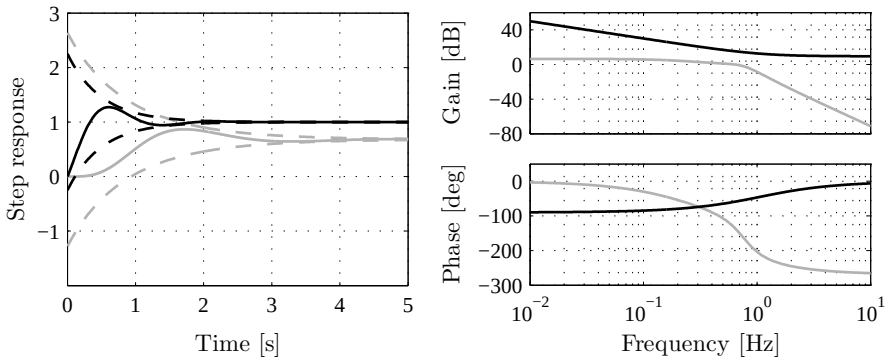

Figure 4.3: Results of the exponential bounds relaxation. (a) New (solid black) and original (solid grey) step responses, original bounds (dashed grey), and new bounds (dashed black), (b) Bode diagrams of the original (grey) and the new (black) controller.

system satisfies the specified bounds and additionally results in zero steady-state tracking error. Upon examination of Figure 4.3(b) this can be explained by the fact that controller (4.49) exhibits an overall higher gain and hence results in a higher bandwidth of the closed-loop system resulting in a faster response, while it also implements integrating action providing the steady-state accuracy. Although there is some conservatism introduced by the fact that upper and lower bounds are used, this example demonstrates that a significant increase of the performance with respect to the time response can be obtained using this method.

4.5.2 Application of the multivariate polynomial relaxation

In this section, the multivariate polynomial relaxation from Section 4.3.2 is used to obtain suitable values of q_0, q_1, q_2 to improve the step response of closed-loop system (4.37). Following (4.30) we obtain (see Appendix A.3)

$$\begin{aligned} &w_1(u,v) = u^2 - v^2, \quad r_1(u,v) = 2uv, \\ &w_2(u,v) = u^4 + v^4 - 6u^2v^2, \quad r_2(u,v) = 4vu^3 - 4uv^3, \end{aligned} \tag{4.52}$$

yielding the time response

$$y(u,v,\lambda) = y_0 + (2a_1(u^2-v^2)+4b_1uv)\lambda + (2a_2(u^4+v^4-6u^2v^2)+8b_2(vu^3-uv^3))\lambda^2, \tag{4.53}$$

which is a multivariate polynomial with 3 independent variables (u, v, λ) and three decision variables (q_0, q_1, q_2). As mentioned in Section 4.4, the exponential bounds relaxation is used to shape the exponential bounds of the step response and is not well-suited to constrain the overshoot. The multivariate polynomial relaxation on the other hand can be used for such problems. Therefore, in this section the problem is to find $q(s)$ such that the overshoot γ is small and that, as before, the steady-state error of the step response is zero. Therefore, the total problem is posed as

$$\begin{aligned} \min_{q_0,q_1,q_2} \quad & 10|1-y_0| + \gamma \\ \text{s.t.} \quad & (4.40) \\ & \gamma - y(u,v,\lambda) \geq 0 \quad \forall (u,v,\lambda) \in \mathcal{F}, \end{aligned} \tag{4.54}$$

where

$$\mathcal{F} := \left\{ (u,v,\lambda) \in \mathbb{R}^3 \mid u^2 + v^2 - 1 = 0, \quad 0 \leq \lambda \leq 1 \right\}. \tag{4.55}$$

Since the explicit relation between u, v and λ is lost in (4.55), this is a relaxed problem and some conservatism is introduced. As already mentioned in Section 4.3.2, since multivariate polynomials are involved, problem (4.54) is hard to solve but it can be approximated as closely as desired by a hierarchy of convex relaxations, see Appendix A.2. Indeed, to make problem (4.54) computationally tractable, we replace the non-negativity condition by a stronger condition in terms of sums-of-squares to formulate a hierarchy of upper bounds $\tilde{\gamma}$ on γ resulting in the optimization problem

$$\begin{aligned} \min \quad & 10|1-y_0| + \tilde{\gamma} \\ \text{s.t.} \quad & (4.40) \\ & \tilde{\gamma} - y(u,v,\lambda) = c_1(u,v,\lambda)(u^2+v^2-1) \\ & + s_0(u,v,\lambda) + s_1(u,v,\lambda)\lambda \\ & + s_2(u,v,\lambda)(1-\lambda) + b_{12}(u,v,\lambda)\lambda(1-\lambda), \end{aligned} \tag{4.56}$$

where c_1 is a polynomial in u, v, λ and $s_0,\ s_1,\ s_2,\ b_{12}$ are sums-of-squares polynomials in u, v, λ. The size of this optimization problem depends on the order of the

multipliers $c_1,\ s_0,\ s_1,\ s_2,\ b_{12}$. This order can be used as a tuning knob in (4.56) to adjust the trade-off between the desired accuracy and the computational complexity. Although it is a priori not clear what the order of the multipliers should be to arrive at the global minimum of γ (if it is attainable), a standard method is to increase the order until not much improvement in $\tilde{\gamma}$ is observed anymore or until one is satisfied with the obtained value of $\tilde{\gamma}$. The obtained minimum values of $\tilde{\gamma}$ for various orders of the multipliers are given in Table 4.1. Based on

	order multipliers					
	1	2	3	4	5	10
$\tilde{\gamma}$	19.9	2.00	2.00	1.50	1.50	1.50

Table 4.1: Upper bound $\tilde{\gamma}$ for various orders of the multipliers.

the figures in this table we expect that the global minimum of γ is equal to 1.50 (although no guarantee can be given as (4.56) remains a relaxation of (4.54)), and the corresponding Youla-Kučera parameter is given by

$$q(s) = -32.0 - 12.9s - 1.49s^2, \tag{4.57}$$

which yields the controller

$$C(s) = \frac{1.49s^3 + 14.4s^2 + 44.9s + 100}{s^3 + 3.51s^2 + 15.1s}. \tag{4.58}$$

The step responses of both the original closed-loop with the d-minimal controller (4.34) and of the closed-loop with controller (4.58) are depicted in Figure 4.4(a). Figure 4.4(b) shows the Bode diagram of the corresponding controllers. Indeed,

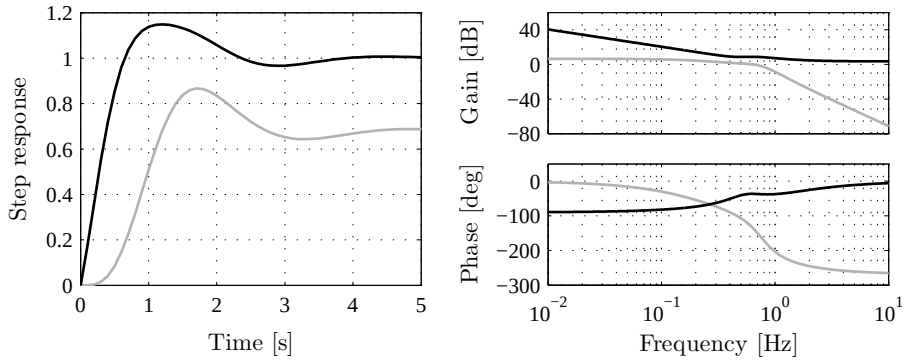

(a) (b)

Figure 4.4: Results of the multivariate polynomial relaxation. (a) New (black) and original (grey) step responses, (b) Bode diagrams of the original (grey) and the new (black) controller.

the optimized controller exhibits integrating action resulting in zero steady-state error. Although the obtained lower bound $\tilde{\gamma} = 1.50$ in fact equals the global maximum $\gamma = 1.50$ on $\mathcal{F}$ (which is verified by gridding $\mathcal{F}$ and computing its maximum), it does not equal the actual maximum of the step response $y_{\max} = 1.15$. This is due to the replacement of constraint (4.23) with the relaxation (4.32) and can be understood from Figure 4.5, which shows the cylindrical relaxed set $\mathcal{F}$ together with the original non-convex set

$$\mathcal{F}_{\text{original}} := \left\{(u, v, \lambda) \in \mathbb{R}^3 \mid u = \cos(\tau),\ v = \sin(\tau),\ \lambda = e^{-\tau}, \quad \forall\ \tau \in [0, \infty]\right\}. \tag{4.59}$$

As can be seen, the maximum of the actual time response (4.53), i.e., the maximum on the set $\mathcal{F}_{\text{original}}$ (which equals 1.15), does not correspond with the maximum on the set $\mathcal{F}$ (which equals 1.50).

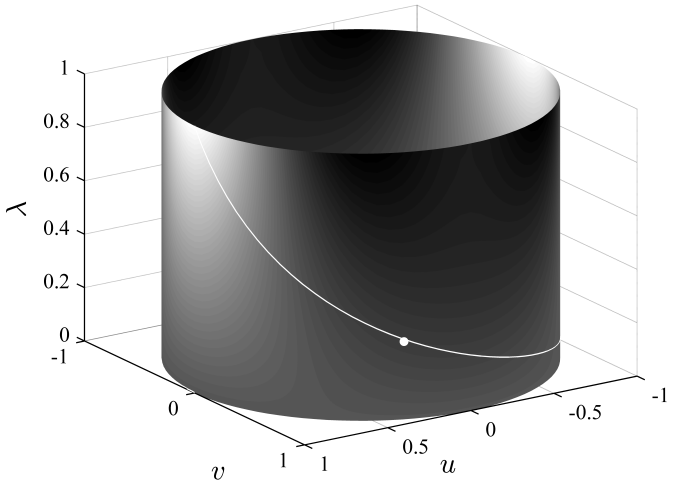

Figure 4.5: Relaxed set $\mathcal{F}$ (light and dark denote low and high values, respectively), the original set $\mathcal{F}_{\text{original}}$ (white line) together with its maximum (white dot).

Reduction of conservatism

As stated in Section 4.3.2, to reduce the conservatism introduced by (4.32), one can attempt to approximate the connection between constraints (4.23) and (4.29) with a polynomial. For this specific example, it turns out that this approximation indeed reduces the gap between the upper bound $\tilde{\gamma}$ and the actual overshoot γ. The function $\lambda = e^{-\tau}$ can be approximated by series expansion of u and v.

Figure 4.6(a) depicts the third order polynomial approximation

$$\lambda = \ell(u, v) = 0.12u - 0.059v + 0.45u^2 + 0.011v^2 + 0.29u^3 + 0.25v^3 \quad (4.60)$$

on the interval $\tau \in [0, 2\pi]$ (the period of u and v). From this figure it is obvious that there is a large deviation between the approximation and $e^{-\tau}$ on the interval $\tau \in [4, 2\pi]$. This caused by the fact that the approximation in terms of $\cos(\tau)$ and $\sin(\tau)$ is always a periodic function while $e^{-\tau}$ is not. However, since we consider a step response, the maximum value of the response is expected to occur before $\tau = 4$ and therefore the deviation might not pose a problem. The approximation

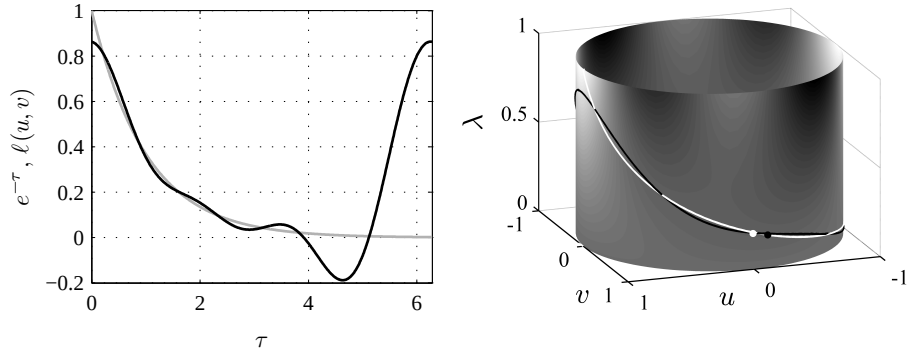

(a) (b)

Figure 4.6: Approximation $\lambda = \ell(u, v)$. (a) Function $e^{-\tau}$ (grey) and 3^{th} order polynomial approximation $\ell(u, v)$ (black), (b) Relaxed set $\mathcal{F}$ (light and dark denote low and high values, respectively), the original set $\mathcal{F}_{\text{original}}$ (white line) together with its maximum (white dot), and the approximate set $\mathcal{F}_{\text{approx}}$ (black line) together with its maximum (black dot).

of the original set $\mathcal{F}_{\text{original}}$ is given by

$$\mathcal{F}_{\text{approx}} := \left\{(u, v, \lambda) \in \mathbb{R}^3 \mid u = \cos(\tau),\ v = \sin(\tau), \quad \lambda = \ell(u, v), \quad \forall\ \tau \in [0, \infty]\right\} \quad (4.61)$$

and is depicted in Figure 4.6(b) together with $\mathcal{F}$ and $\mathcal{F}_{\text{original}}$. When equality (4.60) is used in the optimization problem (4.56), the resulting Youla-Kučera parameter and upper bound $\tilde{\gamma}$ are

$$q(s) = -32.00 - 15.43s - 2.278s^2, \quad \tilde{\gamma} = 1.0857, \quad (4.62)$$

resulting in the controller

$$C(s) = \frac{2.28s^3 + 17.7s^2 + 47.4s + 100}{s^3 + 2.72s^2 + 12.6s}. \quad (4.63)$$

The step responses of both the closed-loop system with controller (4.58) and that of the closed-loop with controller (4.63) are shown in Figure 4.7(a). The Bode diagrams of the corresponding controllers is depicted in Figure 4.7(b). Because

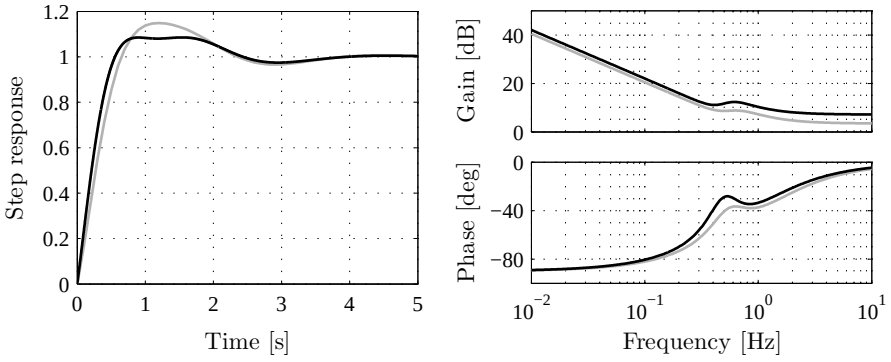

(a) (b)

Figure 4.7: Results with the approximation $\lambda = \ell(u, v)$. (a) Step responses with controller (4.58) (grey) and with controller (4.63) (black), (b) Bode diagrams of controller (4.58) (grey) and of controller (4.63) (black).

of the approximation (4.60), the obtained lower bound $\tilde{\gamma} = 1.0857$ is very close to the actual maximum $y_{\max} = 1.0855$. The global maximum on $\mathcal{F}$ is 1.74 indicating that indeed the minimizer over $\mathcal{F}$ is different from the minimizer on $\mathcal{F}_{\text{approx}}$ (and $\mathcal{F}_{\text{original}}$).

This example showed that after controller design by pole placement it is possible to shape the transient time response of the system by assigning zeros to the closed-loop system through a suitable extension of the controller under pole invariance. In case of a step response, the exponential bounds relaxation is specifically suited for improving the rise-time and settling-time while the multivariate polynomial relaxation can be applied for overshoot minimization.

Remark 4.6 Although the polynomial approximation (4.60) has been shown to be beneficial with respect to the overshoot for this example, it cannot be expected that this will generally be the case. It is obvious from Figure 4.6(a) that approximation (4.60) differs from the actual curve $e^{-\tau}$. This will always be the case since a polynomial function of $\cos(\tau)$ and $\sin(\tau)$ is a periodic function while $e^{-\tau}$ is not. A priori, it is not clear what the effect of this deviation will be. In general, the best we can do is optimizing over the set $\mathcal{F}$, but for certain problems (such as this example) we can do better by including an approximation of the relation between constraints (4.23) and (4.29). In contrast to the relaxation proposed in Section 4.5.1, this relaxation method is suitable to constrain the response by a fixed constant, e.g. $|y(t)| \leq \gamma$, as was illustrated by the overshoot minimization example. □

In the next section we discuss the practical applicability of the proposed method for a more complex plant and also implement it on an experimental setup.

4.6 Experiment and discussion

In this section we apply the control design method to the fourth order dual rotary motion system depicted in Figure 3.5. The measured frequency response and the identified model are depicted in Figure 4.8. The model is described by the transfer

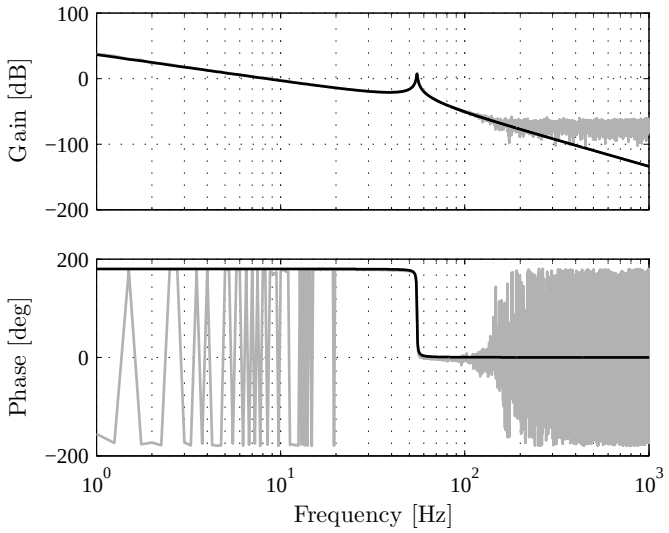

Figure 4.8: Measured frequency response (grey) and estimated model (black).

function

$$P(s) = \frac{b(s)}{a(s)} = \frac{3.16 \cdot 10^8}{s^2(s^2 + 3.43s + 1.20 \cdot 10^5)}. \tag{4.64}$$

The system exhibits a lightly damped resonance with natural frequency 55 Hz and damping ratio 0.005. In general, such resonances are not desirable in any closed-loop transfer.

4.6.1 Handling lightly damped poles

From a control point of view, there are several possibilities to handle lightly damped poles. One could design a controller based on the method as described in

Section 4.3 to move these poles to more favorable locations. Suppose we would like to have a second order Youla-Kučera parameter $q(s)$ at our disposal, then we need to place 10 poles according to degree constraint (4.6). As discussed in Section 4.4, the pole locations should be chosen such that their least common multiple m is small. Therefore, to show the applicability of the method involving both real and complex poles, the following closed-loop pole locations are chosen: $-5 \pm 10j$, $-10 \pm 20j$, -15, $-20 \pm 10j$, -25, and $-30 \pm 70j$. Solving the corresponding Diophantine equation results in the d-minimal controller attaining these poles. However, this controller is unstable. Furthermore, it introduces extra zeros in the closed-loop resulting in a step response which is far from ideal.
A better (and commonly used) method to handle lightly damped poles in the system is the use of a notch filter. To this end, part of the freedom in the control design is used to place a notch filter. This is done by fixing two of the zeros of the controller at the resonance frequency and adding two corresponding closed-loop poles to complete the notch filter. In practice, this amounts to first removing the resonating poles from the model, then designing a controller following the method as before including two closed-loop poles corresponding to the notch filter, and finally placing back the poles in the model and adding zeros to the controller. Summarizing, the design process that we will follow is the following:

- remove the lightly damped poles from the model,
- specify the desired closed-loop pole locations including one pair corresponding to the removed poles,
- shape the transient response using the algorithm presented in Section 4.3,
- add the removed poles to the system model and the corresponding zeros to the controller.

In this case we do not explicitly account for the dynamic response caused by the lightly damped poles, but by sensible placement of the zeros, it is possible to reduce this response significantly.

Removing the lightly damped poles yields the second order model

$$P_r(s) = \frac{b_r(s)}{a_r(s)} = \frac{3.16 \cdot 10^8}{s^2}, \tag{4.65}$$

and since $a_r(s)$ and $b_r(s)$ are coprime, arbitrary pole placement can be achieved. We take a second order Youla-Kučera parameter $q(s)$ since based on experience we expect this to be sufficient. Therefore we need to place 8 poles, including the poles of the notch filter. The characteristic equation of the closed-loop transfer function corresponding to the desired pole locations, $-10 \pm 20j$, -15, $-20 \pm 10j$, -25, and $-30 \pm 70j$, equals

$$\begin{aligned} z(s) = s^8 &+ 160s^7 + 1.6 \cdot 10^4 s^6 + 9.8 \cdot 10^5 s^5 + 3.6 \cdot 10^7 s^4 \\ &+ 8.7 \cdot 10^8 s^3 + 1.4 \cdot 10^{10} s^2 + 1.3 \cdot 10^{11} s + 5.4 \cdot 10^{11}. \end{aligned} \tag{4.66}$$

The combination of the order of the closed-loop and the choice of the closed-loop poles results in a relatively large difference between the smallest and largest coefficient in the characteristic equation. Hence, as discussed in Section 4.4, the desired pole locations are scaled by a factor of 22 to obtain the characteristic equation

$$\begin{aligned} z(s) = {} & s^8 + 7.3s^7 + 33.8s^6 + 91.9s^5 + 154.2s^4 \\ & + 169s^3 + 120.8s^2 + 51.7s + 9.9, \end{aligned} \tag{4.67}$$

which poses no problem for the Diophantine solver and the LMI solver, which is SeDuMi [138] in our case. The d-minimal controller resulting in the desired pole locations can be obtained by solving the Diophantine equation (4.4). The control goal is to track a step reference of 10 radians. A Youla-Kučera parameter of the form $q(s) = q_0 + q_1 s + q_2 s^2$ can be designed, which maintains the specified closed-loop poles and at the same time improves the time response with respect to overshoot and settling-time.

4.6.2 Results of the exponential bounds relaxation

As discussed in Section 4.4, we propose the following bounds as a starting point for the optimization of the time response.

$$\begin{aligned} g_u(\lambda) &= g_{u_{\text{original}}}(\lambda) + c_u \\ &= 10.0 + 56.5e^{-10t} + 340e^{-15t} + 496e^{-20t} - 278e^{-25t} + 0.19e^{-30t}, \\ g_l(\lambda) &= g_{l_{\text{original}}}(\lambda) + c_l \\ &= 10.0 - 56.5e^{-10t} + 340e^{-15t} - 496e^{-20t} - 278e^{-25t} - 0.19e^{-30t}, \end{aligned} \tag{4.68}$$

with $c_u = c_l = 0$ since the original response of the d-minimal controller already had a zero steady-state error. The experimentally obtained step response of the closed-loop system with the d-minimal controller and the bounds (4.68) are depicted in Figure 4.9. The coefficient of the most dominant term e^{-10t} is minimized in the optimization process, yielding a similar optimization problem as (4.47) with objective function $p(a_1, b_1) = |a_1| + |b_1|$. The resulting Youla-Kučera parameter is given by

$$q(s) = -0.036 - 0.0014s - 1.9 \cdot 10^{-6} s^2, \tag{4.69}$$

resulting in the new bounds

$$\begin{aligned} g_{u_{\text{new}}}(t) &= 10.0 + 0e^{-10t} + 215e^{-15t} + 309e^{-20t} - 266e^{-25t} + 1.59e^{-30t}, \\ g_{l_{\text{new}}}(t) &= 10.0 - 0e^{-10t} + 215e^{-15t} - 309e^{-20t} - 266e^{-25t} - 1.59e^{-30t}. \end{aligned} \tag{4.70}$$

The experimentally obtained step response of the closed-loop system with this new controller and the new bounds (4.70) are also depicted in Figure 4.9. The

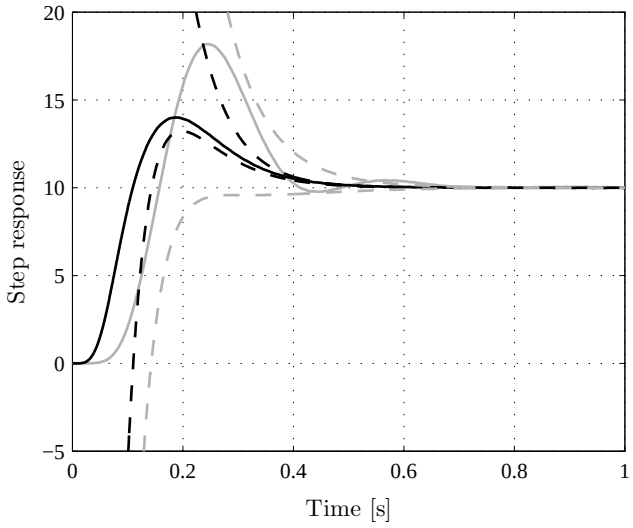

Figure 4.9: New (black) and original (grey) step responses, new bounds (dashed black) and the original bounds (dashed grey).

fact that the responses are not totally within the bounds is explained by the presence of unmodeled dynamics such as friction. The simulated responses correspond very well to the experimental responses and are hence not shown. The new controller meets the new bounds, and the step response has less overshoot and settles significantly faster than the original one, while the closed-loop pole locations remain unchanged. The Bode diagrams of the original and new controller are depicted in Figure 4.10(a), the corresponding open-loop diagrams are shown in Figure 4.10(b). The notch in the controller cancels the effect of the lightly damped poles and the new controller attains a slightly higher bandwidth. The most important difference, however, is its high-frequent behavior. The controller, and hence the open- and closed-loop, possess more gain at high frequencies. Given the fact that in this experiment this is beneficial with respect to the overshoot and the settling-time of the step response, one should keep in mind that undesired high frequent signals such as noise are also amplified by the new controller. This is a direct consequence of optimizing the controller for a specific reference signal.

4.7 Conclusions

In this chapter we extended recent results on the control of linear systems subject to time-domain constraints [56]. In that work, a controller is synthesized via a closed-loop pole placement method and it is shown that additional design freedom

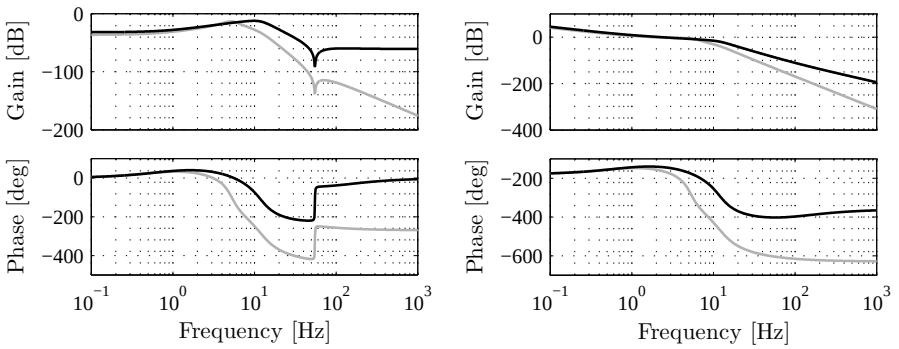

Figure 4.10: (a) Bode diagrams of the original (grey) and the new (black) controller, (b) Bode diagrams of the original (grey) and the new (black) open-loop.

in terms of the Youla-Kučera parameter can be used to satisfy time-domain constraints on closed-loop system signals by solving an LMI optimization problem. However, the method proposed in [56] is only applicable in case input signals are used that have no complex poles in their Laplace transform and in case only distinct negative real closed-loop poles are assigned. In order to extend the method to both inputs and closed-loop systems with complex conjugate poles, we proposed two relaxations which enable the assignment of complex conjugate poles, but at the expense of introducing some conservatism.

The first relaxation, called the exponential bounds relaxation, makes use of exponential upper and lower bounds on the response to any Laplace transformable input. Although this gives rise to potential conservatism, an example showed that by prescribing polynomial time-domain bounds, the system's performance to a step input can be improved with respect to the settling-time and the steady-state error. A drawback of this approach is the fact that fixed bounds on closed-loop signals such as an overshoot constraint cannot be handled. This drawback is not present in the second relaxation, the multivariate polynomial relaxation, since this one does not rely on exponential bounds. Although this approach has some degree of conservatism as well, an example showed that the overshoot to a step response can effectively be reduced using this method. Summarizing, in case of a step response, the exponential bounds relaxation is specifically suited for improving the rise-time and settling-time while the multivariate polynomial relaxation can be applied for overshoot reduction.

The practical applicability of the exponential bounds relaxation was demonstrated by means of an experiment on a fourth order motion system that exhibits a resonance. The order of the system and the prescribed locations of the closed-loop poles resulted in a numerically tractable optimization problem through the application of time scaling.

Chapter 5

Time-domain performance based nonlinear state feedback control of linear systems

This chapter describes a method to design a nonlinear state feedback controller that meets a set of prescribed time-domain constraints that are not attainable by linear state feedback. Using a constrained polynomial interpolation technique, an input signal is computed that satisfies the desired time-domain constraints on the input and state trajectories. The computed input trajectory is approximately mapped on the state trajectory, such that a nonlinear state feedback law is obtained. Stability of the resulting closed-loop polynomial system is analyzed using sum-of-squares techniques. An illustrative example is presented, showing that the proposed nonlinear controller outperforms linear static state feedback. To validate the proposed method, experiments on a fourth-order motion system are carried out.

5.1 Introduction

The tasks of controlled motion systems generally boil down to tracking reference signals, rejecting disturbances, or regulating the system from some initial condition to a desired equilibrium position. As an example, point-to-point motions, as are common for pick-and-place systems, fall within the last category. For this kind of systems, speed and accuracy are the main performance qualifiers. As a

consequence, it is important that the motion is carried out as fast and accurate as possible while time-domain constraints such as limitations on the actuator input and the overshoot are satisfied. Similar constraints hold when the goal of a controller is to regulate the system back to a desired operating point when a disturbance moved the system away from this operating point.
If the initial conditions and the desired operating point are known, it is possible to compute the corresponding optimal input signals that drive the system as fast as possible to the desired point while satisfying the prescribed constraints. This can, for instance, be done via input shaping techniques [11], the Pontryagin maximum principle, or dynamic programming [10]. These computed input signals could then be applied in a feedforward fashion to obtain the desired motions. However, it is well-known that the use of feedforward results in a lack of robustness of the steered system. Therefore, additional feedback is commonly applied in order to stabilize the system. In this chapter, we propose an alternative to the above feedforward approach in the form of a nonlinear state feedback controller. This nonlinear controller is designed to approximate the optimal feedforward signal from the measured states in the nominal case, i.e., for the initial condition the nonlinear design was made for. The obtained controller regulates the system back to the desired operating point and satisfies the prescribed constraints for the nominal design, while the closed-loop system is robust against small variations in the plant and disturbances because of the feedback.
There already exist methods to compute a nonlinear (piecewise linear) state feedback controller for linear systems that satisfy prescribed constraints. If these prescribed constraints are only input constraints, it is well-known that the bang-bang controller is time optimal for linear systems. Unfortunately, in case also state constraints are imposed, a generic method to design such a feedback controller is not available for continuous-time systems. As a solution, one can resort to a discrete-time approximation of the system and either use implicit MPC with on-line optimization or explicit MPC [9], where a controller is designed that can cope with time-domain constraints by solving the off-line constrained optimization explicitly. The explicit control law basically is a piecewise linear state feedback which is to be evaluated for different regions of the state-space, and often leads to a complex description in the sense of the number of regions. This number depends on the length of the optimization horizon and the number of constraints, and can be very high for practical applications, which prohibits real-time implementation for motion systems. On-line optimization is generally computationally demanding and can therefore also not be applied to motion systems. Our proposed design yields a low complexity controller, i.e., a controller with a closed-form solution, that regulates the system back to the desired operating condition as fast as possible while nominally satisfying the prescribed time-domain constraints. Although the design method is heuristic at some point, certain properties such as stability can be a posteriori verified.
The proposed controller synthesis consists of three parts. In the first part the time sequence of a control signal is computed that steers the given linear motion system from a certain initial condition to the desired operating condition as fast as possible and meets certain constraints on the input and output signals. As

mentioned before, this time sequence could for instance be computed via input shaping techniques, the Pontryagin maximum principle, or dynamic programming. These techniques, however, can require much effort to pose the problem. As a suitable alternative, we use the approach proposed in [55], with which a control signal can be computed in a straightforward way using a constrained polynomial interpolation technique, and that meets the imposed time-domain constraints. The time sequences of the corresponding state trajectories are also available using this approach. The second part is the design of a feedback controller that maps these state trajectories to the computed input signal in an approximate manner. Since this input signal can be a complicated signal, it is expected that a nonlinear controller has more potential to generate a control signal that is close to the computed input than a linear controller has. Therefore, as a starting point, we propose to use a nonlinear (polynomial) full-state feedback controller. Stability analysis of the resulting closed-loop system is the final part of the controller synthesis. Since the closed-loop system is chosen polynomially, sum-of-squares techniques, see [105–107, 112, 113], can be used to a posteriori analyze its stability properties.
The computation of an input signal that meets certain time-domain constraints is discussed in Section 5.2. In Section 5.3, a nonlinear full-state feedback law is constructed and the (local) stability of the resulting closed-loop system is analyzed. An illustrative example is given in Section 5.4 and a comparison is made between the best linear and nonlinear static full-state feedback controllers. The proposed method is validated experimentally on a fourth-order motion system in Section 5.5.

5.2 Computation of the time-optimized input signal for a given control task

In this section, we shortly review the constrained polynomial interpolation technique from [55] for completeness and show in the end how it can be used in the context of time-optimal control. Consider a SISO linear time-invariant system in state-space description

$$\begin{aligned} \dot{x}(t) &= Ax(t) + Bu(t) \\ y(t) &= Cx(t) + Du(t), \end{aligned} \tag{5.1}$$

where $x(t) \in \mathbb{R}^n$ is the state-vector, $u(t) \in \mathbb{R}$ is the control input-vector, $y(t) \in \mathbb{R}$ is the output vector at time $t \in \mathbb{R}_+$, A, B, C and D are matrices of appropriate dimensions, and the initial state $x(0)$ is taken to be 0. The goal is to compute a control signal u in the given finite time-interval $t \in [t_0,\ t_f]$ such that the system's input u, output y and their respective k^{th}-order derivatives $u^{(k)},\ y^{(k)}$ meet the

interpolation constraints

$$\begin{array}{rcl} u^{(k_j)}(t_j) & = & u_j \\ y^{(k_j)}(t_j) & = & y_j \end{array} \quad \text{for } j \;=\; 0,\; \ldots,\; M, \tag{5.2}$$

and the bounds

$$\begin{array}{rcccl} u_i^{\min} & \leq & u^{(k_i)}(t) & \leq & u_i^{\max} \\ y_i^{\min} & \leq & y^{(k_i)}(t) & \leq & y_i^{\max} \end{array} \quad \text{for } i \;=\; 0,\; \ldots,\; N \text{ and all } t \in [t_0,\; t_f], \tag{5.3}$$

where $k_i, k_j \geq 0$ are given integers, $u_j, y_j,\ j{=}0, \ldots, M$, and $u_i^{\min}, u_i^{\max}, y_i^{\min}, y_i^{\max}$, $i{=}0, \ldots, N$ are given real numbers and M and N are the number of interpolation and bound constraints, respectively. To this end, system (5.1) can be expressed in the Laplace domain (using $x(0){=}0$) as a right coprime polynomial matrix fraction

$$y(s) = b_r(s)a_r^{-1}(s)u(s), \tag{5.4}$$

with $a_r = \sum_m a_{r,m}s^m$ and $b_r = \sum_m b_{r,m}s^m$ their polynomial expansion where $a_{r,m}$ and $b_{r,m}$ denote the m^{th} element of a_r and b_r, respectively. Under the coprimeness assumption on the pair $(a_r(s), b_r(s))$ there exists a polynomial matrix pair $(x_l(s), y_l(s))$ that satisfies the Bézout identity

$$x_l(s)a_r(s) + y_l(s)b_r(s) = 1. \tag{5.5}$$

The flat output [85] of system (5.4) is defined in the Laplace domain by

$$x^f(s) = x_l(s)u(s) + y_l(s)y(s). \tag{5.6}$$

By virtue of the Bézout identity (5.5), the input u and the output y can be expressed in the Laplace domain as linear combinations of the flat output $x^f(s)$

$$\begin{array}{rcccl} u(s) & = & a_r(s)x^f(s) & = & (\sum_m a_{r,m}s^m)x^f(s) \\ y(s) & = & b_r(s)x^f(s) & = & (\sum_m b_{r,m}s^m)x^f(s), \end{array} \tag{5.7}$$

or, equivalently in the time-domain as linear combinations of $x^f(t)$ and its k^{th}-order derivatives $x^{f(k)}(t)$ via

$$\begin{array}{rcl} u(t) & = & \sum_m a_{r,m}x^{f(m)}(t) \\ y(t) & = & \sum_m b_{r,m}x^{f(m)}(t). \end{array} \tag{5.8}$$

Therefore, algebraic time-domain constraints on u and y can be translated into algebraic constraints on the flat output vector x^f. The interpolation constraints (5.2) can then be written as

$$\begin{array}{rcl} \sum_m a_{r,m}x^{f(m+k_j)}(t_j) & = & u_j \\ \sum_m b_{r,m}x^{f(m+k_j)}(t_j) & = & y_j \end{array} \quad j \;=\; 0,\; \ldots,\; M. \tag{5.9}$$

The bound constraints (5.3) as a function of the flat output are transformed into

$$\begin{array}{rcccl} u_i^{\min} & \leq & \sum_m A_{r,m} x^{f(m+k_i)}(t) & \leq & u_i^{\max} \\ y_i^{\min} & \leq & \sum_m B_{r,m} x^{f(m+k_i)}(t) & \leq & y_i^{\max}, \end{array} \tag{5.10}$$

which can be converted into the non-negativity constraints

$$g_i(t) \geq 0, \quad t \in [t_0, t_f], \quad i = 1, 2, \ldots, 2N \tag{5.11}$$

on a set of scalar polynomials $g_i(t)$. We will approximate $x^f(t)$ by a polynomial of given degree μ of the form

$$x^f(t) = \sum_{\mu} x_\mu^f t^\mu. \tag{5.12}$$

In this case, the interpolation constraints (5.9) are linear in the coefficients x_μ^f of the polynomial $x^f(t)$ and hence the set of all interpolation constraints can be written as

$$F x_{c\mu}^f = f, \tag{5.13}$$

where F is a given matrix, f is a given vector and $x_{c\mu}^f$ denotes the column vector consisting of the coefficients x_μ^f of the flat output polynomial that need to be determined. The coefficient vectors g_i of $g_i(t)$ depend affinely on the coefficient vector $x_{c\mu}^f$ via

$$G_i x_{c\mu}^f + c_i = g_i, \quad i = 1, 2, \ldots, 2N, \tag{5.14}$$

for a given vector G_i and scalar c_i. The original trajectory planning problem with bound constraints can therefore be cast into an equivalent problem requiring positivity of a univariate polynomial problem (5.11) on an interval and subject to linear constraints (5.13) and (5.14). This can be reformulated as an LMI problem as discussed in Section 4.2.2.
An input signal can now be computed for a specific control task over a fixed interval $[t_0,\ t_f]$ that satisfies (5.9) and (5.10). Although it was assumed that the initial condition of system (5.1) was zero during the derivation of this LMI problem, initial conditions other than zero can be imposed through the interpolation constraints (5.9). Since we are interested in driving the system from a given initial condition to its equilibrium as fast as possible, the minimum value of t_f needs to be determined such that the constraints are still satisfied. However, direct optimization of the minimum time t_f is a non-convex problem and is hence performed via a bisection method.

5.3 Nonlinear state feedback and stability

This section focusses on the design of a state feedback law, based on the computed time-optimized input and state signals, as obtained in the previous section.

5.3.1 Construction of the nonlinear state feedback

The input signal obtained by the method of the previous section can be applied to the system in order to realize the optimized response. However, such a feedforward approach is known to be sensitive to small variations in the plant dynamics, disturbances, and to unmodeled dynamics. Furthermore, the input signal is specifically computed for a single initial condition, and nonlinear feedforward cannot cope with regulation of other initial conditions. Therefore, to make the performance and stability more robust for such variations, we aim at designing a closed-loop configuration. The computed input signal is constructed from the system's state trajectories to obtain the feedback law. More specifically, a polynomial feedback law is considered as (i) polynomial feedbacks have a relatively simple structure, (ii) every continuous function in a compact time interval can be uniformly approximated as closely as desired by a polynomial function, as stated by the Weierstrass approximation theorem [77], and (iii) stability properties of polynomial (closed-loop) systems can be evaluated in a systematic way, as will be discussed in Section 5.3.2. To compute the polynomial state feedback law, the following least-squares data-fitting problem is considered:

$$\begin{array}{ll} \text{Find} & \theta \\ \text{such that} & \sum_i^{N_{\text{fit}}} (F(\theta, x_1^*(t_i), \ldots, x_n^*(t_i)) - u^*(t_i))^2 < \gamma_{\text{fit}} \end{array} , \tag{5.15}$$

where $u(t)$ is the optimized input signal obtained from Section 5.2, γ_{fit} is the desired level of accuracy, and N_{fit} is a given number that determines the number of data-points that is used in the data-fitting problem. Index i is used to specify each data-point corresponding to time t in the interval $[t_0,\ t_f]$, $x_j^*(t_i)$ denotes the value of the j^{th} state at time t_i of the optimized state trajectory x^*, and n represents the number of states. The function $F(\theta, x_1^*, \ldots, x_n^*)$ contains all possible monomials in n states for a given degree d, and with coefficients θ. For example, if $n=2$, the function $F(\theta, x_1^*, x_2^*)$ is described by

$$F(\theta, x_1, x_2) \quad = \quad \sum_{p=0}^{d_p} \sum_{q=0}^{d_q} \theta_{pq} x_1^p x_2^q. \tag{5.16}$$

The resulting closed-loop system is given by

$$\dot{x} = f(x) = Ax + BF(\theta^*, x), \tag{5.17}$$

where $F(\theta^*, x)$ is the nonlinear state feedback polynomial obtained from (5.15).

5.3.2 Stability and estimation of the region of attraction

In case we are interested in regulation to the origin, a minimal requirement on (5.17) would be stability of the origin for all initial conditions of interest. However,

as closed-loop system (5.17) is completely described by polynomial differential equations, it generally has multiple equilibria. As a consequence, the system does not stabilize to the origin for all initial conditions. In these cases it is of interest to determine the region of attraction, as defined by [75]

$$R_A := \{x_0 \in \mathbb{R}^n \mid \phi(t, x_0) \to 0 \text{ as } t \to \infty\}, \tag{5.18}$$

where $\phi(t, x_0)$ denotes the solution of (5.17) that starts at initial state x_0 at time $t=0$. To assess the stability of such a nonlinear system and verify that the region of attraction corresponding to the origin is sufficiently large to include all initial states of interest, a general method is to search for Lyapunov functions to prove global or local stability. A powerful tool to compute Lyapunov functions and estimates of the region of attraction for polynomial systems can be based on using the sum-of-squares (SOS) method, see Appendix A.1 and [106]. Local asymptotic stability of the origin of (5.17) can be guaranteed by finding a continuously differentiable Lyapunov function $V : \mathcal{D} \to \mathbb{R}$ in some region $\mathcal{D} \subseteq \mathbb{R}^n$ of the state-space that contains the origin and satisfies

$$V(0) = 0 \text{ and } V(x) > 0 \text{ for all } x \in \mathcal{D} \setminus \{0\}, \tag{5.19}$$

$$\dot{V}(x) = \frac{\partial V}{\partial x} f(x) < 0 \text{ for all } x \in \mathcal{D} \setminus \{0\}. \tag{5.20}$$

When asymptotic stability of the origin is established, an estimate of the region of attraction is given by the largest level set of the Lyapunov function $V(x)$

$$\Omega_\gamma = \{x \in \mathbb{R}^n \mid V(x) \leq \gamma\}, \tag{5.21}$$

which is bounded and strictly contained in $\mathcal{D}$.
It is well-known that for linear systems the existence of a quadratic Lyapunov function of the form $V(x) = x^T P x$ is necessary and sufficient to prove stability. However, for systems with polynomial vector fields, the existence of a quadratic Lyapunov function is only sufficient to prove stability, and hence, considering only quadratic Lyapunov functions is generally conservative. To reduce this conservatism, we consider Lyapunov functions that are polynomial in the states. In this case, (5.19) and (5.20) become polynomial (non)negativity conditions. To consider also strict inequalities, we modify (5.19) and (5.20) into $V(x) \geq \varphi_1(x)$ and $\frac{\partial V}{\partial x} f(x) \leq -\varphi_2(x)$, respectively, where

$$\varphi_\ell(x) = \sum_{i=1}^{n} \sum_{j=1}^{d} \epsilon_{ij} x_i^{2j}, \quad \ell = 1, 2, \tag{5.22}$$

such that

$$\sum_{j=1}^{d} \epsilon_{ij} > \beta \;\forall\; i = 1, \ldots, n, \tag{5.23}$$

with β a positive number and $\epsilon_{ij} \geq 0$ for all i and j. If we select $\mathcal{D}$ with 0 in the interior of $\mathcal{D}$ as

$$\mathcal{D} = \{x \in \mathbb{R}^n \mid a(x) \leq 0\}, \tag{5.24}$$

with $a(x)$ a suitable polynomial, problem (5.19), (5.20) transforms into checking positivity of polynomials on a semialgebraic set

$$V(x) - \varphi_1(x) \geq 0, -\frac{\partial V}{\partial x} f(x) - \varphi_2(x) \geq 0 \quad \text{for all} \quad x \in \mathcal{D}, \tag{5.25}$$

for which an equivalent LMI problem can be formulated, see Appendix A.2.
The estimate of the region of attraction (5.21) is in general conservative and in order to obtain good estimates of the region of attraction, one has to iterate between choosing $V(x)$ and $a(x)$, for instance in the following manner [105]. First, initialize the region of interest $a(x)$ as a ball of radius ζ, i.e., $a(x) = x^T x - \zeta$ and search for a second order Lyapunov function $V(x)$ through maximizing ζ via a bisection algorithm. Then determine the largest level set of $V(x)$ that is completely contained in the set $\frac{\partial V}{\partial x} f(x) < 0$, and use the level set $V(x) - \gamma$ as the new region of interest $a(x)$. Increase the order of the Lyapunov function by 2 and search for a new Lyapunov function while maximizing γ. Iterate this procedure until a satisfactory estimate, i.e., such that (5.21) includes the initial state values for which the control task has been designed, is obtained. In case the order of closed-loop system (5.17) becomes very high, an alternative to the single high degree Lyapunov function is the use of composite Lyapunov functions in order to keep the number of decision variables low [140].

5.3.3 Discussion on the synthesis procedure

A priori, it is not known what mapping $F(\theta, x)$ of the states should be used to construct a feedback law that yields satisfactory performance and robustness for all initial conditions of interest. Furthermore, the parameter θ in (5.15) influences the region of attraction as well. Since no LMI-based method is known that simultaneously constructs a feedback law yielding satisfactory performance and optimizes the region of attraction, we propose an iterative procedure to synthesize the nonlinear state feedback. Start by considering a function $F(\theta, x)$ of low degree d, choose the accuracy γ_{fit} and compute an estimate of the region of attraction via the algorithm in Section 5.3.2. If the performance is satisfactory, i.e., the system's response to the initial condition obtained by the feedback is close to the initially constructed optimal time trajectory, but the provable region of attraction is too small, one can try to decrease the accuracy (increase γ_{fit}) to arrive at a feedback with a larger provable region of attraction. If both are unsatisfactory, increase the degree d of the feedback. Iterate until both the performance and the region of attraction are satisfactory. Unfortunately, convergence is not guaranteed and the synthesis remains in some sense based on trial-and-error. Furthermore, at this

point no guarantees can be given that the performance constraints will not be violated for an arbitrary initial condition within the found region of attraction. Hence, an important topic for future research is to improve the initial ideas presented in this chapter, leading to a systematic method to analyze and design the closed-loop with respect to constraint violation.

5.4 Illustrative Example

In this section the proposed method is illustrated by an example. Operations on polynomials were performed with the Polynomial Toolbox 2.5 [89], whereas the LMI problems were solved using the Yalmip [88] interface, and solver SeDuMi 1.1 [138].

5.4.1 Computation of the desired input signal

Consider the following second order motion system

$$\dot{x}(t) = \begin{bmatrix} 0 & 1 \\ 0 & 0 \end{bmatrix} x(t) + \begin{bmatrix} 0 \\ 1 \end{bmatrix} u(t), \quad x(t_0) = \begin{bmatrix} 1 \\ 0 \end{bmatrix}, \tag{5.26}$$

where the state vector $x(t) = [x_1(t), x_2(t)]^T$ at time $t \in \mathbb{R}_+$ contains the position and velocity of a mass m in [m] and $[\frac{\text{m}}{\text{s}}]$, respectively. Furthermore, $m = 1$ kg and the input $u(t)$ at time $t \in \mathbb{R}_+$ is the force F in [N] applied to the mass. We assume that the actuator can deliver a force with a maximum of 10 N. The goal is to drive the system from its initial condition to the zero equilibrium as fast as possible, subject to additional constraints. The interpolation constraints (5.2) are: $x_1(0) = 1,\ x_2(0) = x_1(t_f) = x_2(t_f) = u(t_f) = \dot{u}(t_f) = 0$, where the final time t_f is to be minimized. To guarantee the absence of overshoot and input saturation, the following bound constraints (5.3) are added

$$\begin{array}{rcccl} 0 & \leq & x_1(t) & \leq & 1 \\ -10 & \leq & u(t) & \leq & 10. \end{array} \tag{5.27}$$

The order of the polynomial function (5.12) approximating the trajectory of the flat output x_f still has to be chosen. In general, a higher order of the polynomial results in a faster response, since more freedom is provided to minimize the final time t_f. However, a higher order also requires more computations, since the size of the resulting LMI problem becomes larger. Therefore, a trade-off should be made between the computational burden and the approximation error of the solution. The state trajectories and required input obtained with a seventh order flat output polynomial are depicted in Figure 5.1(a), the computation of which can be found in Appendix A.4. In the same figure, the well-known bang-bang solution is depicted. This solution is known to be time-optimal for this problem

without the constraint $\dot{u}(t_f) = 0$, and results in the final time $t_f = 0.63$ s. From the response in Figure 5.1, it can be seen that no overshoot occurs and the initial position and velocity as well as the conditions at the optimized final time $t_f = 0.76$ are satisfied. Furthermore, for this time-optimized control signal, the actuator signal does not violate the imposed saturation constraint. It can be concluded that indeed all interpolation and bound constraints are satisfied.

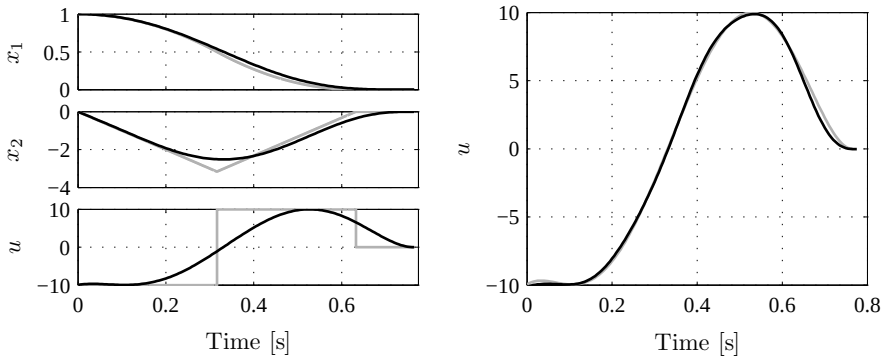

(a) (b)

Figure 5.1: (a) State trajectories $x_1(t), x_2(t)$ and required input $u(t)$ corresponding to the polynomial optimization problem (black) and the bang-bang solution (grey), (b) optimized input signal $u(t)$ (grey) and mapped feedback (black).

5.4.2 Construction of the nonlinear state feedback

A nonlinear state feedback law can now be obtained by mapping the desired state trajectories x_1, x_2 onto the computed input signal u. In this case, a mapping was found consisting of all possible monomials of degree 1 up to 4, described by

$$\begin{aligned} F(x) = &-297.63x_1 - 31.92x_2 + 203.56{x_1}^2 + 87.34x_1x_2 - 6.58{x_2}^2 + 132.35{x_1}^3 \\ &+ 142.99{x_1}^2x_2 + 12.74x_1{x_2}^2 - 9.22{x_2}^3 - 48.34{x_1}^4 - 199.35{x_1}^3x_2 \\ &+ 7.92{x_1}^2{x_2}^2 - 3.74x_1{x_2}^3 - 1.17{x_2}^4. \end{aligned} \tag{5.28}$$

This mapping is depicted in Figure 5.1(b). The resulting closed-loop system is then described by the polynomial differential equations

$$\begin{aligned} \dot{x}_1 &= x_2 \\ \dot{x}_2 &= F(x). \end{aligned} \tag{5.29}$$

Since the resulting closed-loop system is of second order, stability can easily be assessed by inspecting the phase portrait. The phase portrait and equilibria of the resulting closed-loop are shown in Figure 5.2.

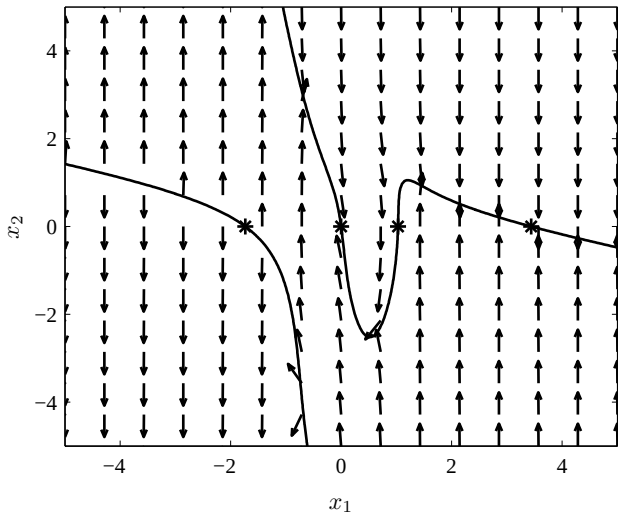

Figure 5.2: Phase portrait of the resulting closed-loop system, together with the hypersurface given by $F(x)=0$ and the equilibria (stars).

5.4.3 Stability and performance analysis

Since (5.29) has four equilibria, the origin is not a global attractor and as a consequence the region of attraction of the origin is not $\mathbb{R}^2$. To obtain an estimate of the region of attraction Ω_γ and to determine if all initial states of interest are inside this region, the method as described in Section 5.3.2 is used. Starting by searching for the largest level set of a second order Lyapunov function in a circular area around the origin, the first estimate of the region of attraction is depicted in Figure 5.3(a). In this figure, the dark grey area denotes the region where $\frac{\partial V}{\partial x} f(x) > 0$, the light grey area is the area where $\frac{\partial V}{\partial x} f(x) < 0$, and the solid black line is the largest level set of $V(x)$ contained in the area where $\frac{\partial V}{\partial x} f(x) < 0$, i.e., an approximation of the region of attraction. The arrows denote the direction of the vector field of the closed-loop system and the dashed black line is the hypersurface given by $F(x)=0$. The estimates of the region of attraction with the subsequent higher order Lyapunov functions are depicted in Figure 5.3(b)-(d). When an eighth order Lyapunov function is used, the provable region of attraction includes the initial state $[1\ 0]^T$, and hence the designed feedback law is stabilizing for the posed regulation problem. The system's response (taking into account the bounds

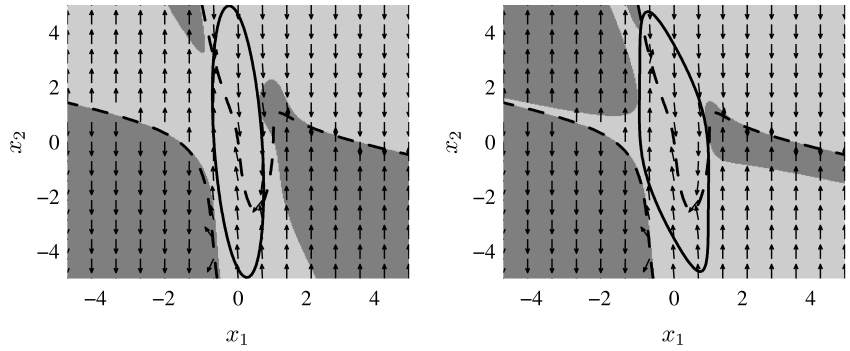

Figure 5.3: Estimates of the region of attraction (solid) for increasing order of the Lyapunov functions together with the hypersurface given by $F(x) = 0$ (dashed). (a) Second order Lyapunov function, (b) fourth order Lyapunov function, (c) sixth order Lyapunov function, (d) eight order Lyapunov function.

on the input) with respect to the initial conditions $x_0 = [1\ 0]^T$, $x_0 = [0.7\ 0]^T$, and $x_0 = [0.4\ 0]^T$ (all within the region of attraction) are depicted in Figure 5.4 (obtained via simulation). The performance is measured by the standard regulation indicators fall-time t_{fall}, settling-time t_{s} and percentage overshoot p_{os} of the response, defined by

$$\begin{aligned} t_{\text{fall}} &= \min\{T \in \mathbb{R}_+ \mid x_1(T) = 0.1x_0\} - \min\{T \in \mathbb{R}_+ \mid x_1(T) = 0.9x_0\} \\ t_{\text{s}} &= \min\{T \in \mathbb{R}_+ \mid |x_1(t)| \leq 0.02 \text{ for all } t \geq T\} \\ p_{\text{os}} &= |\min\{x_1(t) \mid t \geq 0\}| \times 100\%, \end{aligned} \tag{5.30}$$

and shown in Table 5.1. Since the goal of the method focusses on regulating the system to its origin as fast as possible without overshoot, satisfactory performance is obtained when the settling-time is close to the computed optimized final time $t_f = 0.76$ s, the rise-time is small, and there is little overshoot. As can be seen in Table 5.1, the interpolation and bound constraints are almost satisfied and the responses exhibit satisfactory settling-times and overshoot. While stability with

x_0	t_{fall}	t_{s}	p_{os}
[1.0 0]	0.38	0.62	0.10
[0.7 0]	0.30	0.51	0.15
[0.4 0]	0.23	0.39	0.26

Table 5.1: Performance measures for various initial conditions.

respect to different initial conditions (robust stability) can be analyzed through the computed region of attraction, it cannot be guaranteed that robust performance, i.e., satisfactory performance for each initial condition, is obtained for this region. Some insight in the performance can be obtained by means of simulation. As can be observed from the phase portrait, although the feedback is stabilizing

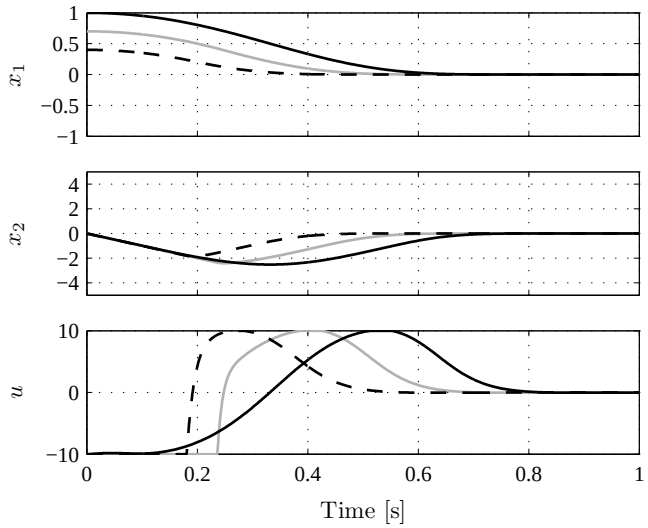

Figure 5.4: Response to various initial conditions: $x_0 = [1\ 0]^T$ (solid black), $x_0 = [0.7\ 0]^T$ (solid grey), $x_0 = [0.4\ 0]^T$ (dashed black).

for the initial state $x_0 = [1\ 0]^T$, the closed-loop is unstable when a starting position is used that is slightly larger than 1. If a larger region of attraction is desired, another design should be made. Following the procedure of Section 5.3.3, a ninth order flat output vector is used (resulting in a final time $t_f = 0.75$), and a state feedback is taken of third order, resulting in a globally stabilizing feedback. This

feedback is given by

$$F(x) = -4.83x_1 - 22.13x_2 + 7.86{x_1}^2 + 19.19x_1x_2 - 12.42{x_2}^2 - 13.51{x_1}^3 - 1.41{x_1}^2x_2 + 4.69x_1{x_2}^2 - 2.14{x_2}^3, \tag{5.31}$$

and a Lyapunov function proving global stability is

$$V(x) = 1.43{x_1}^2 + 0.07x_1x_2 + 0.03{x_2}^2. \tag{5.32}$$

The phase portrait of the resulting closed-loop and the response to various initial conditions are depicted in Figure 5.5. As can be seen from Figure 5.5(a), the

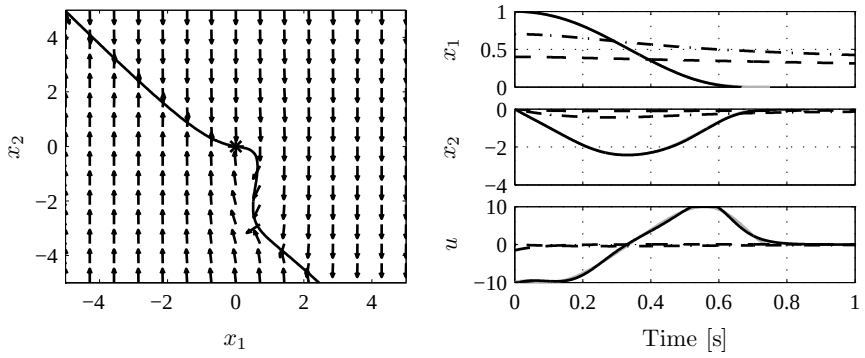

(a) (b)

Figure 5.5: (a) Phase portrait of the resulting closed-loop system, together with the hypersurface given by $F(x) = 0$, (b) response to various initial conditions, $x_0 = [1\ 0]^T$ (solid black), $x_0 = [0.7\ 0]^T$ (dash-dot black), $x_0 = [0.4\ 0]^T$ (dashed black). The computed optimized signals $x_1(t), x_2(t), u(t)$ are shown in grey.

origin is a global attractor. The regulation performance of this controller is given in Table 5.2. From this table it is clear that the performance of other initial

x_0	t_{fall}	t_{s}	p_{os}
[1.0 0]	0.38	0.61	1.30
[0.7 0]	8.79	16.48	0.0
[0.4 0]	10.09	17.94	0.0

Table 5.2: Performance measures for various initial conditions.

conditions than the one the design was made for is worse when compared to Table 5.1, especially when the settling-time is considered. Thus although a much larger region of attraction is obtained, i.e., the entire state-space, the regulation performance is worse than in the previous design.

5.4.4 Linear vs. nonlinear state feedback

The closed-loop system (5.29) has been obtained, which guarantees that starting from initial condition $x_0 = [1\ 0]^T$, the system returns to the origin. The computed input signal and desired state trajectories (see Figure 5.1(a)) could not be mapped onto a static linear state feedback. It is interesting to see what the actual benefit of the nonlinear state feedback controller (5.28) is over a static linear state feedback controller. This linear state feedback controller must satisfy the input constraint $|u(t)| = |-Kx(t)| \leq 10$ N and is optimized for minimum fall-time, settling-time and overshoot. In order to find the static linear state feedback controller that satisfies the input constraint and has the smallest fall-time, settling-time and overshoot, trade-off curves [13] can be created. The trade-off plot between fall-time and overshoot is depicted in Figure 5.6(a) and is obtained by varying the pole-locations of the closed-loop system $\dot{x}(t) = (A - BK)x(t)$ and considering the response to initial condition $x_0 = [1\ 0]^T$, where only the controllers that satisfy the actuator constraint are admitted. The best static linear state feedback controller was determined by minimizing the Euclidian norm of the three time-domain specifications, resulting in an optimal solution with respect to the three performance constraints. The simulated responses to initial conditions $x_0 = [1\ 0]^T$, $x_0 = [0.7\ 0]^T$, and $x_0 = [0.4\ 0]^T$, together with the corresponding inputs are shown in Figure 5.6(b). Implementation of the optimal linear controller for $x_0 = [1\ 0]^T$ results in a fall-time of 0.78 s, settling-time of 1.19 s and an overshoot of 1.6%. The proposed nonlinear controller (5.28) yields for the same initial condition a fall-time of 0.38 s, a settling-time of 0.62 s and 0.10% overshoot. From these figures it can be concluded that the proposed nonlinear state feedback controller outperforms its linear counterpart, at least for the chosen initial conditions within the found region of attraction.

Remark 5.1 Until now only regulation of the states to the zero equilibrium has been considered. To be able to perform pick-and-place tasks where the goal is to drive the system from a given initial state to a desired final state, an error-space approach can be used. Consider for example the problem of driving system (5.26) from initial condition $x(0) = [0\ 0]^T$ to final condition $x(t_f) = [1\ 0]^T$ as fast as possible. Analogously to the procedure from Section 5.4.1, a time-optimized input signal u can be computed that satisfies the bound constraints (5.27) and the interpolation constraints $x_1(0) = x_2(0) = x_2(t_f) = u(t_f) = \dot{u}(t_f) = 0$ and $x_1(t_f) = 1$. The main difference is that in the pick-and-place control setup, the error is regulated to the zero equilibrium instead of the states. Therefore, the computed input signal $u(t)$ is constructed by a nonlinear feedback of the form

$$u = F(\theta, e_1, e_2) \quad = \quad \sum_{p=0}^{d_p} \sum_{q=0}^{d_q} \theta_{pq} e_1^p e_2^q, \tag{5.33}$$

where $e_1(t) = 1 - x_1(t)$, and $e_2(t) = -x_2(t)$. The closed-loop system in terms of

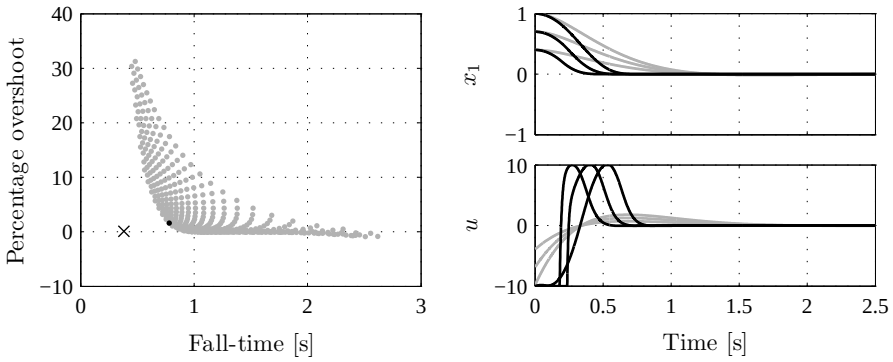

(a) (b)

Figure 5.6: Comparison linear and nonlinear state feedback. (a) Trade-off plot between fall-time and overshoot: linear state feedback controllers (grey dots), best linear state feedback controller (black dot), nonlinear state feedback controller (5.28) (cross), (b) response of the best linear state feedback controller (grey), and of the nonlinear state feedback controller (black).

the error is given by

$$\begin{aligned} \dot{e}_1(t) &= e_2(t) \\ \dot{e}_2(t) &= -f(e(t)), \end{aligned} \tag{5.34}$$

and stability can be verified by searching for Lyapunov functions that are a function of the error. □

5.5 Practical example

In this section experimental results on the fourth-order dual rotary motion system depicted in Figure 3.5 are presented. The first mass is driven by a motor and the positions of both masses are measured by encoders. In order to obtain the required state-space model, frequency response measurements have been performed, followed by parametric identification. The resulting state-space representation is given by

$$\dot{x}(t) = \begin{bmatrix} 0 & 1 & 0 & 0 \\ -46464 & -2.9452 & 46464 & -2.9452 \\ 0 & 0 & 0 & 1 \\ 57013 & 3.6138 & -57013 & -3.6138 \end{bmatrix} x(t) + \begin{bmatrix} 0 \\ 4894.8 \\ 0 \\ 0 \end{bmatrix} u(t), \tag{5.35}$$

with $x(t) = [\theta_1(t)\ \dot{\theta}_1(t)\ \theta_2(t)\ \dot{\theta}_2(t)]^T$ containing the positions and velocities of the two masses in [rad] and $[\frac{\text{rad}}{\text{s}}]$ respectively and $u(t)$ the input in [V]. The frequency response function of the transfer from the input to θ_1 and θ_2, together with the identified model are depicted in Figure 5.7(a) and (b), respectively. In order to

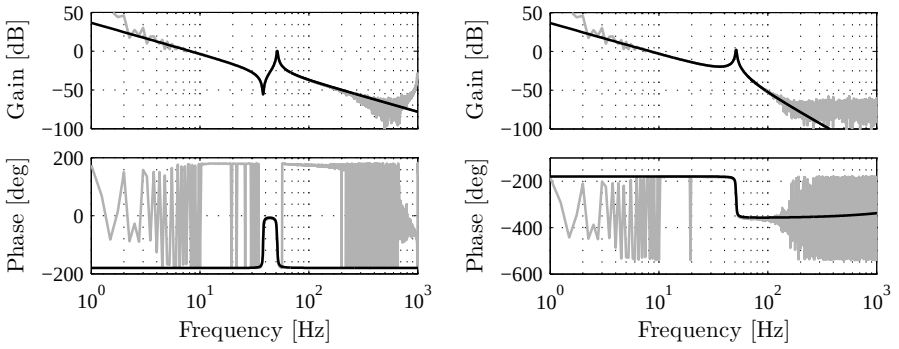

Figure 5.7: Measured frequency response function (grey) and identified model (black). (a) From the input u to θ_1, (b) from the input u to θ_2.

design a state feedback that drives the system from its initial position to the zero equilibrium, an input is computed with the constrained polynomial interpolation technique. The following interpolation constraints are imposed: $\theta_1(0) = \theta_2(0) = 100, \quad \dot{\theta}_1(0) = \dot{\theta}_2(0) = \theta_1(t_f) = \dot{\theta}_1(t_f) = \theta_2(t_f) = \dot{\theta}_2(t_f) = u(t_f) = \dot{u}(t_f) = 0$, where the final time t_f needs to be minimized. The rotational speed of the motor is limited to 450 $\frac{\text{rad}}{\text{s}}$ and since overshoot and actuator saturation are undesirable, the following bound constraints are formulated

$$\begin{array}{rcccl} -450 & \leq & \dot{\theta}_1(t) & \leq & 450, \\ 0 & \leq & \theta_1(t) & \leq & 100, \\ -2.5 & \leq & u(t) & \leq & 2.5. \end{array} \tag{5.36}$$

A 6^{th}-order flat output polynomial was generated, with a minimized final time of $t_f = 0.44$ s. The time trajectories are transformed into a state feedback law by using the second order nonlinear function

$$\begin{aligned} F(x) = &-0.231\theta_1 - 1.93 \cdot 10^{-2}\dot{\theta}_1 - 0.232\theta_2 + 1.472 \cdot 10^{-3}\theta_1^2 \\ &+ 9.376 \cdot 10^{-5}\theta_1\dot{\theta}_1 + 4.168 \cdot 10^{-5}\dot{\theta}_1^2 + 1.472 \cdot 10^{-3}\theta_1\theta_2 \\ &+ 9.376 \cdot 10^{-5}\dot{\theta}_1\theta_2 + 1.472 \cdot 10^{-3}\theta_2^2. \end{aligned} \tag{5.37}$$

This nonlinear state feedback law is implemented on the experimental setup. Only the positions of the two masses can be measured and since full-state feedback is

considered, the two velocities have to be reconstructed. For this purpose a model-based linear full-state observer is designed to obtain an estimate of both velocities. The results of this experiment, together with the designed state trajectories and the input signal are depicted in Figure 5.8. As can be seen, the system is regulated to the origin from its initial position in the optimized final time t_f, without overshoot, and the actuator and velocity constraints are satisfied.

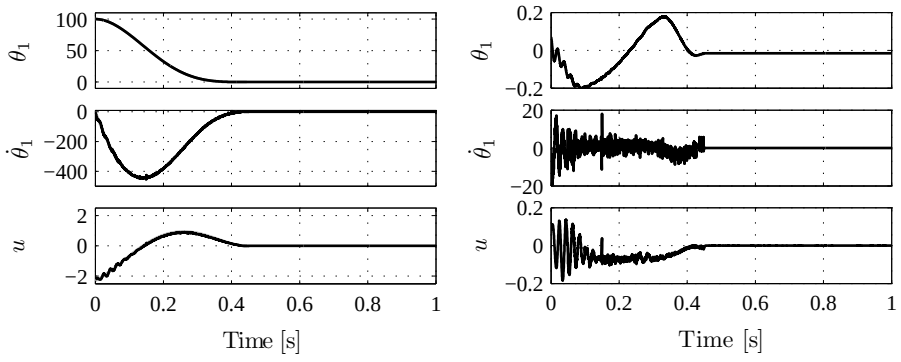

(a) (b)

Figure 5.8: (a) Calculated system signals θ_1, $\dot{\theta}_1$, u (grey) and the experimental results (black), (b) difference between the calculated system signals θ_1, $\dot{\theta}_1$, u and the experimental results.

Some slight differences occur between the experimental and calculated system signals, as is obvious from Figure 5.8(b). The main reason lies in the fact that the system is represented by a fourth order linear model, while in reality there is some unmodeled dynamics and some friction, even though it may be small. Furthermore, an observer is implemented to provide an *estimate* of the velocities. Although this gives a good approximation, it will not exactly resemble the actual velocity profile. These observations support the idea that the closed-loop approach is robust for small variations. Another reason for a closed-loop approach was mentioned, namely robustness with respect to different initial conditions. In Figure 5.9(a) the responses to initial conditions $x_0 = [100\ 0\ 100\ 0]^T$ (solid black), $x_0 = [60\ 0\ 60\ 0]^T$ (dashed black), and $x_0 = [20\ 0\ 20\ 0]^T$ (solid grey) are depicted. As can be seen, the performance is satisfactory since other initial conditions than the one designed for are regulated to zero while fulfilling the imposed constraints. In case a negative initial condition is used for θ_1, the proposed feedback law (5.37) results in an unstable closed-loop due to the even terms. To obtain a stabilizing feedback law for both positive and negative initial conditions for θ_1, the even terms of (5.37) are premultiplied by the sign of the first state of the system resulting in

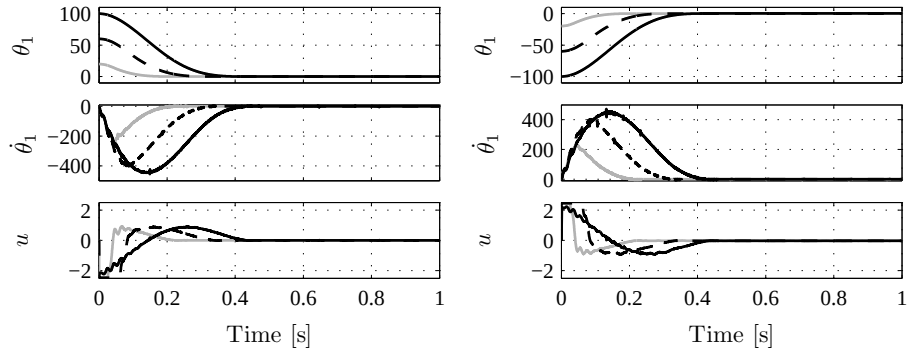

(a) (b)

Figure 5.9: Response to different initial conditions. (a) Positive valued initial conditions, (b) negative valued initial conditions.

the control law

$$\begin{aligned} F(x) = &-0.231\theta_1 - 1.93 \cdot 10^{-2}\dot{\theta}_1 - 0.232\theta_2 + 1.472 \cdot 10^{-3}\,\mathrm{sign}(\theta_1)\theta_1^2 \\ &+ 9.376 \cdot 10^{-5}\,\mathrm{sign}(\theta_1)\theta_1\dot{\theta}_1 + 4.168 \cdot 10^{-5}\,\mathrm{sign}(\theta_1)\dot{\theta}_1^2 \\ &+ 1.472 \cdot 10^{-3}\,\mathrm{sign}(\theta_1)\theta_1\theta_2 + 9.376 \cdot 10^{-5}\,\mathrm{sign}(\theta_1)\dot{\theta}_1\theta_2 \\ &+ 1.472 \cdot 10^{-3}\,\mathrm{sign}(x_1)\theta_2^2. \end{aligned} \tag{5.38}$$

This nonlinear feedback is the same as (5.37) in case positive valued initial conditions are used for θ_1 and is also able to regulate the system when it is subject to negative valued initial condition as is shown in Figure 5.9(b).

5.6 Conclusions and recommendations

In this chapter, a time-domain performance based approach for nonlinear state feedback controller design for linear systems has been presented. The application of the method focussed on regulating the system to its origin (or another state of interest) as fast as possible without overshoot. The nominal design is done for one specific initial condition but the resulting nonlinear controller is able to regulate the system for other initial conditions as well, as long as they are within the region of attraction of the closed-loop system. However, although the closed-loop system is guaranteed to be stable for these other initial conditions, satisfaction of constraints or specifications on the performance cannot be a priori guaranteed and should be considered using simulations. The presented simulation and experimental cases showed that satisfactory performance for a range of initial conditions

can be achieved, and that the proposed nonlinear state feedback controller can outperform its linear counterpart.
Although only regulation was considered, pick-and-place tasks in which the goal is to drive the system from a given initial condition to a given final state while taking into account time-domain specifications can be handled by considering an error-space approach. Furthermore, the state feedback design could also be effective in a disturbance setting. Indeed, if the system is subject to non-persisting external disturbances (like shocks), the controller will regulate the system to its origin as long as the disturbances do not steer the system to a state outside the region of attraction. One should design the controller for a set of initial conditions which contains the states to which the expected disturbances can drive the system.
At this moment however, the ideas presented in this chapter should be regarded as first steps towards a general systematic design method suitable for actual use in applications, since there are certain issues that still require further attention. Firstly, as stated in Section 5.3.3, the method lacks a procedure to systematically analyze the performance (including the violation of bounds) after a feedback law is obtained. Secondly, it would be interesting to combine the computation of the nonlinear state feedback with the construction of a Lyapunov function during the design, such that stability is guaranteed a priori. Ideally, the two issues mentioned above would be blended into one approach. This would result in a method to compute a nonlinear polynomial state feedback law that a priori guarantees stability and performance for a given set of initial conditions, while taking the specified time-domain constraints into account for one or more specific initial conditions. A third issue is the computational tractability of the method when the plant dynamics become more complicated. This is due to the fact that the constraint polynomial interpolation and the stability analysis are performed using LMIs. The currently available LMI solvers are not always able to come up with solutions for large problems, even if those problems are feasible. As the feedback law is computed a priori, i.e., off-line, the LMI computation does not hamper real-time application of the resulting controller. The polynomial feedback law itself is computationally cheap since only additions and multiplications of the state signals are performed. Another topic for future research is to investigate the possibility to track different reference signals (other than pick-and-place actions) with the proposed method.

Part III

Reset Control

Chapter 6

Introduction

This part of the thesis deals with the notion of reset control. In this chapter, previous research is discussed, two motivating examples from literature are presented and the contributions are stated.

6.1 Literature survey

A reset controller is a linear time-invariant system whose states, or subset of states, reset to zero whenever its input and output satisfy certain conditions. Reset control action has certain resemblance with a number of popular non-smooth control strategies including relay control [141], sliding mode control [27] and switching control [15]. A common feature of these methods is a switching surface used to trigger changes in the control signal. Distinctively, reset control employs the same (linear) control law on both sides of the switching surface. The rationale behind reset control can best be understood when considering an integrating controller in particular. An integrator 'sums' the error over time in order to achieve a zero steady-state error. However, when the error becomes zero for the first time, the integrator still has the 'summed' error stored in its states, and the subsequent 'emptying' of the integrator causes the error to overshoot. To reduce the overshoot, it might be beneficial to reset the state of this integrator to zero as soon as its input (the error) becomes zero. This way the integrator state, containing the 'summed' error, is emptied instantaneously, and hence the overshoot is avoided. This concept was indeed validated by simulations in recent publications [6, 23], showing a significant decrease of overshoot in the step response.
The concept of reset control was first introduced in 1958 by means of the resetting integrator of Clegg [26]. The describing function of the Clegg integrator has the

same magnitude plot as a linear integrator, but its performance limiting phase lag is only 38.1° instead of the normal 90°. However, the use of this Clegg integrator is not straightforward as its overall behavior was hard to analyze. As a consequence, it was not until 1974 that it was first used in a control design procedure in [78]. Subsequently, in [62], a *first order reset element (FORE)* was introduced, together with a controller design procedure based on frequency domain techniques. An overview of these results is given in [18].
In the late '90s there has been renewed interest in reset control systems, resulting in various stability analysis techniques. The first results were reported in [63] and [23], stating stability criteria for zero-input closed-loops with a second order plant and a Clegg integrator or a FORE, respectively. However, these criteria involve explicit computation of the reset times and closed-loop solutions, and are hard to generalize to higher order systems.
In following publications, stability conditions were formulated using Lyapunov-based conditions. This was first done in [5], in which only second order closed-loops with constant inputs were considered. These results have been extended in [24] to a sufficient criterion for bounded-input bounded-output (BIBO) stability, and later to the so-called H_β-condition [60]. The potential advantages of reset controllers over linear ones have been demonstrated both in simulations [6, 23] and experiments [18, 24, 154], and are especially apparent during the transient response. A clear overview of this work for general reset systems is provided in [7].
A closer view on the H_β-condition reveals that it is in fact a reformulation of Lyapunov-based stability linear matrix inequalities (LMIs) using the Kalman-Yakubovich-Popov (KYP) lemma, in order to provide computable conditions to check the stability of zero-input reset control systems. The analysis consists of two stability LMIs, one corresponding to the *flowing* of the closed-loop (i.e., smooth evolution of the state) and the other to the *reset* of the controller. These LMIs are coupled as a common quadratic Lyapunov function is employed. Therefore the H_β-condition is rather conservative, and is only necessary and sufficient for *quadratic* stability. Moreover, since the flowing LMI is solved for the complete state-space, it requires the linear part of the closed-loop dynamics to be stable, which already indicates some of the conservatism present in this approach.
This conservatism was reduced in some part by more recent publications [101, 151], where the authors suggested a slightly different resetting condition. Indeed, their idea to reset when controller in- and output have opposite sign instead of when the input is zero, results in a much smaller flow region. Therefore, the linear closed-loop does not need to be stable anymore and the stability bounds of the reset system are sharpened. Secondly, *piecewise quadratic* Lyapunov functions [72] were used, thereby allowing more flexibility in the Lyapunov function to capture a broader class of stability problems. Additionally, the analysis has been extended such that the closed-loop $\mathcal{L}_2$ gain from input to output of a reset control system can be approximated by an upperbound. So far, the work in [101, 151] is the most general analysis framework for reset control systems currently available in literature. However, it is not generally applicable, since it treats only FOREs and Clegg integrators. Furthermore, it does not include a solution to the tracking

problem, since its system description assumes a zero reference. In [152], this last issue is partly resolved as constant reference signals are considered.

6.2 Motivating examples

In this section, two examples from literature are presented comparing reset control to linear feedback. The goal is to demonstrate that reset control can outperform linear feedback control in certain circumstances. The first example is to show that the overshoot and settling-time to a step response can be reduced by using reset control.

6.2.1 Reducing overshoot and settling-time

This example is taken from [23]. Consider the closed-loop setup depicted in Figure 6.1, with plant P given by the transfer function

$$P(s) = \frac{s+1}{s(s+0.2)}, \tag{6.1}$$

and controller C the first order reset element given by the state-space description

$$\begin{aligned} \dot{x}_c &= -x_c + e, \quad && e \neq 0, \\ x_c^+ &= 0, && e = 0, \\ u &= x_c. \end{aligned} \tag{6.2}$$

Here, x_c is the reset controller state, $e = r - y$ the tracking error, and u the controller output. The superscript $+$ in x_c^+ is used to denote the time instant directly after a reset, since a reset is instantaneous. In absence of resetting, the

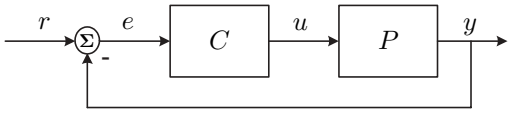

Figure 6.1: Closed-loop setup with a reset controller.

resulting closed-loop system is called the *base-linear system*. The step response of the reset control system and its base-linear system are depicted in Figure 6.2. As can be seen, the overshoot in the reset control system is reduced to approximately 40% as compared to almost 70% in the base-linear system's response. The reset controlled system also settles significantly faster than its linear counterpart. This simple comparison shows some of the potential benefits of introducing resets in control loops to improve the transient response of feedback control systems.

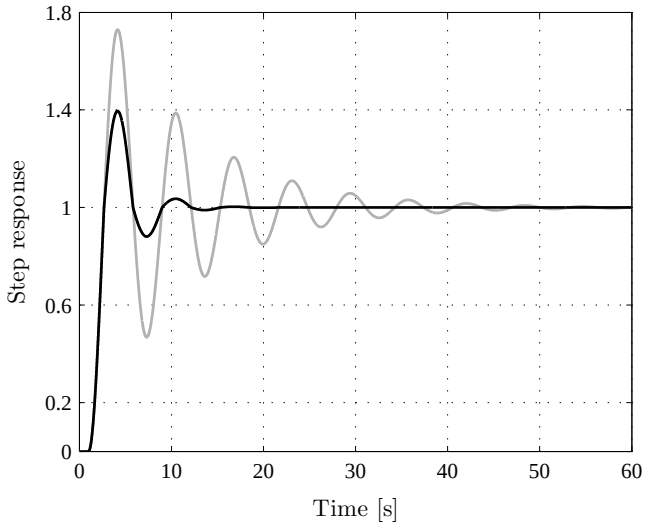

Figure 6.2: Step response of the reset control system (black) and its base linear system (grey).

6.2.2 Overcoming limitations of linear control

The next example (taken from [6]) will show that a reset control system is able to perform accordingly to specifications that are not feasible with linear feedback control. Again, consider the closed-loop setup depicted in Figure 6.1, but now with plant P given by the transfer function

$$P(s) = \frac{1}{s}. \tag{6.3}$$

In [94], it was shown that if a linear controller C stabilizes the plant, the tracking error e due to a unit-step input $r(t)=1(t)$ satisfies

$$\int_0^\infty e(t)dt = \frac{1}{K_v}, \tag{6.4}$$

where the velocity constant K_v is defined by

$$K_v := \lim_{s\to 0} sP(s)C(s). \tag{6.5}$$

In itself, (6.4) does not imply overshoot in the step response. However, if the following notion of rise-time t_r is introduced [94]

$$t_r = \sup\left\{T \geq 0 | y(t) \leq \frac{t}{T}, t \in [0,T]\right\}, \tag{6.6}$$

it can be verified (see [6]) that if $t_r > \frac{2}{K_v}$ the unit step response $y(t)$ overshoots. Now consider the following design objectives:

(i) The steady-state error should not be larger than 1 when tracking a unit-ramp input $r(t)=t$.

(ii) The rise-time should be larger than 2 seconds when tracking a unit-step $r(t)=1(t)$.

(iii) No overshoot should be present in the step response.

To meet the error specification (i) on the ramp response, the linear feedback system must have a velocity error constant that satisfies $K_v \geq 1$. Since $t_r > 2 \geq \frac{2}{K_v}$, no stabilizing linear controller exists that meets all specifications. The tracking error of the reset control system with the FORE (6.2) to the unit-ramp input $r(t)=t$ is depicted Figure 6.3(a), while Figure 6.3(b) shows the step response. As can be

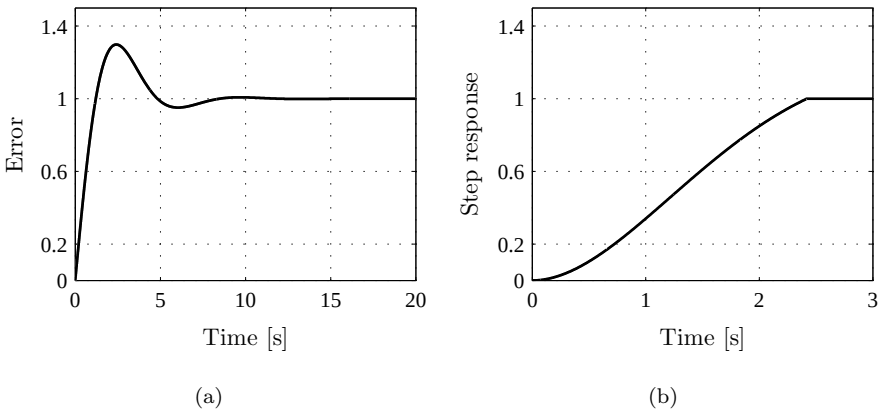

Figure 6.3: Performance of the reset control system. (a) Tracking error to a unit-ramp input, (b) output response to a unit-step input.

seen in the figures, all specifications are met by the reset controller, which is impossible to achieve with a linear feedback controller. More examples can be found in literature. For instance, an experimental demonstration involving disturbance attenuation and sensor-noise suppression for a tape-speed control system can be found in [154]. An experimental example of reset control overcoming limitations of linear feedback control on a flexible mechanical system is provided in [23].

6.3 Contribution

This thesis extends the results in the field of reset control in two directions, namely the work in [101, 151] on $\mathcal{L}_2$ gains of reset control systems is extended, and new contributions are presented in analyzing the $\mathcal{H}_2$ norm. Chapter 7 is an extension

of [101, 151] in several ways. First, it generalizes the $\mathcal{L}_2$ gain analysis to general reset control systems fitting into the common $\mathcal{H}_\infty$ framework using augmented plants, whereas [101, 151] are restricted to the Clegg integrator and FOREs. Second, arbitrary tracking problems are included in our results, as opposed to [152] which only considers constant reference signals. We will show that this might introduce conservatism, for which a solution will be provided via input filtering.
Another important extension in this thesis is the performance analysis via the computation of the $\mathcal{H}_2$ norm. Although the calculation of the $\mathcal{L}_2$ gain is very useful to express the performance of a reset control system, it is typically a steady-state measure. The advantage of reset control over linear control is especially apparent during the transient behavior of constrained problems [6]. Indeed, it has been shown that reset controllers are able to reduce the overshoot of step responses, thereby decreasing the total energy of the error signal, see Section 6.2. This observation shows similarities with one of the interpretations of the $\mathcal{H}_2$ norm, which can be seen as the total output energy (of e.g. the tracking error) of a closed-loop system to either an impulse input or non-zero initial values. For this reason, in Chapter 8 an LMI-based analysis method to calculate upperbounds on the $\mathcal{H}_2$ norm of a closed-loop reset control system is derived. The results can be used to approximate the energy content of the output resulting from specific input signals. We will use the same reset condition as in [151] and also adopt piecewise quadratic Lyapunov functions to reduce conservatism of the analysis.
Moreover, we provide simple though convincing examples to illustrate the accuracy of our proposed $\mathcal{L}_2$ gain and $\mathcal{H}_2$ norm calculations and show that, for an input constrained $\mathcal{H}_2$ problem, reset control can indeed outperform a linear controller designed by a common nonlinear optimization method.
Finally, in Chapter 9, we will shortly reflect on synthesis possibilities, the usefulness of $\mathcal{H}_\infty$ and $\mathcal{H}_2$ controllers for reset control systems and the practical use of reset control in general.

6.4 Notation

The set of real numbers is denoted by $\mathbb{R}$ and the set of nonnegative real numbers is denoted by $\mathbb{R}_+$. The set of real symmetric matrices is denoted by $\mathbb{S}$, the set of real symmetric matrices with nonnegative elements is denoted by $\mathbb{S}_+$. The identity matrix of dimension $n \times n$ is denoted by $I_n \in \mathbb{R}^{n\times n}$. Given two vectors x_1, x_2 we write (x_1, x_2) to denote $[x_1^T, x_2^T]^T$. A vector $x \in \mathbb{R}^n$ is nonnegative, denoted by $x \geq 0$, if its elements x_i satisfy $x_i \geq 0$ for $i = 1, \ldots, n$. A symmetric matrix $A \in \mathbb{R}^{n\times n}$ is positive definite, denoted by $A \succ 0$, if $x^T Ax > 0$ for all $x \in \mathbb{R}^n \backslash \{0\}$. A sequence of scalars $(u^1, u^2, \ldots, u^k)$ is called lexicographically nonnegative, written as $(u^1, u^2, \ldots, u^k) \geq_\ell 0$, if $(u^1, u^2, \ldots, u^k) = (0, 0, \ldots, 0)$ or $u^j > 0$ where $j = \min\{p \mid u^p \neq 0\}$. For a sequence of vectors $(x^1, x^2, \ldots, x^k)$ with $x^j \in \mathbb{R}^n$, we write $(x^1, x^2, \ldots, x^k) \geq_\ell 0$ when $(x_i^1, x_i^2, \ldots, x_i^k) \geq_\ell 0$ for all $i = 1, \ldots, n$. Likewise, we write $(x^1, x^2, \ldots, x^k) \leq_\ell 0$ to denote a lexicographically nonpositive sequence of vectors, meaning that $-(x^1, x^2, \ldots, x^k) \geq_\ell 0$.

Chapter 7

$\mathcal{L}_2$ gain performance analysis of reset control systems

In this chapter we present a general LMI-based analysis method to determine an upperbound on the $\mathcal{L}_2$ gain performance of a reset control system. These computable and sufficient conditions for $\mathcal{L}_2$ stability, based on piecewise quadratic Lyapunov functions, are suitable for all LTI plants and linear-based reset controllers, thereby generalizing the results available in literature. Moreover, the results extend the existing literature by providing solutions to arbitrary tracking and measurement noise problems, while reducing conservatism by using strictly proper input filters.

7.1 General system description

In this section we present a mathematical description of the reset controller and the resulting closed-loop. These descriptions are chosen to fit into the common multichannel $\mathcal{H}_\infty$ framework, as depicted in Figure 7.1.

7.1.1 Plant dynamics

The augmented plant P contains the system to be controlled, together with possible input- and output-weightings. We consider an LTI augmented plant P given

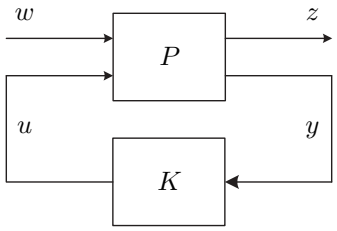

Figure 7.1: General multichannel closed-loop system.

by the minimal state-space description

$$\begin{aligned} \dot{x}_p &= Ax_p + Bu + B_w w \\ z &= C_z x_p + D_{zw} w + D_z u \\ y &= Cx_p + D_w w, \end{aligned} \tag{7.1}$$

where $x_p(t) \in \mathbb{R}^{n_p}$ is the augmented plant state, $w(t) \in \mathbb{R}^{n_w}$ and $z(t) \in \mathbb{R}^{n_z}$ are the exogenous input and the to be controlled output, respectively, at time $t \in \mathbb{R}$ and $A, B_w, B, C_z,\ D_{zw}, D_z, C, D_w$ are matrices of appropriate dimensions. The controller input and output at time $t \in \mathbb{R}$ are denoted by $y(t), u(t) \in \mathbb{R}$. There is no direct feedthrough from u to y, as is for instance the case for many motion systems. Note that we consider SISO controllers only, since reset control for MIMO systems is still a widely open area as the proper formulation of reset conditions in the MIMO case is far from trivial.

7.1.2 Reset controller

The reset controller K is modeled as a linear controller, which resets whenever its input y and output u satisfy a certain condition. To be more precise, the controller is described by

$$\begin{aligned} \dot{x}_k &= A_K x_k + B_K y && \text{if } (y,u) \in \mathfrak{C}' \\ x_k^+ &= A_r x_k && \text{if } (y,u) \in \mathfrak{D}' \\ u &= C_K x_k + D_K y, \end{aligned} \tag{7.2}$$

where $x_k(t) \in \mathbb{R}^{n_k}$ is the controller state at time $t \in \mathbb{R}$ and A_K, B_K, C_K, D_K are matrices of appropriate dimensions. The superscript $+$ in x_k^+ is used to denote the time instant directly after a reset, since a reset is instantaneous. Given (7.1) and (7.2), the closed-loop state becomes $x = (x_p, x_k)$, where $x \in \mathbb{R}^n$ and $n = n_p + n_k$. The reset controller can be considered as a hybrid system with a *flow set* $\mathfrak{C}'$ and a *reset set* $\mathfrak{D}'$ using the framework in [101]. As long as $(y,u) \in \mathfrak{C}'$ the controller behaves linearly and its output u flows conform (A_K, B_K, C_K, D_K). Loosely speaking, when $(y,u) \in \mathfrak{D}'$ the state is changed instantaneously from x_k to x_k^+ by the discrete map corresponding to $A_r \in \mathbb{R}^{n_k \times n_k}$. Various choices for A_r are theoretically possible, but a reasonable and appropriate choice, commonly

used in literature, is

$$A_r = \begin{bmatrix} I_{n_k - n_r} & 0 \\ 0 & 0_{n_r} \end{bmatrix},$$

stating that the last n_r of the n_k controller states are reset to zero, while the others remain unchanged. The reset set $\mathfrak{D}'$ can be defined in various ways, but here we follow [101, 151], where resets occur whenever the controller input and output have opposite signs, i.e., when $yu \leq 0$. Compared to [7], where the condition was $e = 0$, this choice reduces the size of the flow set and allows a considerable relaxation of the stability and performance conditions as we will see later. As mentioned before, the formulation of suitable reset conditions becomes much more complicated for MIMO systems, where $y \in \mathbb{R}^{n_y}$, $u \in \mathbb{R}^{n_u}$ and possibly $n_y \neq n_u$. In that case there are many possible reset conditions, and at present time it is not clear which choices are meaningful. Hence, only SISO controllers are considered and the controller flows whenever $y \geq 0, u \geq 0$ or $y \leq 0, u \leq 0$, which means that

$$\mathfrak{C}' := \left\{ \begin{bmatrix} y \\ u \end{bmatrix} \in \mathbb{R}^2 : E_f \begin{bmatrix} y \\ u \end{bmatrix} \geq 0 \quad \text{or} \quad E_f \begin{bmatrix} y \\ u \end{bmatrix} \leq 0 \right\} \tag{7.3a}$$

$$\mathfrak{D}' := \left\{ \begin{bmatrix} y \\ u \end{bmatrix} \in \mathbb{R}^2 : E_R \begin{bmatrix} y \\ u \end{bmatrix} \geq 0 \quad \text{or} \quad E_R \begin{bmatrix} y \\ u \end{bmatrix} \leq 0 \right\}, \tag{7.3b}$$

where

$$E_f = \begin{bmatrix} 1 & 0 \\ 0 & 1 \end{bmatrix} \quad \text{and} \quad E_R = \begin{bmatrix} -1 & 0 \\ 0 & 1 \end{bmatrix}.$$

The flow set (7.3a) and reset set (7.3b) can also be expressed in terms of x and w. Therefore we introduce a transformation matrix T

$$\left[\begin{array}{c} y \\ \hline u \end{array}\right] = T \left[\begin{array}{c} x \\ \hline w \end{array}\right] = \left[\begin{array}{c|c} T_{yx} & T_{yw} \\ \hline T_{ux} & T_{uw} \end{array}\right] \left[\begin{array}{c} x_p \\ x_k \\ \hline w \end{array}\right],$$

where

$$\left[\begin{array}{c|c} T_{yx} & T_{yw} \\ \hline T_{ux} & T_{uw} \end{array}\right] = \left[\begin{array}{cc|c} C & 0 & D_w \\ \hline D_K C & C_K & D_K D_w \end{array}\right],$$

such that

$$\mathfrak{C} := \left\{ \begin{bmatrix} x \\ w \end{bmatrix} \in \mathbb{R}^{n+n_w} : E_f T \begin{bmatrix} x \\ w \end{bmatrix} \geq 0 \text{ or } E_f T \begin{bmatrix} x \\ w \end{bmatrix} \leq 0 \right\} \tag{7.4a}$$

$$\mathfrak{D} := \left\{ \begin{bmatrix} x \\ w \end{bmatrix} \in \mathbb{R}^{n+n_w} : E_R T \begin{bmatrix} x \\ w \end{bmatrix} \geq 0 \text{ or } E_R T \begin{bmatrix} x \\ w \end{bmatrix} \leq 0 \right\}. \tag{7.4b}$$

For later reference, we also introduce

$$\left[\begin{array}{c|c} T_x & T_w \end{array}\right] = \left[\begin{array}{c|c} T_{yx} & T_{yw} \\ T_{ux} & T_{uw} \end{array}\right].$$

The sets $\mathfrak{C}$ and $\mathfrak{D}$ depend on the input w when $D_w \neq 0$, which is a case not considered in [101, 151]. However, this situation is of importance, as typically in tracking problems the case $D_w \neq 0$ occurs. Indeed, consider the problem depicted in Figure 7.2, where P denotes a dynamical system with input u and output y_p, and K denotes the controller. The signals r and e are the reference signal and the tracking error, respectively. In this case $w = r$, $y = z = e$, and $D_w = 1 \neq 0$, due

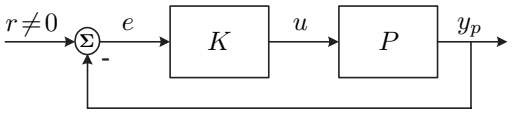

Figure 7.2: Simple tracking problem.

to the direct feedthrough of r in e. This means that the flow and reset regions $\mathfrak{C}$ and $\mathfrak{D}$ in (7.4) explicitly depend on w. Hence, the input r clearly influences the reset moment, since resets are defined to occur at sign changes of u and e. In the analysis of [101, 151] this dependence on w was omitted, since $\mathfrak{C}$ and $\mathfrak{D}$ are only defined in terms of x (e.g. in [101, 151] $\mathfrak{C} := \{x \in \mathbb{R}^n : x^T M x \geq 0\}$). Therefore, the results from [101, 151] are not applicable for tracking problems, but for input disturbance rejection type of problems only. Although tracking problems are considered in [152], they are restricted to cases with a constant reference signal and a reset controller of type FORE only, whereas our result can handle any reference signal and general reset controllers.

7.1.3 Closed-loop dynamics

The dynamics of the augmented plant and the reset controller can be combined into one description for the closed-loop dynamics Σ given by

$$\Sigma : \begin{cases} \dot{x} &= \mathcal{A}x + \mathcal{B}w & \text{if } (x,w) \in \mathfrak{C} \\ x^+ &= \mathcal{A}_R x & \text{if } (x,w) \in \mathfrak{D} \\ z &= \mathcal{C}x + \mathcal{D}w, \end{cases} \tag{7.5}$$

where

$$\left[\begin{array}{c|c} \mathcal{A} & \mathcal{B} \\ \hline \mathcal{C} & \mathcal{D} \end{array}\right] = \left[\begin{array}{cc|c} A + BD_KC & BC_K & B_w + BD_KD_w \\ B_KC & A_K & B_KD_w \\ \hline C_z + D_zD_KC & D_zC_K & D_{zw} + D_zD_KD_w \end{array}\right]$$

$$\mathcal{A}_R = \begin{bmatrix} I_{n_p} & 0 \\ 0 & A_r \end{bmatrix}.$$

The linear closed-loop system without resets is given by

$$\begin{aligned} \dot{x} &= \mathcal{A}x + \mathcal{B}w \\ z &= \mathcal{C}x + \mathcal{D}w, \end{aligned} \tag{7.6}$$

and, as in Section 6.2, is called the *base linear system.*
The reset controller will be chosen such that multiple resets at one point in time are excluded, in order to guarantee local existence of solutions. For convenience, we consider inputs that belong to the set of real Bohl functions, denoted by $\mathbb{B}$. A function $w : \mathbb{R} \to \mathbb{R}^{n_w}$ is called a real Bohl function if $w(t) = He^{Ft}v$ for all $t \in \mathbb{R}$ for some matrices $H \in \mathbb{R}^{n_w \times n_F}, F \in \mathbb{R}^{n_F \times n_F}$, and a vector $v \in \mathbb{R}^{n_F}$. The order o_w of a Bohl function $w(t)$ is defined as the minimum value of n_F for which there exist $H \in \mathbb{R}^{n_w \times n_F}, F \in \mathbb{R}^{n_F \times n_F}$, and a vector $v \in \mathbb{R}^{n_F}$ such that $w(t) = He^{Ft}v$ for all $t \in \mathbb{R}$. To guarantee local solutions, we assume that the closed-loop system can flow after each reset on at least a non-trivial time interval. The following assumption formalizes this statement.

Assumption 7.1 *The system* (7.5) *is such that for all signals w of interest*

$$\begin{bmatrix} x(t) \\ w(t) \end{bmatrix} \in \mathfrak{D} \quad \Rightarrow \quad x^+ = \mathcal{A}_R x \in \mathcal{F}_{\mathfrak{C}}(w), \tag{7.7}$$

where $\mathcal{F}_{\mathfrak{C}}(w)$ is given by

$$\mathcal{F}_{\mathfrak{C}}(w) := \{x_0 \in \mathbb{R}^n \mid \exists \epsilon > 0 \quad \forall \tau \in [0, \epsilon) \ (x(\tau, x_0, w), w(\tau)) \in \mathfrak{C}\}, \tag{7.8}$$

where $x(\tau, x_0, w)$ denotes the state trajectory of (7.5) *at time τ with initial state x_0 and input w.*

This assumption implies that smooth continuation is possible after a reset from the state x^+. The following lemma characterizes the smooth continuation set $\mathcal{F}_{\mathfrak{C}}(w)$ using lexicographic orderings, which can be used to verify (7.7).

Lemma 7.2 *Given the system* (7.5)*, the set $\mathcal{F}_{\mathfrak{C}}(w)$ as defined in* (7.8)*, can be characterized for $w \in \mathbb{B}$ by*

$$\mathcal{F}_{\mathfrak{C}}(w) = \left\{ x_0 \in \mathbb{R}^n : \begin{pmatrix} \begin{bmatrix} \mathcal{O}_y & \mathcal{T}_y \end{bmatrix} \begin{bmatrix} x_0 \\ \mathbf{w}_0 \end{bmatrix} \geq_\ell 0 \text{ and } \begin{bmatrix} \mathcal{O}_u & \mathcal{T}_u \end{bmatrix} \begin{bmatrix} x_0 \\ \mathbf{w}_0 \end{bmatrix} \geq_\ell 0 \end{pmatrix} \right. \\ \left. \text{or} \quad \begin{pmatrix} \begin{bmatrix} \mathcal{O}_y & \mathcal{T}_y \end{bmatrix} \begin{bmatrix} x_0 \\ \mathbf{w}_0 \end{bmatrix} \leq_\ell 0 \text{ and } \begin{bmatrix} \mathcal{O}_u & \mathcal{T}_u \end{bmatrix} \begin{bmatrix} x_0 \\ \mathbf{w}_0 \end{bmatrix} \leq_\ell 0 \end{pmatrix} \right\}, \tag{7.9}$$

where

$$\mathbf{w}_0 = \begin{bmatrix} w(0) \\ \dot{w}(0) \\ \ddot{w}(0) \\ \vdots \\ w^{n+o_w-1}(0) \end{bmatrix}, \ \mathcal{O}_y = \begin{bmatrix} T_{yx} \\ T_{yx}\mathcal{A} \\ T_{yx}\mathcal{A}^2 \\ \vdots \\ T_{yx}\mathcal{A}^{n+o_w-1} \end{bmatrix}, \ \mathcal{O}_u = \begin{bmatrix} T_{ux} \\ T_{ux}\mathcal{A} \\ T_{ux}\mathcal{A}^2 \\ \vdots \\ T_{ux}\mathcal{A}^{n+o_w-1} \end{bmatrix},$$

$$\mathbf{T}_y = \begin{bmatrix} T_{yw} & 0 & 0 & \cdots & 0 \\ T_{yw}\mathcal{B} & T_{yw} & \ddots & \ddots & \vdots \\ T_{yw}\mathcal{A}\mathcal{B} & T_{yw}\mathcal{B} & T_{yw} & \ddots & 0 \\ \vdots & \ddots & \ddots & \ddots & \vdots \\ T_{yw}\mathcal{A}^{n+o_w-2}\mathcal{B} & \cdots & T_{yw}\mathcal{A}\mathcal{B} & T_{yw}\mathcal{B} & T_{yw} \end{bmatrix},$$

$$\mathbf{T}_u = \begin{bmatrix} T_{uw} & 0 & 0 & \cdots & 0 \\ T_{uw}\mathcal{B} & T_{uw} & \ddots & \ddots & \vdots \\ T_{uw}\mathcal{A}\mathcal{B} & T_{uw}\mathcal{B} & T_{uw} & \ddots & 0 \\ \vdots & \ddots & \ddots & \ddots & \vdots \\ T_{uw}\mathcal{A}^{n+o_w-2}\mathcal{B} & \cdots & T_{uw}\mathcal{A}\mathcal{B} & T_{uw}\mathcal{B} & T_{uw} \end{bmatrix}.$$

Proof: The proof is based on inspecting the values of y and u and their derivatives at time $\tau = 0$, and combining them with (7.4a). Utilizing the fact that the functions y and u are Bohl functions of order at most $n+o_w$, the Cayley-Hamilton theorem is used to obtain a finite characterization involving only the first $(n+o_w-1)$ derivatives (see [51] for more details). ■

Note that during implementation of the reset controller reset takes precedence over flow. Under Assumption 7.1 local existence of solutions is guaranteed. However, in principle the reset times may accumulate (so-called Zeno behavior). Therefore, we assume that either Zenoness is absent or otherwise, the solution can be continued beyond the accumulation point in such a way that global existence of solutions is guaranteed.

7.2 Preliminaries

In the remainder of this chapter, by asymptotic stability of system (7.5) we mean asymptotic stability of the zero-input system, i.e., when $w = 0$. Before we state the results on $\mathcal{L}_2$ stability, we need the following definitions. Let $||v||_2$ denote the 2-norm of a signal $v(t)$, defined by the square root of

$$||v||_2^2 = \int_0^\infty v^T(t)\, v(t)\, dt. \tag{7.10}$$

Definition 7.3 *The $\mathcal{L}_2$ gain $||\Sigma||_\infty$ of Σ in (7.5) is defined as the square root of*

$$||\Sigma||_\infty^2 = \sup_{0<||w||_2<\infty} \frac{||z||_2^2}{||w||_2^2}, \tag{7.11}$$

where z is the output of system (7.5) for initial state $x(0)=0$ and input $w \in \mathcal{L}_2$.

Definition 7.4 [144] *System* (7.5) *with state* $x \in \mathbb{R}^n$*, input* $w \in \mathbb{R}^{n_w}$ *and output* $z \in \mathbb{R}^{n_z}$ *is dissipative w.r.t. a supply function* $s : \mathbb{R}^{n_w} \times \mathbb{R}^{n_z} \to \mathbb{R}$ *if there exists a positive definite continuous function* $V : \mathbb{R}^n \to \mathbb{R}$*, sometimes called a storage function, such that* $V(0) = 0$ *and*

$$V(x(t_1)) - V(x(t_0)) \leq \int_{t_0}^{t_1} s(w(t), z(t))dt \tag{7.12}$$

for all $t_1 \geq t_0$ *and all tuples* (w, x, z) *that satisfy* (7.5)*.*

The following lemma will be of use in the sequel.

Lemma 7.5 *System* (7.5) *has a finite* $\mathcal{L}_2$ *gain from input* w *to output* z *smaller than or equal to* γ*, if system* (7.5) *is dissipative w.r.t. the supply function*

$$s(w, z) = \gamma^2 w^T w - z^T z. \tag{7.13}$$

Proof: If system (7.5) is dissipative with respect to the supply function (7.13), then Definition 7.4 implies that

$$V(x(t_1)) - V(x(t_0)) \leq \int_{t_0}^{t_1} \left(\gamma^2 w^T(t)w(t) - z^T(t)z(t)\right) dt \tag{7.14}$$

for all $t_1 \geq t_0$ and all tuples (w, x, z) that satisfy (7.5). Since $V(0)=0$, integrating (7.14) from $t_0 = 0$ to t_1 with initial condition $x(0) = 0$ and using that $V(x(t_1)) \geq 0$, yields

$$\int_0^{t_1} \left(\gamma^2 w^T(t)w(t) - z^T(t)z(t)\right) dt \geq 0.$$

Using $w \in \mathcal{L}_2$ and letting $t_1 \to \infty$ we obtain that

$$\gamma^2 ||w||_2^2 - ||z||_2^2 \geq 0$$

for all $w \in \mathcal{L}_2$, or equivalently

$$\sup_{0<||w||_2<\infty} \frac{||z||_2}{||w||_2} \leq \gamma,$$

which completes the proof. ■

7.3 Common Lyapunov function

In order to approximate the $\mathcal{L}_2$ gain of a reset control system we apply Lemma 7.5 to the closed-loop system (7.5) by selecting a certain structure for V. The minimal

value of γ for which (7.12) holds with supply function (7.13) depends on the particular structure chosen for V. However, at this point, motivated by the linear behavior of the closed-loop in a large part of the state-space, we first restrict our attention to quadratic Lyapunov functions of the form $V(x) = x^T P x$. Using this structure, the following result is obtained.

Theorem 7.6 *The reset control system* (7.5) *is globally asymptotically stable with an $\mathcal{L}_2$ gain $||\Sigma||_\infty \leq \gamma$ if there exist $P \in \mathbb{S}^{n\times n} \succ 0$ and $U, U_R \in \mathbb{S}_+^{2\times 2}$ such that*

$$\begin{bmatrix} \mathcal{A}^T P + P\mathcal{A} + T_x^T E_f^T U E_f T_x & P\mathcal{B} + T_x^T E_f^T U E_f T_w & \mathcal{C}^T \\ \mathcal{B}^T P + T_w^T E_f^T U E_f T_x & -\gamma I + T_w^T E_f^T U E_f T_w & \mathcal{D}^T \\ \mathcal{C} & \mathcal{D} & -\gamma I \end{bmatrix} \prec 0 \tag{7.15a}$$

$$\begin{bmatrix} \mathcal{A}_R^T P \mathcal{A}_R - P + T_x^T E_R^T U_R E_R T_x & T_x^T E_R^T U_R E_R T_w \\ T_w^T E_R^T U_R E_R T_x & T_w^T E_R^T U_R E_R T_w \end{bmatrix} \preceq 0. \tag{7.15b}$$

Proof: First of all, note that the storage function $V(x) = x^T P x$ is continuously differentiable. Moreover, since $P \succ 0$, $V(x) > 0$ for $x \neq 0$ and thus, V is positive definite. Furthermore,

$$\begin{aligned} \begin{bmatrix} x \\ w \end{bmatrix} \in \mathfrak{C} \quad \Rightarrow \quad & \begin{bmatrix} x \\ w \end{bmatrix}^T T^T E_f^T U E_f T \begin{bmatrix} x \\ w \end{bmatrix} = \\ & \begin{bmatrix} x \\ w \end{bmatrix}^T \begin{bmatrix} T_x^T E_f^T U E_f T_x & T_x^T E_f^T U E_f T_w \\ T_w^T E_f^T U E_f T_x & T_w^T E_f^T U E_f T_w \end{bmatrix} \begin{bmatrix} x \\ w \end{bmatrix} \geq 0 \end{aligned} \tag{7.16a}$$

$$\begin{aligned} \begin{bmatrix} x \\ w \end{bmatrix} \in \mathfrak{D} \quad \Rightarrow \quad & \begin{bmatrix} x \\ w \end{bmatrix}^T T^T E_R^T U_R E_R T \begin{bmatrix} x \\ w \end{bmatrix} = \\ & \begin{bmatrix} x \\ w \end{bmatrix}^T \begin{bmatrix} T_x^T E_R^T U_R E_R T_x & T_x^T E_R^T U_R E_R T_w \\ T_w^T E_R^T U_R E_R T_x & T_w^T E_R^T U_R E_R T_w \end{bmatrix} \begin{bmatrix} x \\ w \end{bmatrix} \geq 0, \end{aligned} \tag{7.16b}$$

since $U, U_R \in \mathbb{S}_+^{2\times 2}$ only have nonnegative elements. Since (7.15a) is strict, we have that $\mathcal{A}^T P + P\mathcal{A} + T_x^T E_f^T U E_f T_x^T \prec 0$ and thus, since $V(x) = x^T P x$, we have that

$$\left\langle \frac{\partial V}{\partial x}, \mathcal{A}x \right\rangle < -\varepsilon V \quad \text{if } \left[\begin{smallmatrix} x \\ w \end{smallmatrix}\right] \in \mathfrak{C}, x \neq 0, \tag{7.17}$$

for some $\varepsilon > 0$. Combining (7.16b) with (7.15b) gives

$$x^T(\mathcal{A}_R^T P \mathcal{A}_R - P)x \leq 0 \qquad \text{if } \left[\begin{smallmatrix} x \\ w \end{smallmatrix}\right] \in \mathfrak{D}, \tag{7.18}$$

and thus, since $V(x) = x^T P x$, we have that

$$V(x^+) \leq V(x) \quad \text{when } \left[\begin{smallmatrix} x \\ w \end{smallmatrix}\right] \in \mathfrak{D}. \tag{7.19}$$

Continuous differentiability and positive definiteness of V together with (7.17) and (7.19), and the fact that V is radially unbounded imply that system (7.5) with input $w = 0$ is globally asymptotically stable [50].
To prove that $||\Sigma||_\infty \leq \gamma$ we will show that the inequalities in (7.15) imply, for $V(x) = x^T P x$ and $s(w, z) = \gamma^2 w^T w - z^T z$, that

$$\left\langle \frac{\partial V}{\partial x}, \mathcal{A}x + \mathcal{B}w \right\rangle \leq s(w, z) \quad \text{when } \left[\begin{smallmatrix} x \\ w \end{smallmatrix}\right] \in \mathfrak{C}. \tag{7.20}$$

Indeed, if (7.20) holds, then, since (7.19) also holds, we have that for all $t_1 \geq t_0$

$$V(x(t_1)) - V(x(t_0)) \leq \int_{t_0}^{t_1} s(w(t), z(t))dt, \tag{7.21}$$

showing that (7.5) is dissipative with respect to the supply rate $s(w, z)$. Invoking Lemma 7.5 would then show that (7.5) has an $\mathcal{L}_2$ gain $||\Sigma||_\infty \leq \gamma$.
To show that (7.20) holds, combine (7.16a) with the Schur complement of (7.15a) and employ the S-procedure, to derive

$$\begin{bmatrix} x \\ w \end{bmatrix}^T \begin{bmatrix} \mathcal{A}^T P + P\mathcal{A} + \mathcal{C}^T\mathcal{C} & P\mathcal{B} + \mathcal{C}^T\mathcal{D} \\ \mathcal{B}^T P + \mathcal{D}^T\mathcal{C} & \mathcal{D}^T\mathcal{D} - \gamma^2 I \end{bmatrix} \begin{bmatrix} x \\ w \end{bmatrix} < 0 \quad \text{if } \begin{bmatrix} x \\ w \end{bmatrix} \in \mathfrak{C}, x \neq 0. \tag{7.22}$$

Since $V(x) = x^T P x$, (7.22) is just a reformulation of (7.20), which completes the proof. ■

7.4 Piecewise quadratic Lyapunov function

As stated in the previous section, the minimal value of γ for which (7.12) holds depends on the chosen structure of V, i.e., the value of γ will in general only be an upperbound on the actual value of $||\Sigma||_\infty$ when imposing a structure on V. Therefore, the result in Theorem 7.6 can be conservative. Since we are dealing with a nonlinear closed-loop system, the V that yields the smallest value of γ might be a very complicated function. For the sake of computability we choose to use *piecewise quadratic (PWQ) storage functions* [72, 151]. This choice is motivated by the flexibility of PWQ functions, since they approximate many functions arbitrarily close by using an increasing number of regions, while still resulting in LMIs to check the dissipativity inequality (7.12). These LMIs have the advantage that they can be efficiently solved. Nevertheless, some conservatism remains given a finite number of regions, which implies that the obtained minimal value of γ will only be an upperbound on the actual $\mathcal{L}_2$ gain.
The PWQ storage functions are obtained by partitioning the flow set $\mathfrak{C}'$ into smaller regions $\mathfrak{C}'_i$ and assigning a different quadratic storage function $V_i(x) = x^T P_i x$ to each of them [151]. There are many ways the flow set can be partitioned, here we choose the partitioning as depicted in Figure 7.3. The angles θ_i and θ_{i-1} uniquely define two lines

$$u\cos(\theta_{i-1}) = y\sin(\theta_{i-1}) \quad u\cos(\theta_i) = y\sin(\theta_i),$$

which bound each region $\mathfrak{C}'_i$ as

$$\left.\begin{array}{l} u \geq \frac{\sin(\theta_{i-1})}{\cos(\theta_{i-1})} y \\ u \leq \frac{\sin(\theta_i)}{\cos(\theta_i)} y \end{array}\right\} \Rightarrow \begin{bmatrix} -\sin(\theta_{i-1}) & \cos(\theta_{i-1}) \\ \sin(\theta_i) & -\cos(\theta_i) \end{bmatrix} \begin{bmatrix} y \\ u \end{bmatrix} = E_i \begin{bmatrix} y \\ u \end{bmatrix} \geq 0. \tag{7.23}$$

These angles should be chosen such that $0 < \theta_0 < \theta_1 < \ldots < \theta_N = \frac{\pi}{2}$. Here we choose to distribute θ_i equidistantly, so $\theta_i = \frac{i}{N}\frac{\pi}{2}$, where $i = 0, \ldots, N$ and N is the

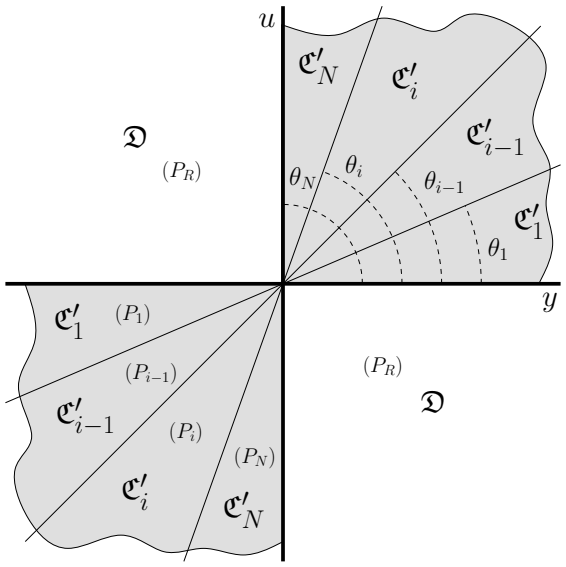

Figure 7.3: Partitioning of the (y, u)-space.

number of regions. Using the coordinate transformation matrix T, we can now define regions $\mathfrak{C}_i$ and $\mathfrak{D}$ as

$$\mathfrak{C}_i := \left\{ \begin{bmatrix} x \\ w \end{bmatrix} \in \mathbb{R}^{n+n_w} \colon E_i T \begin{bmatrix} x \\ w \end{bmatrix} \geq 0 \text{ or } E_i T \begin{bmatrix} x \\ w \end{bmatrix} \leq 0 \right\} \tag{7.24a}$$

$$\mathfrak{D} := \left\{ \begin{bmatrix} x \\ w \end{bmatrix} \in \mathbb{R}^{n+n_w} \colon E_R T \begin{bmatrix} x \\ w \end{bmatrix} \geq 0 \text{ or } E_R T \begin{bmatrix} x \\ w \end{bmatrix} \leq 0 \right\}, \tag{7.24b}$$

where

$$E_i = \begin{bmatrix} -\sin(\theta_{i-1}) & \cos(\theta_{i-1}) \\ \sin(\theta_i) & -\cos(\theta_i) \end{bmatrix}, \quad E_R = \begin{bmatrix} -1 & 0 \\ 0 & 1 \end{bmatrix}.$$

Using a symmetric matrix $U_i \in \mathbb{S}_+$, a region can be defined with the following quadratic form

$$\begin{bmatrix} x \\ w \end{bmatrix}^T T^T E_i^T U_i E_i T \begin{bmatrix} x \\ w \end{bmatrix} \geq 0.$$

Note that, due to the positive elements of U_i, this region always includes the region $\mathfrak{C}_i$ in the sense that

$$\begin{bmatrix} x \\ w \end{bmatrix} \in \mathfrak{C}_i \Rightarrow \begin{bmatrix} x \\ w \end{bmatrix}^T T^T E_i^T U_i E_i T \begin{bmatrix} x \\ w \end{bmatrix} \geq 0. \tag{7.25}$$

A similar argument holds for the region $\mathfrak{D}$. Moreover, using $T = \left[\begin{array}{c|c} T_x & T_w \end{array}\right]$, we introduce

$$E_i T = \left[\begin{array}{c|c} E_i T_x & E_i T_w \end{array}\right] = \left[\begin{array}{c|c} E_{x,i} & E_{w,i} \end{array}\right], \tag{7.26a}$$

$$E_R T = \left[\begin{array}{c|c} E_R T_x & E_R T_w \end{array}\right] = \left[\begin{array}{c|c} E_{x,R} & E_{w,R} \end{array}\right]. \tag{7.26b}$$

The boundaries of the regions are defined by

$$\begin{bmatrix} -\sin(\theta_i) & \cos(\theta_i) \end{bmatrix} T \begin{bmatrix} x \\ w \end{bmatrix} = \Phi_i \begin{bmatrix} x \\ w \end{bmatrix} = 0, \tag{7.27}$$

whose solutions are in the kernel of Φ_i. We can also use an image representation for these boundaries using full column rank matrices $W_{\Phi i} \in \mathbb{R}^{(n+n_w)\times(n+n_w-1)}$ such that $\mathrm{im}(W_{\Phi i}) = \ker(\Phi_i)$, where $\mathrm{im}(W_{\Phi i})$ denotes the image of $W_{\Phi i}$.

7.4.1 General analysis

Using this partitioning we can formulate a theorem on the calculation of an upperbound on the $\mathcal{L}_2$ gain.

Theorem 7.7 *The reset control system* (7.5) *with a partitioning of the flow set given by* (7.24) *is globally asymptotically stable with an $\mathcal{L}_2$ gain $||\Sigma||_\infty \leq \gamma$ if, for a given N, there exists $P_i, P_R \in \mathbb{S}^{n\times n}$ and $U_i, U_{R_0}, U_{R_i}, U_{RI_i}, V_i, V_R \in \mathbb{S}^{2\times 2}_+$, $i = 1, \ldots, N$ such that*

$$\begin{bmatrix} \mathcal{A}^T P_i + P_i \mathcal{A} + E_{x,i}^T U_i E_{x,i} & P_i \mathcal{B} + E_{x,i}^T U_i E_{w,i} & \mathcal{C}^T \\ \mathcal{B}^T P_i + E_{w,i}^T U_i E_{x,i} & -\gamma I + E_{w,i}^T U_i E_{w,i} & \mathcal{D}^T \\ \mathcal{C} & \mathcal{D} & -\gamma I \end{bmatrix} \prec 0, \qquad i = 1, \ldots, N \tag{7.28a}$$

$$\begin{bmatrix} \mathcal{A}_R^T P_R \mathcal{A}_R - P_R + E_{x,R}^T U_{R_0} E_{x,R} & E_{x,R}^T U_{R_0} E_{w,R} \\ E_{w,R}^T U_{R_0} E_{x,R} & E_{w,R}^T U_{R_0} E_{w,R} \end{bmatrix} \preceq 0 \tag{7.28b}$$

$$\begin{bmatrix} \mathcal{A}_R^T P_i \mathcal{A}_R - P_R + E_{x,R}^T U_{R_i} E_{x,R} + \mathcal{A}_R^T E_{x,i}^T U_{RI_i} E_{x,i} \mathcal{A}_R & E_{x,R}^T U_R E_{w,R} + \mathcal{A}_R^T E_{x,i}^T U_{RI_i} E_{w,i} \\ E_{w,R}^T U_R E_{x,R} + E_{w,i}^T U_{RI_i} E_{x,i} \mathcal{A}_R & E_{w,R}^T U_R E_{w,R} + E_{w,i}^T U_{RI_i} E_{w,i} \end{bmatrix} \preceq 0, \quad i = 1, \ldots, N \tag{7.28c}$$

$$\begin{bmatrix} P_i - E_{x,i}^T V_i E_{x,i} & -E_{x,i}^T V_i E_{w,i} \\ -E_{w,i}^T V_i E_{x,i} & -E_{w,i}^T V_i E_{w,i} \end{bmatrix} \succ 0, \qquad i = 1, \ldots, N \tag{7.28d}$$

$$\begin{bmatrix} P_R - E_{x,R}^T V_R E_{x,R} & -E_{x,R}^T V_R E_{w,R} \\ -E_{w,R}^T V_R E_{x,R} & -E_{w,R}^T V_R E_{w,R} \end{bmatrix} \succ 0 \tag{7.28e}$$

$$W_{\Phi i}^T \begin{bmatrix} P_i - P_{i+1} & 0 \\ 0 & 0 \end{bmatrix} W_{\Phi i} = 0, \qquad i = 1, \ldots, N-1 \tag{7.28f}$$

$$W_{\Phi 0}^T \begin{bmatrix} P_R - P_1 & 0 \\ 0 & 0 \end{bmatrix} W_{\Phi 0} = 0 \tag{7.28g}$$

$$W_{\Phi N}^T \begin{bmatrix} P_N - P_R & 0 \\ 0 & 0 \end{bmatrix} W_{\Phi N} = 0. \tag{7.28h}$$

Proof: To prove that system (7.5) with input $w = 0$ is globally asymptotically stable, we will show that the assumptions (7.28) imply that the storage function V, defined as $V(x) = V_i(x) := x^T P_i x$ when $\left[\begin{smallmatrix} x \\ w \end{smallmatrix}\right] \in \mathfrak{C}_i$ and $V(x) = x^T P_R x$ when $\left[\begin{smallmatrix} x \\ w \end{smallmatrix}\right] \in \mathfrak{D}$, is locally Lipschitz continuous, positive definite and that

$$\left\langle \frac{\partial V_i}{\partial x}, \mathcal{A}x \right\rangle < -\varepsilon V \qquad \text{if } \left[\begin{smallmatrix} x \\ w \end{smallmatrix}\right] \in \mathfrak{C}_i, x \neq 0 \tag{7.29a}$$

$$V(x^+) - V(x) \leq 0 \qquad \text{if } \left[\begin{smallmatrix} x \\ w \end{smallmatrix}\right] \in \mathfrak{D}, \tag{7.29b}$$

for some $\varepsilon > 0$. Indeed, if (7.29) are established, then local Lipschitz continuity and positive definiteness together with the radially unboundedness of V imply

global asymptotic stability [50].
Continuity of the piecewise quadratic function V follows from constraints (7.28f), (7.28g) and (7.28h) as these imply that $x^T P_i x = x^T P_{i+1} x$, $x^T P_R x = x^T P_1 x$, $x^T P_N x = x^T P_R x$ for all $\left[\begin{smallmatrix} x \\ w \end{smallmatrix}\right]$ on the corresponding boundaries. Consequently, V is Lipschitz continuous. Furthermore, V is positive definite. To show this, note that $V_i, V_R \in \mathbb{S}_+^{2\times 2}$ have only nonnegative elements, which implies that

$$\begin{aligned} \left[\begin{smallmatrix} x \\ w \end{smallmatrix}\right] \in \mathfrak{C}_i \quad \Rightarrow \quad & \begin{bmatrix} x \\ w \end{bmatrix}^T T^T E_i^T V_i E_i T \begin{bmatrix} x \\ w \end{bmatrix} = \\ & \begin{bmatrix} x \\ w \end{bmatrix}^T \begin{bmatrix} E_{x,i}^T V_i E_{x,i} & E_{x,i}^T V_i E_{w,i} \\ E_{w,i}^T V_i E_{x,i} & E_{w,i}^T V_i E_{w,i} \end{bmatrix} \begin{bmatrix} x \\ w \end{bmatrix} \geq 0 \end{aligned} \tag{7.30a}$$

$$\begin{aligned} \left[\begin{smallmatrix} x \\ w \end{smallmatrix}\right] \in \mathfrak{D} \quad \Rightarrow \quad & \begin{bmatrix} x \\ w \end{bmatrix}^T T^T E_R^T V_R E_R T \begin{bmatrix} x \\ w \end{bmatrix} = \\ & \begin{bmatrix} x \\ w \end{bmatrix}^T \begin{bmatrix} E_{x,R}^T V_R E_{x,R} & E_{x,R}^T V_R E_{w,R} \\ E_{w,R}^T V_R E_{x,R} & E_{w,R}^T V_R E_{w,R} \end{bmatrix} \begin{bmatrix} x \\ w \end{bmatrix} \geq 0. \end{aligned} \tag{7.30b}$$

Therefore, for $\left[\begin{smallmatrix} x \\ w \end{smallmatrix}\right] \in \mathfrak{C}_i$ (not necessarily for all x) it holds that for $x \neq 0$

$$V(x) = x^T P_i x \overset{(7.28d)}{>} \begin{bmatrix} x \\ w \end{bmatrix}^T T^T E_i^T V_i E_i T \begin{bmatrix} x \\ w \end{bmatrix} \geq 0. \tag{7.31}$$

The same applies for $\left[\begin{smallmatrix} x \\ w \end{smallmatrix}\right] \in \mathfrak{D}$ using (7.28e). Furthermore, (7.28a) implicitly implies that $x^T \left(\mathcal{A}^T P_i + P_i \mathcal{A} + E_{x,i}^T U_i E_{x,i}\right) x < 0$ which implies (7.29a). It only remains to be shown that (7.29b) holds. The state x^+ after reset is either an element of $\mathfrak{D}$ or $\mathfrak{C}_i$. In case $x^+ \in \mathfrak{D}$, (7.28b) is equivalent to

$$x^T (\mathcal{A}_R^T P_R \mathcal{A}_R - P_R) x \leq 0 \qquad \text{for } \left[\begin{smallmatrix} x \\ w \end{smallmatrix}\right], \left[\begin{smallmatrix} x^+ \\ w \end{smallmatrix}\right] \in \mathfrak{D}. \tag{7.32}$$

In case $x^+ \in \mathfrak{C}_i$, (7.28c) implies that

$$x^T (\mathcal{A}_R^T P_i \mathcal{A}_R - P_R) x \leq 0 \qquad \text{when } \left[\begin{smallmatrix} x \\ w \end{smallmatrix}\right] \in \mathfrak{D}, \left[\begin{smallmatrix} x^+ \\ w \end{smallmatrix}\right] \in \mathfrak{C}_i. \tag{7.33}$$

The combination of (7.32) and (7.33) is equivalent to (7.29b).
To prove that $||\Sigma||_\infty \leq \gamma$ we will show that the assumptions (7.28) imply that for $s(w,z) = \gamma^2 w^T w - z^T z$,

$$\left\langle \frac{\partial V_i}{\partial x}, \mathcal{A}x + \mathcal{B}w \right\rangle \leq s(w,z) \qquad \text{if } \left[\begin{smallmatrix} x \\ w \end{smallmatrix}\right] \in \mathfrak{C}_i. \tag{7.34}$$

Indeed, if (7.34) holds, then, since (7.29b) holds, we have that for all $t_1 \geq t_0$

$$V(x(t_1)) - V(x(t_0)) \leq \int_{t_0}^{t_1} s(w(t), z(t)) dt, \tag{7.35}$$

showing that (7.5) is dissipative w.r.t. the supply function $s(w,z) = \gamma^2 w^T w - z^T z$, and hence that $||\Sigma||_\infty \leq \gamma$ by virtue of Lemma 7.5.
Combining (7.30a) with the Schur complement of (7.28a) via the S-procedure yields that

$$\begin{bmatrix} x \\ w \end{bmatrix}^T \begin{bmatrix} \mathcal{A}^T P_i + P_i \mathcal{A} + \mathcal{C}^T \mathcal{C} & P_i \mathcal{B} + \mathcal{C}^T \mathcal{D} \\ \mathcal{B}^T P_i + \mathcal{D}^T \mathcal{C} & \mathcal{D}^T \mathcal{D} - \gamma^2 I \end{bmatrix} \begin{bmatrix} x \\ w \end{bmatrix} \leq 0 \qquad \text{if } \left[\begin{smallmatrix} x \\ w \end{smallmatrix}\right] \in \mathfrak{C}_i, \tag{7.36}$$

which is equivalent to (7.34), and hence the proof is complete. ■

Minimizing (7.28) over γ for a given N returns an upperbound on the actual $\mathcal{L}_2$ gain. This upperbound can be lowered by increasing the number of partitions N, see [72]. Unfortunately, it is still not guaranteed that γ will approach the actual $\mathcal{L}_2$ gain $||\Sigma||_\infty$ when $N \to \infty$.
Theorem 7.7 is a generalization of previous stability results and is applicable to all augmented plants and reset controllers that fit into the common multichannel $\mathcal{H}_\infty$ framework described in Section 7.1. It therefore extends the work in [101, 151], which only considers FOREs (including the Clegg integrator). Furthermore, this analysis includes tracking problems in their general form, while [152] is only applicable for setpoint tracking.

7.4.2 Input filtering

The analysis in Theorem 7.7 is capable of providing an upperbound on the actual $\mathcal{L}_2$ gain of any closed-loop reset control system. However, in some situations the upperbound may be very conservative, like in tracking problems as in Figure 7.2. The cause of this high upperbound, as is shown next, is that $D_w \neq 0$ in those situations.
First note that $T \in \mathbb{R}^{2\times(n+n_w)}$ and $\Phi_i \in \mathbb{R}^{1\times(n+n_w)}$. Hence, the kernel of Φ_i is spanned by $n+n_w-1$ independent columns, so $W_{\Phi i} \in \mathbb{R}^{(n+n_w)\times(n+n_w-1)}$. Moreover, (7.28f) can be rewritten by removing its zeros, such that

$$W'^{T}_{\Phi i}(P_i - P_{i+1})W'_{\Phi i} = 0, \tag{7.37}$$

where $W'_{\Phi i} \in \mathbb{R}^{n\times(n+n_w-1)}$ are the matrices consisting of the first n rows of $W_{\Phi i}$. If $D_w = 0$, the boundaries of the regions $\mathfrak{C}_i$ are described by

$$\Phi_i \begin{bmatrix} x \\ \hline w \end{bmatrix} = \left[\begin{array}{cc} \Phi_{i_x} & \Phi_{i_w} \end{array}\right] \begin{bmatrix} x \\ \hline w \end{bmatrix} = \left[\begin{array}{c|c} -\sin(\theta_i)T_{yx} + \cos(\theta_i)T_{ux} & 0 \end{array}\right] \begin{bmatrix} x \\ \hline w \end{bmatrix} = 0,$$

and since the last n_w entries of Φ_i are zero, the structure of $W_{\Phi i}$ is such that only $n-1$ of the $n+n_w-1$ columns of $W'_{\Phi i}$ are linearly independent. Therefore, its rank is $n-1$, and since $P_i \in \mathbb{R}^{n\times n}$, there is design freedom in $P_i - P_{i+1}$ to satisfy (7.37).
However, when $D_w \neq 0$ the rank of $W'_{\Phi i}$ is equal to n, yielding a unique solution to (7.37), namely $P_i - P_{i+1} = 0$ for all i. This means that $V(x) = x^T P x$. Hence, Theorem 7.7 simplifies to the common quadratic Lyapunov function analysis of Theorem 7.6, which gives rise to a possibly conservative upperbound on the $\mathcal{L}_2$ gain.
This conservatism also allows a more comprehensible interpretation. Each region $\mathfrak{C}_i$ has its own Lyapunov function V_i, which solely depends on x, while (7.24) shows that the region itself is defined in terms of both x and w. Figure 7.4 illustrates this for the simple case where $x, w \in \mathbb{R}$. Since V only depends on x (depicted by the dashed vertical line), continuity of V across the borders between the regions with P_1, P_i, and P_{i+1} requires that $V_1(x) = V_i(x) = V_{i+1}(x)$ for all (x, w) on the boundary, i.e., for all $x \in \mathbb{R}^n$.

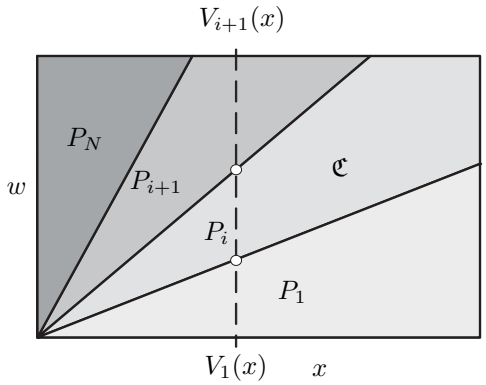

Figure 7.4: Common Lyapunov function.

This issue arises in any situation where $D_w \neq 0$, including measurement noise attenuation and tracking problems. This drawback can be avoided by forcing $D_w = 0$, which can be done by including strictly proper input filters for exogenous signals that enter the closed-loop before the controller. This is illustrated in Figure 7.5, where we have exogenous signals $\bar{r}$, $\bar{\eta}$, replacing the original reference r and noise η. Since these strictly proper filters have no direct feedthrough of the

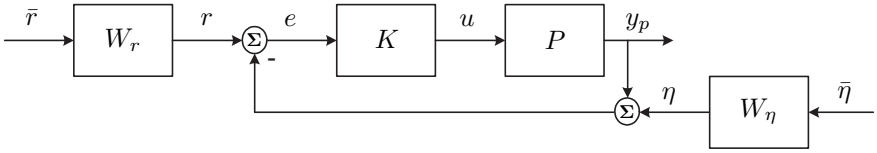

Figure 7.5: Closed-loop with filtered inputs.

input, there is also no direct feedthrough from w (containing $\bar{r}$ and $\bar{\eta}$) to y in the augmented plant in (7.1), so $D_w = 0$. By including input filters in the augmented plant we assume to have a priori knowledge of these inputs (as is often the case in practice), which is then via the filter states contained inside the state vector x_p. Possible input filters include:

- unit step: $W(s) = \frac{1}{(s+\varepsilon)}$,
- unit ramp: $W(s) = \frac{1}{(s+\varepsilon)^2}$,
- sine wave with frequency ω: $W(s) = \frac{\omega}{(s+\varepsilon)^2+\omega^2}$,

where s is the Laplace variable and $\varepsilon > 0$ is a small offset. This offset is standard in $\mathcal{H}_2$ and $\mathcal{H}_\infty$ problems for linear systems to ensure closed-loop stability. Using these filters, the Lyapunov function V also depends on the input knowledge (as

the state variables corresponding to w are now included in x_p and thus in x), while $\mathfrak{C}_i$ and $\mathfrak{D}$ no longer depend on w, i.e.,

$$\mathfrak{C}_i := \{x \in \mathbb{R}^n : E_i T_x x \geq 0 \quad \text{or} \quad E_i T_x x \leq 0\} \tag{7.38a}$$
$$\mathfrak{D} := \{x \in \mathbb{R}^n : E_R T_x x \geq 0 \quad \text{or} \quad E_R T_x x \leq 0\}\,. \tag{7.38b}$$

Theorem 7.7 can now be simplified.

Theorem 7.8 *The reset control system* (7.5) *with* $D_w = 0$ *and a partitioning of the flow set given by* (7.38) *is globally asymptotically stable with an* $\mathcal{L}_2$ *gain* $||\Sigma||_\infty \leq \gamma$ *if, for a given* N*, there exists* $P_i, P_R \in \mathbb{S}^{n\times n}$ *and* $U_i, U_{R_0}, U_{R_i}, U_{RI_i}, V_i$, $V_R \in \mathbb{S}_+^{2\times 2}$, $i = 1, \ldots, N$ *such that*

$$\begin{bmatrix} \mathcal{A}^T P_i + P_i \mathcal{A} + E_{x,i}^T U_i E_{x,i} & P_i \mathcal{B} & \mathcal{C}^T \\ \mathcal{B}^T P_i & -\gamma I & \mathcal{D}^T \\ \mathcal{C} & \mathcal{D} & -\gamma I \end{bmatrix} \prec 0, \qquad i = 1, \ldots, N \tag{7.39a}$$
$$\mathcal{A}_R^T P_R \mathcal{A}_R - P_R + E_{x,R}^T U_{R_0} E_{x,R} \preceq 0 \tag{7.39b}$$
$$\mathcal{A}_R^T P_i \mathcal{A}_R - P_R + E_{x,R}^T U_{R_i} E_{x,R} + \mathcal{A}_R^T E_{x,i}^T U_{RI_i} E_{x,i} \mathcal{A}_R \preceq 0, \quad i = 1, \ldots, N \tag{7.39c}$$
$$P_i - E_{x,i}^T V_i E_{x,i} \succ 0, \qquad i = 1, \ldots, N \tag{7.39d}$$
$$P_R - E_{x,R}^T V_R E_{x,R} \succ 0 \tag{7.39e}$$
$$\overline{W}_{\Phi i_x}^T (P_i - P_{i+1}) \overline{W}_{\Phi i_x} = 0, \qquad i = 1, \ldots, N-1 \tag{7.39f}$$
$$\overline{W}_{\Phi 0_x}^T (P_R - P_1) \overline{W}_{\Phi 0_x} = 0 \tag{7.39g}$$
$$\overline{W}_{\Phi N_x}^T (P_N - P_R) \overline{W}_{\Phi N_x} = 0, \tag{7.39h}$$

where $\operatorname{im}(\overline{W}_{\Phi i}) = \ker(\begin{bmatrix} -\sin(\theta_i) & \cos(\theta_i) \end{bmatrix} T_x)$.

Theorem 7.8 is similar to the result in [151]. However, this result is applicable to all possible LTI plants and reset controllers, which fit the $\mathcal{H}_\infty$ framework, as long as $D_w = 0$. In contrast to [151] it can cope with measurement noise attenuation and tracking problems, as long as these inputs are filtered with a strictly proper filter. Since the analysis in Theorem 7.8 encompasses a priori knowledge of the inputs, it can be performed for a broad class of desired input types (and corresponding input filters).

7.5 Example

In order to illustrate the relevance of the derived analysis method, the above result is applied to a simulation example. The system used in this example is taken from [60, 101], and extended with a tracking problem. Consider a second order LTI plant, represented by $G(s) = \frac{s+1}{s(s+0.2)}$. This system should track a step reference $r(t) = 1(t)$, which can be represented by the input filter $W_r(s) = \frac{1}{s+\varepsilon}$. Similarly as in [60, 101], we only allow first order low-pass controllers K to achieve this. The goal is to compare the tracking performance of a linear controller of this form,

i.e., $K(s) = \frac{1}{s+\beta}$, where β is a free variable, with its resetting counterpart, also known as a FORE. This reset controller K is characterized by

$$A_K = \beta, \quad B_K = C_K = 1, \quad D_K = A_r = 0,$$

yielding closed-loop matrices of the form

$$\mathcal{A} = \begin{bmatrix} A & B \\ C & \beta \end{bmatrix}, \quad \mathcal{B} = \begin{bmatrix} B_w \\ 0 \end{bmatrix}, \quad \mathcal{C} = \begin{bmatrix} C & 0 \end{bmatrix}, \quad \mathcal{D} = 0.$$

The closed-loop layout is shown in Figure 7.6. The $\mathcal{L}_2$ gain of both the linear

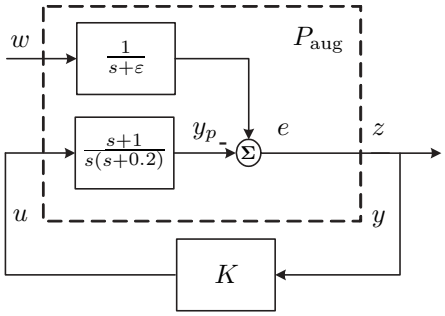

Figure 7.6: Closed-loop layout.

and the reset closed-loop are compared in Figure 7.7(a) for varying pole values β. The linear control curve is obtained using standard $\mathcal{H}_\infty$ techniques, i.e., by minimizing γ in the LMI

$$\begin{bmatrix} \mathcal{A}^T P + P\mathcal{A} & P\mathcal{B} & \mathcal{C}^T \\ \mathcal{B}^T P & -\gamma I & \mathcal{D}^T \\ \mathcal{C} & \mathcal{D} & -\gamma I \end{bmatrix} \prec 0, \tag{7.40}$$

where $P \succ 0$. Theorem 7.8 is used for the reset control curve (with $N = 100$). The $\mathcal{L}_2$ gains for this tracking problem differ significantly from the result in [101], which only considered disturbance rejection.
A second difference with [101] is that the reset controller yields a smaller $\mathcal{L}_2$ gain than its linear counterpart for any value of β. This is not a general result, but is caused by the structure of this specific example. It can be shown that the minimum value of γ that is a solution to (7.40), is also a feasible solution to (7.39). Namely, for $P_R = P_i = P = \begin{bmatrix} P_{11} & P_{12} \\ P_{12}^T & P_{22} \end{bmatrix}$ relations (7.39f)-(7.39h) are satisfied, and (7.39d) and (7.39e) are also satisfied as $P \succ 0$. Furthermore, we have that

$$\mathcal{A}_R = \begin{bmatrix} I & 0 \\ 0 & 0 \end{bmatrix}, \quad E_{x,R}^T U_R E_{x,R} = \begin{bmatrix} C^T U_{R_{11}} C & -C^T U_{R_{12}} C_k \\ -C_k^T U_{R_{12}}^T C & C_k^T U_{R_{12}} C_k \end{bmatrix} \tag{7.41}$$

with $U_{R_{11}}, U_{R_{12}}, U_{R_{22}} \geq 0$, and hence (7.39b) and (7.39c) reduce to

$$\begin{bmatrix} C^T U_{R_{11}} C & -P_{12} - C^T U_{R_{12}} C_k \\ -P_{12}^T - C_k^T U_{R_{12}}^T C & -P_{22} + C_k^T U_{R_{22}} C_k \end{bmatrix} \preceq 0. \tag{7.42}$$

This implies that $U_{R_{11}} = 0$ and hence that $P_{12} = -C^T U_{R_{12}} C_k$. With $\mathcal{A}$, $\mathcal{B}$, $\mathcal{C}$ and $\mathcal{D}$ as defined above, it can be shown that the Lyapunov matrix P with this specific structure is an optimal solution to (7.40), and hence for this example the linear $\mathcal{L}_2$ gain is always an upperbound for Theorem 7.8.
To verify the accuracy of the LMI analysis from Theorem 7.8, a describing function analysis of the closed-loop behavior is performed (a technique already used by Clegg [26]). Therefore, pure sinusoidal inputs w of various frequencies at each value of β are applied to the closed-loop, and the amplitude of the fundamental frequency present in the output z is identified. The peak amplitude over all frequencies is then an estimation $\gamma_{\min}$ of the $\mathcal{L}_2$ gain. Figure 7.7(b) shows this $\gamma_{\min}$ of the describing function. From this figure we can conclude that the describing function analysis matches our LMI $\mathcal{L}_2$ analysis very well, underlining the accuracy of Theorem 7.8. Figure 7.7(a) does not necessarily imply that reset control

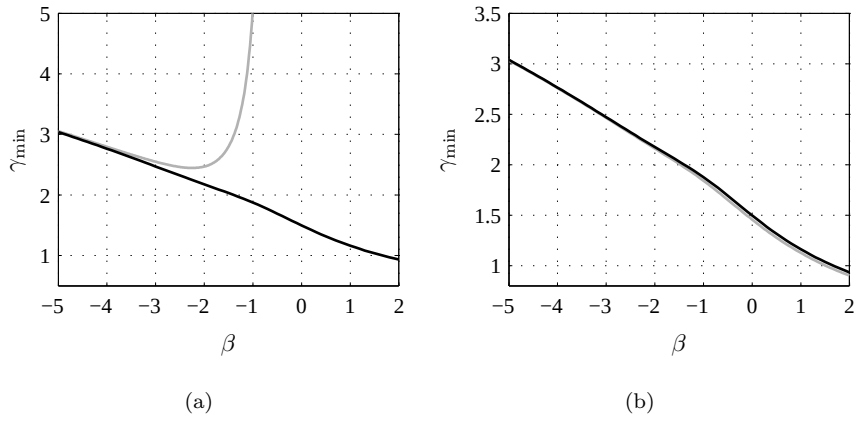

Figure 7.7: (a) Estimated closed-loop $\mathcal{L}_2$ gains using linear (grey) and reset control (black), as a function of β, (b) results using LMI analysis (black) and describing function analysis (grey).

outperforms any linear controller in $\mathcal{H}_\infty$ sense. We have restricted ourselves to linear controllers K with transfer function $\frac{1}{s+\beta}$, but of course one can find other controllers with lower $\mathcal{L}_2$ gains (e.g. with a larger controller gain or of a higher order).

Chapter 8

$\mathcal{H}_2$ performance analysis of reset control systems

The focus in this chapter is to determine the performance of a SISO reset control system in $\mathcal{H}_2$ sense. We derive convex optimization problems in terms of LMIs to compute an upperbound on the $\mathcal{H}_2$ norm, using dissipativity theory with piecewise quadratic Lyapunov functions. Finally, for an input constrained $\mathcal{H}_2$ problem, we show that reset control can indeed outperform a linear controller designed by a common nonlinear optimization method.

8.1 Preliminaries

The results on the $\mathcal{H}_2$ analysis of reset control systems use some common $\mathcal{H}_2$ theory for linear systems of the form

$$\Sigma : \left\{ \begin{array}{rcl} \dot{x} & = & \mathcal{A}x + \mathcal{B}w \\ z & = & \mathcal{C}x, \end{array} \right. \tag{8.1}$$

where $\mathcal{A} \in \mathbb{R}^{n \times n}$, $\mathcal{B} \in \mathbb{R}^{n \times n_w}$, and $\mathcal{C} \in \mathbb{R}^{n_z \times n}$ are the system matrices, $x(t) \in \mathbb{R}^n$ is the state, and $w(t) \in \mathbb{R}^{n_w}$ and $z(t) \in \mathbb{R}^{n_z}$ denote the input and output at time $t \in \mathbb{R}$, respectively. We shortly summarize some of these results here (see [14, 127] for details).

It is well-known that one of the possible interpretations of the $\mathcal{H}_2$ norm for linear systems is the total energy content of the output z due to an impulsive input w. The response of system (8.1) to such an impulsive input is equivalent to

the response when the system is subjected to the initial condition $x_0 = \mathcal{B}_j$ or e.g. $x_0 = \mathcal{B}_i + \mathcal{B}_j$ (with $i \neq j$), corresponding to simultaneous impulses on both channels i and j, where $\mathcal{B}_j$ denotes the j-th column of $\mathcal{B}$ corresponding to the j-th input. In this chapter we use the latter interpretation that corresponds to $w = 0$, as this transforms to the context of reset control in a straightforward manner.

Definition 8.1 *Consider the asymptotically stable linear system* (8.1) *with initial state $x_0 \in \mathbb{R}^n$ and no input ($w = 0$). The total output energy in z is then defined by:*

$$\int_0^\infty z^T z \, dt = \int_0^\infty x_0^T e^{\mathcal{A}^T t} \mathcal{C}^T \mathcal{C} e^{\mathcal{A} t} x_0 \, dt. \tag{8.2}$$

The square root of this integral is called the $\mathcal{H}_2$ norm for x_0 and is denoted by $||\Sigma||_{2,x_0}$.

To calculate (8.2), the observability gramian

$$M := \int_0^\infty e^{\mathcal{A}^T t} \mathcal{C}^T \mathcal{C} e^{\mathcal{A} t} dt \tag{8.3}$$

can be used, so that the squared $\mathcal{H}_2$ norm is equal to

$$||\Sigma||_{2,x_0}^2 = \int_0^\infty z^T z \, dt = x_0^T M x_0. \tag{8.4}$$

It is well-known (see e.g. [14]) that for Hurwitz matrices $\mathcal{A}$ the observability gramian M is the solution to the Lyapunov equality

$$\mathcal{A}^T M + M\mathcal{A} + \mathcal{C}^T \mathcal{C} = 0. \tag{8.5}$$

The $\mathcal{H}_2$ norm of a linear system can also be obtained using the concept of dissipativity, see Definition 7.4. For the initial state $\mathcal{H}_2$ problem there is no input and we are only interested in the energy content of the output. Hence we select the supply function $s(w, z) = -z^T z$. Using quadratic storage functions $V(x) = x^T P x$, the differential form of (7.12) yields

$$\begin{aligned} \left\langle \tfrac{\partial V}{\partial x}, \mathcal{A}x + \mathcal{B}w \right\rangle &\leq s(w, z) \qquad \forall x \\ x^T(\mathcal{A}^T P + P\mathcal{A})x + x^T \mathcal{C}^T \mathcal{C} x &\leq 0 \qquad \forall x \\ \mathcal{A}^T P + P\mathcal{A} + \mathcal{C}^T \mathcal{C} &\preceq 0, \end{aligned} \tag{8.6}$$

which is an LMI in the design variable P. Additionally, global asymptotic stability can be taken into account by choosing V a positive definite Lyapunov function (i.e., requiring that $P \succ 0$) and changing (8.6) in a strict matrix inequality. The actual $\mathcal{H}_2$ norm $||\Sigma||_{2,x_0}$ can be upperbounded by using (7.12), where we set $t_0 = 0$, $s(w, z) = -z^T z$, let $t_1 \to \infty$ and use $V(x(t_1)) > 0$. Indeed, then we obtain

$$||\Sigma||_{2,x_0}^2 = \int_0^\infty z^T z \, dt \leq V(x(t_0)) = x_0^T P x_0. \tag{8.7}$$

The actual $\mathcal{H}_2$ norm can therefore be approximated by minimizing γ^2 subject to the LMIs

$$\begin{aligned} \mathcal{A}^T P + P\mathcal{A} + \mathcal{C}^T\mathcal{C} &\prec 0 && \text{(8.8a)} \\ x_0^T P x_0 &< \gamma^2, && \text{(8.8b)} \end{aligned}$$

which should be solved for $P \succ 0$ and γ^2. The infimum of this optimization problem retrieves $||\Sigma||^2_{2,x_0}$. These LMIs are, of course, closely related to (8.4) and (8.5).

8.2 System description

Reset control has been shown to be advantageous when the transient response to specific input signals (such as step functions) is considered, see e.g. Section 6.2. Reset controllers show less overshoot than their linear counterparts and hence, are expected to have less energy in the closed-loop output, here being the tracking error. Therefore, in this chapter we do not consider the general system description as in Section 7.1 but we focus on the augmented layout depicted in Figure 8.1, consisting of various input filters, a linear plant P and a reset controller K. The

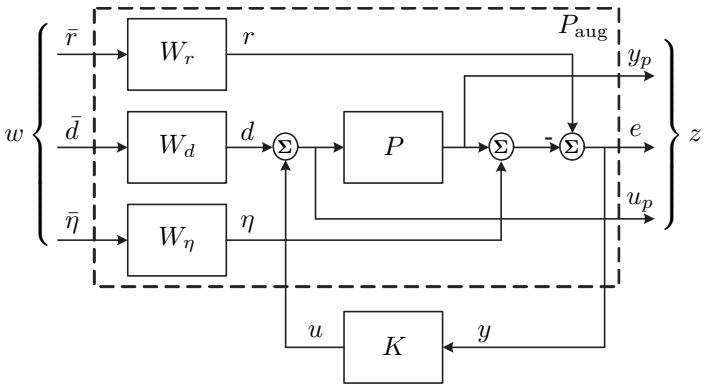

Figure 8.1: Closed-loop layout with input w and output z.

goal is to calculate the total output energy of the unfiltered output z, consisting of the signals e (tracking error), u_p (control) and y_p (plant output) or a subset of these signals, subject to certain *specific* inputs, i.e., the signals r (reference), d (disturbance) and η (measurement noise) or a subset of these inputs. Again, we only consider SISO plants and controllers. The inputs are assumed to be known a priori, and this knowledge is captured in the input filters W_r, W_d and W_η, whose inputs are bundled in the exogenous input w. Possible input filters have already been discussed in Section 7.4.2. Note that when an impulse input is applied to these filters, their outputs indeed approximate a step, ramp or sine wave respectively. Hence, the total energy in z as a result of such specific signals

in r, d or η gets arbitrarily close to the total output energy of the impulse response from w to z, which is an interpretation of the $\mathcal{H}_2$ norm. It is well-known that the $\mathcal{H}_2$ norm of a linear system is bounded only if the corresponding closed-loop transfer matrix between w and z is strictly proper [127, 134]. As in the closed-loop system the transfer matrix between r and e is defined by the sensitivity function, which is biproper, a strictly proper filter W_r is needed to obtain a strictly proper transfer matrix from $\bar{r}$ to e. A similar reasoning can be applied to the other input signals, which implies that the following assumption is required to ensure a bounded $\mathcal{H}_2$ norm.

Assumption 8.2 *The input filters W_r, W_d and W_η are all strictly proper.*

The strict properness of these filters is quite natural in practice, as is also indicated by the three examples in Section 7.4.2. As discussed in Section 8.1, to compute the $\mathcal{H}_2$ norm we will use the initial condition setting and assume $w=0$. However, in order to be able to select appropriate initial states $x_0=\mathcal{B}_j$ later on, we will elaborate on the plant and controller dynamics without this assumption for now. The dynamics of the reset controller is discussed in Section 7.1.2, but here we make a slight adjustment. The strict properness of the weighting functions implies that there is no direct feedthrough between the input w and the controller input signal e (i.e., $D_w=0$) or between w and z (i.e., $D_{zw}=0$). This simplifies (7.4a) and (7.4b) to

$$\mathfrak{C} := \{x \in \mathbb{R}^n : E_f T_x x \geq 0 \quad \text{or} \quad E_f T_x x \leq 0\} \tag{8.9a}$$

$$\mathfrak{D} := \{x \in \mathbb{R}^n : E_R T_x x \geq 0 \quad \text{or} \quad E_R T_x x \leq 0\}, \tag{8.9b}$$

which now only depend on x.
We combine the augmented plant and the reset controller into one closed-loop system, described by Σ as

$$\Sigma : \begin{cases} \dot{x} &= \mathcal{A}x + \mathcal{B}w & \text{if } x \in \mathfrak{C} \\ x^+ &= \mathcal{A}_R x & \text{if } x \in \mathfrak{D} \\ z &= \mathcal{C}x + \mathcal{D}w, \end{cases} \tag{8.10}$$

where, using $D_w=0$ and $D_{zw}=0$,

$$\left[\begin{array}{c|c} \mathcal{A} & \mathcal{B} \\ \hline \mathcal{C} & \mathcal{D} \end{array}\right] = \left[\begin{array}{cc|c} A+BD_KC & BC_K & B_w \\ B_KC & A_K & 0 \\ \hline C_z+D_zD_KC & D_zC_K & 0 \end{array}\right], \; \mathcal{A}_R = \begin{bmatrix} I_{n_p} & 0 \\ 0 & A_r \end{bmatrix}.$$

At this point we return to the assumption that $w=0$ and consider non-zero initial values of the input filters. Hence, we take $w=0$ and $x_0=\mathcal{B}_j$. Note that $x_0=\mathcal{B}_i+\mathcal{B}_j$ where $i \neq j$ is also a valid initial condition corresponding to simultaneous impulses on both channels i and j. Again, to guarantee local existence of solutions, we adopt Assumption 7.1, and Lemma 7.2 reduces to

Lemma 8.3 *Given the system* (8.10)*, the set $\mathcal{F}_\mathfrak{C}$ in Assumption 7.1 can be characterized by two lexicographic orderings, i.e.,*

$$\mathcal{F}_\mathfrak{C} = \{x_0 \in \mathfrak{C} : \left(E_f T_x x_0, E_f T_x \mathcal{A} x_0, E_f T_x \mathcal{A}^2 x_0, \ldots, E_f T_x \mathcal{A}^{n-1} x_0\right) \geq_\ell 0 \\ \text{or} \; \left(E_f T_x x_0, E_f T_x \mathcal{A} x_0, E_f T_x \mathcal{A}^2 x_0, \ldots, E_f T_x \mathcal{A}^{n-1} x_0\right) \leq_\ell 0\}.$$

We are now ready to present the main results on the LMI-based calculation of an upperbound on the $\mathcal{H}_2$ norm of reset control systems, which is defined as follows.

Definition 8.4 *The squared $\mathcal{H}_2$ norm of reset control system* (7.5) *corresponding to an initial value $x_0 \in \mathbb{R}^n$ is equal to the squared total output energy and is defined as*

$$||\Sigma||_{2,x_0}^2 = \int_0^\infty z^T z \, dt, \tag{8.11}$$

where z denotes the output trajectory corresponding to (7.5) *and initial state x_0 (and $w=0$).*

8.3 Common Lyapunov function

Although a reset control system behaves in a hybrid manner, the mathematical description of its dynamics (8.10) shows that both the flow and the reset part can be described in a linear fashion. This motivates our choice to focus first on a common quadratic Lyapunov function $V(x) = x^T P x$ as also done in Section 7.3.

Theorem 8.5 *Consider the reset control system* (8.10) *with $\mathfrak{C}$ and $\mathfrak{D}$ as defined in* (8.9)*. This system is globally asymptotically stable and its $\mathcal{H}_2$ norm $||\Sigma||_{2,x_0} \leq \gamma$ if there exist $P \succ 0$ and $U_f, U_R \in \mathbb{S}_+^{2\times 2}$ such that*

$$\mathcal{A}^T P + P\mathcal{A} + \mathcal{C}^T\mathcal{C} + T_x^T E_f^T U_f E_f T_x \prec 0 \tag{8.12a}$$

$$\mathcal{A}_R^T P \mathcal{A}_R - P + T_x^T E_R^T U_R E_R T_x \preceq 0 \tag{8.12b}$$

$$\gamma^2 - x_0^T P x_0 \geq 0. \tag{8.12c}$$

Proof: The storage function $V(x) = x^T P x$ is continuously differentiable. Since $P \succ 0$, $V(x) > 0$ for $x \neq 0$ and hence, V is positive definite. Note that

$$x \in \mathfrak{C} \quad \Rightarrow \quad x^T T_x^T E_f^T U_f E_f T_x x \geq 0 \tag{8.13a}$$

$$x \in \mathfrak{D} \quad \Rightarrow \quad x^T T_x^T E_R^T U_R E_R T_x x \geq 0, \tag{8.13b}$$

since $U_f, U_R \in \mathbb{S}_+^{2\times 2}$ only have nonnegative elements. Furthermore, (8.12a) is strict, which implies that $\mathcal{A}^T P + P\mathcal{A} + \mathcal{C}^T\mathcal{C} + T_x^T E_f^T U_f E_f T_x \prec 0$ and thus

$$\left\langle \frac{\partial V}{\partial x}, \mathcal{A}x \right\rangle < -\varepsilon V \quad \text{if } x \in \mathfrak{C}, x \neq 0, \tag{8.14}$$

for some $\varepsilon > 0$. Combining (8.13b) with (8.12b) gives

$$x^T(\mathcal{A}_R^T P \mathcal{A}_R - P)x \leq 0 \qquad \text{if } x \in \mathfrak{D}, \tag{8.15}$$

and thus

$$V(x^+) \leq V(x) \quad \text{when } x \in \mathfrak{D}. \tag{8.16}$$

Continuous differentiability and positive definiteness of V together with (8.14) and (8.16), and the fact that V is radially unbounded imply that system (8.10) is globally asymptotically stable [50].
The proof that $||\Sigma||_{2,x_0} \leq \gamma$ is based on showing that assumptions (8.12) imply, for $V(x) = x^T P x$ and $s(w,z) = -z^T z$, that

$$\left\langle \frac{\partial V}{\partial x}, \mathcal{A}x \right\rangle \leq s(w,z) \quad \text{when } x \in \mathfrak{C}\backslash\{0\}. \tag{8.17}$$

Indeed, if (8.17) would hold then, since (8.16) also holds, we have that for all $t_1 \geq t_0$

$$V(x(t_1)) - V(x(t_0)) \leq \int_{t_0}^{t_1} s(w(t), z(t)) dt, \tag{8.18}$$

showing that (8.10) is dissipative w.r.t. the supply function $s(w,z) = -z^T z$. Using that $V(x(t_1)) \geq 0$ and letting $t_1 \to \infty$, the combination of (8.18) and (8.12c) yields

$$||\Sigma||_{2,x_0}^2 = \int_0^\infty z^T(t) z(t)\, dt = -\int_0^\infty s(w(t), z(t)) dt \leq V(x(0)) \leq \gamma^2. \tag{8.19}$$

To show (8.17), combine (8.13a) with (8.12a) to yield that

$$x^T(\mathcal{A}^T P + P\mathcal{A} + \mathcal{C}^T\mathcal{C})x < 0 \qquad \text{if } x \in \mathfrak{C}\backslash\{0\}, \tag{8.20}$$

which is just a reformulation of (8.17). Hence, the proof is complete. ■

8.4 Piecewise quadratic Lyapunov function

Although Theorem 8.5 provides an easy way to determine an upperbound on the $\mathcal{H}_2$ norm for a specific x_0, it can be conservative for the same reasons as discussed in Section 7.4. Therefore, we propose here also the use of piecewise quadratic Lyapunov functions based on the same partitioning of the flow set as in Section 7.4. The corresponding regions $\mathfrak{C}_i$ and $\mathfrak{D}$ are given by

$$\mathfrak{C}_i := \{x \in \mathbb{R}^n : E_{x,i} x \geq 0 \quad \text{or} \quad E_{x,i} x \leq 0\} \tag{8.21a}$$
$$\mathfrak{D} := \{x \in \mathbb{R}^n : E_{x,R} x \geq 0 \quad \text{or} \quad E_{x,R} x \leq 0\}. \tag{8.21b}$$

Using this partitioning, the calculation of an $\mathcal{H}_2$ upperbound can be performed using the following theorem.

Theorem 8.6 *The reset control system* (8.10) *is globally asymptotically stable with an $\mathcal{H}_2$ norm $||\Sigma||_{2,x_0} \leq \gamma$ if, for a given N, there exists $P_i, P_R \in \mathbb{S}^{n\times n}$ and $U_i, U_{R_0}, U_{R_i}, U_{RI_i}, V_i, V_R \in \mathbb{S}_+^{2\times 2}$ such that*

$$\mathcal{A}^T P_i + P_i \mathcal{A} + \mathcal{C}^T\mathcal{C} + E_{x,i}^T U_i E_{x,i} \prec 0, \qquad i = 1, \ldots, N \tag{8.22a}$$

$$\mathcal{A}_R^T P_R \mathcal{A}_R - P_R + E_{x,R}^T U_{R_0} E_{x,R} \preceq 0 \tag{8.22b}$$
$$\mathcal{A}_R^T P_i \mathcal{A}_R - P_R + E_{x,R}^T U_{R_i} E_{x,R} + \mathcal{A}_R^T E_{x,i}^T U_{RI_i} E_{x,i} \mathcal{A}_R \preceq 0, \quad i = 1, \ldots, N \tag{8.22c}$$
$$P_i - T_x^T E_i^T V_i E_i T_x \succ 0, \qquad i = 1, \ldots, N \tag{8.22d}$$
$$P_R - T_x^T E_R^T V_R E_R T_x \succ 0 \tag{8.22e}$$
$$W_{\Phi i}^T (P_i - P_{i+1}) W_{\Phi i} = 0, \qquad i = 1, \ldots, N-1 \tag{8.22f}$$
$$W_{\Phi 0}^T (P_R - P_1) W_{\Phi 0} = 0 \tag{8.22g}$$
$$W_{\Phi N}^T (P_N - P_R) W_{\Phi N} = 0 \tag{8.22h}$$
$$\gamma^2 - x_0^T P_j x_0 \geq 0, \qquad j \in I(x_0) \tag{8.22i}$$

where $I(x_0) := \{i \mid x_0 \in \mathfrak{C}_i\}$ *denotes the indices of the regions that contain* x_0.

Proof: The function V defined as $V(x) = V_i(x) := x^T P_i x$ when $x \in \mathfrak{C}_i$ and $V(x) = x^T P_R x$ when $x \in \mathfrak{D}$, is a continuous piecewise quadratic function due to continuity constraints (8.22f), (8.22g) and (8.22h) and is thus locally Lipschitz continuous as can be proven similarly as in the proof of Theorem 7.7. Furthermore, V is positive definite. To show this, note that for $x \in \mathfrak{C}_i \backslash \{0\}$ (not necessarily for all x) it holds that

$$V(x) = x^T P_i x \overset{(8.22d)}{>} x^T T_x^T E_i^T V_i E_i T_x x \geq 0 \tag{8.23}$$

as $x \in \mathfrak{C}_i \Rightarrow x^T T_x^T E_i^T V_i E_i T_x x \geq 0$ due to the fact that $V_i \in \mathbb{S}_+^{2\times 2}$ has nonnegative elements. The same applies for $x \in \mathfrak{D}$ using (8.22e). Using (8.22a) and (8.22b) similarly as in the proof of Theorem 8.5 again shows global asymptotic stability, as V is proven to be a Lyapunov function for the reset system.
Furthermore, applying (8.22a), (8.22b), and (8.22c) similarly as in the dissipativity part of the proofs of Theorems 8.5 and 7.7 gives

$$\left\langle \frac{\partial V_i}{\partial x}, \mathcal{A}x \right\rangle < -z^T z \qquad \text{if } x \in \mathfrak{C}_\mathrm{i},\ x \neq 0 \tag{8.24a}$$
$$V(x^+) - V(x) \leq 0 \qquad \text{if } x \in \mathfrak{D}. \tag{8.24b}$$

Clearly, (8.24a) and (8.24b) guarantee that

$$V(x(t_1)) - V(x(t_0)) \leq \int_{t_0}^{t_1} s(w(t), z(t)) dt, \tag{8.25}$$

which in turn yields that $||\Sigma||_{2,x_0}^2 \leq V(x(0)) \leq \gamma^2$ as in the proof of Theorem 8.5. ∎

This upperbound can be lowered by increasing the number of subregions N, thereby increasing the tightness of the approximation of the actual $\mathcal{H}_2$ norm. Hence, as the solution to the LMIs in Theorem 8.5 is always a solution to (8.22) for some U_i, U_R, V_i, V_R, Theorem 8.6 is always less conservative than Theorem 8.5.

8.5 Example

As mentioned before, performance improvement by using reset control is especially apparent in the transient closed-loop behavior of constrained problems, which motivates our choice to consider the $\mathcal{H}_2$ norm of reset control systems. Indeed, in this section we show, by means of an input constrained $\mathcal{H}_2$ problem, that reset control can perform better than linear control in a specific situation. Consider a closed-loop system with an integrator plant, $G(s)=\frac{1}{s}$, which should track a unit step reference $r(t)=1(t)$. The goal is to minimize the energy in the tracking error e for this specific reference, subject to a maximum allowed control signal u to the plant (see Figure 8.2), as is usually the case in practical situations. Hence, the design problem is

$$\min_{K} \quad \sqrt{\int_0^\infty e^2\,dt} \tag{8.26a}$$

$$\text{subject to} \quad |u(t)| \leq 1 \qquad \forall t \geq 0. \tag{8.26b}$$

The theoretically best non-linear controller for this specific problem is described by the discontinuous feedback law

$$u = \text{sign}(e), \tag{8.27}$$

since this controller produces the maximum control signal as long as possible, and vanishes as soon as the plant output reaches the desired value. This way the plant reacts as fast as possible, without any overshoot, realizing a minimal amount of energy in e, i.e., $\sqrt{1/3} \approx 0.577$. The closed-loop response resulting from this discontinuous feedback is depicted in Figure 8.4 by the black line. We now try to approach this optimal performance by using both linear and reset control. First, the optimal linear controller will be designed. Common multi-objective controller design methods rely on norm-based optimization functionals and constraints [127], whereas problem (8.26) is given in terms of time-domain signals. A common attempt to capture the essence of time-domain specifications such as (8.26b) is the reformulation into the frequency domain [64]. As such, we could approximate problem (8.26) via a multiobjective problem, schematically represented in Figure 8.3, and formulated as

$$\min_{K} \quad \gamma_2 = ||T_{11}||_2 \tag{8.28a}$$

$$\text{subject to} \quad ||T_{22}||_\infty < \gamma_\infty, \tag{8.28b}$$

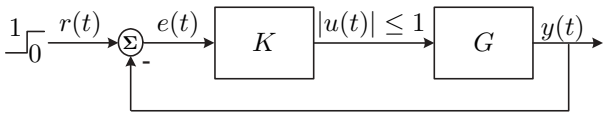

Figure 8.2: Closed-loop for design problem (8.26).

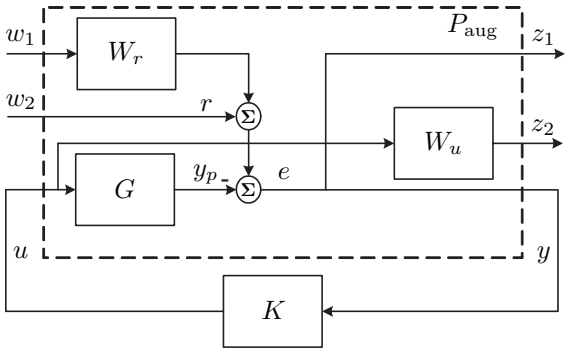

Figure 8.3: Augmented plant for multiobjective problem (8.28).

where T_{11} denotes the transfer function from w_1 to z_1, T_{22} is the transfer between w_2 and z_2, and $\gamma_\infty = 1$. Note that here $W_u(s) = 1$ and $W_r(s) = \frac{1}{s+\varepsilon}$.
The standard method to approximate the optimum for (8.28) is by requiring a common Lyapunov function for both specifications, and applying a linearizing change of variables [127]. Using this method, the static linear controller $K = 1$ with an actual $\mathcal{H}_2$ norm from w_1 to z_1 of $\sqrt{1/2} \approx 0.707$ is obtained. The closed-loop response of this controller is also shown in Figure 8.4 by the grey line. However,

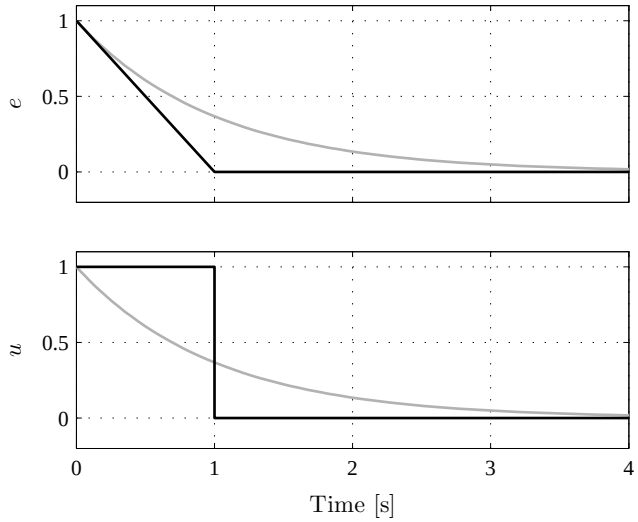

Figure 8.4: Closed-loop responses using the hybrid feedback (black) and the mixed objective controller (grey).

both the transition from (8.26) to (8.28) and the common Lyapunov solution method are conservative, meaning that the controller $K = 1$ is not necessarily the optimal linear one for the original problem (8.26). There are more advanced

optimization techniques available to solve (8.28) with less conservatism, but still these techniques do not necessarily return the optimal controller for (or an exact lower- or upperbound on the objective of) the original problem (8.26).

Another method to obtain some optimal linear controller for (8.26), is the use of numerical optimization tools like `fminsearch` in Matlab to specify the constraint and objective of (8.26) in the time-domain. For now, only first-order controllers are considered. After numerous iterations with various initial conditions, the solution eventually converged to the controller parameterized by

$$\left[\begin{array}{c|c} A_{K,\text{lin}} & B_{K,\text{lin}} \\ \hline C_{K,\text{lin}} & D_{K,\text{lin}} \end{array}\right] = \left[\begin{array}{c|c} -1.4775 & 0.6602 \\ \hline 2.4794 & 0.9259 \end{array}\right], \tag{8.29}$$

with an $\mathcal{H}_2$ norm of 0.599. The closed-loop response with this controller is shown in Figure 8.5 by the grey line.

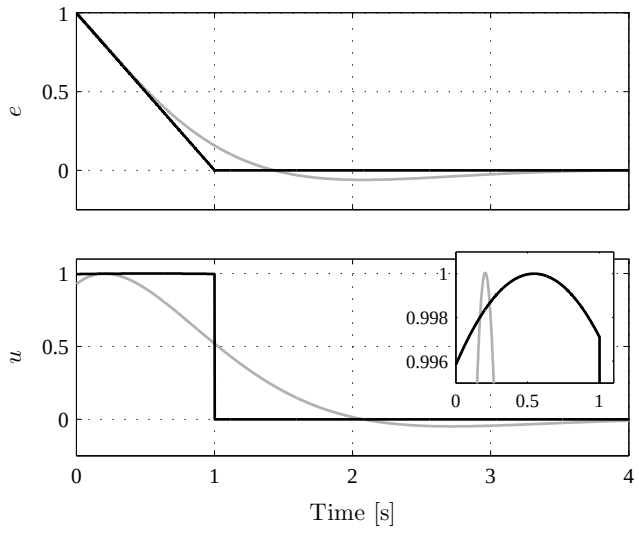

Figure 8.5: Closed-loop responses u and e using linear controller (8.29) (grey), and the reset controller (8.30) (black). The inlay shows a close-up of the flow behavior of the reset controller in u.

A similar approach can be used to find a first order reset controller. Again using various initial conditions, the solution converged to the controller parameterized by $A_r = 0$ and

$$\left[\begin{array}{c|c} A_K & B_K \\ \hline C_K & D_K \end{array}\right] = \left[\begin{array}{c|c} 0.9831 & -0.3843 \\ \hline -2.6201 & 0.9958 \end{array}\right]. \tag{8.30}$$

The black lines in Figure 8.5 show its closed-loop response. Theorem 8.6 can now

be applied to approximate the $\mathcal{H}_2$ norm, using the plant parameters

$$A = \begin{bmatrix} 0 & 0 \\ 0 & -\varepsilon \end{bmatrix}, \quad B = \begin{bmatrix} 1 \\ 0 \end{bmatrix}, \quad B_w = \begin{bmatrix} 0 \\ 1 \end{bmatrix},$$
$$C = C_z = \begin{bmatrix} -1 & 1 \end{bmatrix}, \quad D_z = 0.$$

By increasing the number of subregions N, the upperbound on the $\mathcal{H}_2$ norm becomes less conservative, and for $N = 30$ we obtain $\gamma = 0.579$. The actual energy content in e obtained by the reset controller, calculated by numerical integration of the energy in e, equals 0.578, which shows the accuracy of Theorem 8.6. It can be seen in Figure 8.5 that the time-domain performance of the reset controller is comparable to the discontinuous controller (8.27). When the order of the linear controller increases, the response starts to resemble the hybrid response, see Figure 8.6. Although the $\mathcal{H}_2$ norm decreases with increasing controller order, the first order reset controller still yields a lower one. All results are summarized in Table 8.1. Hence, when considering only first order controllers, the obtained

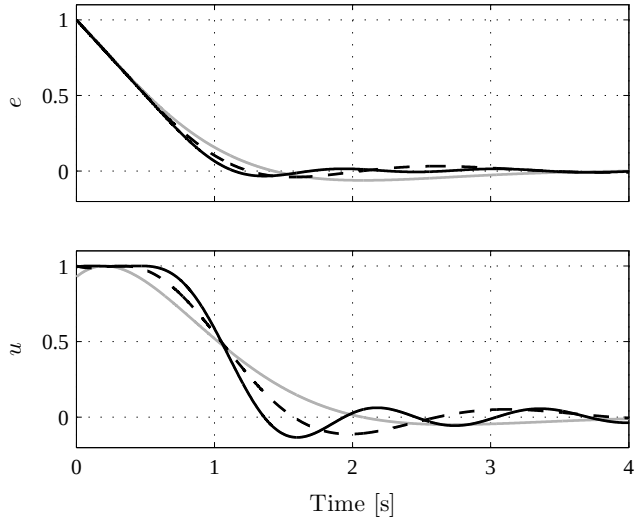

Figure 8.6: Closed-loop responses u and e using linear controllers of order 1 (solid grey), 2 (dashed black), and 4 (solid black).

reset controller clearly outperforms the linear controller.
We emphasize that it is not guaranteed that the constructed controllers are the

Table 8.1: $\mathcal{H}_2$ norms for various controllers

		linear control order			reset control			
	hybrid	1	2	4	N=3	N=5	N=10	N=30
Numerical int.	0.577	0.599	0.586	0.580	0.578	0.578	0.578	0.578
LMI approx.	-	0.599	0.586	0.580	0.665	0.606	0.584	0.579

optimal ones for problem (8.26), since the nonlinear optimization routine is not necessarily converging to the global optimum.

Chapter 9

Discussion

In this chapter the results obtained in Chapters 7 and 8 are reflected upon. We discuss the possibilities of reset controller synthesis, implementation issues, and finalize by stating the conclusions.

9.1 Discussion

Previous publications have shown in simulations [6, 23] and experiments [18, 24, 154] that reset control can outperform linear control in some situations. The $\mathcal{H}_\infty$ and $\mathcal{H}_2$ analysis tools presented in Chapters 7 and 8, respectively, can be very useful to quantify this ability. The main problem, however, is the actual synthesis of a reset controller that outperforms a linear controller. In this section, we reflect on the possibilities for controller synthesis, and on practical implementation issues.

9.1.1 Synthesis

Using standard LMI-based $\mathcal{H}_\infty$ and $\mathcal{H}_2$ analysis techniques, it is possible to design the corresponding optimal linear controllers for an LTI system, e.g. by using the synthesis method from [127]. The synthesis of a reset controller, however, is still an open question. With the currently available knowledge it seems impossible to formulate $\mathcal{H}_\infty$ or $\mathcal{H}_2$ synthesis LMIs to find the optimal reset controller. This problem is to a large extend caused by the $E_{\cdot,\cdot}^T U . E_{\cdot,\cdot}$ terms in the analysis LMIs in Theorems 7.6, 7.7, 7.8, 8.5, and 8.6 which introduce bilinear combinations of design variables. Unfortunately, these nonlinearities cannot be eliminated using the procedure from [47] or linearized via the change of variables introduced in

[127]. Therefore, it is not straightforward to arrive at synthesis LMIs. Resorting to bilinear matrix inequality (BMI) solvers, of which some are available without guarantees on finding solutions if they exist, is one option. An alternative way can be to use recent results on optimization of matrix valued polynomials by sum-of-squares methods [58].

Furthermore, it is questionable whether reset control can ever outperform linear controllers in terms of the $\mathcal{L}_2$ gain or $\mathcal{H}_2$ performance. Indeed, as is shown in [76] and [116], for LTI plants there exists no nonlinear (possibly time-varying) controller which yields a lower $\mathcal{L}_2$ gain than the optimal linear controller. Unfortunately, we expect reset control to be no exception to this. We therefore point out that Examples 2 and 3 in [101] do not provide a fair comparison between linear and reset controllers; in both examples it is easy to find linear controllers with lower $\mathcal{H}_\infty$ norms, and hence better performance when quantified in terms of the $\mathcal{L}_2$ gain. However, the performance improvement of reset controllers with respect to linear controllers can be shown by transient response performance qualifiers such as rise-time, overshoot, and settling-time as in the examples of Section 6.2. Therefore, it is still of interest to be able to characterize the $\mathcal{L}_2$ gain and $\mathcal{H}_2$ performance of reset control systems.

9.1.2 Design issues

Although reset control might seem very advantageous, its usage and implementation is far from straightforward. To illustrate this, reconsider the relaxation of the resetting condition, i.e., reset when $yu \leq 0$ instead of when $y = 0$. For some controllers, like low-pass filters, these two conditions are equivalent, but for others the former performs much worse in an implementation than the latter. This is especially true for controllers with a derivative action, such as lead filters. This derivative action acts like a 'brake' since it reverses the sign of the control signal u when the desired setpoint is approached. The $yu \leq 0$ reset condition then requires a state reset, but also resets this 'braking action', causing a large overshoot instead of preventing it. Hence, $y = 0$ is preferred for implementation reasons, while $yu \leq 0$ clearly has advantages for analysis of the $\mathcal{L}_2$ gain and $\mathcal{H}_2$ norm (note that an analysis with $yu \leq 0$ does not guarantee anything for the $y = 0$ implementation).

Still, even with an $y = 0$ implementation, reset actions tend to counteract derivative controllers, thereby diminishing damping effects. Resets change the dynamical behavior of the (otherwise linear) controller drastically. This observation makes the design of reset controller even more complicated. As an example, simply resetting the states of an $\mathcal{H}_\infty$ optimal linear controller will generally make its performance much worse. That makes the 32 year old frequency-based design of Horowitz [62] still the only currently available synthesis method for reset controllers.

9.2 Summary and conclusions

Motivated by recent publications on the potential advantages of reset control, we have developed a set of analysis LMIs with which the $\mathcal{L}_2$ gain and the $\mathcal{H}_2$ norm of any reset control system that fits into the linear-based generalized plant framework can be approximated. With respect to the $\mathcal{L}_2$ gain, the work in [151] is generalized, while the results on the $\mathcal{H}_2$ norm have not been reported in literature before. The proposed analysis methods can also be applied to tracking and measurement noise problems. The possible conservatism present in the $\mathcal{L}_2$ gain approximation can be removed by including strictly proper input filters for the latter control problems. The introduction of piecewise quadratic Lyapunov functions, which are much more flexible than quadratic ones, results in tighter approximations. Examples have shown the accuracy of the proposed calculations of the $\mathcal{L}_2$ gain and $\mathcal{H}_2$ norm. Furthermore, we have presented an example which shows that reset control can be close to the performance of the optimal (discontinuous) controller for a constrained $\mathcal{H}_2$ problem, while a common optimization method to design a linear controller provides a worse $\mathcal{H}_2$ performance. Finally we reflected on synthesis possibilities and practical design issues.
The initial goal of studying reset control was to formulate a method with which reset controllers could be synthesized. Unfortunately, it turned out that the standard methods to arrive at controller synthesis inequalities, i.e., parameter elimination and the linearizing change of variables, are not applicable to the specific structure of the reset analysis LMIs. Possible solution directions for synthesis are the use of BMI solvers and sum-of-squares decompositions of matrix valued polynomials. However, taking into account the results in [76] and [116], it is not likely that there exists a reset controller yielding a lower $\mathcal{L}_2$ gain than the optimal linear controller. Therefore, any synthesis method resulting in a reset controller that outperforms the optimal linear controller in some sense should not only be based on the $\mathcal{L}_2$ gain, but should rather take performance measures into account which reflect the advantages of reset control, e.g. transient measures such as overshoot and settling-time. Since this is not a trivial procedure even for linear control systems, it is not clear at this point how to proceed for reset controllers. Concluding, the analysis results that are derived in this part of the thesis are well-suited to determine (upperbounds on) the $\mathcal{L}_2$ gain and $\mathcal{H}_2$ norm of a closed-loop reset system with a given reset controller, however, reset controller synthesis is still an open issue.

Part IV

Linear Parameter Varying Control

Chapter 10

Gain scheduling & LPV techniques

In this chapter we shortly review LPV control and discuss the proposed concept to use LPV methods to design nonlinear controllers for linear motion systems in order to improve the performance.

10.1 Introduction

In this part of the thesis we consider linear parameter varying (LPV) controllers for LTI systems. This is a subclass of nonlinear controllers for which systematic analysis and synthesis methods exist. In standard LPV control systems, the main characteristic of the plants that are considered is their dependency on a real-valued parameter vector $\delta(t)$. The general layout that is used for an LPV control problem formulation is depicted in Figure 10.1. The plant, denoted by $P(\delta(t))$, contains the parameter dependent system to be controlled, together with possible input- and output-weightings. The controller K has input $y \in \mathbb{R}^{n_y}$ and output $u \in \mathbb{R}^{n_u}$, while $w \in \mathbb{R}^{n_w}$ is the exogenous input and $z \in \mathbb{R}^{n_z}$ denotes the controlled output. In case the actual value of the parameter vector is not known, it is common to design a robust controller $K = C_R$ to account for the possible parameter variation in the plant $P(\delta(t))$. However, when measurements of $\delta(t)$ are available, the parameter variation can be taken into account in the design of the controller, resulting in a parameter dependent controller $K = C_{PD}(\delta(t))$. Whereas a robust controller C_R results in a stable closed-loop system for all possible parameter values and variations at the expense of performance, the explicit parameter dependence of $C_{PD}(\delta(t))$ could lead to an overall higher performance

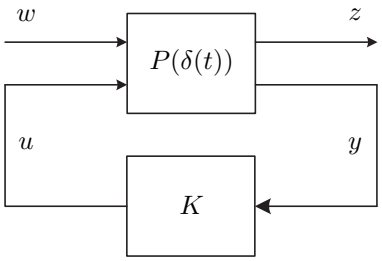

Figure 10.1: General closed-loop gain scheduled and LPV system.

while still maintaining closed-loop stability.
Several control techniques can be classified as a form of LPV control. These include the switching of control gains according to operating conditions or time, as well as complete controller switching and or blending [121]. Normally, the LPV approach can be regarded as the continuous variation of controller parameters according to the current value of the scheduling variables, which can be exogenous or endogenous measured signals. The scheduling variables are usually linked to the dynamics of the system which has to be controlled, i.e., LPV controllers are usually designed for plants whose parameters are varying. In our proposed approach, however, the plant is considered to be linear and time-invariant, and the parameter dependence is introduced through the performance requirements. These performance requirements are represented by weighting filters as is common in loop shaping in the $\mathcal{H}_\infty$ framework [134], see also Figure 10.2. The weighting functions W_e, W_u, and W_{y_p} are used to shape the sensitivity function S, the control sensitivity function R, and the complementary sensitivity function T, respectively. The weighting filters used in our approach are parameter dependent as

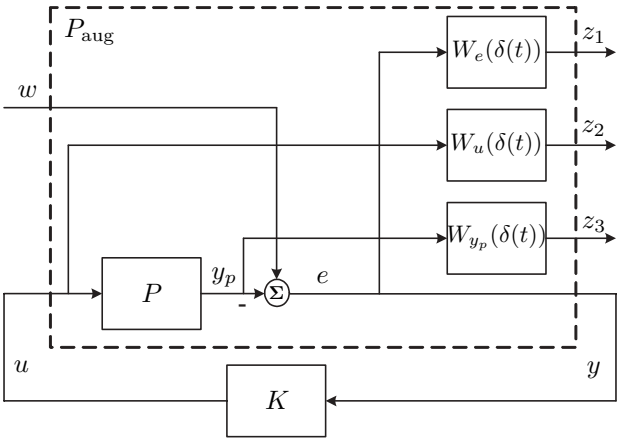

Figure 10.2: General closed-loop LPV setup.

opposed to the standard $\mathcal{H}_\infty$ design method for linear systems, where a trade-off between multiple performance objectives is achieved using LTI weighting filters resulting in a fixed LTI controller. The introduction of parameter dependent performance requirements enables the merging of multiple trade-offs in a single (nonlinear) controller, thereby enriching the spectrum of achievable trade-offs. As an example, consider the standard SISO control scheme depicted in Figure 10.3 with LTI controller C and LTI plant P. Suppose that the reference signal r has

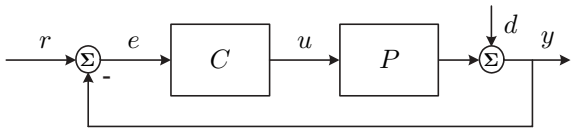

Figure 10.3: Standard control scheme.

frequency content up to 10 Hz and there are no disturbances d present. An LTI controller $C = C_1$ has been designed such that certain requirements on the tracking error e are satisfied, resulting in the sensitivity function S_1 as depicted in Figure 10.4 by the black line. Now suppose that at some point a disturbance d that has frequency content from 10 to 30 Hz enters the system. It is obvious from Figure 10.4 that this disturbance will be amplified in the output y by the controller C_1. If this disturbance leads to unacceptable errors, another controller C_2 has to be designed that does not have this effect, for instance one resulting in sensitivity function S_2 which is also depicted in Figure 10.4. However, due to the waterbed effect (see Section 2.2.2), reducing the disturbance amplification between 10 and 30 Hz implies that the reference tracking below 10 Hz deteriorates. Such a trade-off is always present when applying fixed linear controllers. If the disturbance could be measured, this measurement could be used to enable an LPV controller to adapt to the current operating condition, which would result in a momentary sensitivity function that is well-suited for this operating condition. This can be done by specifying scheduling performance requirements represented by S_1 and S_2 via the weighting function $W_e(\delta)$ where δ is a measure of the momentary disturbance in this case. Notice that this can be seen as a form of adaptive control. A similar approach has been used in [31], where an LPV controller is designed for a DC motor that switches between the following two trade-offs for the closed-loop: (i) a fast response and high control energy versus (ii) a slow response combined with low control energy. The switching is performed via an exogenous scheduling variable, the value of which is a priori selected by the user. An LPV controller for a compact disc player was designed in [28]. In that work, the rotation frequency of the disc was used as the scheduling variable. The result was a controller with a notch filter that shifts its attenuation frequency accordingly to the disc's rotation frequency.

Both the designs from [31] and [28] use an exogenous scheduling variable. However, it is also possible to use a loop variable as the scheduling variable, resulting in a truly nonlinear controller. This idea is pursued in this part of the thesis. We propose a systematic method to design a nonlinear controller that exhibits error

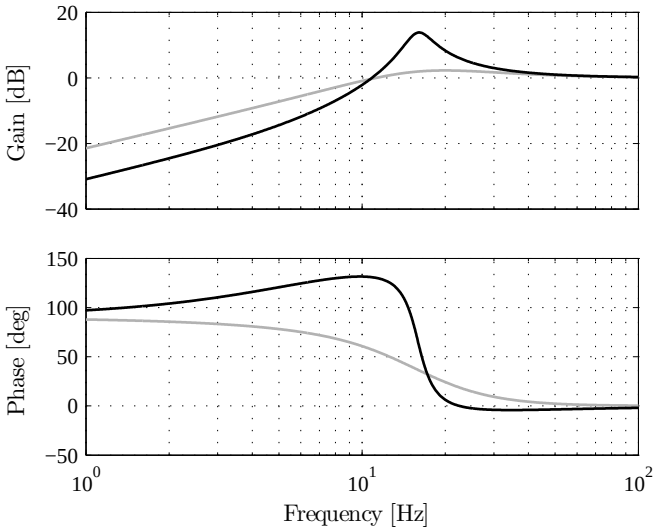

Figure 10.4: Sensitivity functions S_1 (black) and S_2 (grey).

dependent damping in order to improve the time-domain characteristics of the step response in Chapter 11. In Chapter 12, an LPV controller is designed for a vibration isolation system to improve the overall disturbance rejection properties. This is done by using spectral information of the loop signals to adapt the controller to the disturbances that are acting on the system. In the following section, we start by discussing the available procedures for designing an LPV controller.

10.2 LPV synthesis procedures

The design procedure of an LPV controller for a parameter dependent plant generally boils down to four basic steps [121]:

(i) Computation of an LPV model of the (augmented) plant to be controlled.

(ii) Design of controllers for the LPV plant model from (i). This can be done in various ways, e.g. multi controller design, interpolation between various linear controllers, or controller design taking the parameter variation directly into account.

(iii) Implementation of these controllers in such a way that the controller coefficients are scheduled accordingly to the scheduling signals.

(iv) Performance assessment. This mainly depends on the chosen design process in step (ii). If issues such as stability and performance are already taken into account during the design, there is no need for an a posteriori analysis. However, if the design is rather ad hoc and intuitive, extensive simulation is a common way to check stability and performance.

Basically, there are two methods to design a parameter dependent controller, namely by (i) classical gain-scheduling, which boils down to interpolating controllers that are designed for various fixed values of the scheduling variable, and (ii) direct LPV controller synthesis.

10.2.1 Classical gain-scheduling

In the classical gain scheduling approach, linear controllers are designed for a grid of parameter values, which results in an indexed set of controllers. In order to go from this indexed set to a parameterized controller family, two basic options are available. The first is hard switching between the controllers when the plant goes from one operating region to another, and the second way is to interpolate the indexed controllers with respect to the parameter in a smoother way. Hard switching between controllers is in general not desirable because of the transients that can occur when switching, and in most cases it is difficult to guarantee stability due to the hybrid nature. For the second approach, several possibilities are available of which the most common are the interpolation between the state-space controller coefficients [65], and interpolating the gain, poles and zeroes of the controller transfer functions [104]. However, this is mostly done in an ad hoc fashion, and stability is not guaranteed at all intermediate parameter values. There also exist theoretically justified methods that guarantee stabilization at the interpolated operating points [136, 150], but at the cost of conservatism. When finally an interpolated gain scheduled controller is available, the final step is to implement the controller and to assess the closed-loop performance. This implementation step is not straightforward since the choice of the gain scheduled controller realization can result in hidden coupling and greatly influences the closed-loop performance [84, 121]. Performance analysis for this approach is mostly restricted to extensive simulation.

10.2.2 Direct LPV synthesis

As opposed to the above mentioned gridding approach, direct LPV controller synthesis is based on robust control techniques and results in a parameter dependent controller that has guaranteed stability and performance over the complete parameter interval. Consider the general parameter dependent continuous-time system representing an LTI system augmented with parameter dependent weight-

ing filters, given by

$$\begin{aligned} \dot{x}(t) &= A(\delta(t))x(t) + B_w(\delta(t))w(t) + B(\delta(t))u(t) \\ z(t) &= C_z(\delta(t))x(t) + D_{zw}(\delta(t))w(t) + D_z(\delta(t))u(t) \\ y(t) &= C(\delta(t))x(t) + D_w(\delta(t))w(t) + D(\delta(t))u(t) \end{aligned} , \tag{10.1}$$

where $x(t) \in \mathbb{R}^n$ is the state vector, $u(t) \in \mathbb{R}^{n_u}$ the command input, $y(t) \in \mathbb{R}^{n_y}$ the measured output, $z(t) \in \mathbb{R}^{n_z}$ the output of the performance channel, and $w(t) \in \mathbb{R}^{n_w}$ the input of the performance channel at time $t \in \mathbb{R}$. The state-space matrices $A, B_w, B, C_z, D_{zw}, D_z, C, D_w$, and D are rational functions of $\delta(t) \in \mathbb{R}^N$, the (time-varying, real-valued) parameter vector. In LPV control, it is assumed that the parameter $\delta(t)$ is contained in an a priori given set $\boldsymbol{\delta} \subseteq \mathbb{R}^N$. The actual parameter curve is unknown a priori, but can be measured in real time. In the LPV systems we consider, this $\boldsymbol{\delta}$ is a box where each parameter δ_i lies within a given interval $[\underline{\delta}_i, \overline{\delta}_i]$, and is described by

$$\boldsymbol{\delta} := \text{convex hull}(\boldsymbol{\delta}_g), \quad \boldsymbol{\delta}_g := \{\delta \in \mathbb{R}^N : \ \delta_i \in \{\underline{\delta}_i, \overline{\delta}_i\}, \ i = 1, \ldots, N\}, \tag{10.2}$$

where N is the number of parameters. Furthermore, we assume that the rate of variation of the scheduling parameters is not bounded, i.e., the parameters are allowed to vary arbitrarily fast. The LPV design procedure consists of synthesizing a parameter dependent controller of the form

$$\begin{aligned} \dot{x}^c(t) &= A^c(\delta(t))x^c(t) + B^c(\delta(t))y(t) \\ u(t) &= C^c(\delta(t))x^c(t) + D^c(\delta(t))y(t), \end{aligned} \tag{10.3}$$

where $x^c(t) \in \mathbb{R}^{n_c}$ is the controller state at time $t \in \mathbb{R}$ and A^c, B^c, C^c and D^c are parameter dependent matrices of appropriate dimensions. The procedure to synthesize the LPV controller (10.3) can be decomposed in several steps:

1 Formulate the synthesis problem as an extension of the $\mathcal{H}_\infty$ synthesis problem, see e.g. [127], resulting in parameter dependent decision variables and LMIs to be solved. This results in an infinite dimensional optimization problem:
   - as functions of δ: the decision variables belong to an infinite dimensional space.
   - as parameterized by δ in an interval: there is an infinite number of constraints.

2 Restrict the decision variables, functions of δ, to a finite dimensional set, e.g. by restricting them to be constant, affine, multi-affine, quadratic, polynomial, piecewise affine, spline, or rational. This introduces conservatism, the extent of which depends on the specific problem at hand.

3 Revert the infinite number of LMIs (due to parameter dependency in an interval) to a finite set of parameter independent LMIs. This can be done in several ways:

- gridding: solve the LMIs for a grid of the parameter space. The drawback of this approach is that stability and performance cannot be guaranteed at the intermediate values of δ.
- solve at vertices: solve the LMIs at the vertices of a polytopic overapproximation of the parameter space. This approach is only nonconservative for affine parameter dependence. Some methods have been proposed to use the polytopic approach to more general classes of parameter dependence (quadratic/polynomial/PWA), others have been proposed to transform the parameter dependent LMI (quadratic/rational) into an affine one. However, both of these methods introduce conservatism.
- multipliers: this approach utilizes a (scaled) small-gain setting which introduces extra variables, called multipliers or scalings. These multipliers try to describe the nature of the parameter dependency, and the more precise this description is, the less conservative the results will be.

Detailed information about these synthesis procedures can be found in for instance [1, 28, 31, 103, 124, 128, 129] and [4, 29, 30, 147, 149].
An advantage of the classical gain-scheduling method is that the design of the indexed set of controllers is fairly straightforward. A disadvantage is that there is no guaranteed performance for the parameter values between, and even at, the interpolated points. Furthermore, if stability has not been taken into account during the interpolation step (which is generally the case), extensive simulation may be the only way to check stability. The main advantage of the direct LPV synthesis method is that there is a solid theoretical foundation for guaranteed stability and performance for all (infinite number of) values of the scheduling parameter in the interval. The disadvantage is twofold: firstly the synthesis is much more involved since the currently available solvers that are required are very sensitive to the numerical tuning of the optimization parameters, and secondly, possibly conservatism is introduced because of the synthesis procedure.

Chapter 11

An LPV approach to the Lewis servo

In this chapter, we propose a systematic method to design a nonlinear controller for a linear motion system to improve the transient response to a step reference. This is done by representing the desired performance requirements via parameter dependent weighting functions and synthesizing an LPV controller that results in the desired performance.

11.1 Introduction

In 1953, J.B. Lewis introduced the use of nonlinear feedback to improve the rise-time and overshoot of the transient response of a servo mechanism [87]. He achieved this by introducing variable damping in a second order closed-loop system instead of using a constant damping coefficient. To illustrate his reasoning, consider the second order closed-loop system depicted in Figure 11.1 in the standard form

$$T(s) = \frac{y_p(s)}{r(s)} = \frac{\omega_n^2}{s^2 + 2\zeta\omega_n s + \omega_n^2}, \tag{11.1}$$

where s is the Laplace variable, $y_p(s)$ is the Laplace transform of the output $y_p(t) \in \mathbb{R}$, ω_n denotes the natural frequency and ζ is the damping coefficient. Furthermore, $u(s)$ will denote the Laplace transform of the input $u(t) \in \mathbb{R}$. In case system (11.1) is subjected to a unit step input $r(t) = 1(t)$, common performance qualifiers are the rise-time t_r, the maximum percentage overshoot p_os, and the

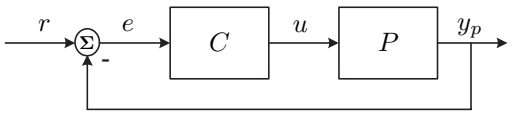

Figure 11.1: Standard closed-loop setup.

settling-time t_s, defined by

$$\begin{aligned} t_r &= \min\{T \in \mathbb{R}_+ \mid y_p(T) = 0.9 \lim_{t\to\infty} y_p(t)\} - \\ &\quad \min\{T \in \mathbb{R}_+ \mid y_p(T) = 0.1 \lim_{t\to\infty} y_p(t)\}, \\ t_s &= \min\{T \in \mathbb{R}_+ \mid |y_p(t) - 1| \leq \varepsilon, \text{ for all } t \geq T\}, \\ p_{os} &= \max\{y_p(t) - 1 \mid t \geq 0\} \times 100\%, \end{aligned}$$

where ε is the allowed error, for instance $\varepsilon = 0.02$. Desired properties of the step response are typically (i) a small rise-time t_r, and (ii) a low percentage overshoot p_{os}. However, it is well-known that there is a trade-off between the speed of the response and the amount of overshoot of this system when subjected to a step input. For large values of the damping ratio ζ there is little to no overshoot, but as ζ decreases, the response develops an overshoot. On the other hand, large values of the damping ratio also imply a sluggish response, while the speed of response increases when the damping ratio decreases, see Figure 11.2.
Lewis' rationale was based on the observation that the rise-time is a measure that is typically of interest when the servo error $e(t)$ is large, while the overshoot comes into play when the servo error is small. Therefore, the trade-off between these two measures, dictated by ζ, could possibly be circumvented if different values of the damping ratio ζ are used for different values of the servo error. In other words, by making the damping ratio a function of the error signal $e(t)$, it would perhaps be possible to have a small rise-time combined with a low percentage overshoot. Indeed, if $\zeta = 1 - \frac{1}{2}\sqrt{2}e$, we have relatively low damping when the response is far from its final value, while we have relatively high damping when the response is near its steady-state value. The resulting closed-loop servo system is called the Lewis servo. The step response of system (11.1) with natural frequency $\omega_n = \sqrt{2}$ with the error dependent damping is depicted in Figure 11.2. Comparing the Lewis servo with the responses for various constant damping ratios, it can be seen that the rise-time of the system with nonlinear damping is close to that of the linear system with damping coefficient $\zeta = 0.6$, while there is virtually no overshoot. The practical effectiveness of a similar method where a PD controller with nonlinear damping is used to control a servo motor has been shown in [48].
The major drawback of both the Lewis design and the nonlinear PD controller from [48] is their ad-hoc approach. These designs are merely based on engineering insight, instead of systematically designing a controller based on a desired (nonlinear) performance requirement. Furthermore, stability can only be analyzed afterwards using Lyapunov techniques [48]. For simple systems with simple requirements (such as varying damping in a second order closed-loop system) the

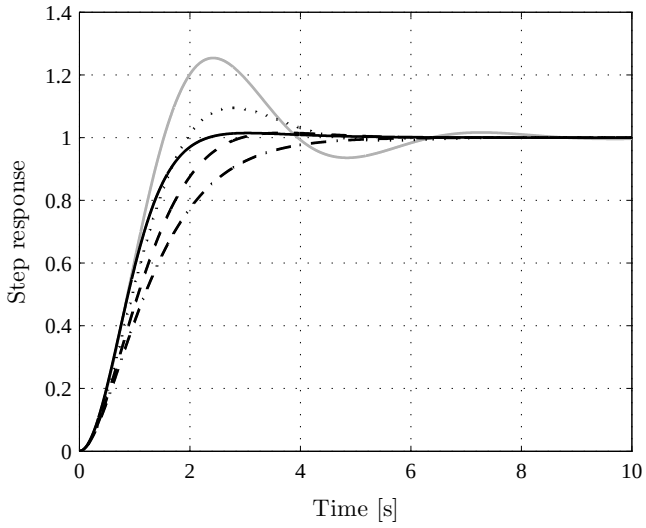

Figure 11.2: Step responses: $\zeta = 1.0$ (dash-dot), $\zeta = 0.8$ (dashed), $\zeta = 0.6$ (dotted), $\zeta = 0.4$ (solid grey), and Lewis servo (solid).

design and analysis can be done by hand. However, when more complex systems and/or performance requirements are considered, it is not obvious how a controller can be designed that achieves the desired performance. This clearly indicates the need for more systematic design methodologies that can exploit the benefits as demonstrated via the Lewis servo.
A well-developed framework for controller synthesis using predefined performance requirements is $\mathcal{H}_\infty$ loop shaping. The performance requirements that are used in this framework are formulated in the frequency domain through weighting functions, which are LTI and fixed for such a design. Unfortunately, a performance specification as varying damping cannot be expressed by such a fixed weighting function. A natural extension to be able to cope with varying performance specifications is the use of weighting functions that depend on some parameter δ, see Figure 10.2. In this chapter, we will apply both the classical gain-scheduling method as well as the direct LPV synthesis approach to the design of a Lewis servo-like closed-loop system. For this purpose, parameter dependent weighting functions are designed to characterize the error dependent performance requirements. We start by considering the Lewis servo as the closed-loop system of a servomotor and a nonlinear controller in Section 11.2, and design the nonlinear controller by hand. In Section 11.3, $\mathcal{H}_\infty$ controllers are designed for a grid of the parameter interval and an LPV controller is obtained by interpolation of the various $\mathcal{H}_\infty$ controllers. Finally, in Section 11.4 an LPV controller is synthesized based on the methods proposed in [31, 124, 128]. We end by stating the conclusions in Section 11.5.

11.2 The Lewis servo as a closed-loop system

Since the Lewis servo as described above is a relatively simple system, it is possible to design a controller by hand that results in the desired step response characteristic. As is standard in classical gain scheduled controller design, the scheduling parameter is treated as a constant during the design [121]. Therefore, define $\delta = 2\zeta\omega_n = 2\sqrt{2} - 2e$ and assume for now that δ is a constant. Closed-loop system (11.1) can then be obtained by controlling a simple model of a servomotor given by

$$P(s) = \frac{1}{s^2}, \tag{11.2}$$

by controller

$$C(s) = \frac{\omega_n^2 s}{s + \delta}. \tag{11.3}$$

The resulting closed-loop system in state-space representation is given by (now we do not need to assume that δ is constant)

$$\begin{aligned} \dot{x}_1 &= x_2 \\ \dot{x}_2 &= -\omega_n^2 x_1 - \delta x_2 + \omega_n^2 r \\ y_p &= x_1, \end{aligned} \tag{11.4}$$

with input/output behavior governed by the differential equation

$$\ddot{y}_p + \delta \dot{y}_p + \omega_n^2 y_p = \omega_n^2 r. \tag{11.5}$$

If the nonlinear damping ratio $\delta = 2\sqrt{2} - 2e$, with $e = r - x_1$ and the natural frequency $\omega_n = \sqrt{2}$ are substituted in closed-loop system (11.4), the desired Lewis servo, given by

$$\begin{aligned} \dot{x}_1 &= x_2 \\ \dot{x}_2 &= -2x_1 - (2\sqrt{2} - 2r + 2x_1)x_2 + 2r \\ y_p &= x_1 \end{aligned} \tag{11.6}$$

is obtained with input/output behavior governed by the nonlinear differential equation

$$\ddot{y}_p + (2\sqrt{2} - 2r + 2y_p)\dot{y}_p + 2y_p = 2r. \tag{11.7}$$

The actual implementation of the nonlinear damping ratio is done through the controller. There are several ways in which the controller could be implemented. It turns out that the chosen realization is key for the resulting closed-loop performance.

11.2.1 Observer canonical form

The generalized plant depicted in Figure 10.2, with performance channel output $z = e = (w - y_p)$, performance channel input $w = r$, and measured output $y = e$ is described in state-space form as

$$\begin{bmatrix} \dot{x_1} \\ \dot{x_2} \\ z \\ y \end{bmatrix} = \begin{bmatrix} 0 & 1 & 0 & 0 \\ 0 & 0 & 0 & 1 \\ -1 & 0 & 1 & 0 \\ -1 & 0 & 1 & 0 \end{bmatrix} \begin{bmatrix} x_1 \\ x_2 \\ w \\ u \end{bmatrix}, \tag{11.8}$$

while the controller (11.3) can be represented in the observer canonical form by

$$\begin{bmatrix} \dot{x^c} \\ u \end{bmatrix} = \begin{bmatrix} -\delta & -2\delta \\ 1 & 2 \end{bmatrix} \begin{bmatrix} x^c \\ y \end{bmatrix}. \tag{11.9}$$

Closed-loop system (11.8), (11.9) is given by

$$\begin{aligned} \dot{x} &= \begin{bmatrix} 0 & 1 & 0 \\ -2 & 0 & 1 \\ 2\delta & 0 & -\delta \end{bmatrix} x + \begin{bmatrix} 0 \\ 2 \\ -2\delta \end{bmatrix} w \\ y_p &= \begin{bmatrix} 1 & 0 & 0 \end{bmatrix} x, \end{aligned} \tag{11.10}$$

with $x = \begin{bmatrix} x_1 \, x_2 \, x^c \end{bmatrix}^T$ resulting in the input/output behavior

$$\ddot{y}_p + \delta \dot{y}_p + 2y_p = 2w, \tag{11.11}$$

which is equal to (11.5). For constant values of the scheduling parameter δ, controller (11.9) indeed results in the desired behavior. Unfortunately, this is not the case if the controller is implemented by setting $\delta = 2\sqrt{2} - 2e$. The step response of closed-loop system (11.8), (11.9) with $\delta = 2\sqrt{2} - 2e$ is depicted in Figures 11.3(a) and (b) for two different values of the step size $w = r(t)$. The corresponding step responses of the desired closed-loop system (11.6) are also shown in these figures. From these figures, it is obvious that controller (11.9) does not result in the desired closed-loop performance. This is due to the hidden coupling [121] that is introduced by setting $\delta = 2\sqrt{2} - 2e$. The observation that the response differs from the desired response when the supposedly constant parameter δ is replaced by a function of the actual scheduling signal can be made more explicit when the nonlinear differential equations of closed-loop system (11.10), i.e.,

$$\dot{y}_p = x_2 \tag{11.12a}$$

$$\dot{x}_2 = -2y_p + x^c + 2w \tag{11.12b}$$

$$\begin{aligned} \dot{x}^c = {} & 2(2\sqrt{2} - 2w + 2y_p)y_p - (2\sqrt{2} - 2w + 2y_p)x^c \\ & -2(2\sqrt{2} - 2w + 2y_p)w \end{aligned} \tag{11.12c}$$

are considered. From equations (11.12a) and (11.12b) we obtain

$$\ddot{y}_p = -2y_p + x^c + 2w \Rightarrow x^c = \ddot{y}_p + 2y_p - 2w, \tag{11.13}$$

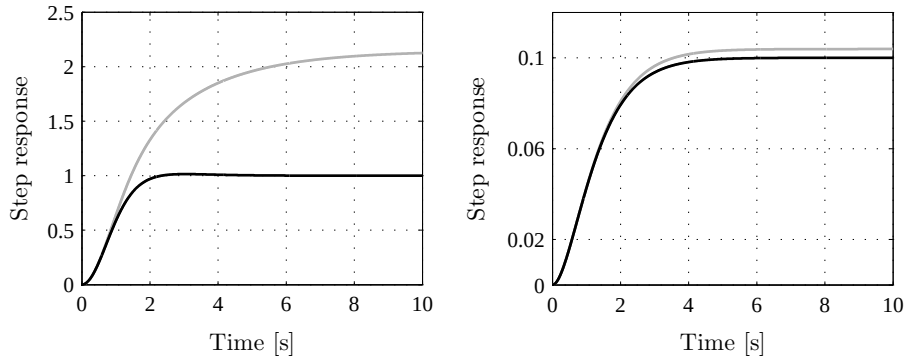

(a) (b)

Figure 11.3: Step response with controller (11.9) (grey) and of system (11.6) (black) for different step sizes. (a) $w=1$, (b) $w=0.1$.

which can be substituted in (11.12c) to yield the input/output behavior

$$\dddot{y}_p + (2\sqrt{2} - 2w + 2y_p)\ddot{y}_p + 2\dot{y}_p = 2\dot{w}. \tag{11.14}$$

Clearly, this behavior is not equivalent to the desired behavior (11.7). This is due to additional nonlinear terms that are introduced when the supposedly static scheduling parameter δ is replaced by the state and input dependent scheduling signal $\delta = 2\sqrt{2} - 2e$. This phenomenon is known as hidden coupling [121].

11.2.2 Controller canonical form

The controller can also be represented in controller canonical form via

$$\begin{bmatrix} \dot{x^c} \\ u \end{bmatrix} = \begin{bmatrix} -\delta & 1 \\ -2\delta & 2 \end{bmatrix} \begin{bmatrix} x^c \\ y \end{bmatrix}, \tag{11.15}$$

resulting in the closed-loop system

$$\begin{aligned} \dot{x} &= \begin{bmatrix} 0 & 1 & 0 \\ -2 & 0 & -2\delta \\ -1 & 0 & -\delta \end{bmatrix} x + \begin{bmatrix} 0 \\ 2 \\ 1 \end{bmatrix} w \\ y_p &= \begin{bmatrix} 1 & 0 & 0 \end{bmatrix} x, \end{aligned} \tag{11.16}$$

with $x = \begin{bmatrix} x_1 \, x_2 \, x^c \end{bmatrix}^T$. If the scheduling parameter δ is again considered to be constant, the resulting input/output behavior equals (11.5). Hence, for constant values of the scheduling parameter δ, controller (11.15) also results in the desired behavior. The input/output behavior resulting from implementing controller (11.15) with $\delta = 2\sqrt{2} - 2e$ can be obtained by analyzing the closed-loop

system (11.16), i.e.,

$$\begin{aligned} \dot{y}_p &= x_2 && \text{(11.17a)} \\ \dot{x}_2 &= -2y_p - 2(2\sqrt{2} - 2w + 2y_p)x^c + 2w && \text{(11.17b)} \\ \dot{x}^c &= -y_p - (2\sqrt{2} - 2w + 2y_p)x^c + w. && \text{(11.17c)} \end{aligned}$$

From equation (11.17b) we have that $(2\sqrt{2} - 2(w - y_p)) = \frac{1}{2}\ddot{y}_p - y_p - w$ which is substituted in (11.17c) to yield

$$\dot{x}^c = \frac{1}{2}\ddot{y}_p \Rightarrow x^c = \frac{1}{2}\dot{y}_p, \tag{11.18}$$

where the latter implication is justified by the fact that all initial conditions are zero, i.e., $x^c(0) = \dot{y}_p(0) = 0$. Substitute (11.18) in (11.17b) to arrive at the input/output behavior

$$\ddot{y}_p + (2\sqrt{2} - 2w + 2y_p)\dot{y}_p + 2y_p = 2w, \tag{11.19}$$

which now is equivalent to the desired nonlinear behavior (11.7). Hence, if plant (11.2) is controlled by nonlinear controller (11.15) implemented with $\delta = 2\sqrt{2} - 2e$, the characteristic behavior of the Lewis servo is obtained.

The design of the nonlinear controller (11.15) was done by hand. This was possible since for this simple example the structure of the controller could be established by engineering insight. Still, the controller implementation is not straightforward since it has been shown that different realizations can lead to different behavior. When more involved performance specifications or plants are considered, engineering insight might not be adequate or error prone to come up with a satisfying controller. Therefore, the goal is to be able to systematically design a controller for system (11.2) which results in a closed-loop behavior similar to the Lewis servo. We will pursue this goal in the next section by designing an LPV controller via $\mathcal{H}_\infty$ controller interpolation.

11.3 LPV control by $\mathcal{H}_\infty$ controller interpolation

In this section we will design an LPV controller resulting in a closed-loop system that mimics the behavior of the Lewis servo by interpolating several controllers that are designed for a grid of the parameter range. These controllers are designed via loop shaping in the mixed sensitivity framework, depicted in Figure 11.4. The standard mixed sensitivity $S/R/T$ design is formulated as [134]

$$\left\| \begin{array}{c} W_e(s)S(s) \\ W_u(s)R(s) \\ W_{y_p}(s)T(s) \end{array} \right\|_\infty < 1, \tag{11.20}$$

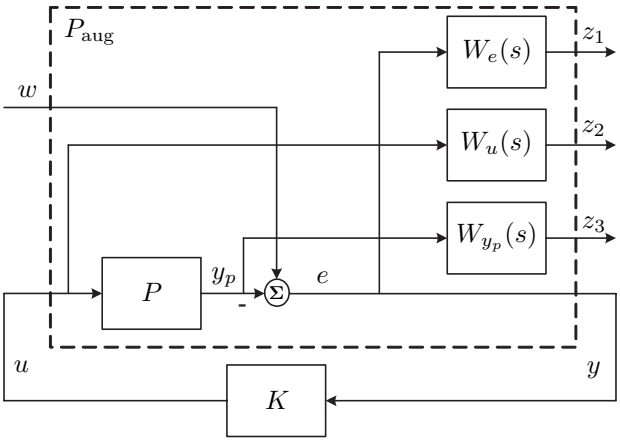

Figure 11.4: General mixed sensitivity setup.

where $W_e(s), W_u(s)$, and $W_{y_p}(s)$ are functions weighting the sensitivity function $S(s)$, the control sensitivity function $R(s)$ and the complementary sensitivity function $T(s)$, respectively. These weighting functions can be used to shape these sensitivity functions in order to meet certain specifications. The mixed sensitivity framework is described in state-space form by

$$\begin{aligned} \begin{bmatrix} z \\ y \end{bmatrix} &= P(s) \begin{bmatrix} w \\ u \end{bmatrix} \\ u &= K(s)y, \end{aligned} \tag{11.21}$$

where $z = [z_1^T \ z_2^T \ z_3^T]^T$ and where the generalized plant P is given by

$$P = \left[\begin{array}{c|c} P_{11} & P_{12} \\ \hline P_{21} & P_{22} \end{array}\right] = \left[\begin{array}{c|c} W_e & -W_eG \\ 0 & W_u \\ 0 & W_yG \\ \hline I & -G \end{array}\right]. \tag{11.22}$$

The closed-loop transfer function over the performance channel from w to z is given by

$$z = \mathcal{F}_\ell(P, K)w, \tag{11.23}$$

where

$$\mathcal{F}_\ell(P, K) = (P_{11} + P_{12}K(I - P_{22}K)^{-1}P_{21}) = \begin{bmatrix} W_eS \\ W_uR \\ W_yT \end{bmatrix} \tag{11.24}$$

is the lower LFT [32, 155] of P and K. To obtain a closed-loop system that performs accordingly to the specifications that are imposed through the sensitivity

weighting functions, a controller K has to be designed which renders

$$\|\mathcal{F}_\ell(P,K)\|_\infty = \left\| \begin{array}{c} W_eS \\ W_uR \\ W_yT \end{array} \right\|_\infty = 1. \tag{11.25}$$

This is done in the LMI framework [127]. Since this is a state-space approach, we need to express the generalized plant as

$$P : \left\{ \begin{array}{rcl} \dot{x} & = & Ax + B_w w + Bu \\ z & = & C_z x + D_{zw} w + D_z u \\ y & = & Cx + D_w w + Du \end{array} \right. . \tag{11.26}$$

The state-space representations of the plant and weighting functions are given by

$$G : \left\{ \begin{array}{rcl} \dot{x} & = & A_g x + B_g u \\ y_p & = & C_g x + D_g u \end{array} \right. , \qquad W_e : \left\{ \begin{array}{rcl} \dot{x}_{we} & = & A_{we} x_{we} + B_{we} e \\ z_1 & = & C_{we} x_{we} + D_{we} e \end{array} \right.$$

$$W_u : \left\{ \begin{array}{rcl} \dot{x}_{wu} & = & A_{wu} x_{wu} + B_{wu} u \\ z_2 & = & C_{wu} x_{wu} + D_{wu} u \end{array} \right. , \; W_{y_p} : \left\{ \begin{array}{rcl} \dot{x}_{wy} & = & A_{wy} x_{wy} + B_{wy} y_p \\ z_3 & = & C_{wy} x_{wy} + D_{wy} y_p. \end{array} \right.$$

By taking $x = \left[x_g^T \; x_{we}^T \; x_{wu}^T \; x_{wy}^T \right]^T$ and $z = \left[z_1^T \; z_2^T \; z_3^T \right]^T$, a state-space representation of the generalized plant P is given by

$$\begin{array}{rcl} \dot{x} & = & \left[\begin{array}{cccc} A_g & 0 & 0 & 0 \\ -B_{we}C_g & A_{we} & 0 & 0 \\ 0 & 0 & A_{wu} & 0 \\ B_{wy}C_g & 0 & 0 & A_{wy} \end{array} \right] x + \left[\begin{array}{c} 0 \\ B_{we} \\ 0 \\ 0 \end{array} \right] w + \left[\begin{array}{c} B_g \\ -B_{we}D_g \\ B_{wu} \\ B_{wy}D_g \end{array} \right] u \\ z & = & \left[\begin{array}{cccc} -D_{we}C_g & C_{we} & 0 & 0 \\ 0 & 0 & C_{wu} & 0 \\ D_{wy}C_g & 0 & 0 & C_{wy} \end{array} \right] x + \left[\begin{array}{c} D_{we} \\ 0 \\ 0 \end{array} \right] w + \left[\begin{array}{c} -D_{we}D_g \\ D_{wu} \\ D_{wy}D_g \end{array} \right] u \\ y & = & \left[\begin{array}{cccc} -C_g & 0 & 0 & 0 \end{array} \right] x + Iw - D_g u, \end{array} \tag{11.27}$$

which is in the form (11.26). Appropriate weighting functions to portray the transient performance specifications are discussed next.

11.3.1 Weighting functions describing Lewis servo behavior

To describe the Lewis servo behavior, a set of generalized plants (11.27) that exhibit different trade-offs with respect to rise-time and overshoot have to be obtained. To this end, weighting filters have to be designed which express this trade-off. In general, the reformulation of time-domain specifications into frequency domain requirements via weighting functions are either approximate, conservative, or both. However, for second order closed-loop systems the percentage

overshoot to a unit step input can be directly controlled by bounding the $\mathcal{H}_\infty$ norm of the closed-loop transfer function via

$$||T||_\infty = \frac{\ln(o_s)^2 + \pi^2}{2\pi \ln(\frac{1}{o_s})}, \tag{11.28}$$

as explained in Appendix B.2, where o_s is the desired overshoot (in the same unit as the plant output y_p). Although relation (11.28) is only valid for second order closed-loop systems, it is argued in [64] that it provides a good estimate when the system is not of second order, but when it is of a higher order where the lowest pole pair is dominant. To suppress residual vibrations and sensor noise, it is common to additionally specify high frequent roll-off for the complementary sensitivity function T. The overshoot and the roll-off specification can be specified via the weighting function

$$W_{y_p}(s) = \left(\frac{\tau_y^2}{\rho_y}\right) \frac{s^2 + \delta_w s + \rho_y}{s^2 + 2\tau_y s + \tau_y^2}, \tag{11.29}$$

where ρ_y is a parameter that can be used to influence the frequency where the peak $||T||_\infty$ occurs, τ_y is a generally large (in comparison to the desired bandwidth) constant to shape the complementary sensitivity at high frequencies, and δ_w is the parameter that can be used to specify the $\mathcal{H}_\infty$ norm of the closed-loop transfer function.
A common way to increase the rise-time of a system is to increase its bandwidth. This can be done by the weighting function on the sensitivity function

$$W_e(s) = \lambda_e \frac{s + \rho_e}{s + \tau_e}, \tag{11.30}$$

where λ_e is a parameter normally used to guarantee a certain modulus margin, τ_e is a generally small (compared to the desired bandwidth) constant to shape the sensitivity at low frequencies, and ρ_e can be used to increase the bandwidth.
When only restrictions are placed upon the sensitivity S and the complementary sensitivity T, it can be expected that in some cases the controller will be of a high-gain type, causing controller outputs that are far above the actuator capabilities. To prevent this, we use the frequency independent weighting function

$$W_u(s) = \lambda_u. \tag{11.31}$$

The parameters ρ_e and ρ_y influence the bandwidth of the closed-loop system and are obtained via an iterative procedure to make sure that the resulting rise-times are similar to those of the Lewis servo (11.6). The constants τ_e and τ_y are used to make the weighting functions W_e and W_{y_p} proper. The parameter δ_w is used to describe the desired values of the overshoot for the various designs. From the step response data of the Lewis servo (11.4) with constant scheduling parameter δ, it is observed that the overshoot o_s varies between 0.38 for $\delta = 2\sqrt{2} - 2$ ($e = 1$) and 0 for $\delta = 2\sqrt{2}$ ($e = 0$), see Table 11.1. In this same table, the corresponding

e	1	0.8	0.6	0.4	0.2	0
o_s	0.38	0.22	0.11	0.039	0.005	0
$\|\|T\|\|_\infty$	1.79	1.28	1.06	-	-	-

Table 11.1: Overshoot o_s of the Lewis servo for various values of the scheduling parameter e and the corresponding bound on $||T||_\infty$ according to (11.28).

bound on the complementary sensitivity function according to (11.28) is given. For the LPV synthesis later on, it is convenient to scale the scheduling parameter δ between 0 and 1 such that $\delta = 0$ corresponds to low damping ($o_s = 0.38$) while $\delta = 1$ corresponds to high damping ($o_s = 0$). The resulting weighting filters are given by

$$\begin{aligned} W_{y_p}(s) &= \left(\frac{100^2}{2}\right)\frac{s^2+\delta_w s+2}{s^2+200s+100^2} \\ W_e(s) &= 0.12\frac{s+0.3}{s+0.0003} \\ W_u(s) &= \frac{1}{30}, \end{aligned} \tag{11.32}$$

where $\delta_w = 2\sqrt{2}-2+2\delta$ to express the desired overshoot for $\delta \in [0,1]$. The Bode diagrams of the weighting functions are depicted in Figure 11.5.

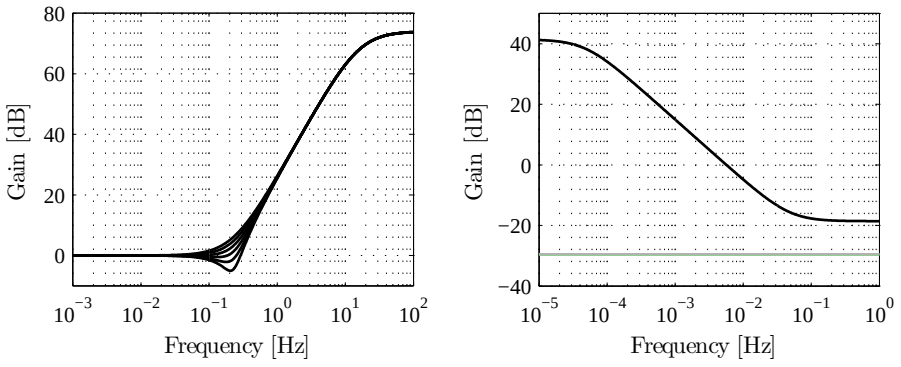

(a) (b)

Figure 11.5: Bode diagrams of the weighting functions. (a) W_{y_p} for $\delta \in \{0, 0.2, 0.4, 0.6, 0.8, 1\}$, (b) W_e (black) and W_u (grey).

11.3.2 Controller synthesis and interpolation

To design an LPV controller via interpolation, a set of $\mathcal{H}_\infty$ controllers is designed at the following grid of the parameter interval

$$\delta \in \{0,\ 0.1,\ 0.2,\ 0.3,\ 0.4,\ 0.5,\ 0.6,\ 0.7,\ 0.8,\ 0.9,\ 1\}. \tag{11.33}$$

The sampled weighting functions and the plant are substituted in (11.27) to arrive at a set of generalized plants. The subsequent controller synthesis for each of these generalized plants is performed via LMI optimization [127]. The Bode diagrams of the resulting fifth order $\mathcal{H}_\infty$ controllers for several values of $\delta \in [0, 1]$ are depicted in Figure 11.6(a), while the step responses of the closed-loop system are shown in Figure 11.6(b). As can be seen, the weighting functions (11.32) indeed specify

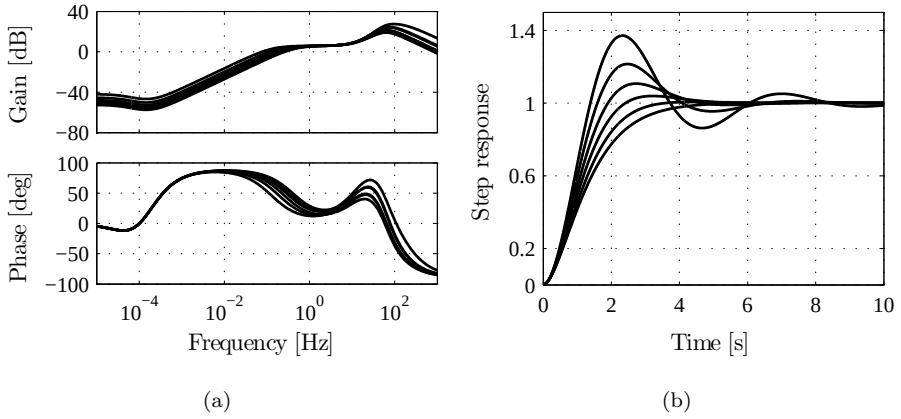

Figure 11.6: (a) Bode diagrams of the resulting $\mathcal{H}_\infty$ controllers for $\delta \in \{0,\ 0.2,\ 0.4,\ 0.6,\ 0.8,\ 1\}$, (b) closed-loop step responses corresponding to the $\mathcal{H}_\infty$ controllers.

various damping characteristics for different values of δ.
Due to the controller synthesis method, additional poles and zeros are introduced at relative high frequencies compared to the bandwidth of the system. These are not related to the desired specifications, but are an inherent effect of the synthesis method. Since it is not expected that these poles and zeros significantly contribute to the dynamic response, they are removed to facilitate interpolation. The resulting second order controllers are depicted in Figure 11.7(a). Since the step responses of the reduced order $\mathcal{H}_\infty$ and the full order $\mathcal{H}_\infty$ controllers almost coincide, see Figure 11.7(b), the controller reduction is justified. To obtain an LPV controller, the obtained $\mathcal{H}_\infty$ controllers are interpolated using δ. This can be done in several ways, of which the most common are the interpolation between the state-space controller coefficients [65], and interpolating the gain, poles and zeroes of the controller transfer functions [104]. The elements of the state-space matrices

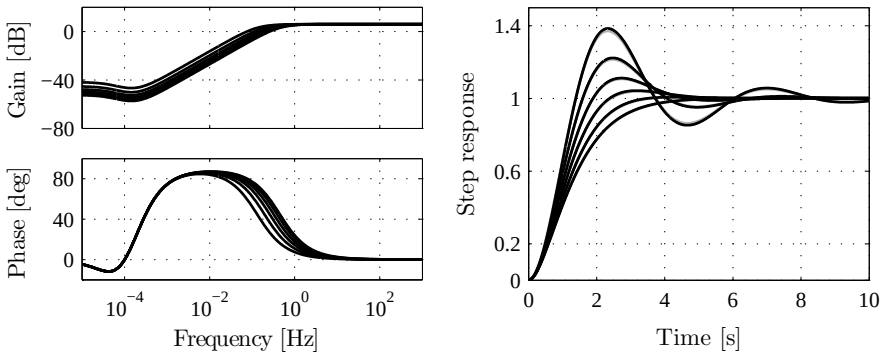

(a) (b)

Figure 11.7: (a) Bode diagrams of the reduced order $\mathcal{H}_\infty$ controllers, (b) closed-loop step responses of the full order $\mathcal{H}_\infty$ (grey) and of the reduced order $\mathcal{H}_\infty$ controllers (black).

of the reduced order $\mathcal{H}_\infty$ controllers together with the interpolated elements are shown in Figure 11.8. From this figure it is clear that affine interpolation of the state-space matrices is a suitable choice for this interpolation problem. Therefore, we construct the LPV controller by affine interpolation of the state-space matrices in the form

$$A^c(\delta) = A_0^c + A_1^c\delta, \quad B^c(\delta) = B_0^c + B_1^c\delta, \quad C^c(\delta) = C_0^c + C_1^c\delta, \quad D^c(\delta) = D_0^c + D_1^c\delta.$$

The state-space matrices are interpolated using the grid (11.33). Several state-space representations of the controllers can be used for interpolation, leading to different results. Both in the frequency domain as well as in the time-domain the controller canonical form results in the best results. The resulting LPV controller is given by

$$\begin{aligned}
A^c(\delta) &= \begin{bmatrix} 0 & 1.00 \\ -0.0002 & -0.8102 \end{bmatrix} + \begin{bmatrix} 0 & 0 \\ 0 & -1.95 \end{bmatrix}\delta \\
B^c(\delta) &= \begin{bmatrix} 0 \\ 1 \end{bmatrix} \\
C^c(\delta) &= \begin{bmatrix} -0.0005 & -1.60 \end{bmatrix} + \begin{bmatrix} 0 & -3.88 \end{bmatrix}\delta \\
D^c(\delta) &= 1.98.
\end{aligned} \tag{11.34}$$

When an LPV controller is obtained by interpolation, it is generally not possible to guarantee that the desired performance (and even stability) is achieved when the controller is implemented using the actual scheduling variable. The performance and stability of the resulting LPV controller can be verified a posteriori via LPV analysis [126], but here we assess the stability and performance via simulation. According to the damping function $\zeta = 1 - \frac{1}{2}\sqrt{2}e$ of the Lewis servo, the controller is

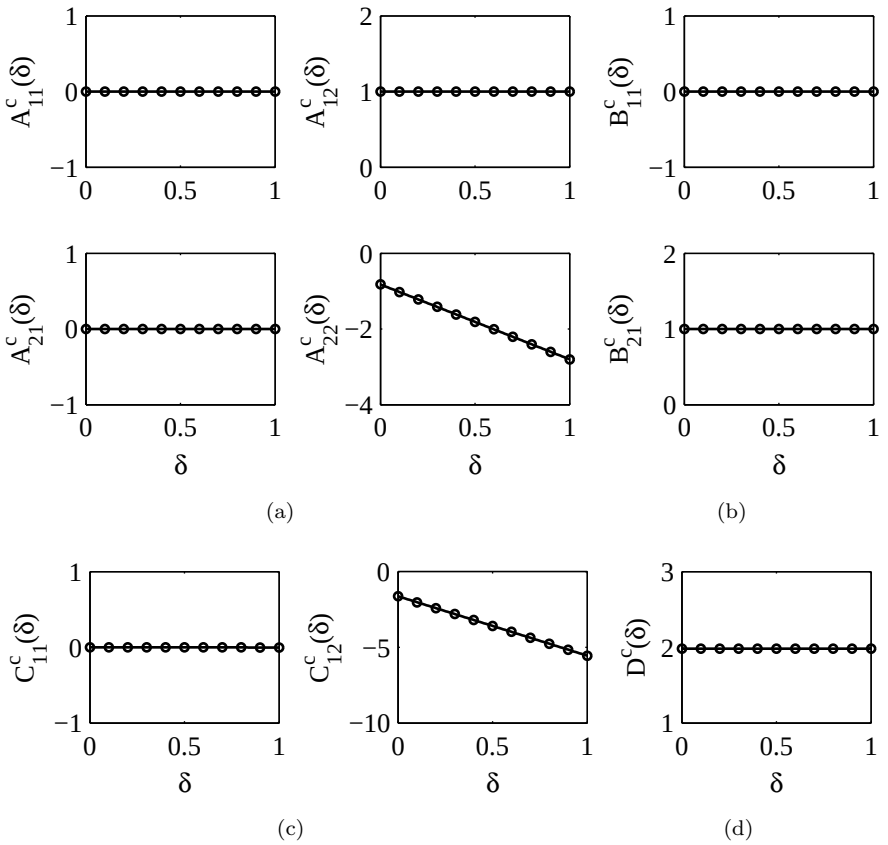

Figure 11.8: Interpolated state-space matrices. Pointwise $\mathcal{H}_\infty$ controller values (circles) and affine interpolation (solid). (a) $A^c(\delta)$, (b) $B^c(\delta)$, (c) $C^c(\delta)$, (d) $D^c(\delta)$.

implemented with $\delta = 1-e$, where e is the measured error signal. In Figure 11.9(a) the step responses of the LPV controller (11.34) for various constant values of the scheduling parameter δ is depicted together with that of the LPV controller implemented with $\delta = 1-e$. Figure 11.9(b) shows the corresponding controller output signals. This figure shows that the actual nonlinear controller that is obtained by implementing the interpolated LPV controller (11.34) with $\delta = 1-e$ is indeed stabilizing and leads to closed-loop behavior that is very similar to that of the Lewis servo (compare to Figure 11.2). Although the interpolation approach has been shown to work for this relatively simple example, in general no a priori guarantees with respect to stability and performance of the closed-loop system can be given. A direct LPV controller synthesis method taking into account stability and performance over the complete parameter interval during the design is presented in the next section. The reason for designing the LPV controller via interpolation is twofold. Firstly, since the LPV synthesis method is

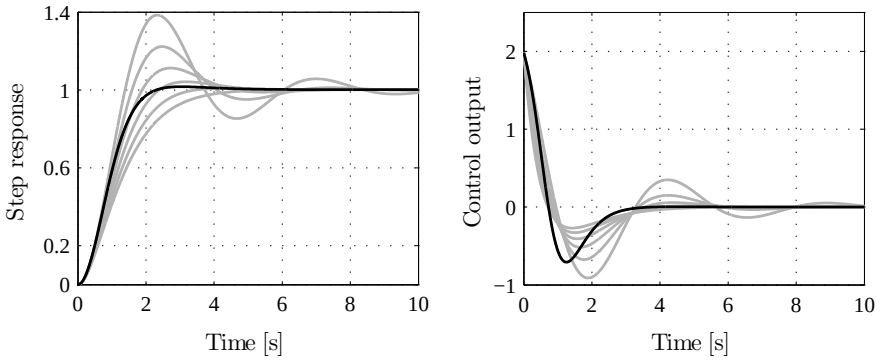

(a) (b)

Figure 11.9: Time-domain simulation results of the interpolated LPV controller (11.34) at the constant values $\delta \in \{0,\ 0.2,\ 0.4,\ 0.6,\ 0.8,\ 1\}$ (grey) and for $\delta = 1 - e$ (black). (a) Step responses, (b) control output.

similar in nature to the $\mathcal{H}_\infty$ synthesis method but numerically more complex, it is advantageous to know that the generalized plant descriptions with the various weighting functions are numerically tractable. Secondly, an LPV controller was designed which fulfills the desired specifications, and hence we know that there exists at least one controller that solves the posed problem.

11.4 Direct LPV controller design

In the previous section the weighting functions (11.32) were sampled at various values in the parameter interval $\delta \in [0, 1]$, $\mathcal{H}_\infty$ controllers were designed for these values, and the state-space representations of the reduced order controllers were affinely interpolated to arrive at an LPV controller. As discussed, the major drawback of this design procedure is the ad-hoc approach of interpolation. It is not straightforward to find a representation that is suitable for interpolation, and furthermore, stability and performance of the interpolated controller is not guaranteed. Therefore, the goal of this section is to directly design an LPV controller, based on a parameter dependent generalized plant.
If the parameter dependent state-space matrices of the weighting functions (11.32) are substituted in (11.27), a parameter dependent generalized plant in the form (10.1) is obtained. Since this generalized plant depends on only one parameter, and since this parameter δ is contained in the box $[0, 1]$, the control synthesis method proposed in [31] (see also Appendix B.1) can be used. The parameterized LPV controller that is obtained via this method results in a closed-loop system of which the stability and desired performance is guaranteed for each constant

value of the parameter in the interval $[0, 1]$. Therefore, a subsequent interpolation step is not necessary. We apply the method proposed in [31] to design the LPV controller with first order rationally depending decision variables. Via a bisection algorithm, the minimum achievable $\mathcal{H}_\infty$ norm is determined to be 1.0024, and hence we can conclude that the LPV controller achieves the desired performance and that in this synthesis problem there is no relaxation gap. The Bode diagrams of the obtained fifth order LPV controller for various constant values of δ are depicted in Figure 11.10. Stability and performance are both taken into ac-

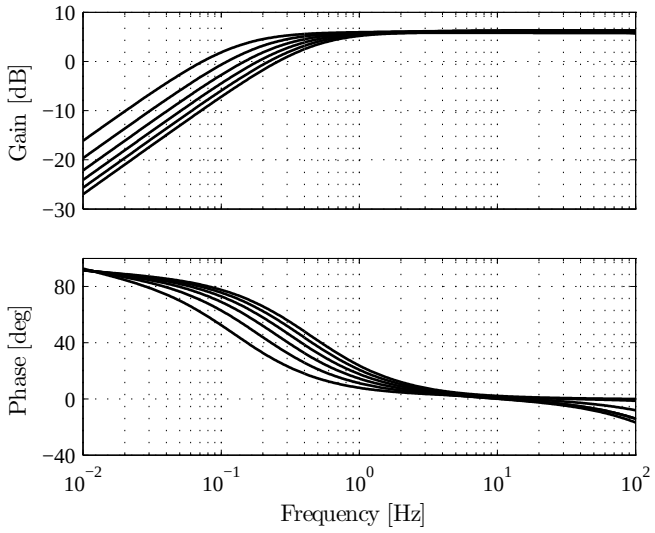

Figure 11.10: Bode diagrams of the LPV controller with constant parameters in the set $\delta \in \{0,\ 0.2,\ 0.4,\ 0.6,\ 0.8,\ 1\}$.

count during the design for all constant parameter values in the interval $\delta \in [0, 1]$. However, there are no guarantees that the LPV controller achieves the desired performance when it is used as a nonlinear controller by setting $\delta = 1 - e$ in accordance with the Lewis servo. In Figure 11.11(a) the step response of the nonlinear controller in feedback with system (11.2) together with the step responses of the base linear system for various constant parameter values are depicted. The corresponding controller output signals are shown in Figure 11.11(b). As can be seen, the nonlinear controller performs as desired since it mimics the step response of the Lewis servo (compare to Figure 11.2).

Remark 11.1 It is well-known from $\mathcal{H}_\infty$ synthesis that at optimality, the resulting controllers are often ill-conditioned [126]. Similar phenomena occur for the LPV synthesis procedure. Time simulations performed with the controller presented in this section take a long time. The LPV controller that is synthesized with an $\mathcal{H}_\infty$ norm that equals 1.003 instead of 1.0024 still performs desirably while time simulations take considerably less time. □

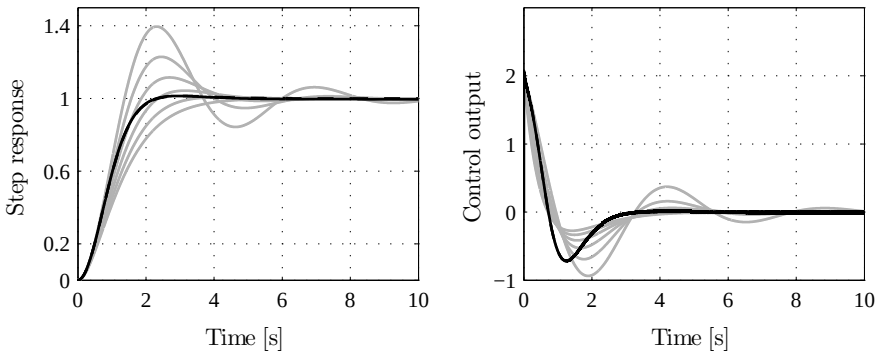

(a) (b)

Figure 11.11: Time-domain simulation results of the LPV controller (solid), the Lewis controller (dashed), and the base linear controllers for $\delta \in \{0, 0.2, 0.4, 0.6, 0.8, 1\}$ (grey). (a) Step responses, (b) control output.

11.5 Conclusions

In this chapter we proposed a systematic procedure to design a nonlinear controller that, when it is used to control a simple model of a servomotor, results in a closed-loop performance that resembles the Lewis servo. While the original Lewis servo [87] was designed by hand using engineering insight, we showed that a systematic design can be made using the well-developed framework of $\mathcal{H}_\infty$ loop shaping in combination with parameter dependent weighting functions and LPV synthesis procedures. The synthesis of the resulting LPV controller was performed via two approaches.

The first method comprised the interpolation of $\mathcal{H}_\infty$ controllers that were designed for constant weighting functions, obtained by gridding the parameter dependent weighting functions. Although an advantage of this approach is that the design of the $\mathcal{H}_\infty$ controllers is rather straightforward since there are many off-the-shelf synthesis tools available, interpolation of the resulting controllers is generally not straightforward. There are many possibilities to interpolate the controllers, resulting in LPV controllers with different closed-loop performance. It is not clear a priori which interpolation methods results in the desired performance (if some do at all) and which do not. The common way to assess the performance is via (extensive) simulation. It turned out that in our problem setting, affine interpolation of the state-space matrices of the synthesized $\mathcal{H}_\infty$ controllers resulted in an LPV controller which achieved closed-loop performance similar to the Lewis servo. Since closed-loop stability and performance are not guaranteed when the interpolation approach is used, we also designed an LPV controller via the second method of direct LPV synthesis.

The advantage of direct LPV synthesis is that there is no need for an interpolation step and that closed-loop stability and performance are taken into account during the synthesis procedure. The main drawback of the method is that certain relaxations are needed to arrive at a tractable problem and that these relaxations generally lead to conservative synthesis results. Because of our specific problem setting, the LPV synthesis procedure was not conservative and as a consequence resulted in a closed-loop system of which the stability and desired performance is guaranteed for all constant parameter values in the considered interval. Although there are no guarantees for stability and performance when the controller is implemented with the proposed scheduling law, simulations showed that Lewis servo-like behavior was obtained by this LPV controller.
Although the designed nonlinear controller results in a closed-loop system with a step response characteristic which seems to overcome the limitations regarding the trade-off with respect to rise-time and overshoot, it cannot be concluded that this nonlinear controller outperforms the 'best' linear controller. The resulting nonlinear controller is a fifth order controller while the by hand designed linear controllers used to illustrate the trade-off were first order controllers. It may well be that there exist higher order linear controllers that achieve similar performance as the nonlinear controller. However, it is not clear how such a linear controller could be designed, while the major advantage of our proposed approach is that a (nonlinear) controller that achieves the desired nonlinear performance criteria can be designed in a systematic way .

Chapter 12

LPV control of an active vibration isolation system

As stated in Chapter 10, the closed-loop performance of motion systems that suffer from non-stationary disturbances could benefit from knowledge of these disturbances. Indeed, if the disturbance could be measured, this measurement could be used to enable an LPV controller to adapt itself to the current operating condition, resulting in a closed-loop system with an overall increased performance. In this chapter, this idea is applied to an active vibration isolation system which suffers from non-stationary disturbances.

12.1 Introduction

In high-precision motion systems, vibrations of unknown frequency and amplitude can limit the performance. These vibrations can for instance be induced by floor vibrations that are transferred to the system or by forces that directly act on the system such as airflow from the air conditioning. Examples of processes where this occurs include high-resolution measurement equipment such as scanning electron microscopes used for sub-micron imaging, and photolithographic wafer steppers and scanners used to fabricate integrated circuits. For these systems, the typical amplitudes of the induced vibrations are of the same magnitude as the dimensions of the measured or manufactured objects, and therefore these vibrations limit the performance. To provide such systems with a vibration free platform, vibration isolation systems are used, where disturbance isolation is achieved either passively, actively, or both. Figure 12.1(a) shows a schematic representation of

such a vibration isolation system. Herein, k, b are the isolator stiffness and damping, respectively, d represents the floor vibrations and f_d denotes the disturbance forces that act directly on the payload. The payload displacement in vertical direction is denoted by y, and f_a is the force generated by the actuator. The goal of a vibration isolation system is to minimize the effect of the environmental disturbances d and f_d on the vertical velocity $v = \dot{y}$ of the payload. The passive part of the vibration isolation system consists of a heavy payload supported by elastic springs and damping units, resulting in a mechanical low-pass system with typical resonance frequencies between 2 and 5 Hertz. Since the passive system is generally weakly damped, disturbance amplification at the natural frequency is often observed. Increasing the structural damping of the system may offer a solution, however, a major disadvantage of passive damping is that the disturbance rejection properties deteriorate. This is illustrated in Figure 12.1(b), where a typical frequency response of the transfer from f_d to y is depicted. Moreover,

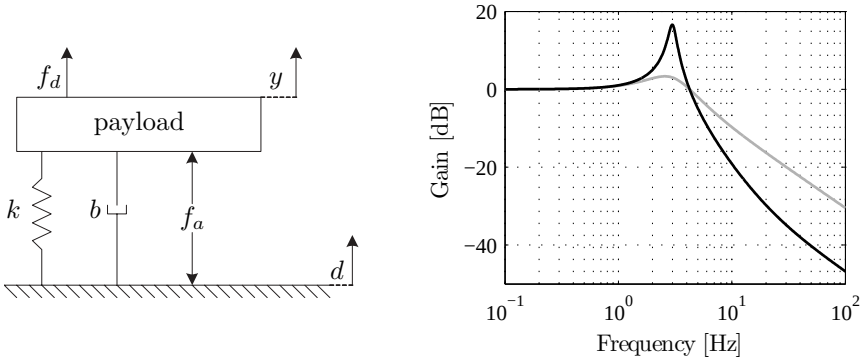

(a) (b)

Figure 12.1: (a) Schematic representation of a vibration isolation system, (b) mechanical low-pass characteristic of a passive isolation system with low (black) and high (grey) structural damping.

the passive type is, in principle, unable to attenuate disturbances f_d that directly act on the payload such as an exiting force generated in a mounted operating machine, airflow from the air conditioning, and acoustic excitations. By applying active damping near the natural frequency of the passive system, i.e., by active vibration isolation, a significant benefit in vibration isolation can be obtained.
In the active vibration isolation system (AVIS) we consider, active vibration isolation is achieved by controlled actuation of the payload, based on feedback of its absolute velocity. The absolute velocity is obtained via geophones while the actuation is performed by means of Lorentz actuators. A picture of the AVIS is shown in Figure 12.2(a). The schematic of one of the controlled vibration isolators is depicted in Figure 12.2(b), where $u = f_a$ is the controller output, $v = \dot{y}$ is the payload velocity in vertical direction, G denotes the transfer function of an

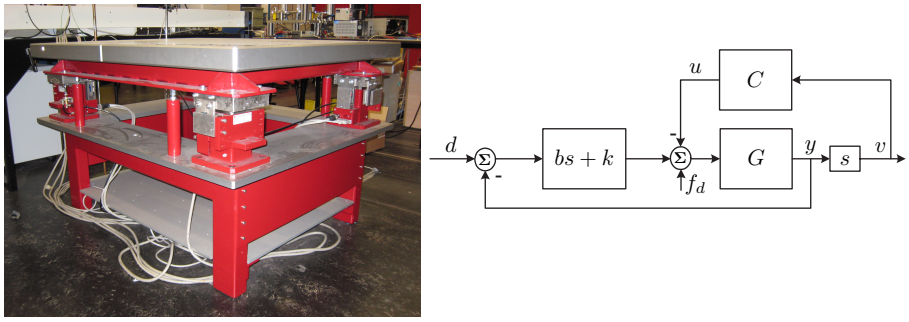

(a) (b)

Figure 12.2: (a) Active Vibration Isolation System (AVIS), (b) schematic of the controlled isolation system.

isolator module, and C is the controller. A fourth-order model of an isolator of the AVIS is given by the transfer function [53]

$$G(s) = \frac{m_2 s^2 + b_{12} s + k_{12}}{m_1 m_2 s^4 + (m_1 + m_2)(b_{12} s^3 + k_{12})}, \tag{12.1}$$

with $m_1 = 950$ kg, $m_2 = 50$ kg, $b_{12} = 3 \cdot 10^2$ Nsm^{-1}, and $k_{12} = 1.75 \cdot 10^6$ Nm^{-1}. The isolator's passive stiffness and damping are $k = 4.25 \cdot 10^5$ Nm^{-1} and $b = 2 \cdot 10^3$ Nsm^{-1}, respectively. To reduce the effect of disturbances near the resonance frequency, controller C is designed as the complex valued damper [53]

$$C(s) = k_d \left(\frac{s}{s + \omega_{hp}} \right)^2 \left(\frac{\omega_{lp}}{s + \omega_{lp}} \right)^2, \tag{12.2}$$

which consists of a gain k_d, combined with a low-pass filter with cut-off frequency ω_{lp}, and a high-pass filter with cut-off frequency ω_{hp}. The choices for ω_{hp} and ω_{lp} are related to the limitations of the sensors and actuators, respectively. Since the geophones produce unreliable output below 0.1 Hz, and since actuator limitations occur beyond 100 Hz, the cut-off frequencies are chosen as $\omega_{hp} = 0.2\pi$ rad/s and $\omega_{lp} = 200\pi$ rad/s, and the gain is $k_d = 3 \cdot 10^4$ Nsm^{-1}. This controller is designed to preserve the desirable properties at high frequencies of the passive isolator, while it significantly reduces the effect of disturbances around the resonance frequency. In Figure 12.3 the Bode diagram of the uncontrolled plant (i.e., of the passive vibration isolation system)

$$P_p(s) = \frac{v(s)}{f_d(s)} = \frac{sG(s)}{1 + (bs + k)G(s)}, \tag{12.3}$$

is compared with that of the the controlled plant (i.e., of the active vibration isolation system)

$$P_a(s) = \frac{v(s)}{f_d(s)} = \frac{sG(s)}{1 + (bs + k)G(s) + sC(s)G(s)}. \tag{12.4}$$

The maximum amplitude occurs around the resonance frequency, which implies that the plant still is most sensitive to disturbances in this frequency region. However, the sensitivity in this region is reduced by about a factor 17. The price paid is a slightly increased amplitude between 10 and 20 Hz.

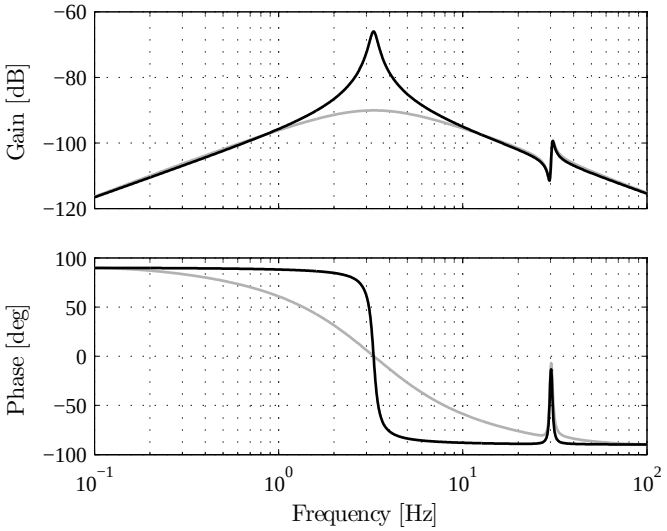

Figure 12.3: The Bode diagram of the transfer function from the environmental disturbance f_d to the measured output v of the passive isolation system (black) and of the active isolation system (grey).

12.1.1 Problem setting

In this chapter, the payload of the AVIS is used as an experimental benchmark representing a metrology frame that needs to be isolated from environmental disturbances. This means that the amplitude of the vertical velocity v should be controlled to be as low as possible. A machine is mounted to this metrology frame that performs periodic tasks, which result in non-stationary environmental disturbances f_d with frequency content between 4 and 10 Hz, depending on the specific task that is performed. This machine is represented by a rotational imbalance, depicted in Figure 12.4. The induced disturbances f_d are not known beforehand and cannot be measured directly. As a consequence, direct disturbance compensation via feedforward cannot be applied. Although other disturbance sources are present as well, the periodic disturbance generated by the mounted machine is expected to dominate the measured output. All that is known about the induced

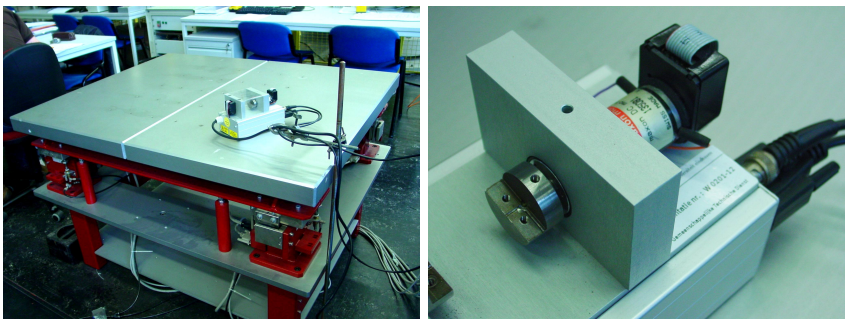

(a) (b)

Figure 12.4: (a) The active vibration isolator platform including the mounted rotating imbalance, (b) a close-up of the rotating imbalance.

disturbance is that it consists of a single, time-varying frequency in the range 4 to 10 Hz. Although controller (12.2) reduces the effect of disturbances in this range, the achieved isolation performance is considered not to be adequate. To improve the isolation performance, controller (12.2) will be adjusted in order to provide additional disturbance reduction.

12.1.2 Proposed approach

A classical solution to reduce disturbances at specific frequencies is the use of an inverted notch filter in the controller to increase the gain at that frequency. Such a notch filter results in a decreased sensitivity for disturbances in a small frequency range around the center frequency of the notch. Unfortunately, a classical notch filter cannot be applied to the posed problem for two reasons. Firstly, the frequency of the expected periodic disturbance varies in an interval between 4 and 10 Hz, while a fixed notch is only effective around a single frequency. Secondly, even if the disturbance signal would be stationary instead of time-varying (for instance when the mounted machine is operating in a stationary condition), the actual disturbance frequency, and hence the target center frequency of the notch, is not known beforehand.
In this chapter, we propose a solution to improve the isolation performance that circumvents these two problems. The problem of the unknown frequency will be tackled by devising an algorithm that identifies the dominating disturbance frequency from available measured data from the AVIS. The problem of frequency variation can be solved by extending controller (12.2) with an LPV notch instead of a classical LTI notch. This way, the controller can adapt the center frequency of the notch to the identified disturbance frequency, resulting in an improved isolation performance at that frequency. A schematic overview of the proposed control architecture is shown in Figure 12.5. In the next section, the algorithm

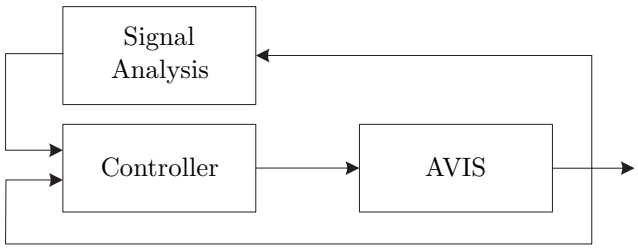

Figure 12.5: Proposed control architecture.

that is used to identify the disturbance frequency is discussed.

12.2 Time-frequency analysis

The problem as stated in Section 12.1.1 requires a frequency identifier that is able to determine the actual frequency of the disturbance from the measured signals of the AVIS. Since the proposed LPV controller is required to adapt itself to the disturbance that acts on the system, ideally the exact disturbance frequency at the current time instant should be available. Unfortunately, the Heisenberg uncertainty principle [37] implies that it is not possible to have both a high time resolution Δt (accuracy with which the moment in time where the frequency is present can be determined), and a high frequency resolution Δf (accuracy with which the frequency can be determined). The uncertainty principle states that the product of Δt and Δf is constant and lower bounded. This means that it is possible to identify a frequency component f_a with either a high frequency resolution and a low time resolution, or with a high time resolution and a low frequency resolution, but not with both. Since in practical applications low frequency components often last a long period of time, while high frequency components often appear as short bursts, a so-called multiresolution spectrum is desirable. Such a multiresolution spectrum combines a high frequency resolution (with a corresponding low time resolution) for low frequencies with a high time resolution (and hence a low frequency resolution) for high frequencies.
To obtain the frequency spectrum of a measured signal, various methods are available, of which the Fourier transform (FT) [37] is probably the most widely used. Unfortunately, the FT offers only the global frequency content of the signal without any time information. An adapted version of the FT, called the short time Fourier transform (STFT) [137], is able to retrieve both frequency and time information of the signal. The major disadvantage of the STFT, however, is that is has a fixed resolution, i.e., the desired multiresolution spectrum cannot be obtained by this transform. The wavelet transform [37] was developed as an alternative approach to the short time Fourier transform to make a multiresolution analysis possible. More information about the wavelet transform is provided in Appendix

C. The shape of the wavelet is the design parameter that determines the achieved time and frequency resolution of the multiresolution spectrum. The frequency resolution Δf of the wavelet transform is proportional to the frequency that is analyzed (the analysis frequency f_a). This implies that low analysis frequencies have a high frequency resolution and a low time resolution, while high frequency component analysis results in a high time resolution with a low frequency resolution. Furthermore, since the spectral analysis has to be performed in real-time, delay is inevitably introduced in the analysis method, see Appendix C.2. This delay depends on the frequency and time resolution. Therefore, the shape of the wavelet should be designed in such a way that, for the application at hand, an acceptable trade-off between frequency resolution, time resolution, and analysis delay is obtained.

We will use the real-time spectrum analyzer to estimate the dominating disturbance frequency in the range 4 to 10 Hz. This estimated frequency will be used to schedule a notch filter. Since the use of a notch filter results in a decreased sensitivity for disturbances in a small frequency range around the center frequency of the notch, the estimated frequency of the disturbance should be close to the actual frequency. Furthermore, we require that a disturbance frequency of 4 Hz can be identified in 0.75 seconds, while frequency components of 10 Hz should be identified in 0.3 seconds. The corresponding wavelet is designed in Appendix C.2.2.

The real-time algorithm is designed (see Appendix C.2) in such a way that the multiresolution spectrum is computed for 1000 analysis frequencies f_a ranging logarithmically from $f_a = {}^{120}/_{1024}$ to $f_a = 120$ Hz. By gridding the analyzed frequencies this way, the maximum relative error between the identified frequency and the actual frequency equals 0.35%, see Appendix C.2.3. In Figure 12.6 an example of an obtained spectrum is presented. The analyzed signal consists of a sinusoid of which the frequency is switched between 4 and 10 Hz every 5 seconds, combined with randomly distributed noise. The time series is depicted in the upper part of Figure 12.6(a). The results of the real-time spectrum analyzer (C.5) are depicted in the lower part of Figure 12.6(a). The estimated amplitudes of the analyzed frequencies are normalized and represented using colors. Dark red indicates no frequency content, while dark blue indicates the frequencies with the highest estimated amplitude. The corresponding estimated dominating frequency is depicted in 12.6(b) together with the actual switching signal that is used to change the frequency of the input signal. The delay that is introduced by the real-time implementation (C.5) can be seen when figure (a) is compared to (c), where the spectrum is computed without this delay using (C.4). In the remainder of this chapter the computation with (C.4) is referred to as the *off-line* computation. By changing the wavelet, the achieved frequency resolution can be increased resulting in the off-line computed spectrum depicted in Figure 12.6(d). If this resolution would be used in the real-time implementation, the introduced delay would be significantly increased. The real-time frequency analyzer (C.5) will be used to schedule the controller as discussed in the next section.

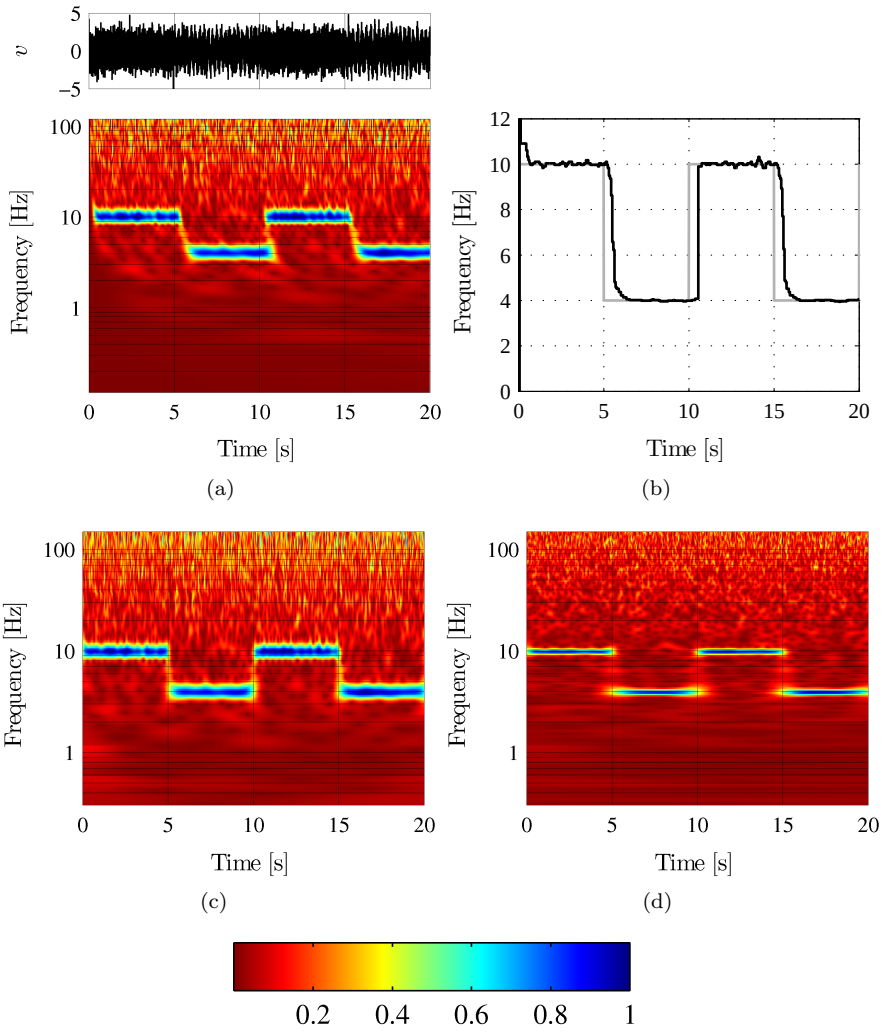

Figure 12.6: (a) Analyzed signal v and computed spectrum via (C.5), (b) estimated frequency of dominant frequency (black) together with the switching signal (grey), (c) computed spectrum via (C.4), (d) computed spectrum via (C.4) using a wavelet with a higher frequency resolution.

12.3 Controller design

The frequency of the dominating disturbance that acts on the system can be identified by the algorithm that was discussed in the previous section. This information can be used to adapt controller (12.2) in order to improve the isolation performance at that frequency. Such a controller can be designed via the LPV syn-

thesis framework using frequency and parameter dependent weightings expressing the desired performance as discussed in Chapter 10 and applied in Chapter 11. For this specific application however, it is expected that the desired performance can be achieved by extending controller (12.2) with an LPV notch filter, the center frequency of which is adapted to the identified disturbance frequency. Therefore, in this section we will design the controller by hand and analyze the closed-loop stability afterwards.
An LTI notch filter is described by the transfer function

$$H_n(s) = \frac{s^2 + 2\beta_1(2\pi f_n)s + (2\pi f_n)^2}{s^2 + 2\beta_2(2\pi f_n)s + (2\pi f_n)^2}, \tag{12.5}$$

where f_n is the center frequency in Hz, and β_1 and β_2 are parameters that can be used to alter the reduction factor and the width of the notch. Although ideally all three parameters f_n, β_1, and β_2 should be adapted depending on the disturbance characteristic, in this chapter we only consider the adaptation of the center frequency f_n. Several factors play a role in the determination of the constant reduction factor and width of the notch filter. If only steady-state disturbance rejection around the center frequency f_n is considered, a wide notch with a large reduction factor is desirable. Indeed, a wide notch will not only reduce disturbances at f_n, but has also good disturbance rejection properties for frequencies near f_n, while a larger reduction factor results in a higher reduction. Unfortunately, there are also downsides to using such a notch filter. Widening the filter reduces the disturbances in a larger area around the center frequency, but at the same time results in amplification of disturbances in another, larger, frequency region. This is illustrated in Figure 12.7(a), where the frequency responses of the original actively controlled plant (12.4) is compared to that of the same controlled plant including a notch filter of different widths. The same holds if the reduction factor of the notch is increased. This effect is basically due to the waterbed effect (see Section 2.2.2). Another issue related to the width and reduction factor of a notch is its transient response time. A short transient response time of the notch filter is desirable since it allows a fast adaptation of the controller to the current disturbance frequency. A wider notch filter has a shorter transient response time than a narrow one, just as a filter with a smaller reduction factor has a shorter transient response time than one with a higher reduction factor. The effect on the transient response caused by widening the notch filter is illustrated in Figure 12.7(b), where the response of the controlled plant to a sinusoidal disturbance of 10 Hz is depicted with the same notch filters of different width.
The transient response time of the notch filter depends on the center frequency similarly as the frequency identification time of the real-time frequency analyzer. Therefore, in a good overall controller design, the transient response time of the notch filter for a certain frequency, and the time it takes to identify that frequency should be matched. Since the delay of the real-time frequency analyzer is equal to 3 periods of the analyzed frequency (see (C.7)), we will use a notch that reduces the amplitude of a sinusoidal disturbance with a frequency corresponding to the center frequency f_n to approximately half of the final reduction in 3 periods. Furthermore, we choose a reduction factor of 30. The above discussion results in

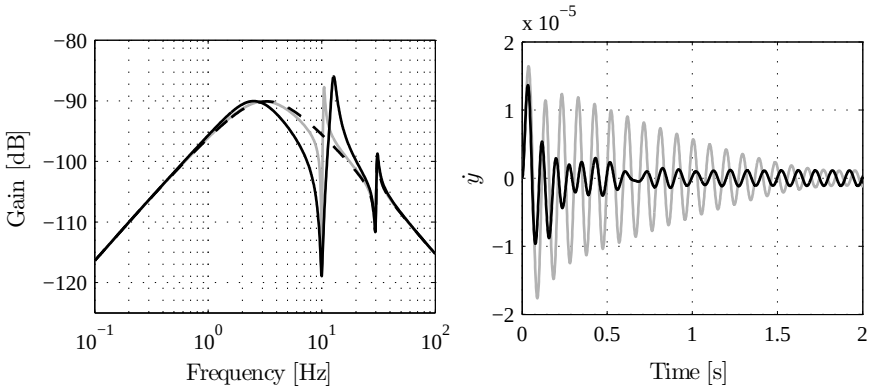

(a) (b)

Figure 12.7: Bode diagram of the original controlled plant (12.4) (dashed) and two notches of different widths (solid black and grey). (a) Effect of widening the notch on the frequency response, (b) effect of widening the notch on the transient response time.

$\beta_1 = 0.6$ and $\beta_2 = 0.02$.

12.3.1 State-space realization and stability

To arrive at a closed-loop state-space system from disturbance input f_d to measured output v, we start by representing the uncontrolled AVIS (the passive vibration isolation system) (12.3) in state-space form as

$$\begin{aligned} \dot{x} &= Ax + Bf_d \\ v &= Cx, \end{aligned} \tag{12.6}$$

where $x \in \mathbb{R}^4$ is the state vector, and A, B, C are matrices of appropriate dimensions. The state-space description of the original controller (12.2) is given by

$$\begin{aligned} \dot{x_o^c} &= A_o^c x_o^c + B_o^c v \\ u &= C_o^c x_o^c, \end{aligned} \tag{12.7}$$

where $x_o^c \in \mathbb{R}^4$ is the original controller state vector, and A_o^c, B_o^c, C_o^c are matrices of appropriate dimensions. This controller will be augmented with a notch filter that adapts itself to the dominating disturbance. The LTI notch filter (12.5) can be changed to an LPV notch by using the center frequency as the scheduling variable, i.e., $\delta := 2\pi f_n$. This LPV notch can be represented by various state-space realizations. It is well-known that the complexity and conservatism of

the stability and performance analysis of LPV systems depends on the type of parameter dependence of that system [126]. For instance, systems that are affinely parameterized allow a quadratic stability analysis without a relaxation gap, and hence we aim for an affinely parameterized closed-loop system. Since the state-space description of the controlled AVIS is affine in the controller state-space matrices, an affinely parameterized state-space description of the controller results in an affinely parameterized state-space description of the controlled AVIS.
Changing the center frequency of a notch filter will linearly change its eigenvalues, and hence the LPV notch will be described by the modal canonical state-space representation

$$\left[\begin{array}{c|c} \dot{x}_\delta^c & \\ \hline u & \end{array}\right] = \left[\begin{array}{c|c} A_\delta^c(\delta) & B_\delta^c(\delta) \\ \hline C_\delta^c(\delta) & D_\delta^c(\delta) \end{array}\right] \left[\begin{array}{c|c} x_\delta^c & \\ \hline v & \end{array}\right], \tag{12.8}$$

where $x_\delta^c \in \mathbb{R}^2$ is the notch state vector and where

$$\left[\begin{array}{c|c} A_\delta^c(\delta) & B_\delta^c(\delta) \\ \hline C_\delta^c(\delta) & D_\delta^c(\delta) \end{array}\right] = \left[\begin{array}{cc|c} -\delta\beta_2 & -\delta\sqrt{-\beta_2^2+1} & \delta \\ \delta\sqrt{-\beta_2^2+1} & -\delta\beta_2 & \delta \\ \hline \frac{(\beta_1-\beta_2)\left(\beta_2^2-\beta_2\sqrt{-\beta_2^2+1}-1\right)}{\beta_2^2-1} & \frac{(\beta_1-\beta_2)\left(\beta_2^2+\beta_2\sqrt{-\beta_2^2+1}-1\right)}{\beta_2^2-1} & 1 \end{array}\right], \tag{12.9}$$

which is indeed affine in δ. The series connection of (12.8) and the original controller (12.7) results in the affine parameter dependent controller

$$\left[\begin{array}{c|c} \dot{x}_c & \\ \hline u & \end{array}\right] = \left[\begin{array}{c|c} A_c(\delta) & B_c(\delta) \\ \hline C_c(\delta) & D_c(\delta) \end{array}\right] \left[\begin{array}{c|c} x_c & \\ \hline v & \end{array}\right], \tag{12.10}$$

where $x_c^T = [x_\delta^{cT}\ x_o^{cT}]^T$ and

$$\left[\begin{array}{c|c} A_c(\delta) & B_c(\delta) \\ \hline C_c(\delta) & D_c(\delta) \end{array}\right] = \left[\begin{array}{cc|c} A_\delta^c(\delta) & 0 & B_\delta^c(\delta) \\ B_o^c C_\delta^c(\delta) & A_o^c & B_o^c D_\delta^c(\delta) \\ \hline 0 & C_o^c & 0 \end{array}\right]. \tag{12.11}$$

The closed-loop state-space system from disturbance input f_d to measured output v is then given by

$$\left[\begin{array}{c|c} \dot{x}_{cl} & \\ \hline v & \end{array}\right] = \left[\begin{array}{c|c} \mathcal{A}(\delta) & \mathcal{B}(\delta) \\ \hline \mathcal{C}(\delta) & \mathcal{D}(\delta) \end{array}\right] \left[\begin{array}{c|c} x_{cl} & \\ \hline f_d & \end{array}\right], \tag{12.12}$$

where $x_{cl}^T = [x^T\ x_c^T]^T$ and

$$\left[\begin{array}{c|c} \mathcal{A}(\delta) & \mathcal{B}(\delta) \\ \hline \mathcal{C}(\delta) & \mathcal{D}(\delta) \end{array}\right] = \left[\begin{array}{cc|c} A & -BC_c(\delta) & B \\ B_c(\delta)C & A_c(\delta) & 0 \\ \hline C & 0 & 0 \end{array}\right]. \tag{12.13}$$

Note that (12.12) is affine in the scheduling parameter δ. Stability of affine parameter dependent systems such as (12.12) can be assessed by solving a set of

LMIs. The complexity of this set depends on the allowed rate of variation of the scheduling parameter. In our application, the operating condition of the mounted machine may be changed arbitrarily and hence the scheduling parameter may vary arbitrarily fast. The following sufficient condition for the stability of affine dependent systems with an arbitrarily fast rate of variation is well-known.

Theorem 12.1 ([126]) *Affinely parameterized system* (12.12) *with an arbitrarily fast varying parameter* $\delta \in [\underline{\delta}, \overline{\delta}]$ *is quadratically stable if and only if there exists* $K = K^T \succ 0$ *such that*

$$\mathcal{A}(\delta)^T K + K\mathcal{A}(\delta) \prec 0 \quad \textit{for all } \delta \in \{\underline{\delta}, \overline{\delta}\}. \tag{12.14}$$

Our application aims at reducing sinusoidal disturbances within the frequency range 4 to 10 Hz and therefore the scheduling parameter will be restricted to lie within the interval $\delta \in [4, 10]$. The LMI solver SeDuMi [138] is successfully used to find a positive definite matrix $K \in \mathbb{R}^{10\times 10}$, which satisfies (12.14). Based on Theorem 12.1, we now have that system (12.12) is stable for arbitrarily fast parameter variations in the range $\delta \in [4, 10]$.

12.3.2 Interconnection of the signal analyzer and the controller

Since both the real-time spectrum analyzer (C.5) and the LPV controller (12.10) have been designed, they can be interconnected to obtain the complete control setup as was proposed in Figure 12.5. Several measured signals could be used to identify the dominating disturbance frequency. A logical first choice would be to use the vertical velocity v of the AVIS since the goal of the controller is to minimize this velocity. However, a direct consequence of this goal is that the amplitude of the disturbing frequency is largely reduced, and therefore it is difficult to recognize this frequency with the spectrum analyzer. A better alternative is to use the controller output u as the input to the spectrum analyzer. In contrast to the vertical velocity of the AVIS, the amplitude of the disturbance frequency will not decrease due to the suppression of the controller in this signal. As long as the disturbance is acting on the AVIS, its frequency is present in the controller output. A schematic overview of the complete control system as it will be implemented is shown in Figure 12.8.

12.3.3 Simulation

To validate the proposed control setup, a simulation is performed. In this simulation the AVIS is subjected to a sinusoidal disturbance f_d to simulate a disturbance force that acts on the payload. The amplitude of the sinusoid is constant, but

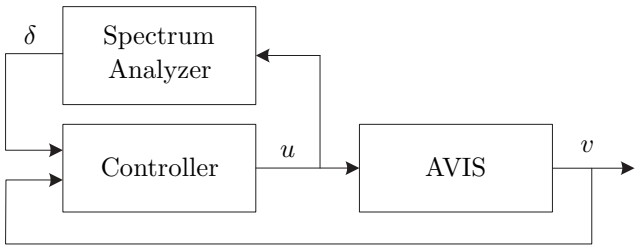

Figure 12.8: Schematic representation of the implementation of the controller and the spectrum analyzer.

the frequency of the disturbance force is continuously varying as is shown in Figure 12.9(a) by the grey line. The controller is implemented in three different ways. During the first 50 seconds, the original LTI controller (12.2) is applied. After 50 seconds the LPV controller (12.10) is used, where the scheduling parameter δ is taken to be the actually applied sinusoidal disturbance f_d. Finally, after 100 seconds, the controller implementation from Figure 12.8 is used and the scheduling parameter is replaced with the estimated frequency of the dominating disturbance. The disturbance isolation performance is depicted in Figure 12.9(b), where the (off-line computed) spectrum of the vertical velocity v is shown. It is obvious that the LPV controller achieves a much better disturbance rejection than the original controller. A slight increase of the vertical velocity is observed when the LPV controller is scheduled with the estimated frequency instead of the actually applied disturbance frequency, especially at low frequencies. This is caused by the delay that is introduced by the real-time spectrum analyzer. The real-time estimated frequency is also shown in Figure 12.9(a) with the black line. It is clear from this figure that the spectrum analyzer performs very well. In the following section the proposed control setup is applied to the experimental setup.

12.4 Experimental results

In this section, experiments will be performed on the experimental setup as depicted in Figure 12.4. The rotating imbalance is used to generate disturbance forces f_d that directly act on the payload. The imbalance is represented by a mass m_d located at a distance e_d from the center of rotation. For constant angular velocities ω_d, the induced disturbance force on the payload equals

$$f_d = m_d e_d \omega_d^2 \sin(\omega_d t). \tag{12.15}$$

These disturbance forces are sinusoids with frequency $\omega_d/2\pi$ Hz and an amplitude that is proportional to ω_d^2. The rotational velocity of the mass can vary in time, but is restricted between 4 and 10 revolutions per second. As mentioned before,

environmental disturbances are present as well, but disturbances from the rotating mass are dominating the disturbance spectrum.
Several experiments are performed. We start with a slow and smoothly varying induced disturbance frequency in Section 12.4.1. Fast changing operating conditions of the mounted machine are mimicked in Section 12.4.2 by switching the rotational velocity of the imbalance between 4 and 10 Hz. The limits of the LPV controller are investigated by rapidly changing the disturbance frequency in Section 12.4.3.

12.4.1 Smooth variations of the disturbance frequency

During this experiment, the rotational velocity ω_d of the imbalance is controlled to vary continuously between 4 and 10 revolutions per second, similar to the simulation in Section 12.3.3. The variation is obtained by using a sinusoidal reference velocity profile for the imbalance with a frequency of 0.02 Hz. The first half of the experiment, up to 50 seconds, the original LTI controller (12.2) is applied to be able to quantify the performance improvement of the LPV controller. After 50 seconds the LPV controller (12.10) is used together with the real-time spectrum analyzer. In Figure 12.10 the results from this experiment can be seen. Figure 12.10(a) shows the estimated frequency of the dominating disturbance by the real-time spectrum analyzer. The measured vertical velocity v of the AVIS and the off-line computed time-frequency spectrum are depicted in Figure 12.10(b). Several observations can be made from this figure. The overall error is decreased between a factor 3 to 5, depending on the disturbance frequency. When the LPV controller is scheduled to increase the performance around 10 Hz an increase in the error level in the frequency range 10 to 15 Hz can be observed. This is in agreement with Figure 12.7, where it was shown that the application of a notch around 10 Hz results in amplification of the environmental disturbances in that range. As a final observation we note that there is a frequency component around 130 Hz in the vertical velocity of the payload. Although this cannot be explained from the first principles model of the isolator (12.1), frequency response measurements show that indeed a resonance frequency is present in this range. It is clear from this experiment that the LPV controller offers a major increase in performance, at least for a slowly and smoothly varying disturbance force.

12.4.2 Switching variations of the disturbance frequency

The stability analysis from Section 12.3.1 showed that the closed-loop system is stable for arbitrary fast variations of the scheduling parameter in the interval $\delta \in [4, 10]$. To verify this experimentally, in this section the disturbance frequency ω_d is varied by switching the reference velocity of the imbalance between 4 and 10 Hz every 20 seconds. Although the reference velocity switches instantly, the actual velocity of the rotating mass changes only as fast as the hardware allows.

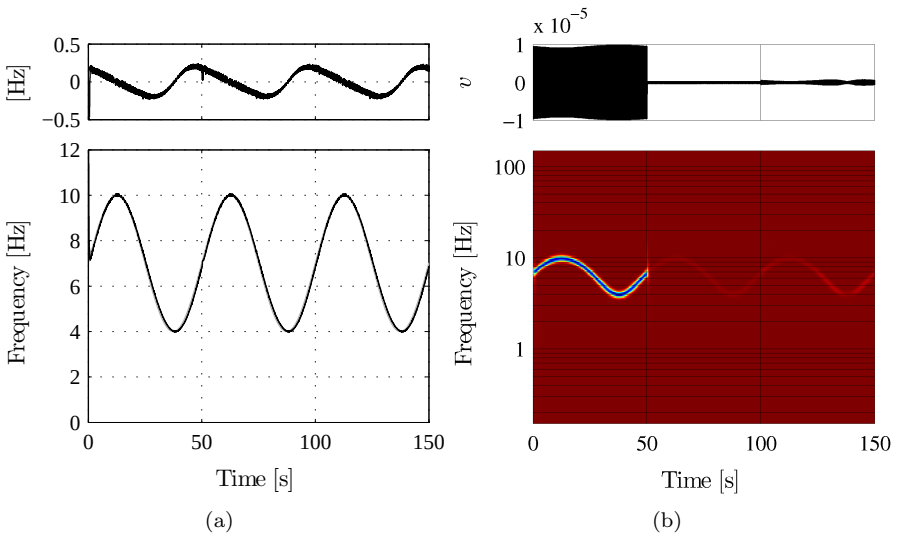

Figure 12.9: Simulation result. (a) Lower: Applied disturbance frequency (grey) and estimated dominating frequency (black), upper: estimation error, (b) the analyzed signal v and the off-line computed spectrum.

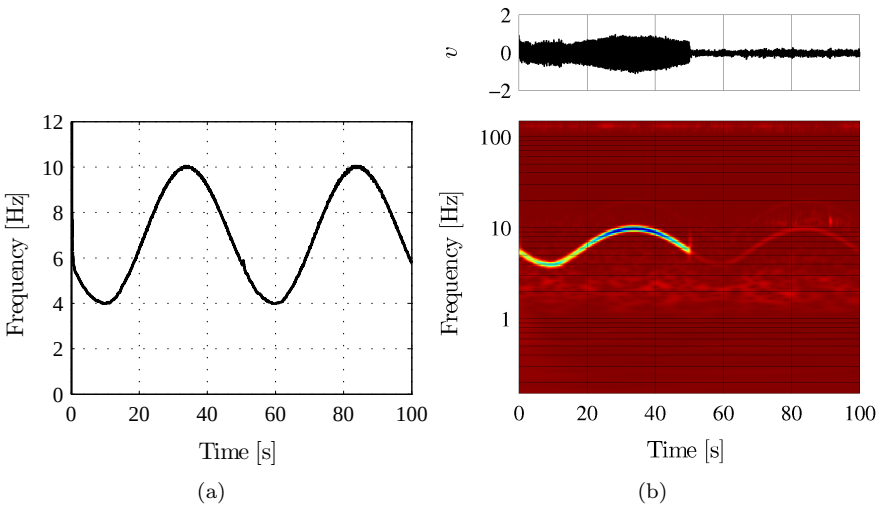

Figure 12.10: Experimental results with a smoothly varying disturbance. (a) Estimated frequency, (b) measured signal v and its off-line computed spectrum.

This is much faster, however, than the adaptation time of the LPV controller. Again, up to 50 seconds the original LTI controller (12.2) is applied, and the LPV controller is used after 50 seconds. The estimated frequency of the dominating disturbance is shown in Figure 12.11(a), while the off-line computed spectrum of the vertical velocity v is shown in Figure 12.11(b). At each switch, the controller needs some time to adapt to the changed disturbance. The needed adaptation time is caused by both the delay introduced by the real-time analyzer and by the time it takes to adjust the notch to the estimated frequency. Since the introduced delay and the transient time of the notch are both inversely proportional to the frequency, the control setup will adapt faster to the 10 Hz disturbance than to the 4 Hz disturbance. Indeed, the 10 Hz disturbance is adequately reduced after approximately 0.7 seconds while it takes approximately 1.5 seconds to adjust to the 4 Hz disturbance. The high frequent components that can be observed at each velocity switch are caused by the high accelerations of the rotating imbalance at those moments. The time span of these high frequent components is a measure for the time that is needed to decelerate and accelerate the imbalance. This time is indeed much smaller than the adaptation time of the LPV controller.

12.4.3 Increasing the rate of variation

To investigate the applicability of the proposed control setup in case the disturbance spectrum varies very fast, the rate of variation of the disturbance frequency is increased continuously in this experiment. The experiment is similar to the experiment of Section 12.4.1. However, the disturbance frequency varies at an increasing rate. The frequency of the sinusoid that is used to vary the disturbance is increased from 0.05 Hz at $t=0$ to 1 Hz at $t=100$ seconds. The first 25 seconds the original LTI controller is used and after 25 seconds the LPV controller is applied. The spectrum of the resulting measured signal v is depicted in Figure 12.12(a). The LPV controller improves the isolation performance up to approximately 200 seconds. When the disturbance changes too fast, the controller is not able to adapt itself. The spikes in the measured vertical velocity coincide with the time span in which the disturbance frequency is increasing. This is caused by the signal analysis method. Since the introduced delay is larger for the detection of low frequencies than for the detection of high frequencies, the delay caused by the low frequency detection results in a larger estimation error if the disturbance frequency is increasing than vice-versa. At this point the LPV controller performs worse than the LTI controller. This is caused by the fact that the disturbance of the actual disturbance differs from the estimated one. If for instance the actual disturbance frequency equals 7 Hz, while the notch is scheduled at 4 Hz, the isolation performance is decreased compared to the LTI controller as discussed in Section 12.3.

To improve the performance of the control setup for fast varying disturbances, the controller needs to adapt itself faster to the variations in the disturbance. To improve the transient time of the notch filter, the reduction factor of the notch is decreased from 30 to a factor 5, i.e, the damping is increased. Although this

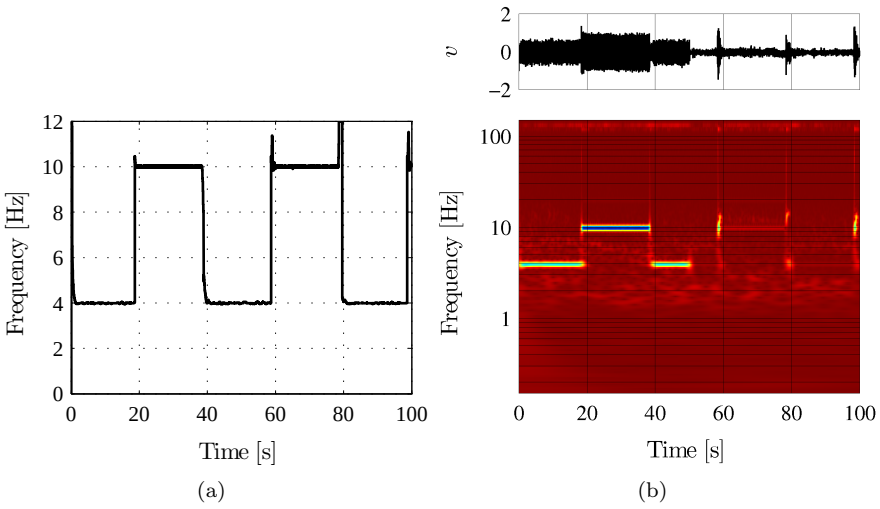

Figure 12.11: Experimental results with a switching disturbance. (a) Estimated frequency, (b) measured signal v and its off-line computed spectrum.

results in less vibration reduction at the center frequency, it is expected that the overall reduction of fast varying disturbances increases. The vertical velocity and

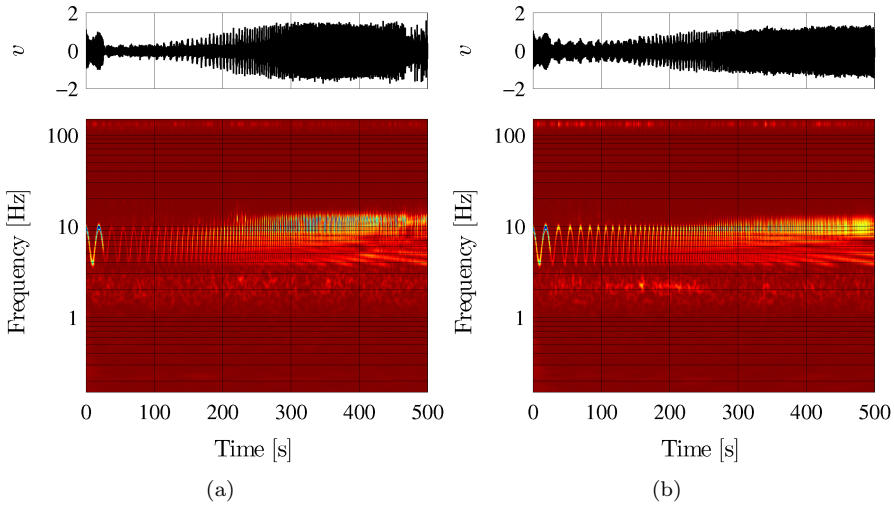

Figure 12.12: Experimental results with a continuously increasing disturbance frequency. (a) LPV controller (12.10), (b) LPV controller with a notch with a lower reduction factor.

the corresponding spectrum that are obtained obtained using the LPV controller with this notch is depicted in Figure 12.12(b). To compare both controllers, the moving average of the absolute vertical velocity v is shown in Figure 12.13. As

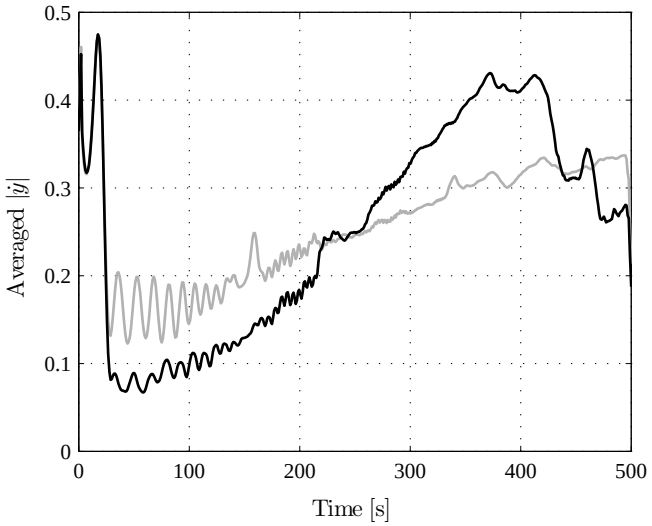

Figure 12.13: The moving average of $|v|$ corresponding to Figures 12.12(a) (black) and 12.12(b) (grey).

expected, the LPV controller with the notch with amplification factor 5 shows less disturbance reduction for slowly varying disturbances compared to controller (12.10). For fast variations, however, this faster adapting controller performs better. If information about the rate of variation of the disturbance is available, this information should be taken into account during the design of the controller. In addition, the frequency resolution of the spectrum analyzer could be lowered as well, resulting in a faster but less accurate disturbance frequency estimate. These parameters should be tuned with respect to the application at hand.

12.5 Conclusions

In this chapter we proposed a nonlinear controller setup for the active control of a vibration isolation system. This setup consists of two parts: (i) a real-time multiresolution spectrum analyzer that is able to identify the currently dominating disturbance, and (ii) an LPV controller that adapts itself to the available disturbance information. This resulted in a control system that is able to adapt itself to the current operating condition resulting in a closed-loop system with an overall increased performance when compared to an LTI controller.

An important design aspect of the spectrum analyzer is the shape of the used wavelet which constitutes the trade-off between the desired frequency accuracy and the introduced time delay. If only stationary disturbances with unknown frequency (or slowly varying non-stationary disturbances) are present, a high frequency resolution is desirable to better be able to differentiate between disturbances that differ only little in frequency. In contrast, when the disturbances vary fast in frequency, it is important to be able to identify them as soon as possible at the cost of a reduced frequency resolution.
A similar discussion applies to the design of the controller. In this chapter, the part of the controller that was scheduled according to the identified disturbance frequency was a notch filter. Such a notch filter has a certain width and reduction factor. These design parameters should be chosen with the application and expected disturbance variation in mind. A wide notch with a large reduction factor results in good disturbance reduction properties around the center frequency of the notch. However, at the same time environmental disturbances in other frequency regions will be amplified by such a notch. A too narrow notch with a small reduction factor on the other hand may not be adequate to reduce the dominating disturbance at the center frequency.
The proposed control system was validated by experiments that were performed on an active vibration isolation system. Compared to the originally designed LTI controller, the LPV control system was able to decrease the error by a factor 3 to 5 in case the disturbance spectrum is dominated by a single sinusoid with varying frequency. If the disturbance frequency varies very fast, the LPV control system is not able to adapt itself to the disturbance. This is both caused by the real-time spectrum analyzer as well as by the controller itself. The desired accuracy of the analyzer and the width and amplification factor of the notch may be altered to match the changed disturbance properties.
Although ideally the center frequency, the width, and the reduction factor of the notch filter should all three be adapted conform to the disturbance, in this chapter we only considered the adaptation of the center frequency. The real-time spectrum analyzer not only offers the frequency of the dominating disturbance, but also its amplitude. This estimated amplitude can be used in conjunction with the given performance specifications to additionally schedule the reduction factor of the notch filter. The spectral analysis of past data can be used to estimate the rate of change of the disturbance spectrum and this information can also be used to schedule the width and amplification factor of the notch filter. All this will be subject of future research.

Part V

Closing

Chapter 13

Conclusions and Recommendations

In this chapter, we reflect on the obtained results in this thesis. We start by stating the overall conclusions. After this we will discuss recommendations for future research.

13.1 Conclusions

This thesis focussed on nonlinear control of linear motion systems. The goal was to:

Develop systematic and generic control synthesis methods for nonlinear feedback controllers for linear motion systems, overcoming the limitations imposed by linear feedback.

The followed approach to arrive at systematic synthesis methods was to take several well-developed linear control design methods as a starting point and use them as a basis to propose nonlinear extensions. These nonlinear extensions are designed to overcome the limitations that are present in the linear control design methods. This strategy was followed in an exploratory way. As such, the concepts that are discussed in this thesis should be seen as first steps towards performance driven nonlinear control design for linear motion systems, as several issues still have to be overcome before complete design solutions are available. We distinguished three nonlinear control approaches:

- Time-domain performance based polynomial state feedback (Part II)
- Reset control (Part III)
- LPV control (Part IV)

Just as there are many design methods for linear control systems such as loop shaping, pole placement, LQG design, $\mathcal{H}_\infty$ design, and so on, there are different methods to design nonlinear controllers for linear systems. Each of these methods (both for linear and nonlinear controller design) has its own advantages and disadvantages. A major problem is the absence of a performance measure that is suitable for the synthesis of both linear and nonlinear control systems. This is encountered throughout the thesis. First of all, the goal of this thesis was to design nonlinear controllers that *outperform* linear controllers. However, it is not clear at this point what is the 'best' *linear* controller for a linear system. The label 'best' should be quantifiable by some performance measure. In this thesis we mainly used time-domain performance measures (such as rise-time, settling time, and overshoot), and the design of the 'best' linear controller with respect to these time-domain measures is still an open problem. Therefore, it is difficult to answer the question if certain nonlinear controllers outperform the 'best' linear controller, as this linear controller is not available in most cases. Determining what is the 'best' nonlinear controller might even be more difficult. As a consequence, the performance of the nonlinear controllers that were proposed in this thesis is not assessed with respect to the performance of the 'best' linear or nonlinear controller, but rather with respect to the performance of the linear controller, which was used as the basis for the corresponding nonlinear controller design. In this respect, it was shown that by adding specific nonlinear elements it was possible to improve the performance of the original linear controller in some sense. In other words, all of the proposed nonlinear controllers are able to outperform the original linear controller.

However, the practical applicability of the proposed design methods is not the same. In our opinion, the LPV approach has the most potential to be used in industry from all the considered approaches. This is expected since the conceptual design steps taken in this approach, i.e., performance specification in the frequency domain and automatic synthesis via $\mathcal{H}_\infty$-like methods, are close to the methods with which industrial control engineers are familiar. The other approaches suffer in more or less severe ways from some 'impracticalities'. The main issue related to the method presented in Chapter 4 is that the original controller should be designed via pole placement. This approach is less adopted in industry because the link to closed-loop performance is not as clear as when, for instance, loop shaping is applied. To make the design of a nonlinear state feedback controller as proposed in Chapter 5 a viable method in practice, the heuristic and approximative nature should be reduced. One of the main issues is that, next to stability, also performance and constraint satisfaction should be guaranteed for a large set of initial conditions, which is currently not the case. The obtained results from Part III are suitable for the analysis of reset control systems. The performance

based synthesis of these kind of controllers could be based on bilinear matrix inequalities (BMIs), but these are generally hard to solve. Moreover, with respect to performance in terms of the $\mathcal{L}_2$ gain, reset control can never outperform linear controllers, since it is shown in [76] and [116] that for LTI plants there exists no nonlinear (possibly time-varying) controller, which yields a lower $\mathcal{L}_2$ gain than the optimal linear controller. However, reset control can be used to improve the transient performance of a control system, possibly with not too much loss of $\mathcal{L}_2$ gain performance.
The above discussion is in agreement with the final conclusion, namely that we do not expect that the application of nonlinear controllers for linear systems is able to 'defeat Bode', i.e., to obtain performance improvement over the complete frequency range at the same time. The main limitation in linear systems is imposed by the waterbed effect and Bode's gain-phase relation, see Section 2.2. Taking into account the nonlinear extensions of the fundamental limitations discussed in Section 2.3, the existence of a similar trade-off as characterized by the waterbed effect seems to be inevitable. It is therefore expected that the benefits of nonlinear control of linear systems are most apparent in specific situations (e.g. for specific disturbance or reference signals) and that there are few to no benefits when worst case performance is considered for large classes of possible input and disturbance signals as is typically the case for performance measures such as the $\mathcal{L}_2$ gain.

13.2 Recommendations

The following recommendations can be made.

- Currently, most performance analysis techniques for nonlinearly controlled motion systems are based on time-domain simulations. Using these simulations, the results in this thesis showed that nonlinear control can outperform a fixed linear controller for practically relevant subclasses of reference and disturbance signals, such as for instance step references and disturbance signals with limited frequency content. Unfortunately, there are not many suitable measures that on the one hand can capture the performance of a system for some subclasses of reference or disturbance signals, while allowing for a systematic synthesis method for (nonlinear) controllers on the other hand. Indeed, for instance, the well-known $\mathcal{H}_\infty$ or $\mathcal{L}_2$ gain criterium suffers from the drawback that it guarantees that the $\mathcal{L}_2$ gain is lower than a certain value for whole classes of disturbances or references, while in practice one is often interested in the performance related to particular disturbance and reference signals. Therefore, it would be beneficial to develop practically relevant performance measures that can be used to asses the performance of both linearly and nonlinearly controlled systems in an improved manner and, as a second step, that allow for a systematic design procedure, which yields the optimal (nonlinear) controller for that measure. From the foregoing it is clear that a suitable performance measure should be based on the

particular class of disturbance and reference signals, which is relevant for the (practical) control problem at hand. The line of work in [108, 111] on convergence might be helpful in setting up such performance measures and corresponding control design methods.

- All proposed design methods in this thesis are based on optimization. Part II used sum-of-squares optimization, while Parts III and IV considered optimization using the dissipativity framework. A common aspect of these optimization problems is that they can be represented via LMIs. At this point, however, although theoretically the optimal solution can be found since these optimization problems are convex, numerically it is not straightforward to actually obtain the optimal solution. This is due to the fact that the currently available solvers, such as for instance SeDuMi [138], are not able to handle large optimization problems and are very sensitive to the numerics. To arrive at the nonlinear control solutions that are presented in this thesis, most of the time a lot of effort was required to tune the problem to arrive at sensible solutions using the available solvers. This can be a problem if the proposed nonlinear controller synthesis methods are to be used in industry, since the optimization problems for real-life applications are normally large and not well-conditioned. Clearly, the development of reliable and less numerically sensitive solvers for LMI problems would be advantageous for this line of work and the application in industry.

- The two relaxations proposed in the optimization of the controller based on time-domain constraints in Chapter 4 are suited for different performance objectives. In case of a step response, the exponential bounds relaxation is specifically suited for improving the rise-time and settling-time, while the multivariate polynomial relaxation can be applied for overshoot minimization. These relaxations could be merged to combine the performance objectives in one problem formulation. Furthermore, to reduce the conservatism of the multivariate polynomial relaxation, the ad hoc polynomial approximation (4.60) was introduced. At this point it is not clear what is the best approximation, and hence, further research is required to arrive at generically applicable approximation methods, which are guaranteed to be effective.

- With respect to the control design method proposed in Chapter 5, there are several issues that still require further attention. Firstly, the method lacks a procedure to systematically analyze the performance (including the violation of input and state constraints) after a feedback law is obtained. Moreover, at this point the performance for other initial conditions than the one designed for cannot be guaranteed during the synthesis. Secondly, it would be interesting to combine the computation of the nonlinear state feedback with the construction of a Lyapunov function during the design, such that some guarantees for the region of attraction can be given a priori. Ideally, the two issues mentioned above should be blended into one approach. This would result in a method to compute a nonlinear polynomial state

feedback law that a priori guarantees stability and performance for a given set of initial conditions, while taking the specified time-domain constraints into account for one or more specific initial conditions.

- The initial goal of studying reset control was to formulate a method with which reset controllers could be synthesized based on efficient computational methods such as LMIs. Unfortunately, it turned out that the standard methods could not reduce the obtained BMIs to LMIs to facilitate controller synthesis. Possible solution directions for synthesis are the use of BMI solvers and sum-of-squares decompositions of matrix valued polynomials as proposed in [57].

- Although the proposed method in Chapter 11 is suitable for systematic control synthesis, the user still has to specify the desired performance through weighting functions. Moreover, the scheduling function has to be designed separately. Ideally, given some performance specification, the corresponding weighting functions and the scheduling functions should be obtained systematically, while both stability and performance should be guaranteed for all possible parameter trajectories. Further research is required to reach this goal leading to a complete synthesis method.

- In Chapter 12 we only considered the adaptation of the center frequency of the proposed LPV notch filter. Ideally, the center frequency, the width, and the reduction factor could all three be adapted depending on the disturbance characteristic. Since the real-time spectrum analyzer not only offers the frequency of the dominating disturbance, but also its amplitude, this estimated amplitude can be used in conjunction with the given performance specifications to additionally schedule the reduction factor of the notch filter. The spectral analysis of past data can be used to estimate the rate of change of the disturbance spectrum, which can also be used to schedule the width and amplification factor of the notch filter.

To conclude, this thesis presented initial steps towards systematic design methods for nonlinear controllers for linear systems, which obtain performance levels that are not attainable by using linear controllers. The obtained results are promising on the one hand, but, on the other hand they also show that still a lot of developments are needed before complete systematic synthesis methods are available. However, the potential benefits for the high-tech industry will drive such further developments in this appealing and challenging area, for which the results presented in this thesis can form a starting point.

Bibliography

[1] P. Apkarian and P. Gahinet. A convex characterization of gain-scheduled H_∞ controllers. *IEEE Trans. Automat. Contr.*, 40(5):853–864, 1995.

[2] A.R. Bailey. Stabilization of control systems by the use of driven limiters. *Proc. IEEE*, 113(1):169–174, 1966.

[3] R. Bass and R. Webber. Optimal nonlinear feedback control derived from quartic and higher-order performance criteria. *IEEE Trans. Automat. Contr.*, 11(3):448–454, 1966.

[4] G. Becker and A. Packard. Robust performance of linear parametrically varying systems using parametrically-dependent linear feedback. *System & Control Letters*, 23(3):205–215, 1994.

[5] O. Beker, C.V. Hollot, Q. Chen, and Y. Chait. Stability of a reset control system under constant inputs. In *Proceedings of the American Control Conference*, pages 3044–3045, San Diego, CA, 1999.

[6] O. Beker, C.V. Hollot, and Y. Chait. Plant with integrator: An example of reset control overcoming limitations of linear feedback. *IEEE Trans. Automat. Contr.*, 46(11):1797–1799, 2001.

[7] O. Beker, C.V. Hollot, Y. Chait, and H. Han. Fundamental properties of reset control systems. *Automatica*, 40(6):905–915, 2004.

[8] A. Bemporad, A. Casavola, and E. Mosca. Nonlinear control of constrained linear systems via predictive reference management. *IEEE Trans. Automat. Contr.*, 42(3):340–349, 1997.

[9] A. Bemporad, M. Morari, V. Dua, and E.N. Pistikopoulos. The explicit linear quadratic regulator for constrained systems. *Automatica*, 38(1):3–20, 2002.

[10] D.P. Bertsekas. *Dynamic programming and optimal control*. Athena Scientific, Belmont, Mass., 2005.

[11] S.P. Bhat and D.K. Miu. Precise point-to-point positioning control of flexible structures. *J. of Dyn. Sys., Meas., and Control*, 112:667–674, December 1990.

[12] H. Bode. *Network analysis and feedback amplifier design*. D. van Nostrand, New York, 1945.

[13] S. Boyd and C. Barratt. *Linear controller design: limits of performance*. Prentice Hall, 1991.

[14] S. Boyd, L. El Ghaoui, E. Feron, and V. Balakrishnan. *Linear Matrix Inequalities in System and Control Theory*. SIAM, Philadelphia, PA, 1994.

[15] M.S. Branicky. Multiple Lyapunov functions and other analysis tools for switched and hybrid systems. *IEEE Trans. Automat. Contr.*, 43(4):475–482, 1998.

[16] J.H. Braslavsky, R.H. Middleton, and J.S. Freudenberg. Effects of time delay on feedback stabilization over signal-to-noise ratio constrained channels. In *Proceedings of the 16th IFAC World Congress*, 2005.

[17] J.H. Braslavsky, R.H. Middleton, and J.S. Freudenberg. Feedback stabilization over signal-to-noise ratio constrained channels. *IEEE Trans. Automat. Contr.*, 52(8):1391–1403, 2007.

[18] Y. Chait and C.V. Hollot. On Horowitzs contributions to reset control. *Int. Journal of Robust and Nonlinear Control*, 12(4):335–355, 2002.

[19] B.M. Chen, T.H. Lee, P. Kemao, and V. Venkataramanan. Composite nonlinear feedback control for linear systems with input saturation: theory and an application. *IEEE Trans. Automat. Contr.*, 48(3):427–439, 2003.

[20] J. Chen. Sensitivity integrals and transformation techniques: a new perspective. *IEEE Trans. Automat. Contr.*, 42:1037–1042, 1997.

[21] J. Chen. Multivariable gain-phase and sensitivity integral relations and design trade-offs. *IEEE Trans. Automat. Contr.*, 43(3):373–385, 1998.

[22] J. Chen. Logarithmic integrals, interpolation bounds, and performance limitations in MIMO feedback systems. *IEEE Trans. Automat. Contr.*, 45(6): 1098–1115, 2000.

[23] J. Chen and Z. Ren. A comparison of small gain versus lyapunov type robust stability bounds. *Int. Journal of Robust and Nonlinear Control*, 11 (15):1407–1414, 2001.

[24] J. Chen, G. Chen, Z. Ren, and L. Qiu. Extended argument principle and integral design constraints part I: a unified formula for classical results. In *Proceedings of the Conference on Decision and Control*, pages 4984–4989, 2000.

[25] J. Chen, G. Chen, Z. Ren, and L. Qiu. Extended argument principle and integral design constraints part II: new integral relations. In *Proceedings of the Conference on Decision and Control*, pages 3081–3086, 2001.

[26] J.C. Clegg. A nonlinear integrator for servomechanisms. *Trans. AIEE*, 77: 41–42, 1958.

[27] R.A. Decarlo, S.H. Zak, and G.P. Matthews. Variable structure control of nonlinear multivariable systems: A tutorial. *Proc. IEEE*, 76(3):212–232, 1988.

[28] M. Dettori. *LMI techniques for control with application to a compact disc player mechanism*. PhD thesis, Technisch Universiteit Delft, Delft, 2001.

[29] M. Dettori and C.W. Scherer. Robust stability analysis for parameter dependent systems using full block S-procedure. In *Proceedings of the Conference on Decision and Control*, volume 3, pages 2798–2799, 1998.

[30] M. Dettori and C.W. Scherer. New robust stability and performance conditions based on parameter dependent multipliers. In *Proceedings of the Conference on Decision and Control*, volume 5, pages 4187–4192, 2000.

[31] M. Dinh, G. Scorletti, V. Fromion, and E. Magarotto. Parameter dependent H_∞ control by finite dimensional LMI optimization: application to trade-off dependent control. *Int. Journal of Robust and Nonlinear Control*, 15(9): 383–406, 2005.

[32] J. Doyle, A. Packard, and K. Zhou. Review of LFTs, LMIs, and μ. In *Proceedings of the Conference on Decision and Control*, volume 2, pages 1227–1232, 1991.

[33] J.C. Doyle, B.A. Francis, and A.R. Tannenbaum. *Feedback control theory*. MacMillan, New York, 1992.

[34] N. Elia. When Bode meets Shannon: control-oriented feedback communication schemes. *IEEE Trans. Automat. Contr.*, 49(9):1477–1488, 2004.

[35] A. Feuer, G.C. Goodwin, and M. Saldago. Potential benefits of hybrid control for linear time invariant plants. In *Proceedings of the American Control Conference*, pages 2790–2794, Albuquerque, NM, 1997.

[36] I.J. Fialho and G.J. Balas. Design of nonlinear controllers for active vehicle suspensions using parameter-varying control synthesis. *Vehicle System Dynamics*, 33:351–370, 2000.

[37] P. Flandrin. *Time-Frequency/Time-scale analysis*. Academic Press, London, UK, 1999.

[38] W.C. Foster, D.L. Gieseking, and W.K. Waymeyer. A nonlinear filter for independent gain and phase (with application). *Trans. ASME J. Basic Eng.*, 78:457 – 462, 1966.

[39] B. Francis and G. Zames. On H_∞-optimal sensitivity theory for SISO feedback systems. *IEEE Trans. Automat. Contr.*, 29(1):9–16, 1984.

[40] G.F. Franklin, J.D. Powell, and A. Emami-Naeini. *Feedback control of dynamic systems*. Prentice Hall, New Jersey, 2002.

[41] J.S. Freudenberg and D. Looze. Right half plane poles and zeros and design tradeoffs in feedback systems. *IEEE Trans. Automat. Contr.*, 30(6):555–565, 1985.

[42] J.S. Freudenberg and D. Looze. A sensitivity tradeoff for plants with time delay. *IEEE Trans. Automat. Contr.*, 32(2):99–104, 1987.

[43] J.S. Freudenberg, R.H. Middleton, and J.H. Braslavsky. Inherent design limitations for linear sampled-data feedback systems. *Int. Journal of Control*, 61(6):1387 – 1421, 1995.

[44] J.S. Freudenberg, R.H. Middleton, and A. Stefanpoulou. A survey of inherent design limitations. In *Proceedings of the American Control Conference*, volume 5, pages 2987–3001, 2000.

[45] V. Fromion and G. Scorletti. Performance and robustness analysis of nonlinear closed loop systems using μ_{nl} analysis: applications to nonlinear PI controllers. In *Proceedings of the Conference on Decision and Control*, volume 3, pages 2480–2485, 2002.

[46] V. Fromion, G. Scorletti, and G. Ferreres. Nonlinear performance of a PI controlled missile: an explanation. *Int. Journal of Control*, 9(8):485–518, 1999.

[47] P. Gahinet and P. Apkarian. A linear matrix inequality approach to H_∞ control. *Int. Journal of Robust and Nonlinear Control*, 4:421–448, 1994.

[48] R. Garrido and A. Soria. Control of a servomechanism using non-linear damping. *Proc. Instn Mech. Engrs, Part I: J. Systems and Control Eng.*, 219(4):295–299, 2005.

[49] A. Gelb and W.E. Vander Velde. *Multiple-Input Describing Functions and Nonlinear System Design*. McGraw-Hill, New York, 1968.

[50] W. Haddad. Nonlinear impulsive dynamical systems, part I: stability and dissipativity. *Int. Journal of Control*, 74(17):1631–1658, 2001.

[51] W. Heemels, J. Schumacher, and S. Weiland. Linear complementarity systems. *SIAM Journal on Applied Mathematics*, 60(4):1234–1269, 2000.

[52] M. Heertjes and M. Steinbuch. Stability and performance of a variable gain controller with application to a DVD storage drive. *Automatica*, 40(4): 591–602, 2004.

[53] M.F. Heertjes, N. van de Wouw, and W.P.M.H. Heemels. Switching control in active vibration isolation. In *Proceedings of the 6th EUROMECH Nonlinear Oscillations Conference (ENOC)*, Saint Petersburg, Russia, 2008.

[54] D. Henrion and J.-B. Lasserre. GloptiPoly: Global optimization over polynomials with Matlab and SeDuMi. *ACM Trans. Math. Soft*, 29:165–194, 2002.

[55] D. Henrion and J.-B. Lasserre. LMIs for constrained polynomial interpolation with application in trajectory planning. *System & Control Letters*, 55 (6):473–477, 2006.

[56] D. Henrion, S. Tarbouriech, and V. Kučera. Control of linear systems subject to time-domain constraints with polynomial pole placement and LMIs. *IEEE Trans. Automat. Contr.*, 50(9):1360–1364, 2005.

[57] C.W.J. Hol. *Strucured controller synthesis for mechanical servo systems: algorithms, relaxations and optimality certificates*. PhD thesis, Technische Universiteit Delft, Delft, 2006.

[58] C.W.J. Hol and C. Scherer. Sum of squares relaxations for polynomial semi-definite programming. In *Proceedings MTNS*, Leuven, Belgium, 2004.

[59] J.H. Holland. *Adaptation in Natural and Artificial Systems*. PhD thesis, University of Michigan, 1975.

[60] C.V. Hollot, O. Beker, Y. Chait, and Q. Chen. On establishing classic performance measures for reset control systems. In S. Moheimani, editor, *Perspectives in Robust Control*, pages 123–148. Springer-Verlag, 2001.

[61] I. Horowitz. *Synthesis of feedback systems*. Academic Press, New York, 1963.

[62] I. Horowitz and P. Rosenbaum. Non-linear design for cost of feedback reduction in systems with large parameter uncertainty. *Int. Journal of Control*, 21:977–1001, 1975.

[63] H. Hu, Y. Zheng, Y. Chait, and C.V. Hollot. On the zero-input stability of control systems with Clegg integrators. In *Proceedings of the American Control Conference*, pages 408–410, Albuquerque, NM, 1997.

[64] J. Hu, H. Unbehauen, and C. Bohn. A practical approach to selecting weighting functions for $\mathcal{H}_\infty$ control and its application to a pilot plant. In *UKACC Int. Conf. Contr.*, volume 2, pages 998–1003, Bochum, Germany, 1996.

[65] R.A. Hyde and K. Glover. The application of scheduled H_∞ controllers to a VSTOL aircraft. *IEEE Trans. Automat. Contr.*, 38(7):1021–1039, 1993.

[66] P.A. Iglesias. Tradeoffs in linear time-varying systems: an analogue of Bode's sensitivity integral. *Automatica*, 37(10):1541–1550, 2001.

[67] P.A. Iglesias. An analogue of Bode's integral for stable nonlinear systems: Relations to entropy. In *Proceedings of the Conference on Decision and Control*, pages 3419–3420, 2001.

[68] P.A. Iglesias. Logarithmic integrals and system dynamics: an analogue of Bode's sensitivity integral for continuous-time, time-varying systems. *Lin. Algebra Appl.*, 343-344:451–471, 2002.

[69] T. Iwasaki and S. Hara. Generalized KYP lemma: unified frequency domain inequalities with design applications. *IEEE Trans. Automat. Contr.*, 50(1): 41–59, 2005.

[70] T. Iwasaki, G. Meinsma, and M. Fu. Generalized S-procedure and finite frequency KYP lemma. *Mathematical Problems in Engineering*, 6:305–320, 2000.

[71] F. Jiang and Z. Gao. An application of nonlinear PID control to a class of truck ABS problems. In *Proceedings of the Conference on Decision and Control*, volume 1, pages 516–521, 2001.

[72] M. Johansson and A. Rantzer. Computation of piecewise quadratic Lyapunov functions for hybrid systems. *IEEE Trans. Automat. Contr.*, 43(4): 555–559, 1998.

[73] R.E. Kalman. Phase-plane analysis of automatic control systems with nonlinear gain elements. *Trans. AIEE*, 73:383 – 389, 1955.

[74] N. Karlsson, M.A. Dahleh, and D. Hrovat. Nonlinear H_∞ control of active suspensions. In *Proceedings of the American Control Conference*, volume 5, pages 3329–3334, 2001.

[75] H.K. Khalil. *Nonlinear systems*. MacMillan, New York, 1992.

[76] P.P. Khargonekar and K.R. Poolla. Uniformly optimal control of linear time-invariant plants: Nonlinear time-varying controllers. *System & Control Letters*, 6(5):303–308, 1986.

[77] E. Kreyzig. *Introductory functional analysis with applications*. John Wiley & Sons, 1978.

[78] K.R. Krishnan and I.M. Horowitz. Synthesis of a non-linear feedback system with significant plant-ignorance for prescribed system tolerances. *Int. Journal of Control*, 19(4):689 – 706, 1974.

[79] V. Kučera. The pole placement equation - a survey. *Kybernetica*, 30:578–584, 1994.

[80] V. Kučera and P. Zagalak. Proper solutions of polynomial equations. In *Proceedings of the 14th IFAC World Congress*, pages 357–362, Beijing, China, 1999.

[81] J.-B. Lasserre. Global optimization with polynomials and the problem of moments. *SIAM Journal on Optimization*, 11:796–817, 2001.

[82] K. Lau. *Time Domain Feedback Performance Limitations - Extensions to Nonlinear, Switched, and Sampled Systems.* PhD thesis, The University of Newcastle, Australia, 2002.

[83] K. Lau, R.H. Middleton, and J.H. Braslavsky. Undershoot and settling time tradeoffs for nonminimum phase systems. *IEEE Trans. Automat. Contr.*, 48(8):1389–1393, 2003.

[84] D.J. Leith and W.E. Leithead. Appropriate realization of gain-scheduled controllers with application to wind turbine regulation. *Int. Journal of Control*, 65(2):223 – 248, 1996.

[85] J. Levine and D.V. Nguyen. Flat output characterization for linear systems using polynomial matrices. *System & Control Letters*, 48(1):69–75, 2003.

[86] E. Levinson. *Gain reduction without phase change. A property of non-linear circuits.* PhD thesis, Polytechnic institute of Brooklyn, 1956.

[87] J.B. Lewis. The use of nonlinear feedback to improve the transient response of a servomechanism. *Trans. AIEE*, 71(II):449–453, 1953.

[88] J. Löfberg. YALMIP : A toolbox for modeling and optimization in MATLAB. In *Proc. CACSD Conference*, Taipei, Taiwan, 2004.

[89] PolyX Ltd. *The polynomial toolbox for matlab.* version 2.5, Prague, Czech Republic, 2001.

[90] G.Y. Luo, D. Osypiw, and M. Irle. On-line vibration analysis with fast continuous wavelet algorithm for condition monitoring of bearing. *Journal of Vibration and Control*, 9(8):931–947, 2003.

[91] N.C. Martins and M.A. Dahleh. Fundamental limitations of performance in the presence of finite capacity feedback. In *Proceedings of the American Control Conference*, volume 1, pages 79–86, 2005.

[92] D.Q. Mayne, J.B. Rawlings, C.V. Rao, and P.O.M. Scokaert. Constrained model predictive control: Stability and optimality. *Automatica*, 36(6):789–814, 2000.

[93] N.H. McClamroch and I. Kolmanovsky. Performance benefits of hybrid control design for linear and nonlinear systems. *Proc. IEEE*, 88(7):1083–1096, 2000.

[94] R.H. Middleton. Trade-offs in linear control system design. *Automatica*, 27 (2):281–292, 1991.

[95] R.H. Middleton and J.H. Braslavsky. On the relationship between logarithmic sensitivity integrals and limiting optimal control problems. *IEEE Trans. Automat. Contr.*, 5:4990–4995, 2000.

[96] R.H. Middleton and J.H. Braslavsky. Towards quantitative time domain design tradeoffs in nonlinear control. In *Proceedings of the American Control Conference*, volume 6, pages 4896–4901, 2002.

[97] R.H. Middleton and G.C. Goodwin. *Digital control and estimation. A unified approach*. Prentice-Hall, Englewood Cliffs, NJ, 1990.

[98] R.H. Middleton, J.K. Ward, J.S. Freudenberg, and A.R. Woodyatt. Performance limitations in the feedback control of a class of resonant systems. In *Proceedings of the Conference on Decision and Control*, volume 2, pages 1845–1850, 1999.

[99] R.H. Middleton, J.H. Braslavsky, and J.S. Freudenberg. Stabilization of non-minimum phase plants over signal-to-noise ratio constrained channels. In *Proceedings of the Asian Control Conference*, 2004.

[100] Y. Nesterov. Squared functional systems and optimization problems. In H. Frenk, K. Roos, T. Terlaky, and S. Zhang, editors, *High performance optimization*, chapter 17, pages 405–440. Kluwer academic publishers, Dordrecht, The Netherlands, 2000.

[101] D. Nešić, L. Zaccarian, and A.R. Teel. Stability properties of reset systems. In *Proceedings of the 16th IFAC World Congress*, Prague (CZ), 2005.

[102] D.S. Ortiz, J.S. Freudenberg, and R.H. Middleton. Inherent design limitations for feedback systems with periodic digital controllers. In *Proceedings of the Conference on Decision and Control*, volume 2, pages 1257–1258, 1996.

[103] A. Packard. Gain scheduling via linear fractional transformations. *System & Control Letters*, 22(2):79–92, 1994.

[104] B. Paijmans, W. Symens, H. Van Brussel, and J.A. Swevers. A gain-scheduling-control technique for mechatronic systems with position-dependent dynamics. In *Proceedings of the American Control Conference*, pages 2933–2398, 2006.

[105] A. Papachristodoulou. *Scalable analysis of nonlinear systems using convex optimization*. PhD thesis, California Institute of Technology, Pasadena, CA, 2005.

[106] A. Papachristodoulou and S. Prajna. A tutorial on sum of squares techniques for systems analysis. In *Proceedings of the American Control Conference*, volume 4, pages 2686–2700, 2005.

[107] P.A. Parrilo. *Structured semidefinite programs and semialgebraic geometry methods in robustness and optimization*. PhD thesis, California Institute of Technology, Pasadena, CA, 2000.

[108] A. Pavlov. *The output regulation problem: A convergent dynamics approach.* PhD thesis, Eindhoven University of Technology, Eindhoven, The Netherlands, 2004.

[109] A. Pavlov, N. van de Wouw, and H. Nijmeijer. Frequency response functions and Bode plots for nonlinear convergent systems. In *Proceedings of the Conference on Decision and Control*, pages 3765–3770, 2006. San Diego.

[110] A. Pavlov, N. van de Wouw, and H. Nijmeijer. Frequency response functions for nonlinear convergent systems. *IEEE Trans. Automat. Contr.*, 52(6): 1159–1165, 2007.

[111] A. Pavlov, N. van de Wouw, and H. Nijmeijer. Global nonlinear output regulation: Convergence-based controller design. *Automatica*, 43(3):456–463, 2007.

[112] S. Prajna, A. Papachristodoulou, and P.A. Parrilo. Introducing SOSTOOLS: a general purpose sum of squares programming solver. In *Proceedings of the Conference on Decision and Control*, volume 1, pages 741–746, 2002.

[113] S. Prajna, A. Papachristodoulou, P. Seiler, and P.A. Parrilo. *SOSTOOLS: Sum of squares optimization toolbox for MATLAB.* Available from `http://www.cds.caltech.edu/sostools` and `http://www.mit.edu/~parrilo/sostools`, 2004.

[114] M. Putinar. Positive polynomials on compact semi-algebraic sets. *Indiana Univ. Math. J.*, 42(3):969984, 1993.

[115] L. Qiu and E.J. Davison. Performance limitations of non-minimum phase systems in the servomechanism problem. *Automatica*, 29(2):337–349, 1993.

[116] S. Rangan. Multiobjective H_∞ problems: Linear and nonlinear control. *System & Control Letters*, 32(3):135–141, 1997.

[117] A. Rantzer. On the Kalman–Yakubovich–Popov lemma. *System & Control Letters*, 28(1):7–10, 1996.

[118] Z. Rekasius. Suboptimal design of intentionally nonlinear controllers. *IEEE Trans. Automat. Contr.*, 9(4):380–386, 1964.

[119] B. Reznick. Some concrete aspects of Hilbert's 17th problem. In *Contemporary Mathematics*, volume 253, pages 251–272. American Mathematical Society, 2000.

[120] L. Rossignol, G. Scorletti, and V. Fromion. Filter design: a finite dimensional convex optimization approach. *Int. Journal of Robust and Nonlinear Control*, 13(14):1317–1335, 2003.

[121] W.J. Rugh and J.S. Shamma. Research on gain scheduling. *Automatica*, 36:1401–1425, 2000.

[122] H. Sandberg and B. Bernhardsson. A Bode sensitivity integral for linear time-periodic systems. *IEEE Trans. Automat. Contr.*, 50(12):2034–2039, 2005.

[123] J. Sandor and D. Williamson. Nonlinear feedback to improve the transient response of a linear servo. *IEEE Trans. Automat. Contr.*, 22(5):863–864, 1977.

[124] C. Scherer. Robust mixed control and LPV control with full block scalings. In L.E. Ghaoui and S.I. Niculescu, editors, *Advances in linear matrix inequality methods in control*. Siam, Philadelphia, 1999.

[125] C. Scherer. Relaxations for robust linear matrix inequality problems with verifications for exactness. *SIAM J. Matrix Anal. Appl.*, 27(2):365–395, 2005.

[126] C. Scherer and S. Weiland. *Lecture notes DISC course on linear matrix inequalities in control*. Dutch Institute of Systems and Control, Delft, The Netherlands, 2005.

[127] C. Scherer, P. Gahinet, and M. Chilali. Multiobjective output-feedback control via LMI optimization. *IEEE Trans. Automat. Contr.*, 42(7):896–911, 1997.

[128] C.W. Scherer. LPV control and full block multipliers. *Automatica*, 37(3): 361–375, 2001.

[129] G. Scorletti and L. El Ghaoui. Improved LMI conditions for gain scheduling and related control problems. *Int. Journal of Robust and Nonlinear Control*, 8(10):845–877, 1998.

[130] M.M. Seron and G.C. Goodwin. Sensitivity limitations in nonlinear feedback control. *System & Control Letters*, 27(4):249–254, 1996.

[131] M.M. Seron, J.H. Braslavsky, and G.C. Goodwin. *Fundamental Limitations in Filtering and Control*. Springer-Verlag, London, 1997.

[132] M.M. Seron, J.H. Braslavsky, P.V. Kokotovic, and D.Q. Mayne. Feedback limitations in nonlinear systems: from Bode integrals to cheap control. *IEEE Trans. Automat. Contr.*, 44(4):829–833, 1999.

[133] J.S. Shamma. Performance limitations in sensitivity reduction for nonlinear plants. *System & Control Letters*, 17(1):43–47, 1991.

[134] S. Skogestad and I. Postletwaite. *Multivariable feedback control - analysis and design*. John Wiley & Sons Ltd, Chichester, England, 2005.

[135] G. Stengle. A Nullstellensatz and a Positivstellensatz in semialgebraic geometry. *Mathematische Annalen*, 207:87–97, 1974.

[136] D.J. Stilwell and W.J. Rugh. Interpolation of observer state feedback controllers for gain scheduling. In *Proceedings of the American Control Conference*, volume 2, pages 1215–1219, 1998.

[137] G. Strang and T. Nguyen. *Wavelets and Filter Banks*. Wellesley-Cambridge Press, 1996.

[138] J. Sturm. Using SeDuMi 1.02, a Matlab toolbox for optimization over symmetric cones. *Optimization methods and software*, 11-12:625–653, 1999.

[139] H.K. Sung and S. Hara. Properties of sensitivity and complementary sensitivity functions in single-input single-output digital control systems. *Int. Journal of Control*, 48(6):2429 – 2439, 1988.

[140] W. Tan and A. Packard. Stability region analysis using sum of squares programming. In *Proceedings of the American Control Conference*, pages 2297–2302, 2006.

[141] Z. Tsypkin. *Relay control systems*. Cambridge University Press, 1984.

[142] V. Venkataramanan, B.M. Chen, T.H. Lee, and G. Guo. A new approach to the design of mode switching control in hard disk drive servo systems. *Control Engineering Practice*, 10(9):925–939, 2002.

[143] M.J. Vrhel, C. Lee, and M. Unser. Rapid computation of the continuous wavelet transform by oblique projections. *IEEE Trans. Signal Processing*, 45(4):891–900, 1997.

[144] J. Willems. Dissipative dynamical systems, part I: General theory. *Archive for Rational Mechanics and Analysis*, 45(5):321–351, 1972.

[145] D. Williamson. Some perspectives on techniques of non-linear compensation. *Journal A*, 19(2):61–72, 1978.

[146] B. Wu and E.A. Jonckheere. A simplified approach to Bode's theorem for continuous-time and discrete-time systems. *IEEE Trans. Automat. Contr.*, 37:1797–1802, 1992.

[147] F. Wu, X.H. Yang, A. Packard, and G. Becker. Induced L_2-norm control for LPV systems with bounded parameter variation rates. *Int. Journal of Robust and Nonlinear Control*, 6(9-10):983–998, 1996.

[148] T. Yamaguchi and H. Hirai. Control of transient response on a servosystem using mode-switching control, and its application to magnetic disk drives. *Control Engineering Practice*, 6(9):1117–1123, 1998.

[149] J. Yu and A. Sideris. H_∞ control with parametric Lyapunov functions. *System & Control Letters*, 30(2-3):57–69, 1997.

[150] Z. Yu, H. Chen, and P.-Y. Woo. Gain scheduled output feedback control based on LTI controller interpolation that preserves LPV H_∞ performance. *J. Intell. Robotics Syst.*, 40(2):183–206, 2004.

[151] L. Zaccarian, D. Nešić, and A.R. Teel. First order reset elements and the Clegg integrator revisited. In *Proceedings of the American Control Conference*, pages 563–568, Portland, OR, 2005.

[152] L. Zaccarian, D. Nešić, and A.R. Teel. Set-point stabilization of SISO linear systems using first order reset elements. In *Proceedings of the American Control Conference*, pages 5808–5809, 2007.

[153] G. Zang and P.A. Iglesias. Nonlinear extension of Bode's integral based on an information-theoretic interpretation. *System & Control Letters*, 50(1): 11–19, 2003.

[154] Y. Zheng, Y. Chait, C.V. Hollot, M. Steinbuch, and M. Norg. Experimental demonstration of reset control design. *Control Engineering Practice*, 8(2): 113–120, 2000.

[155] K. Zhou, J.C. Doyle, and K. Glover. *Robust and Optimal Control*. Prentice Hall, New Jersey, 1996.

Appendix A

Optimization over polynomials

In this appendix, the concept of sum-of-squares polynomials and the problem of checking positivity of a polynomial on a semialgebraic set are discussed briefly.

A.1 Sum-of-squares polynomials

Let the ring $\mathbb{R}[X] := \mathbb{R}[x_1, \ldots, x_n]$ denote the set of polynomials in n variables with real coefficients. These are called multivariate polynomials when $n > 1$. When $n = 1$ we speak of univariate polynomials. A *monomial* in $\mathbb{R}[X]$ is a polynomial of the form $x_1^{m_1} x_2^{m_2} \cdots x_n^{m_n}$ for certain $m_i \in \mathbb{N},\ i = 1, \ldots, n$. A polynomial $p(x) = p(x_1, ..., x_n)$ is called a sum-of-squares (SOS), if it is possible to find polynomials $f_i(x) \in \mathbb{R}[X],\ i = 1, \ldots, m$ such that

$$p(x) = \sum_{i=1}^{m} f_i^2(x). \tag{A.1}$$

From the above expression it is clear that all SOS polynomials are nonnegative for all $x \in \mathbb{R}^n$. However, $p(x) \geq 0$ for all $x \in \mathbb{R}^n$ does not necessarily imply that $p(x)$ is a SOS, as is shown by the Motzkin polynomial [119]. The equivalence between nonnegativity and SOS holds in the following cases [119]:

- univariate polynomials of any even degree,
- quadratic polynomials in any number of variables,
- quartic polynomials in two variables.

The SOS condition (A.1) for $p(x)$ is equivalent to the existence of a decomposition of the form

$$p(x) = Z^T(x)QZ(x), \tag{A.2}$$

where Q is a positive semidefinite matrix and $Z(x)$ is a properly chosen vector of monomials. Equation (A.2) can be checked by expanding $Z(x)^TQZ(x)$ and equating the coefficients of the resulting monomials to the coefficients of $p(x)$. This leads to a set of affine relations in the elements of Q. Since the statement $p(x)$ is a SOS is equivalent to $Q \geq 0$, the problem of finding a Q, which proves that $p(x)$ is indeed a SOS, can be cast as a semidefinite program (SDP) [107]. This approach is also known as the Gram matrix method. Although the condition that $p(x)$ is a SOS is stricter than nonnegativity, checking whether a polynomial is a SOS is much more computationally tractable than checking nonnegativity. From now on, $\sum[X]^2$ denotes the set of all sums-of-squares in $\mathbb{R}[X]$, i.e., $\sum[X]^2 := \{f(x) \in \mathbb{R}[X] \mid f(x) = \sum_{i=1}^m f_i^2(x), \text{ for some } f_i(x) \in \mathbb{R}[X], i = 1, \ldots, m\}$.

A.2 Checking positivity on a semialgebraic set

Consider the problem of checking whether a polynomial $f(x) \in \mathbb{R}[X]$ is nonnegative over a semialgebraic set, i.e., checking whether

$$f(x) \geq 0 \quad \text{for all } x \in \mathcal{K}, \tag{A.3}$$

where

$$\mathcal{K} := \{x \in \mathbb{R}^n \mid g_i(x) \geq 0,\ i = 1, \ldots, m,\ h_j(x) = 0,\ j = 1, \ldots, p\} \tag{A.4}$$

with $g_i(x),\ i = 1, \ldots, m$, and $h_j(x),\ j = 1, \ldots, n$ polynomials in $\mathbb{R}[X]$. This check can be performed with the Positivstellensatz [135].

Theorem A.1 *Let $f(x)$, $g_1(x) \ldots, g_m(x), h_1(x), \ldots, h_p(x)$ be polynomials in $\mathbb{R}[X]$ and let $\mathcal{K}$ be given as in* (A.4)*. Then,* (A.3) *holds if there exist (possibly an infinite number of) polynomials*
$\sigma_i(x), \sigma_{i_1,i_2}(x), \sigma_{i_1,i_2,i_3}(x), \cdots \in \sum[X]^2$ and $\lambda_j(x) \in \mathbb{R}[X]$, such that

$$f(x) = \sigma_0(x) + \sum_j \lambda_j(x)h_j(x) + \sum_i \sigma_i(x)g_i(x) + \sum_{i_1,i_2} \sigma_{i_1,i_2}(x)g_1(x)g_2(x) + \cdots \tag{A.5}$$

Given the set $\mathcal{K}$, we adopt the following assumption.

Assumption A.2 *There exists a polynomial $q \in \mathbb{R}[X]$ of the form*

$$q(x) = u_0(x) + \sum_{i=1}^m u_i(x)g_i(x), \tag{A.6}$$

where $u_0, \ldots, u_m \in \sum[X]^2$, and for which the set $\{x \in \mathbb{R}^n \mid q(x) \geq 0\}$ is compact.

If Assumption A.2 holds, Theorem A.1 is still true if (A.5) is replaced by [114]

$$f(x) = \sigma_0(x) + \sum_j \lambda_j(x) h_j(x) + \sum_i \sigma_i(x) g_i(x). \tag{A.7}$$

In this case the possibly infinite sum in (A.5) is replaced by the finite sum in (A.7). Of course, (A.7) is much easier to verify than (A.5). Assumption A.2 is true if, for instance, the set $\{x \in \mathbb{R}^n \mid g_j(x) \geq 0\}$ is compact for some $j \in \{1, \ldots, m\}$. If $x \in \mathcal{K} \Rightarrow ||x|| \leq C$ for some (known) C then one can add the redundant quadratic constraint $C^2 - ||x||^2 \geq 0$ in the definition of $\mathcal{K}$ to satisfy Assumption A.2.
Testing whether (A.5) holds is a convex problem and if the search for polynomials $\sigma_i(x), \sigma_{i_1,i_2}(x), \sigma_{i_1,i_2,i_3}(x), \ldots, \lambda_j(x)$ is restricted to polynomials of a certain order, this test is an SDP [107]. By increasing the order of the polynomials a hierarchy of convex relaxations is obtained.
In [81], an alternative set of relaxations, equivalent to the SOS ones, is developed in a dual framework. The dual of checking the nonnegativity of a polynomial over a semialgebraic set turns out to be finding a sequence of moments [81] that represent a probability measure with support in that set. To be a valid set of moments, the sequence should form a positive semidefinite moment matrix. Then, each level of relaxation fixes the size of this matrix, i.e., considers moments up a certain order, and therefore solves an SDP. This is similar to fixing the order of the polynomials appearing in the SOS relaxations.
Relaxations using the Positivstellensatz (extended Gram matrix method) are implemented in SOStools [113], while relaxations based on the dual theory of moments are used in GloptiPoly 3 [54] and Yalmip [88].

A.3 Multivariate polynomial relaxation

In this section, we elaborate on the relation between the time-domain response (4.24), repeated here for convenience as

$$y(t) = \sum_{i=0}^{n_r} y_i \lambda^{\overline{p}_i} + \sum_{i=n_r+1}^{n_r+n_c/2+1} \left(a_i 2\cos(\overline{\beta}_i \tau) + b_i 2\sin(\overline{\beta}_i \tau) \right) \lambda^{\overline{\alpha}_i}, \tag{A.8}$$

and the equivalent multivariate polynomial

$$y(t) = \sum_{i=0}^{n_r} y_i \lambda^{\overline{p}_i} + \sum_{i=n_r+1}^{n_r+n_c/2+1} \left(a_i 2 w_i(\cos(\tau), \sin(\tau)) + b_i 2 r_i(\cos(\tau), \sin(\tau)) \right) \lambda^{\overline{\alpha}_i} \tag{A.9}$$

with w_i and r_i, $i = n_r + 1, \ldots, n_r + n_c/2 + 1$ appropriate polynomial functions in two variables. First, note that (A.8) is equivalent to

$$y(t) = \sum_{i=0}^{n_r} y_i \lambda^{\overline{p}_i} + \sum_{i=n_r+1}^{n_r+n_c/2+1} \left((a+jb_i)\left(\cos(\overline{\beta}_i\tau) - j\sin(\overline{\beta}_i)\right) + (a-jb_i)\left(\cos(\overline{\beta}_i\tau) + j\sin(\overline{\beta}_i\tau)\right)\right)\lambda^{\overline{\alpha}_i}. \tag{A.10}$$

De Moivre's formula states that for any $\phi \in \mathbb{R}$ and any integer n

$$(\cos(\phi) + j\sin(\phi))^n = \cos(n\phi) + j\sin(n\phi), \tag{A.11}$$

and hence (A.10) is equal to

$$y(t) = \sum_{i=0}^{n_r} y_i \lambda^{\overline{p}_i} + \sum_{i=n_r+1}^{n_r+n_c/2+1} \left((a+jb_i)\left(\cos(\tau) + j\sin(\tau)\right)^{\overline{\beta}_i} + (a-jb_i)\left(\cos(\tau) + j\sin(\tau)\right)^{\overline{\beta}_i}\right)\lambda^{\overline{\alpha}_i}. \tag{A.12}$$

Indeed, (A.12) is a reformulation of (A.9) for appropriate polynomial functions w_i and r_i, $i = n_r + 1, \ldots, n_r + n_c/2 + 1$ in two variables.
Consider the example from Section 4.5, where $n_r = 0, n_c = 2$, $\overline{\alpha}_1 = -1$, $\overline{\alpha}_2 = -2$, $\overline{\beta}_1 = 2$ and $\overline{\beta}_2 = 4$. Let $u = \cos(\tau)$ and $v = \sin(\tau)$ so that (A.12) yields

$$\begin{aligned} y(t) &= \left((a_1 + jb_1)(u+jv)^2 + (a_1 - jb_1)(u+jv)^2\right)\lambda \\ &\quad + \left((a_2 + jb_2)(u+jv)^4 + (a_2 - jb_2)(u+jv)^4\right)\lambda^2 \\ &= 2a_1\left(u^2 - v^2\right) + 2b_1 2uv + 2a_2\left(u^4 + v^4 - 6u^2v^2\right) + 2b_1\left(4vu^3 - 4uv^3\right). \end{aligned} \tag{A.13}$$

As a consequence, for this example we obtain

$$\begin{aligned} w_1(u,v) &= u^2 - v^2, \quad r_1(u,v) = 2uv \\ w_2(u,v) &= u^4 + v^4 - 6u^2v^2, \quad r_2(u,v) = 4vu^3 - 4uv^3. \end{aligned} \tag{A.14}$$

A.4 Computation of the optimal input signal

In order to clarify the described method, the computations used in the example from Section 5.4 are presented. The system under consideration is described by the differential equation $F(t) = m\ddot{x}(t)$ where the mass m is 1 kg and the input is

the force F, constrained via $|u(t)| \leq 10$ N.
The state-space description is given by (5.26) and the interpolation constraints are $x_1(0) = 1,\ x_2(0) = x_1(t_f) = x_2(t_f) = u(t_f) = \dot{u}(t_f) = 0$. To prevent overshoot and actuator saturation the following bound constraints are imposed

$$\begin{array}{rcccr} 0 & \leq & x_1(t) & \leq & 1, \\ -10 & \leq & u(t) & \leq & 10. \end{array} \tag{A.15}$$

The right polynomial matrix fractions are

$$A_r(s) = -s^2, \quad B_r(s) = -1. \tag{A.16}$$

In order to deal with the constraints, a seventh order flat output polynomial is proposed

$$x^f(t) = x_0^f + x_1^f t + x_2^f t^2 + x_3^f t^3 + x_4^f t^4 + x_5^f t^5 + x_6^f t^6 + x_7^f t^7.$$

The interpolation constraints on the in- and output are converted into constraints on the flat output vector using the polynomial matrix fractions. Since the input and states are related to the internal state via

$$\begin{aligned} u(t) &= A_2 \frac{d^2}{dt^2} x^f(t), \\ x_1(t) &= B_0 x^f(t), \\ x_2(t) &= B_0 \frac{d}{dt} x^f(t), \end{aligned} \tag{A.17}$$

the interpolation constraints can be written as

$$\begin{aligned} x_1(0) &= B_0 x_0^f = 1, \\ x_2(0) &= B_0 x_1^f = 0, \\ x_1(t_f) &= B_0(x_0^f + x_1^f t_f + x_2^f t_f^2 + x_3^f t_f^3 + x_4^f t_f^4 + \\ &\quad x_5^f t_f^5 + x_6^f t_f^6 + x_7^f t_f^7) = 0, \\ x_2(t_f) &= B_0(x_1^f + 2x_2^f t_f + 3x_3^f t_f^2 + 4x_4^f t_f^3 + 5x_5^f t_f^4 + \\ &\quad 6x_6^f t_f^5 + 7x_7^f t_f^6) = 0, \\ u(t_f) &= A_2(2x_2^f + 6x_3^f t_f + 12x_4^f t_f^2 + 20x_5^f t_f^3 + \\ &\quad 30x_6^f t_f^4 + 42x_7^f t_f^5) = 0, \\ \dot{u}(t_f) &= A_2(6x_3^f t_f + 24x_4^f t_f^2 + 60x_5^f t_f^3 + \\ &\quad 120x_6^f t_f^4 + 210x_7^f t_f^5) = 0, \end{aligned} \tag{A.18}$$

where $A_2 = -1$ and $B_0 = -1$. The complete set of interpolation constraints is then given by

$$F x_{c\mu}^f = f, \tag{A.19}$$

with

$$F = \begin{pmatrix} B_0 & 0 & B_0 & 0 & 0 & 0 \\ 0 & B_0 & B_0 t_f & B_0 & 0 & 0 \\ 0 & 0 & B_0 t_f^2 & 2B_0 t_f & 2A_0 & 0 \\ 0 & 0 & B_0 t_f^3 & 3B_0 t_f^2 & 6A_0 t_f & 6A_0 \\ 0 & 0 & B_0 t_f^4 & 4B_0 t_f^3 & 12A_0 t_f^2 & 24A_0 t_f \\ 0 & 0 & B_0 t_f^5 & 5B_0 t_f^4 & 20A_0 t_f^3 & 60A_0 t_f^2 \\ 0 & 0 & B_0 t_f^6 & 6B_0 t_f^5 & 30A_0 t_f^4 & 120A_0 t_f^3 \\ 0 & 0 & B_0 t_f^7 & 7B_0 t_f^6 & 42A_0 t_f^5 & 210A_0 t_f^4 \end{pmatrix}^T, \tag{A.20}$$

$$x_{c\mu}^f = \begin{pmatrix} x_0^f & x_1^f & x_2^f & x_3^f & x_4^f & x_5^f & x_6^f & x_7^f \end{pmatrix}^T, \tag{A.21}$$

and

$$f = \begin{pmatrix} 1 & 0 & 0 & 0 & 0 \end{pmatrix}^T. \tag{A.22}$$

Both bound constraints (A.15) are written as the nonnegativity constraints

$$\begin{aligned} g_1(t) &= x_1(t) - y^{\min} \geq 0 \\ &= (B_0 x_0^f - y^{\min}) + B_0(x_1^f t + x_2^f t^2 + x_3^f t^3 + x_4^f t^4 + x_5^f t^5 + x_6^f t^6 + x_7^f t^7) \geq 0 \\ g_2(t) &= -x_1(t) + y^{\max} \geq 0 \\ &= (y^{\max} - B_0 x_0^f) - B_0(x_1^f t + x_2^f t^2 + x_3^f t^3 + x_4^f t^4 + x_5^f t^5 + x_6^f t^6 + x_7^f t^7) \geq 0 \\ g_3(t) &= u(t) - u^{\min} \geq 0 \\ &= (2A_2 x_2^f - u^{\min}) + A_2(6x_3^f t_f + 12x_4^f t_f^2 + 20x_5^f t_f^3 + 30x_6^f t_f^4 + 42x_7^f t_f^5) \geq 0 \\ g_4(t) &= u^{\max} - u(t) \geq 0 \\ &= (u^{\min} - 2A_2 x_2^f) - A_2(6x_3^f t_f + 12x_4^f t_f^2 + 20x_5^f t_f^3 + 30x_6^f t_f^4 + 42x_7^f t_f^5) \geq 0, \end{aligned} \tag{A.23}$$

where $y^{\min} = 0$, $y^{\max} = 1$, $u^{\min} = -10$ and $u^{\max} = 10$. Coefficients $x_0^f, \ldots, x_7^f$ such that e.g. $g_1(t) \geq 0$ can be computed via Lemma 4.2 as follows. Find symmetric matrices $G_1 = G_1^T$, $J_1 = J_1^T$ of dimension 4 and the coefficients $x_0^f \ldots x_7^f$ solving

the LMIs

$$\begin{aligned}
G_1 &\succeq 0 \\
J_1 &\succeq 0 \\
B_0 x_0^f - y_{\min} &= \operatorname{trace} G_1 H_{-1}^4 + \operatorname{trace} R_1 (t_f H_0^4 - H_{-1}^4) \\
B_0 x_1^f &= \operatorname{trace} G_1 H_0^4 + \operatorname{trace} R_1 (t_f H_1^4 - H_0^4) \\
B_0 x_2^f &= \operatorname{trace} G_1 H_1^4 + \operatorname{trace} R_1 (t_f H_2^4 - H_1^4) \\
B_0 x_3^f &= \operatorname{trace} G_1 H_2^4 + \operatorname{trace} R_1 (t_f H_3^4 - H_2^4) \\
B_0 x_4^f &= \operatorname{trace} G_1 H_3^4 + \operatorname{trace} R_1 (t_f H_4^4 - H_3^4) \\
B_0 x_5^f &= \operatorname{trace} G_1 H_4^4 + \operatorname{trace} R_1 (t_f H_5^4 - H_4^4) \\
B_0 x_6^f &= \operatorname{trace} G_1 H_5^4 + \operatorname{trace} R_1 (t_f H_6^4 - H_5^4) \\
B_0 x_7^f &= \operatorname{trace} G_1 H_6^4 + \operatorname{trace} R_1 (t_f H_7^4 - H_6^4).
\end{aligned} \tag{A.24}$$

LMIs corresponding to the other inequalities in (A.23) should be added together with the linear matrix equality (A.19). Solving the complete set of LMIs while performing bisection on t_f results in the coefficients

$$x_{c\mu}^f = \begin{bmatrix} -1.00 & 0 & 4.98 & -3.20 & 34.3 & -132 & 162 & -64.8 \end{bmatrix} \tag{A.25}$$

resulting in the final time $t_f = 0.7638$ and input signal

$$u(t) = -9.95 + 19.2t - 412t^2 + 0.266 \cdot 10^4 t^3 - 0.486 \cdot 10^4 t^4 + 0.272 \cdot 10^4 t^5. \tag{A.26}$$

Appendix B

LPV synthesis

This appendix describes the method that is used in Section 11.4 to design the LPV controller. Furthermore, the design of a weighting function that can be used to specify closed-loop overshoot requirements is discussed.

B.1 The one parameter case

The method that is reviewed in this appendix is proposed in [31] and it is based on the full-block multiplier approach from [124]. In case an LPV system with only one parameter is considered, a non-conservative multiplier structure is proposed in [31] based on an extension of the Kalman-Yakubovich-Popov (KYP) Lemma [117]. This classical lemma allows to replace an infinite number of inequalities by one matrix inequality through the introduction of an additional multiplier. This is in fact the same way the full-block S-procedure [124] operates. Indeed, the full-block S-procedure for one repeated complex block leads to a complete treatment of variants of the KYP lemma, both for continuous as well as discrete-time systems [125]. Another line of research, [70], [69], and [120] obtained extensions of the KYP lemma independently. In [120], the KYP lemma is extended to the case of LFTs of a real (positive) parameter δ.

Lemma B.1 ([120]) *Let $M(\delta)$ be a rational matrix function of δ, well-posed on $[0,1]$, defined by its LFT realization*

$$M(\delta) = \mathcal{F}_u\left(\left[\begin{array}{cc} A & B \\ C & D \end{array}\right], \delta I\right), \tag{B.1}$$

and let X be a matrix. Then the condition

$$M(\delta)^T X M(\delta) \prec 0 \quad \forall\ \delta \in [0,1], \tag{B.2}$$

holds if and only if there exists a symmetric matrix $S = S^T \succeq 0$ *and a skew-symmetric matrix* $G = -G^T$ *such that*

$$\begin{bmatrix} C^T \\ D^T \end{bmatrix}^T X \begin{bmatrix} C & D \end{bmatrix} + \begin{bmatrix} A^T(S-G) + (S+G)A - 2S & (S+G)B \\ B^T(S-G) & 0 \end{bmatrix} \prec 0. \tag{B.3}$$

This lemma is in fact nothing more than a specialized version of the full-block S-procedure, and is used in [31] to reveal that a rational dependent parameter LMI with rational decision variables can be equivalently recast as a finite number of parameter independent LMIs in case there is only one parameter. As an example, consider the LMI

$$\begin{bmatrix} X(\delta) & I \\ I & Y(\delta) \end{bmatrix} \succ 0 \quad \forall \delta \in \boldsymbol{\delta}, \tag{B.4}$$

where the decision variables $X(\delta)$ and $Y(\delta)$ are chosen to be rational of order 2:

$$X(\delta) = \frac{X_0 + X_1\delta + X_2\delta^2}{1 + d_1\delta + d_2\delta^2}, \quad Y(\delta) = \frac{Y_0 + Y_1\delta + Y_2\delta^2}{1 + d_1\delta + d_2\delta^2}. \tag{B.5}$$

Obviously, (B.4) is equivalent to

$$\begin{bmatrix} -X(\delta) & -2I \\ 0 & -Y(\delta) \end{bmatrix} + \begin{bmatrix} -X(\delta) & -2I \\ 0 & -Y(\delta) \end{bmatrix}^T \prec 0 \quad \forall \delta \in \boldsymbol{\delta}, \tag{B.6}$$

and using (B.5) we obtain

$$\begin{bmatrix} \frac{-X_0 - X_1\delta - X_2\delta^2}{1+d_1\delta+d_2\delta^2} & -2I \\ 0 & \frac{-Y_0 - Y_1\delta - Y_2\delta^2}{1+d_1\delta+d_2\delta^2} \end{bmatrix} + \begin{bmatrix} \frac{-X_0 - X_1\delta - X_2\delta^2}{1+d_1\delta+d_2\delta^2} & -2I \\ 0 & \frac{-Y_0 - Y_1\delta - Y_2\delta^2}{1+d_1\delta+d_2\delta^2} \end{bmatrix}^T \prec 0 \quad \forall \delta \in \boldsymbol{\delta}. \tag{B.7}$$

If $X(\delta)$ and $Y(\delta)$ are well-posed on $\boldsymbol{\delta}$ then (B.7) is equivalent to

$$K + K^T \prec 0 \quad \forall \delta \in \boldsymbol{\delta}, \tag{B.8}$$

with

$$K = \begin{bmatrix} \frac{-X_0 - X_1\delta - X_2\delta^2}{1+c_1\delta+c_2\delta^2} & \frac{-2I - 2d_1 I\delta - 2d_2 I\delta^2}{1+c_1\delta+c_2\delta^2} \\ 0 & \frac{-Y_0 - Y_1\delta - Y_2\delta^2}{1+c_1\delta+c_2\delta^2} \end{bmatrix},$$

where c_1 and c_2 are real scalars such that $1 + c_1\delta + c_2\delta^2 \neq 0$ for any $\delta \in \boldsymbol{\delta}$. It is easily seen that (B.8) equals

$$L^T N + N^T L \prec 0 \quad \forall \delta \in \boldsymbol{\delta} \tag{B.9}$$

where

$$L = \begin{bmatrix} -X_2 & 0 \\ -X_1 & 0 \\ -X_0 & 0 \\ -2d_2 I & -Y_2 \\ -2d_1 I & -Y_1 \\ -2I & -Y_0 \end{bmatrix}, \quad N = \begin{bmatrix} \frac{\delta^2}{1+c_1\delta+c_2\delta^2} & 0 \\ \frac{\delta}{1+c_1\delta+c_2\delta^2} & 0 \\ \frac{1}{1+c_1\delta+c_2\delta^2} & 0 \\ 0 & \frac{\delta^2}{1+c_1\delta+c_2\delta^2} \\ 0 & \frac{\delta}{1+c_1\delta+c_2\delta^2} \\ 0 & \frac{1}{1+c_1\delta+c_2\delta^2} \end{bmatrix},$$

or

$$M(\delta)^T X M(\delta) \prec 0 \quad \forall \delta \in \boldsymbol{\delta}, \tag{B.10}$$

where

$$M(\delta) = \begin{bmatrix} I \\ \hline \frac{\delta^2}{1+c_1\delta+c_2\delta^2} & 0 \\ \frac{\delta}{1+c_1\delta+c_2\delta^2} & 0 \\ \frac{1}{1+c_1\delta+c_2\delta^2} & 0 \\ 0 & \frac{\delta^2}{1+c_1\delta+c_2\delta^2} \\ 0 & \frac{\delta}{1+c_1\delta+c_2\delta^2} \\ 0 & \frac{1}{1+c_1\delta+c_2\delta^2} \end{bmatrix}, \quad X = \begin{bmatrix} L^T & 0 \\ 0 & L^T \end{bmatrix}.$$

There remains one issue, namely the well-posedness of $X(\delta)$ and $Y(\delta)$, which constitutes the equivalence between (B.7) and (B.8). Well-posedness in this case means that $1 + d_1\delta + d_2\delta^2 \neq 0$ for any $\delta \in \boldsymbol{\delta}$. This is guaranteed if and only if

$$\frac{1 + d_1\delta + d_2\delta^2}{1 + c_1\delta + c_2\delta^2} > 0 \quad \forall \delta \in \boldsymbol{\delta}, \tag{B.11}$$

which is equivalent to

$$\begin{bmatrix} \star \\ \star \\ \star \\ \star \end{bmatrix}^T \begin{bmatrix} 0 & -d_2 I & -d_1 I & -I \\ -d_2 I & 0 & 0 & 0 \\ -d_1 I & 0 & 0 & 0 \\ -I & 0 & 0 & 0 \end{bmatrix} \begin{bmatrix} 1 \\ \frac{\delta^2}{1+c_1\delta+c_2\delta^2} \\ \frac{\delta}{1+c_1\delta+c_2\delta^2} \\ \frac{1}{1+c_1\delta+c_2\delta^2} \end{bmatrix} \prec 0 \quad \forall \delta \in \boldsymbol{\delta}. \tag{B.12}$$

The full-block S-procedure [124] can now readily be applied to (B.9) and (B.12). Furthermore, if we restrict the parameter set to be $\boldsymbol{\delta} = [0, 1]$ we know from Lemma B.1 that the full-block S-procedure is exact when the multiplier

$$P = \begin{bmatrix} Q & S \\ S^T & R \end{bmatrix} = \begin{bmatrix} -2S & (S+G) \\ (S+G)^T & 0 \end{bmatrix} \tag{B.13}$$

is used, and hence the decision variables $X_0, X_1, X_2, Y_0, Y_1, Y_2, d_1$, and d_2 can be computed by standard LMI solvers. In a similar fashion other LMIs with rational parameter dependent decision variables can be rewritten in the form (B.10). In [31], the above mentioned approach is used to yield a complete solution to the one parameter LPV control design problem with rational decision variables as stated in the following theorem.

Theorem B.2 ([31]) *Define*

$$\mathcal{X}(\theta)=\frac{\sum_{i=0}^{N}\theta^i\mathcal{X}_i}{1+\sum_{i=1}^{N}\theta^i d_i},\quad \mathcal{Y}(\theta)=\frac{\sum_{i=0}^{N}\theta^i\mathcal{Y}_i}{1+\sum_{i=1}^{N}\theta^i d_i},\quad \mathcal{V}(\theta)=\frac{\sum_{i=0}^{N}\theta^i\mathcal{V}_i}{1+\sum_{i=1}^{N}\theta^i d_i}, \tag{B.14}$$

where $\mathcal{X}_i=\mathcal{X}_i^T\in\mathbb{R}^{n\times n}$, $\mathcal{Y}_i=\mathcal{Y}_i^T\in\mathbb{R}^{n\times n}$, $\mathcal{V}_i\in\mathbb{R}^{(n+n_u)\times(n+n_y)}$, $d\in\mathbb{R}$, *and where*

$$\mathcal{V}(\theta)=\begin{bmatrix}\mathcal{A}(\theta) & \mathcal{B}(\theta)\\ \mathcal{C}(\theta) & \mathcal{D}(\theta)\end{bmatrix}, \tag{B.15}$$

with $\mathcal{A}_i\in\mathbb{R}^{n\times n}$, $\mathcal{B}_i\in\mathbb{R}^{n\times n_y}$, $\mathcal{C}_i\in\mathbb{R}^{n_u\times n}$, *and* $\mathcal{D}_i\in\mathbb{R}^{n_u\times n_y}$.
Given N, *there exist decision variables* $\mathcal{X}(\theta)$, $\mathcal{Y}(\theta)$, *and* $\mathcal{V}(\theta)$, *well-posed on* $[0,1]$, *such that for any* $\theta\in[0,1]$ *the inequalities*

$$\begin{bmatrix}\mathcal{X}(\theta) & I\\ I & \mathcal{Y}(\theta)\end{bmatrix}\succ 0 \tag{B.16}$$

$$\left[\begin{array}{cccc}
\begin{array}{c}A(\theta)\mathcal{X}(\theta)+\mathcal{X}(\theta)A(\theta)^T+\\ B(\theta)\mathcal{C}(\theta)+(B(\theta)\mathcal{C}(\theta)^T\end{array} & \star & \star & \star\\ \hline
\begin{array}{c}\mathcal{A}(\theta)+\\ (A(\theta)+B(\theta)\mathcal{D}(\theta)C(\theta))^T\end{array} & \begin{array}{c}A(\theta)^T\mathcal{Y}(\theta)+\mathcal{Y}(\theta)A(\theta)+\\ \mathcal{B}(\theta)C(\theta)+(\mathcal{B}(\theta)C(\theta))^T\end{array} & \star & \star\\ \hline
(B_w(\theta)+B(\theta)\mathcal{D}(\theta)D_w(\theta))^T & (\mathcal{Y}(\theta)B_w(\theta)+\mathcal{B}(\theta)D_w(\theta))^T & -\gamma I & \star\\ \hline
\begin{array}{c}C_z(\theta)\mathcal{X}(\theta)+\\ D_u(\theta)\mathcal{C}(\theta)\end{array} & \begin{array}{c}C_z(\theta)+\\ D_u(\theta)\mathcal{D}(\theta)C(\theta)\end{array} & \begin{array}{c}D_w(\theta)+\\ D_u(\theta)\mathcal{D}(\theta)D_w(\theta)\end{array} & -\gamma I
\end{array}\right]\prec 0 \tag{B.17}$$

are satisfied, if and only if there exist $\mathcal{X}_i$, $\mathcal{Y}_i$, $\mathcal{V}_i$, *and* d_i, $i=1,\dots,N$ *such that*

(i) there exist $S_0=S_0^T\succ 0$ *and* $G_0=-G_0^T$ *such that*

$$\begin{aligned}&\begin{bmatrix}C_{\Omega_0}^T\\ D_{\Omega_0}^T\end{bmatrix}^T\begin{bmatrix}0 & -\mathcal{W}\\ -\mathcal{W}^T & 0\end{bmatrix}\begin{bmatrix}C_{\Omega_0} & D_{\Omega_0}\end{bmatrix}\\ &+\begin{bmatrix}A_{\Omega_0}^T(S_0-G_0)+(S_0+G_0)A_{\Omega_0}-2S_0 & (S_0+G_0)B_{\Omega_0}\\ B_{\Omega_0}^T(S_0-G_0) & 0\end{bmatrix}\prec 0,\end{aligned} \tag{B.18}$$

with

$$\mathcal{W}:=\begin{bmatrix}\mathcal{R}_{\mathcal{X}} & 2\mathcal{R}_{d,n}\\ 0 & \mathcal{R}_{\mathcal{Y}}\end{bmatrix}$$

$$\mathcal{F}_u\left(\left[\begin{array}{c|c}A_{\Omega_0} & B_{\Omega_0}\\ \hline C_{\Omega_0} & D_{\Omega_0}\end{array}\right],\theta I\right):=\left[\begin{array}{cc}I_{2n} & \\ \hline \mathcal{F}_u(J_n(c_i),\theta I) & 0\\ 0 & \mathcal{F}_u(J_n(c_i),\theta I)\end{array}\right]. \tag{B.19}$$

(ii) there exist $S=S^T\succ 0$ *and* $G=-G^T$ *such that*

$$\begin{aligned}&\begin{bmatrix}C_{\Omega}^T\\ D_{\Omega}^T\end{bmatrix}^T\begin{bmatrix}0 & \mathcal{Z}(\gamma)\\ \mathcal{Z}(\gamma)^T & 0\end{bmatrix}\begin{bmatrix}C_{\Omega} & D_{\Omega}\end{bmatrix}\\ &+\begin{bmatrix}A_{\Omega}^T(S-G)+(S+G)A_{\Omega}-2S & (S+G)B_{\Omega}\\ B_{\Omega}^T(S-G) & 0\end{bmatrix}\prec 0,\end{aligned} \tag{B.20}$$

with

$$\mathcal{Z}(\gamma) = \left[\begin{array}{ccccc} \mathcal{R}_{\mathcal{V}} & 0 & 0 & 0 & 0 \\ \hline 0 & \mathcal{R}_{\mathcal{X}} & \mathcal{R}_{d,n} & 0 & 0 \\ 0 & 0 & \mathcal{R}_{\mathcal{Y}} & 0 & 0 \\ \hline 0 & \mathcal{R}_{d,n} & 0 & 0 & 0 \\ 0 & 0 & 0 & \mathcal{R}_{d,n_w} & 0 \\ 0 & 0 & 0 & \gamma\mathcal{R}_{d,n_w} & 0 \\ 0 & 0 & 0 & 0 & \gamma\mathcal{R}_{d,n_z} \end{array}\right], \tag{B.21}$$

and with

$$\mathcal{F}_u\left(\left[\begin{array}{c|c} A_\Omega & B_\Omega \\ \hline C_\Omega & D_\Omega \end{array}\right], \theta I\right) := \left[\begin{array}{c} F_1(\theta)^T \\ F_2(\theta)F_3(\theta) \end{array}\right], \tag{B.22}$$

where

$$\begin{aligned} F_1(\theta) &= \left[\begin{array}{cc|cc|cccc} 0 & B(\theta) & A(\theta) & 0 & 0 & 0 & 0 & 0 \\ I_n & 0 & 0 & A(\theta)^T & 0 & 0 & 0 & 0 \\ 0 & 0 & 0 & B_w(\theta)^T & B_w(\theta)^T & 0 & -\frac{1}{2}I_{n_w} & 0 \\ 0 & D_z(\theta) & C_z(\theta) & 0 & 0 & D_{zw}(\theta) & 0 & -\frac{1}{2}I_{n_z} \end{array}\right] \\ F_2(\theta) &= \left[\begin{array}{c|cccc} \mathcal{F}_u\left(J_{n+n_y}(c_i), \theta I\right) & 0 & 0 & 0 & 0 \\ 0 & \mathcal{F}_u(J_n(c_i), \theta I) & 0 & 0 & 0 \\ 0 & 0 & \mathcal{F}_u(J_n(c_i), \theta I) & 0 & 0 \\ 0 & 0 & 0 & \mathcal{F}_u(J_n(c_i), \theta I) & 0 \\ 0 & 0 & 0 & 0 & \mathcal{F}_u(J_n(c_i), \theta I) \end{array}\right] \\ F_3(\theta) &= \left[\begin{array}{cccc} I_n & 0 & 0 & 0 \\ 0 & C(\theta) & D_w(\theta) & 0 \\ & & I_{n+n+n_w+n_z} & \end{array}\right]. \end{aligned} \tag{B.23}$$

The state-space representation of a parameter dependent controller is obtained with

$$\begin{aligned} \left[\begin{array}{cc} A_k(\theta) & B_K(\theta) \\ C_K(\theta) & D_K(\theta) \end{array}\right] = \left[\begin{array}{ccc} L(\theta) & -J(\theta) & 0 \\ 0 & 0 & I_{n_u} \end{array}\right] \times \ldots \\ \left(\left[\begin{array}{cc} I_n & 0 \\ 0 & B(\theta) \\ 0 & I_n \end{array}\right] \mathcal{V}(\theta) \left[\begin{array}{cc} \mathcal{X}(\theta)^{-1} & 0 \\ -C(\theta) & I_{n_y} \end{array}\right] + \left[\begin{array}{cc} 0 & 0 \\ A(\theta) & 0 \\ 0 & 0 \end{array}\right]\right), \end{aligned} \tag{B.24}$$

where

$$\left[\begin{array}{cc} L(\theta) & -J(\theta) \end{array}\right] = \mathcal{F}_u\left(I_n, \left(\left[\begin{array}{c} I_n \\ I_n \end{array}\right] \mathcal{X}(\theta) \left[\begin{array}{cc} I_n & \mathcal{Y}(\theta) \end{array}\right] \left[\begin{array}{ccc} I_n & 0 & 0 \\ 0 & -I_n & I_n \end{array}\right]\right)\right). \tag{B.25}$$

This theorem can be used to synthesize an LPV controller with the least possible conservatism. The only conservatism in this approach is the fact that the decision

variables are restricted to be rational functions. However, this conservatism can be arbitrarily reduced by increasing the approximation order at the cost of a high complexity controller.

B.2 Weighting function describing overshoot

In this appendix, we discuss a method to arrive at weighting functions that can be used to specify overshoot requirements on a closed-loop system. Consider the second order closed-loop system

$$T(s) = \frac{\omega_n^2}{s^2 + 2\zeta\omega_n s + \omega_n^2}, \tag{B.26}$$

where ω_n denotes the natural frequency and ζ is the damping coefficient. The magnitude of the frequency response of this system is given by

$$|T(j\omega)| = \frac{\omega_n^2}{\sqrt{(\omega_n^2 - \omega^2)^2 + (2\zeta\omega_n\omega)^2}} = \frac{1}{\sqrt{(1-r^2)^2 + (2\zeta r)^2}}, \tag{B.27}$$

where $r := \frac{\omega}{\omega_n}$. The value of r where the maximum of the magnitude occurs can be obtained by differentiation, which yields

$$\frac{d}{dr}\left(\frac{1}{\sqrt{(1-r^2)^2 + (2\zeta r)^2}}\right) = 0 \Rightarrow r_{\text{peak}} = \sqrt{1-2\zeta^2}. \tag{B.28}$$

This value is only defined for $-\frac{1}{2}\sqrt{2} \leq \zeta \leq \frac{1}{2}\sqrt{2}$. The corresponding value of the magnitude is then given by

$$||T||_\infty = \frac{1}{2\zeta\sqrt{1-\zeta^2}}. \tag{B.29}$$

Equation (B.29) expresses the $\mathcal{H}_\infty$ norm of the transfer function of a second order system in the form (B.26) as a function of the damping coefficient ζ when $|\zeta| \leq \frac{1}{2}\sqrt{2}$.
The overshoot of system (B.26) in the time-domain as a consequence of a unit step input can also be expressed as a function of the damping coefficient as follows. The step response (for $0 \leq \zeta < 1$) is given by

$$y_s(t) = 1 - \frac{e^{-\zeta\omega_n t}}{\sqrt{1-\zeta^2}} \cos\left(\omega_n t\sqrt{1-\zeta^2} - \arcsin\zeta\right). \tag{B.30}$$

The time t_{peak} where the maximum overshoot occurs can be obtained by differentiating this expression, which yields

$$\begin{aligned} \frac{d}{dt}y_s(t) =& \frac{\omega_n}{\sqrt{1-\zeta^2}} e^{-\zeta\omega_n t} \sin\left(\omega_n t\sqrt{1-\zeta^2}\right) = 0 \Rightarrow \\ & \sqrt{1-\zeta^2}\omega_n t = \pi \Rightarrow t_{\text{peak}} = \frac{\pi}{\omega_n\sqrt{1-\zeta^2}}, \end{aligned} \tag{B.31}$$

and hence the maximum overshoot $e_{\max}$ is given by

$$e_{\max}(\zeta) = y_s(t_{\text{peak}}) - 1 = e^{-\frac{\zeta\pi}{\sqrt{1-\zeta^2}}}. \tag{B.32}$$

Combining equation (B.29) and (B.32) yields

$$e_{\max}(||T||_\infty) = e^{-||T||_\infty \pi(1-\sqrt{1-\frac{1}{||T||_\infty^2}})}, \tag{B.33}$$

which expresses the overshoot in the time-domain as a function of the $\mathcal{H}_\infty$ norm of the transfer function when $|\zeta| \leq \frac{1}{2}\sqrt{2}$. Similarly, the following holds as well

$$||T||_\infty = -\frac{\ln(e_{\max})^2 + \pi^2}{2\pi \ln(e_{\max})} = \frac{\ln(e_{\max})^2 + \pi^2}{2\pi \ln(\frac{1}{e_{\max}})}. \tag{B.34}$$

This relation is used in [64] and also provides a good estimate when the system is not a pure second order one, but when it is of a higher order where the lowest frequent pole pair is dominant.
Relation (B.34) indicates that by bounding the $\mathcal{H}_\infty$ norm of the closed-loop transfer function, the percentage overshoot can directly be controlled. However, since (B.34) is only valid for $|\zeta| \leq \frac{1}{2}\sqrt{2}$, the minimal overshoot that can be guaranteed by forcing that $||T||_\infty \leq 1$ is 4.3%. Since $|T(j\omega)|_{\max}$ always appears below the crossover frequency ω_c, the complementary sensitivity function needs to be bounded in the interval $\omega \in [0, \omega_c]$ to be able to control the percentage overshoot.

Appendix C

Real-time spectral analysis

In this appendix, the real-time spectral analysis algorithm that is used in Chapter 12 is discussed. To obtain the frequency spectrum of a measured signal various methods are available, of which the Fourier transform is probably the most widely used. The Fourier transform (FT) [37] provides a way to transform a time signal into the frequency domain by measuring the similarity between the original time-domain signal and an (oscillating) analyzing shape. Unfortunately, the FT offers only the global frequency content of the signal without any time information. An adapted version of the FT, called the short time Fourier transform (STFT) [137], is able to retrieve both frequency and time information of the signal $x(t)$ and is given by

$$X_{STFT}(\tau, f_a) = \int_{-\infty}^{\infty} x(t)g(t-\tau)e^{-j2\pi f_a t}dt. \tag{C.1}$$

The STFT calculates the Fourier coefficient X_{STFT} at time τ corresponding to the analysis frequency f_a. This is done by the convolution of the analyzing shape $e^{-j2\pi f_a t}$ with a windowed part of the original signal, where the window $g(t)$ shifts along the time axis using the translation parameter τ. By calculating the Fourier coefficients for various values of τ and f_a, a time-frequency spectrum is obtained. The major disadvantage of the STFT, however, is that is has a fixed resolution, i.e., a multiresolution spectrum cannot be obtained by this transform. The fixed resolution that is characteristic for the short time Fourier transform is due to the fact that the same constant window $g(t)$ is used for all frequencies f_a. The wavelet transform [37] was developed as an alternative approach to the short time Fourier transform to make a multiresolution analysis possible.

C.1 Wavelet analysis

Wavelet analysis is done in a similar way as the short time Fourier transform (STFT) in the sense that the transform is determined by measuring the similarity between a windowed part of the original time-domain signal, and an analyzing shape. The continuous wavelet transform (CWT) of a signal $x(t)$ is defined as [37]

$$X_{WT}(\tau, s) = \int_{-\infty}^{\infty} \frac{1}{\sqrt{|s|}} W\left(\frac{t-\tau}{s}\right) x(t)\, dt, \tag{C.2}$$

where X_{WT} is the wavelet coefficient at time τ corresponding to the scale s, $W(t)$ is the analyzing function (or *wavelet*), τ is the translation parameter that specifies the location of the wavelet in time, and s is the scale parameter. This scale parameter is similar to the analysis frequency f_a in the STFT. However, in wavelet theory it is common to talk about scales instead of frequencies. The wavelets are normalized by the factor $1/\sqrt{|s|}$ such that they have constant energy at all scales s, and they comprise both the analyzing shape as well as the window shape. The Morlet wavelet [37] for instance is defined as

$$W_m(t) = g(t)e^{-j2\pi f_c t}, \quad g(t) = e^{\frac{t^2}{f_b}}, \tag{C.3}$$

and uses the same analyzing shape as the STFT and a Gaussian window $g(t)$. The parameters f_c and f_b are known as the center frequency and the bandwidth, respectively, and can be used to shape the wavelet. Whereas the STFT is characterized by a constant window $g(t)$ for all frequencies, the wavelet transform features a frequency dependent window via scale parameter s. Hence, by varying s not only the central analysis frequency $f_a = f_c/s$, but also the effective window width is changed. This is depicted in Figure C.1 for two different scales s. The scale s is inversely proportional to the central analysis frequency. This implies that a large scale corresponds to a low analysis frequency and a wide window, resulting in a high frequency resolution and a low time resolution for that frequency. Small scales correspond to high frequency component analysis and shorter windows, resulting in a high time resolution with low frequency resolution for those components. Therefore, if the scale s and the the location of the wavelet in time τ are varied, the set of corresponding wavelet coefficients indeed form a multiresolution spectrum, where the frequency resolution Δf is proportional to the analysis frequency f_a.
Any desired frequency resolution can be achieved by designing a suitable wavelet. However, due to the Heisenberg uncertainty principle [37], in order to obtain a good time resolution, the frequency resolution should be chosen as low as the application allows. The shape of the wavelet determines the achieved time and frequency resolution, and a good wavelet design will provide a time-frequency resolution that comes close to the actual limit imposed by the Heisenberg inequality. Most experimentally obtained signals are discrete rather than continuous in time.

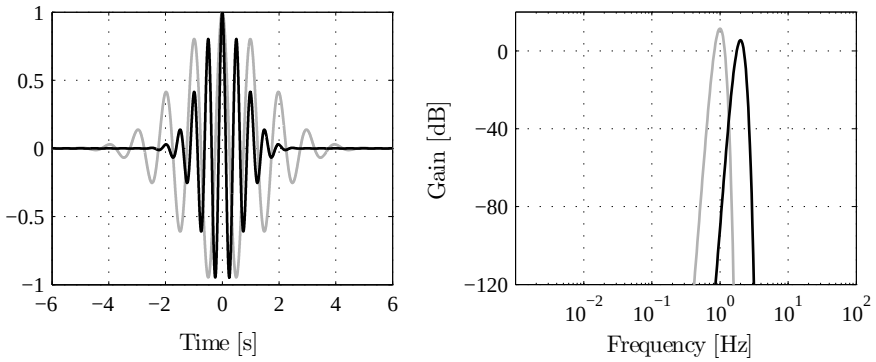

(a) (b)

Figure C.1: The Morlet wavelet ($f_c = 3$ and $f_b = -0.5$) with scales $s = 3$ ($f_a = 1$ Hz)(grey) and $s = 1.5$ ($f_a = 2$ Hz) (black) both represented in the time-domain (a) as well as in the frequency domain (b).

The continuous wavelet transform (C.2) cannot be used to analyze such discrete-time signals. A standard method to perform wavelet analysis for discrete-time signals is the discrete wavelet transform (DWT) [137]. A major drawback of the DWT is that not all frequency resolutions can be achieved. In an attempt to stretch the limit on the achievable frequency resolution that can be obtained by the DWT, wavelet packet decompositions (WPD) [137] were developed. Although any frequency resolution can be achieved, the WPD results in a time-frequency analysis with a fixed time and frequency resolution (similar to the short time Fourier transform), which is also not desirable. In the next section, we propose an adaptation to the CWT such that it can be used for real-time spectral analysis of a measured discrete time signal without the disadvantages that are inherent to the DWT and the WPD.

C.2 Real-time spectral analysis

The continuous wavelet transform (C.2) is the most suitable alternative for performing a time-frequency analysis for a certain frequency (or scale). By varying the location of the wavelet in time (τ) and the scale (s), the CWT results in a multiresolution spectrum with a constant relative frequency resolution and where any desired frequency resolution can be achieved. However, the continuous wavelet transform (C.2) cannot directly be applied to compute the current spectrum of a measured signal, and therefore the CWT has to be adapted as discussed next.

C.2.1 Implementation adaptations

Since the goal of the proposed control method is to minimize the amplitude of the vertical velocity v of the AVIS (see Section 12.1.1), the normalizing factor of the wavelet is changed to $\frac{1}{|s|}$. This way, disturbances of different frequencies, but with equal amplitudes, all result in an equal magnitude when they are transformed.
Secondly, the CWT is only defined for continuous signals. The signals that we consider in this application are not continuous in time, but sampled with sample time ΔT. To arrive at a transform which is able to handle such discrete-time signals $x[k]$, the wavelet transform has to be discretized which can be done by basically two methods. The first method approximates the continuous wavelet $W(t)$ by another continuous function that allows an infinite impulse response (IIR) filter representation [90]. The IIR filter can then be used to process the signal $x[k]$. A drawback of this method is that it is not straightforward to obtain an approximation of the wavelet $W(t)$ that allows an IIR representation. The second method approximates the continuous wavelet transform by a FIR filter implementation via truncation and sampling of the continuous wavelet [143]. The method we propose is in the spirit of [143], but differs with respect to the implementation. To arrive at a FIR filter implementation, the integral (C.2) is approximated by the Riemann sum

$$X_{WT}^{a}(\tau, s) = \sum_{k=-\infty}^{\infty} \frac{1}{|s|} W\left(\frac{k\Delta T - \tau}{s}\right) x[k]\, \Delta T, \tag{C.4}$$

where $X_{WT}^{a}(\tau, s)$ is the wavelet coefficient corresponding to time τ and scale s. In practical applications, the discrete-time signals $x[k]$ are not infinitely long but of finite length with a total measurement time T, resulting in a discrete signal $x[k],\ k = 0, \ldots, N$ with $N = \frac{T}{\Delta T}$ samples. Therefore, the infinite sum in (C.4) should be replaced by a finite sum over $k=0$ to $k=N$. For values of τ near 0 and $N\Delta T$, the wavelet coefficients will be distorted due to leakage as a consequence of the non-smoothness of the corresponding window, see Figure C.2(a) for an illustration when τ is close to $N\Delta T$. A third adaptation is related to the desired real-time implementation of the transform (C.4). Since in (C.4) the wavelet is centered around time τ, both past as well as future data with respect to time τ should be available to compute $X_{WT}^{a}(\tau, s)$. In a real-time implementation this future data is not available if $\tau = t_c$, where t_c denotes the current time. If this future data is taken to be zero, the same problem as illustrated in Figure C.2(a) arises, resulting in distortions of the spectrum due to leakage. To prevent this leakage, the window of the wavelet should be zero at time t_c as depicted in Figure C.2(b). This is only possible if a wavelet W_c is used that has compact support in the time-domain (i.e., its domain is finite). From Figure C.2(b) it is clear that this distortion free method to compute $X_{WT}^{a}(t_c, s)$ is equivalent to computing $X_{WT}^{a}\left(t_c - \frac{1}{2}N_{W_c}(s), s\right)$, where $N_{W_c}(s)$ is the length of the compact domain of wavelet W_c (i.e., the length of the used window). Hence, the price we pay for a distortion free approximation of the wavelet coefficient is the introduction of delay. Indeed, to ensure causality and a distortion free spectrum, the wavelet W_c

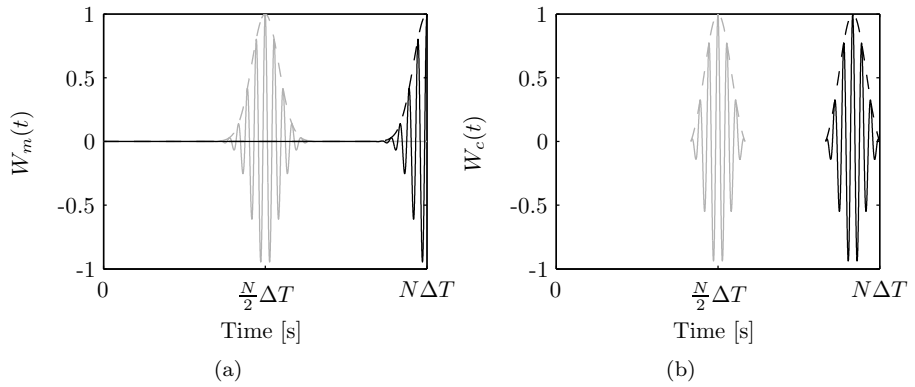

Figure C.2: Wavelets (solid) and corresponding windows (dashed) for different values of τ. (a) Morlet wavelet $W_m(t-\tau)$ for $\tau = N/2$ (grey) and $\tau = N$ (black), (b) wavelet $W_c(t-\tau)$ with compact support for $\tau = N/2$ (grey) and $\tau = N$ (black).

is centered around time $\tau - \frac{1}{2}N_{W_c}(s)$, resulting in the delayed approximation

$$X_{WT}^{da}(\tau, s) = \sum_{k=\lfloor \frac{\tau - N_{W_c}(s)}{\Delta T} \rfloor}^{\frac{\tau}{\Delta T}-1} W_c\left(\frac{k\Delta T - \left(\tau - \frac{1}{2}N_{W_c}(s)\right)}{s}\right) x[k]\,\Delta T, \qquad \text{(C.5)}$$

where the floor function $\lfloor x \rfloor = \max\{n \in \mathbb{Z} \mid x \leq n\}$ is used. Equation (C.5) can be used to calculate the estimate $X_{WT}^{da}(n\Delta T, s)$ of the continuous wavelet transform corresponding to scale s at the current sample n using the last $\lfloor N_{W_c}(s)/\Delta T \rfloor$ samples. By computing $X_{WT}^{da}(n\Delta T, s)$ for a desired set of scales s, an approximation of the momentary multiresolution spectrum of the signal is obtained. The introduced delay of $\frac{1}{2}N_{W_c}(s)$ seconds is not desirable but it is inherent to the requirement of real-time implementation. Since the delay depends on the scale s, it is inversely proportional to the central analysis frequency of the wavelet. Therefore, the analysis of low frequency components in the signal $x[k]$ suffers from larger delays than the analysis of high frequency components.

C.2.2 Wavelet design

As stated in Section C.1, the shape of the wavelet determines the achieved time and frequency resolution. Various wavelets are presented in literature, both real valued and complex valued [37]. The advantage of a complex valued wavelet is that it ensures that the magnitude of the transform is independent of the current phase of the signal.
We will use a complex valued wavelet that is based on the Morlet wavelet (C.3) since this one is suitable for achieving almost any frequency resolution by varying

the center frequency f_c and the bandwidth parameter f_b [37]. Moreover, the Morlet wavelet attains the lower bound on $\Delta f \Delta t$ implied by the uncertainty principle. The choice for the center frequency f_c and the bandwidth f_b depend on the desired time and frequency resolution. For our application it is important that the disturbance frequencies are identified in a short time period since this allows fast controller adaptation to reduce the disturbances. Therefore, we choose the time resolution as $\Delta T = {}^{1.06}/_{f_a}$. This results in a frequency resolution of $\Delta f = 0.075 f_a$. For 4 Hz, the frequency resolution equals 0.3 Hz. This may seem to be an unacceptable value, but the accuracy of the analyzed frequency f_a is generally much higher than Δf. Indeed, when no, or very little, frequency content is present near the analyzed frequency, the Morlet wavelet is able to compute the wavelet coefficient corresponding to f_a almost exactly. This is due to the fact that the gain of the Morlet wavelet falls off reasonably steep around the analyzed frequency, see Figure C.1(b). The frequency resolution Δf will become limiting when a sinusoid with a frequency close to f_a is present in the signal as well. Interference of the two sinusoids causes an inaccurate estimate of the wavelet coefficient. However, since the dominating disturbance acting on the AVIS is expected to be a single sinusoid, the achieved frequency resolution is considered to be acceptable. The corresponding values of the center frequency and the bandwidth are $f_c = 3$ and $f_b = -0.5$, respectively. Although the Morlet wavelet does not have compact support, it decays very fast and the support is nearly compact, see Figure C.1(a). Therefore, it is expected that truncating the Gaussian window in a smooth way to arrive at a compactly supported wavelet will not cause much distortion of the computed coefficient. The resulting truncated wavelet is described by

$$W_c(t) = \begin{cases} \frac{e^{\frac{t^2}{f_b}} - e^{\frac{1}{f_b}}}{1 - e^{\frac{1}{f_b}}} e^{-j2\pi f_c t} & \text{for } |t| \leq 1 \\ 0 & \text{for } |t| > 1 \end{cases}, \tag{C.6}$$

where $f_c = 3$ and $f_b = -0.5$. Wavelet $W_c(\frac{t}{s})$ is depicted in Figure C.3(a) together with the original Morlet wavelet $W_m(\frac{t-\tau}{s})$ for $\tau = 0$, $s = 3$. As already mentioned, the truncation of the wavelet results in distortion of the wavelet coefficient. This distortion is quantified in Figure C.3(b), where the Fourier transforms of both the Morlet wavelet as well as wavelet (C.6) are shown. This representation is a measure of the frequency resolution at scale s. The frequency resolution of the Morlet wavelet is ${}^{\Delta f}/_{f} = 0.075$, and although the frequency resolution for the adapted Morlet wavelet is not defined, it can be seen in Figure C.3(b) that the distortions are small compared to the analyzing frequency (1 Hz in this case). The scale s and the analysis frequency f_a of both the Morlet wavelet and wavelet (C.6) are related as $f_a = {}^{f_c}/_{s}$. The length of the used window in $W_c(\frac{t-\tau}{s})$ equals $N_{W_c}(s) = 2s$. This implies that the delay that is introduced by the real-time implementation via (C.5) in terms of the analyzed frequency is given by

$$\frac{1}{2} N_{W_c}(f_a) = \frac{3}{f_a}, \tag{C.7}$$

and hence, the identification of frequency components of 4 Hz will be delayed by 0.75 seconds, while frequency components of 10 Hz are delayed by 0.3 seconds.

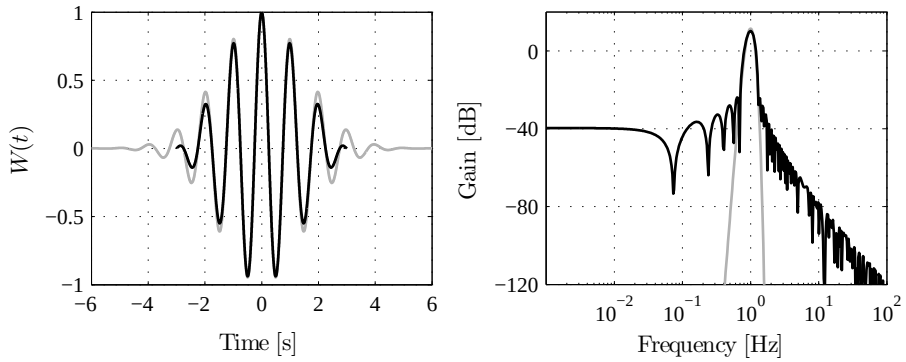

(a) (b)

Figure C.3: The Morlet (grey) and adapted (black) wavelets both represented in the time-domain (a) as well as in the frequency domain (b).

C.2.3 Real-time implementation

The discretized continuous wavelet transform (C.5) with the adapted Morlet wavelet (C.6) can be used to obtain the approximate spectrum of signal $x[k]$ at time $t = n\Delta T$ where n is the current sample by calculating $X_{WT}^{da}(n\Delta T, s)$ for a given set of scales s (and corresponding analysis frequencies f_a).
Basically, the computation of $X_{WT}^{da}(n\Delta T, s)$ boils down to the calculation of the inner product of the $\lfloor {}^{N w_c(s)}/_{\Delta T} \rfloor$-dimensional sampled wavelet vector with the corresponding signal vector. Hence, a straightforward implementation of this computation for a large amount of scales is depicted in Figure C.4. In this figure,

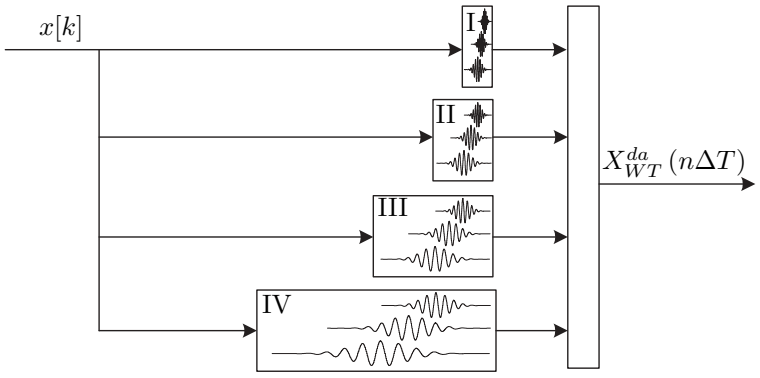

Figure C.4: Straightforward implementation.

the blocks marked by I-IV represent the calculation of the inner product for differ-

ent frequency ranges. Since the frequency resolution Δf of the wavelet transform is proportional to the analysis frequency, the scales are chosen to be logarithmically distributed. The measured signal is sampled at 1000 Hz, and according to Shannon's sampling theorem [137], the highest frequency that can be identified is 500 Hz (at scale $s = 1/500$). Since we are mainly interested in frequencies between 4 and 10 Hz, the highest frequency that will be analyzed is 120 Hz. Each block spans a factor 2 between the lowest and the highest analyzed frequencies. This means that block I computes the wavelet coefficients ranging from 60 to 120 Hz, block II from 30 to 60 Hz, and so forth. In total 10 blocks are used (although only 4 are depicted in Figure C.4 for ease of exposition), and within each block 100 coefficients are computed. This results in a logarithmically spaced frequency spectrum $X_{WT}^{da}(n\Delta T)$ that is computed for 1000 frequencies and that spans a factor $2^{10} = 1024$ in frequency ranging from $f_a = 120/1024$ to $f_a = 120$ Hz. By gridding the analyzed frequencies this way, the maximum relative error between the identified frequency and the actual frequency equals $\left(1 - 2^{\frac{1}{2 \cdot 100}}\right) \times 100\% = 0.35\%$. The implementation as depicted in Figure C.4 is not very efficient. As stated earlier, the computation of the wavelet coefficient for scale s comprises the calculation of the inner product of two $\lfloor 2s/\Delta T \rfloor$-dimensional vectors. This implies that the wavelets that are used in block IV are described by 2^3 times more samples than the wavelets in block I. Especially for low frequencies (large values of s) the computation of the inner product requires much computational effort, hampering real-time implementation. As an alternative to doubling the scale s (halving the analysis frequency) for each subsequent block as in Figure C.4, the to be analyzed vector $x[k]$ can be downsampled by a factor 2, effectively halving the frequencies that are present in the signal. To avoid aliasing, the signal should be low-pass filtered prior to the downsampling. This way the computation of the wavelet coefficients for all frequency ranges can be performed with the low dimensional vectors from block I as shown in Figure C.5. This idea is also used in [143]. Moreover,

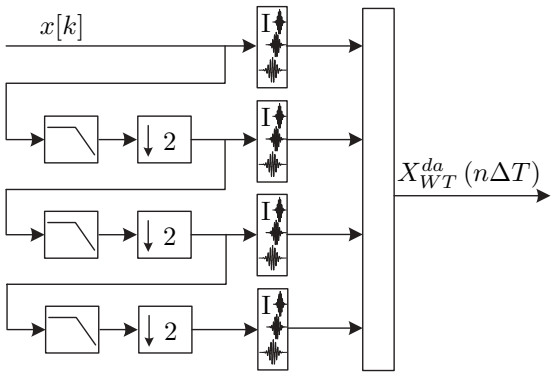

Figure C.5: More efficient implementation.

since downsampling by a factor 2 effectively halves the sampling rate of the vector $x[k]$, the rate of computation of the corresponding wavelet coefficients can be

halved as well. Especially for low frequencies this results in a drastic improvement in efficiency compared to the implementation from Figure C.4. For instance, the computational burden corresponding to the lowest frequency range (tenth block) is $2^9 \cdot 2^9 = 2^{18}$ times less for the implementation of Figure C.5 compared to that of Figure C.4, which enables real-time implementation. The low-pass filtering introduces an extra delay of approximately 1 sample each time it is applied, which amounts to a delay of 0.007 seconds for the analysis frequency of 10 Hz, and 0.015 seconds in case $f_a = 4$ Hz. This is negligible to the delay that is introduced through (C.5).

The real-time spectral analyzer returns an estimate of the frequency content of the measured signal $x[k]$ at the current sample n via the values $X_{WT}^{da}(n\Delta T, s)$ obtained at the chosen set of scales s. The dominating frequency in the spectrum is the one corresponding to the scale s with the highest value X_{WT}^{da}.

Samenvatting

Zowel industriële als commerciële high-tech mechatronische apparaten zoals printers, robotische manipulatoren, CD/DVD spelers, elektronen microscopen en wafer scanners vertegenwoordigen een groot deel van de economie. Deze apparaten moeten hun taken met hoge snelheid en precisie uitvoeren en de alsmaar strengere prestatie-eisen vragen om een herbeschouwing van de huidige ontwerpen. Aangezien de meeste van deze systemen zijn geconstrueerd om lineair gedrag te vertonen, zijn de geïmplementeerde regelstrategiën meestal gebaseerd op de lineaire regeltechniek. Vanwege inherente beperkingen van de lineaire regeltechniek moeten deze geregelde systemen vaak worden voorzien van extra (soms ook mechanische) oplossingen om de geëiste prestaties te halen.
De beperkingen waar men tegenaan loopt tijdens het ontwerp van het regelsysteem zijn fundamenteel van aard en worden deels veroorzaakt door het te regelen systeem zelf en deels door het gebruik van lineaire causale terugkoppeling. Hierdoor rijst de vraag of dit laatste deel van de beperkingen kan worden weggenomen door het toepassen van tijdsvariërende of niet-lineaire terugkoppeling.
In de literatuur kunnen inderdaad verschillende voorbeelden worden gevonden van niet-lineaire terugkoppelingen voor lineaire systemen waaruit blijkt dat deze tot betere prestaties kunnen leiden dan een lineaire terugkoppeling. Het ontbreekt echter aan kennis over de robuustheid, systematische regelaarsynthese en fundamentele beperkingen van dit soort niet-lineaire regelsystemen. Het bovenstaande in acht nemend kan de doelstelling van dit proefschrift als volgt geformuleerd worden:

Ontwikkel systematische en generieke methoden om niet-lineaire regelaars voor lineaire systemen te ontwerpen die de beperkingen, opgelegd door het gebruik van lineaire regelaars, omzeilen.

Dit proefschrift verkent een drietal richtingen om tot een oplossing voor de bovenstaande probleemstelling te komen.

Tijd-domein gebaseerd regelaar ontwerp: Een methode wordt ontwikkeld

om een niet-lineaire toestandsterugkoppeling te ontwerpen die aan een aantal tijd-domein specificaties voldoet die niet gehaald kunnen worden met het gebruik van lineaire toestandsterugkoppeling. Dit wordt bereikt door het gebruik van een reeds bestaande polynomische interpolatietechniek. De stabiliteit van het verkregen niet-lineaire regelsysteem kan worden geanalyseerd met behulp van de zogenaamde "sum-of-squares" techniek. Ook wordt er een uitbreiding gepresenteerd van een methode uit de recente literatuur die gebruikt kan worden om lineaire regelaars van vaste orde te ontwerpen die voldoen aan vooraf gespecificeerde eisen. Deze uitbreiding maakt het mogelijk om gesloten lus systemen met complex geconjugeerde polen te beschouwen, terwijl de oorspronkelijke methode alleen geschikt is voor gesloten lus systemen met reële polen.

Reset regelaars: Dit proefschrift draagt op twee manieren bij aan de theorie op het gebied van reset regelaars, namelijk met betrekking tot de $\mathcal{L}_2$ versterking en tot de $\mathcal{H}_2$ norm. De analyse van de $\mathcal{L}_2$ versterking wordt gegeneraliseerd tot reset systemen die passen in het welbekende en algemene $\mathcal{H}_\infty$ raamwerk. Verder worden er convexe optimalisatie problemen geformuleerd om een bovengrens van de $\mathcal{H}_2$ norm van een reset systeem te berekenen.

LPV regelaars: In standaard lineair parameter afhankelijke (LPV) regelsystemen hangt het te regelen systeem af van één of meerdere reëel waardige parameters. In dit proefschrift echter worden lineaire en tijdsinvariante te regelen systemen beschouwd en wordt de parameterafhankelijkheid geïntroduceerd via de prestatie-eisen. We presenteren een methode om een niet-lineaire regelaar voor een lineair systeem te ontwerpen die de transiënte responsie op een stapvormig referentiesignaal verbetert. Ook presenteren we een niet-lineair regelaarontwerp voor de actieve regeling van een trillingsisolatiesysteem. Dit ontwerp bestaat uit twee delen: (i) een real-time multi-resolutie spectrale analyse algorithme dat de belangrijkste aanwezige verstoring kan identificeren en (ii) een LPV regelaar die zichzelf aanpast aan de huidige verstoring. Op deze manier wordt een regelsysteem verkregen dat zichzelf aanpast aan de huidige verstoringsomstandigheden en op deze manier een betere prestatie tot gevolg heeft dan het originele regelaarontwerp.

In dit proefschrift zijn een aantal initiële stappen gepresenteerd om tot een systematische methode te komen om niet-lineaire regelaars te ontwerpen voor lineaire systemen die beter presteren dan lineaire regelaars. De verkregen resultaten zijn aan de ene kant veelbelovend, aan de andere kant moet er nog veel gedaan worden voordat systematische ontwerpmethoden beschikbaar zijn. De potentiële voordelen voor de high-tech industrie zijn een motivatie om dit uitdagende gebied verder te ontwikkelen. De resultaten die in dit proefschrift zijn gepresenteerd kunnen een basis vormen voor deze verdere ontwikkeling.

Dankwoord

En dan nu: het dankwoord. Ook al staat het (bijna) helemaal achterin, het wordt waarschijnlijk de meest gelezen pagina van dit proefschrift. Met het schrijven ervan breekt dan toch echt het einde aan van een geweldige periode op de TU/e. Niet alleen de laatste 4 promotiejaren maar ook de voorafgaande studiejaren hebben mij in staat gesteld dit proefschrift te schrijven. Alhoewel dit voor mijn gevoel '*mijn* boekje' is, was het nooit tot stand gekomen zonder alle mensen om mij heen. Daarom wil ik graag van de gelegenheid gebruik maken om hen middels dit dankwoord te bedanken.

Maarten Steinbuch wil ik bedanken voor de mogelijkheid die hij me heeft geboden om het promotietraject in deze inspirerende en unieke omgeving te doorlopen. Maarten, ik ben je ook zeer erkentelijk voor de coaching, de motiverende gesprekken en de geboden mogelijkheden om diverse conferenties te bezoeken en cursussen te volgen.
René van de Molengraft wil ik graag bedanken voor de dagelijkse begeleiding. René, je goede ideeën, scherpe inzichten en de stimulerende besprekingen hebben veel bijgedragen aan dit proefschrift. Ik ben erg blij dat je me gevraagd hebt voor het Robocup team, een ervaring die ik niet had willen missen. Vooral de gezelligheid tijdens de vele uurtjes die we eraan besteed hebben wordt erg door mij gewaardeerd.
Last in dit rijtje, maar zeker not least, wil ik Maurice Heemels bedanken. Maurice, ondanks het feit dat je er pas in een later stadium als copromoter bent bijgekomen, is er geen enkele bladzijde van dit proefschrift ongewijzigd gebleven. Ook wil ik je bedanken voor jouw onuitputtelijke bereidheid om de verschillende stukken zeer kritisch door te lezen en te bespreken, mede daarom zit het proefschrift een stuk 'strakker in het jasje'.

Een woord van dank gaat ook uit naar de studenten die geholpen hebben met verschillende delen van dit proefschrift. Chris, Gert, Rolf, Matthijs en Tom, bedankt voor jullie inzet! Zonder jullie had ik nooit alle onderwerpen in dit proefschrift zo uitgebreid kunnen behandelen.

Henk Nijmeijer, Carsten Scherer en Jan Swevers wil ik bedanken voor de bereidheid om plaats te nemen in de kerncommissie. I would also like to thank Didier

Henrion for the suggestions he has offered regarding Chapter 4.

Ik betwijfel of er ergens een gang te vinden is waar zo'n goede werksfeer heerst als op -1. Ik ben altijd met erg veel plezier naar mijn 'werk' gegaan waar vanaf 's ochtend 8 (heb ik mij laten vertellen) tot 's avonds 8 altijd wel collega's aanwezig waren. Laan, Brunuh, Hamers, cdr. Marcos, Martijn, Iciar, Paola, Beast, Buxus, Bonsen, Fix, Mattie, master Doris, Wevers, dr. BVO, JvH, Hofmeister, Kazaa, Koot, TAC, Mallon, Meinders, Melly, Smackdown, Gnaus, T. Ohmi, Rick, Schneiders, JvdW, Gurt en alle andere collega's, bedankt voor de gezelligheid tijdens de lunch, borrels, uitjes, conferenties, vakanties, bankdruk activiteiten (ook Raphaël bedankt) en alle andere activiteiten. Ook de nog niet genoemde leden van het TechUnited Robocup team: Harrie, Rob, Pieter, Patrick, Gerard, Ruud en het office wil ik bij deze bedanken voor de leuke tijden tijdens de klusavonden en de 'zakenreizen'.

Gelukkig heb ik ook genoeg tijd gehad om buiten de universiteit dingen te ondernemen. Het is fijn om zo nu en dan te horen dat er nog andere dingen bestaan dan Bode plaatjes, transfer functies en m-files. Ik wil dan ook graag 'de portiers', mijn tafelvoetbalteam, (ex)AOR collega's, (oud)huisgenoten, (ex)studiegenoten en al mijn andere (niet tot een nader te definiëren groep behorende) vrienden bedanken voor de welkome afleiding.

Graag wil ik mijn familie bedanken voor de getoonde interesse in mijn werk en al de gezelligheid en steun die ik heb mogen ontvangen gedurende alle jaren.
Boven alles wil ik mijn ouders bedanken. Mam, ik was nooit zo ver gekomen zonder jouw grenzeloze liefde, steun en vertrouwen. Pap, ook al heb je mijn promotie niet meer mogen meemaken, ook jouw liefde, steun en vertrouwen hebben mij in staat gesteld dit proefschrift te voltooien. Mijn enige zusje mag natuurlijk niet ontbreken in dit dankwoord. Rinske, je bent er altijd voor mij als het nodig is en dat waardeer ik zeer. Samen met Thijs zorg je ook voor veel gezellige en ontspannen momenten, dank je wel daarvoor!

Tot slot wil ik mijn vriendin bedanken. Lieve Rasa, als geen ander weet jij wat het is om een promotietraject te doorlopen. Je bent dan ook een grote steun voor mij geweest de laatste jaren en ik hoop dat er nog vele mooie jaren mogen volgen.

Curriculum Vitae

Wouter Aangenent was born on October 30th, 1978 in Milsbeek, The Netherlands. After finishing his secondary education at the Elshof College in Nijmegen in 1996, he started his study Mechanical Engineering at the Technische Universiteit Eindhoven (TU/e), where he received his M.Sc. degree (Cum Laude) in 2004. His traineeships were carried out at the TU/e and at Aalborg Universitet, Denmark. His master's thesis was entitled "Data-based LQG control" and was performed at the TU/e. Since April 2004, Wouter has been working as a Ph.D. student in the Control Systems Technology Group at the department of Mechanical Engineering of the TU/e on the topic "Nonlinear Control for Linear Motion Systems", resulting in this thesis.